

To Mom and Dad
who installed a love for nature throughout my life
Could not have done it without your support

致父母：
感谢你们在我成长过程中一路默默支持和付出
成就了我今天的高度

Acknowledgment

First and foremost, I want to express my deepest gratitude to my respectful dissertation advisor, Dr. Eyleen O'Rourke. Within the past 4 years, you provided me the best environment and resources to grow and learn to be a good scientist and a good person; you guided me not only on scientific thinking but also on communication with people, behaving professionally, and overcoming my weaknesses; you mentored me with all your patient and good heart even when I was frustrated and struggled; you provided good advice to me regardless of my stubbornness and arrogance; you were always there helping me when I was in any trouble; you always think about me and satisfied my craving for high-fat food (Thanks for all the coupons for high-fat food)! NO WORDS can express my appreciation to you as the person who truly changed me and pointed me on the path to be successful. And your advice will always guide me in my future career and my life.

Secondly, I want to thank all the members of my dissertation committee, including Dr. Keith Kozminski, Dr. Jason Papin, Dr. Christopher Deppmann, and Dr. Ariel Gomez. In particular, I would like to express my special appreciation to Dr. Keith Kozminski. As my first reader, you are super responsible and reliable in every step I went through in graduate school. You constantly checked on me to make sure I was on the right path, and you were also very patient with me when I was struggling with work and life. I have a personality that is easily distracted by different ideas and goals, while you are the only person who helped me focus and to keep on

track. Moreover, I learned a lot from you regarding professionalism. You guided me on how to communicate properly in science and took you time to carefully revised my extra-long dissertation. You are my idol of a serious scientist and I hope I could have learned more from you! Besides Dr. Keith Kozminski, I also want to thank Dr. Christopher Deppmann, especially for all the guidance and advice when I was struggling. All the advice you provided was very helpful and I was very lucky to be able to talk to one of your very successful students (Dr. Dong Suo) to figure out my path to be successful in graduate school during the rough time. Altogether, I am lucky to have such a great committee to guide me during graduate school.

Next, I want to thank all the undergrads working with me, especially Leila Rayyan, Chenyu Yang, Noel Higgason, and Michael Hilzendeger. I am very grateful that you all could trust me and be my mentees for >2 years out of your 4 years of precious undergraduate time. All of you worked super hard and became a co-author of at least one publication with me, and I am very proud of you! And Leila, I am very grateful that you made birthday celebrations for me every year! I am lucky to be your mentor and I could not make such progress without help from all of you.

Further, I want to thank all my co-workers and friends in graduate school, especially everyone in O'Rourke lab. Anna Way, I enjoy being a friend of you and to be able to share opinions and ideas with you, and I also enjoy working with you not only on science but also on science communication, science policy, and students affairs when we worked together in ComSciCon organizing committee,

GSASC, and PhD plus program. Dr. Vinod Mony, you are the friendliest person I have ever know and I enjoy being around you. Nella Solodukhina, although I did not talk to you much, I appreciate all the reagents and helps from you these years and you are a great lab manager. Shawna Benjamin, Wei Ma, Abbas Ghaddar, MaryKate Horak, Zofia Kołodziejczyk, all of you have been great and helpful co-workers and friends to me! I also want to thank my friends in graduate school, Omar Guessoum, Qijun Tang, Sihang Li, Lindsay Heckle, Dr. Yu Yong, Yang Yu, Shiwei Liu, Yingnan Gao. I was very happy to be your friend and to take the time to hang out with you.

Finally, I want to express my appreciation to all my family members. I want to especially thank my mom and dad for raising me to make me who I am now, and for the unconditional love and support to me. I could not have achieved anything without all the guidance and support from you throughout my childhood and adult life. I also want to recognize my girlfriend Thao Do, for being through all the happy and rough time with me in the past 10 years, and I am grateful that you are still in love with me and decided to continue being my girlfriend even when I was focusing on career and did not spend much time with you in the long-distance relationship. In addition, I want to also acknowledge all my other family members (uncles, aunts, cousins) for taking care of me throughout my childhood, and Thao's family (sister, brother in law, mother, nephews, and niece) for the hospitality when I came visiting in the past 10 years.

Table of Content

CHAPTER I: Introductory chapter	1
1.1 Studying the molecular mechanisms of CCDs in <i>C. elegans</i>	1
1.2 Studying therapeutics for CCDs in <i>C. elegans</i>.....	6
1.3 Introductory remarks.....	7
CHAPTER II: Developing high-throughput RNAi screen to identify fat regulators in obesity	8
Statement of contribution and acknowledgment.....	9
2.1 Abstract	10
2.2 Introduction.....	11
2.3 Materials	14
<i>2.3.1 Bacteria and worm strains.....</i>	<i>14</i>
<i>2.3.2 Reagents.....</i>	<i>17</i>
<i>2.3.3 Supplies and equipment.....</i>	<i>19</i>
2.4 Methods	21
<i>2.4.1 Reagents preparation.....</i>	<i>21</i>
<i>2.4.2 Bacteria RNAi strains preparation</i>	<i>24</i>
<i>2.4.3 Worm preparation</i>	<i>30</i>
<i>2.4.4 RNAi incubation (first day of experiment).....</i>	<i>32</i>
<i>2.4.5 ORO staining.....</i>	<i>33</i>

2.4.6 Image acquisition and data storage	36
2.4.7 High-Content Screening (HCS) Image Processing considerations.....	37
CHAPTER III: Modeling diet-induced obesity and validating GWAS obesity candidate genes in <i>C. elegans</i>	46
Statement of contribution and acknowledgment.....	47
3.1 Abstract	49
3.2 Introduction.....	50
3.3 Materials and Methods	54
3.4 Results.....	62
3.4.1 Meta-analysis of human obesity GWAS variants identifies <i>C. elegans</i> orthologs.....	386 62
3.4.2 Sixteen human-obesity gene candidates alter fat accumulation in standard-diet fed <i>C. elegans</i>	66
3.4.3 High-fructose diet leads to Diet-induced obesity in <i>C. elegans</i>	77
3.4.4 Three human-obesity gene candidates cause DIO in <i>C.</i> <i>elegans</i>	86
3.4.5 DIO suppressors restore <i>C. elegans</i> LD physiology in a tissue-specific manner	90
3.4.6 DIO suppressors restore health biomarkers and lifespan of HFrD-fed <i>C. elegans</i>	95

3.5 Discussion.....	98
3.6 Tables	109
CHAPTER IV: Metabolic profiling and modeling obesity in <i>C. elegans</i>	129
Statement of contribution and acknowledgment.....	130
4.1 Introduction.....	132
4.2 Results and discussion.....	137
4.4 Tables	143
CHAPTER V: Molecular Dissection of a Chemotherapeutic-diet-host- microbiome 4-way interaction in <i>C. elegans</i>	153
Statement of contribution and acknowledgement.....	154
5.1 Abstract	158
5.2 Introduction.....	159
5.3 Material and Methods	163
5.4 Results.....	181
5.4.1 <i>FUdR</i> toxicity in <i>C. elegans</i> is driven by <i>FUMP</i> synthesis and not <i>dTMP</i> depletion in <i>E. coli</i>	181
5.4.2 Dietary thymidine potentiates <i>FUdR</i> toxicity via promoting <i>E.</i> <i>coli</i> <i>FUdR</i> -to- <i>FUMP</i> conversion.....	190
5.4.3 Dietary serine potentiates <i>FUdR</i> toxicity without increasing <i>FUMP</i> levels.....	194
5.4.4 <i>E. coli</i> 's folate-synthesis pathway is required for <i>SE-FUdR</i> toxicity	209

5.4.5 Dietary serine reduces <i>E. coli</i> 's and hence <i>C. elegans</i> 's dTMP pool	216
5.4.6 The host distinctively responds to Lth-FUdR and SE-FUdR toxicity	227
5.5 Discussion.....	250
5.6 Tables	255
CHAPTER VI: Conclusion	269
Summary of this dissertation	269
<i>Simplicity is the ultimate sophistication.....</i>	271
References	278

List of Figures

CHAPTER II

Figure 2. 1 RNAi screening workflow.....	42
Figure 2. 2 Post-HCS image processing workflow	44

CHAPTER III

Figure 3. 1 GWAS obese genes were validated through <i>C. elegans</i> RNAi screen	64
Figure 3. 2	71
Figure 3. 3 GWAS lean genes were validated through <i>C. elegans</i> RNAi screen	73
Figure 3. 4 Human orthologs of <i>C. elegans</i> screen hits are implicated in human obesity	75
Figure 3. 5 Overconsumption of fructose leads to DIO in <i>C. elegans</i>	81
Figure 3. 6	84
Figure 3. 7 <i>C. elegans</i> DIO suppressors were identified through RNAi screen .	88
Figure 3. 8 KD of DIO suppressors leads to LD phenotypes in worms fed RD and HFrD.....	93
Figure 3. 9 KD of DIO suppressors improves <i>C. elegans</i> healthspan and lifespan	96
Figure 3. 10	107

CHAPTER IV

Figure 4. 1 Summary of worm model screens	140
--	------------

CHAPTER V

Figure 5. 1	185
--------------------------	------------

Figure 5. 2 Dietary thymidine enhances FUdR-to-FUMP conversion in <i>E. coli</i>	187
--	------------

Figure 5. 3	192
--------------------------	------------

Figure 5. 4 Dietary serine enhances FUdR toxicity but not FUdR-to-FUMP conversion	199
---	------------

Figure 5. 5 Lth-FUdR and SE-FUdR toxicity do not correlated with <i>E. coli</i> growth, viability, or bacterial virulence.....	202
--	------------

Figure 5. 6	204
--------------------------	------------

Figure 5. 7	206
--------------------------	------------

Figure 5. 8 SE-FUdR toxicity requires <i>E. coli</i> 's folate and pyridoxal phosphate synthesis pathways	212
---	------------

Figure 5. 9 Suppression of SE-FUdR toxicity by <i>E. coli</i> KOs does not correlate with <i>E. coli</i> growth.....	214
--	------------

Figure 5. 10	222
---------------------------	------------

Figure 5. 11 SE-FUdR promotes dTMP depletion in <i>E. coli</i> and <i>C. elegans</i>	224
--	------------

Figure 5. 12 Lth-FUdR activates autophagic cell death in <i>C. elegans</i>	229
---	------------

Figure 5. 13 Validation of EORB1 (an RNAi-competent derivative of HB101) .	232
---	------------

Figure 5. 14	240
---------------------------	------------

Figure 5. 15 Autophagy activation in Lth-FUdR depends on mitochondrial lipid metabolism	243
Figure 5. 16 Host response to Lth-FUdR and SE-FUdR are distinct.....	247

List of Tables

Chapter III

Table 3. 1 Human GWAS obesity genes and <i>C. elegans</i> orthologs from meta-analysis	109
Table 3. 2 Lifespan analysis of worms fed HFrD versus RD	126
Table 3. 3 Lifespan analysis of worms treated with RNAi constructs versus EV in RD and HFrD conditions.....	127

Chapter IV

Table 4. 1 Fat regulators in <i>C. elegans</i> obesity models	143
--	------------

Chapter V

Table 5. 1 List of <i>E. coli</i> genes screened from the Keio <i>E. coli</i> knock-out library	255
Table 5. 2 Hits of Keio screen for mediators of SE-FUdR toxicity	258
Table 5. 3 List of <i>C. elegans</i> genes tested in the EORB1 Lth-FUdR, and SE-FUdR RNAi screens	260
Table 5. 4 <i>C. elegans</i> suppressors and enhancers of Lth-FUdR and SE-FUdR toxicity	266

CHAPTER I: Introductory chapter

Chronic complex diseases (CCDs) and conditions such as cancer, type 2 diabetes, Alzheimer's disease, heart disease, obesity, and other age-related disorders are the leading cause of death and disability in the US (Murphy et al., 2021). CCDs are also a major economic burden (Buttorff et al., 2017; Martin et al., 2021). In the past decade, approximately 50% of the population age 60 or older in the US have been diagnosed with a CCDs and ~25% of this age group has two or more conditions (Anderson and Horvath, 2004; Joly et al., 2013; van den Akker et al., 1998; Wolff et al., 2002). Therefore, it is critical to understand the molecular mechanisms underlying CCDs to develop interventions to alleviate such health, social, and economic burdens.

1.1 Studying the molecular mechanisms of CCDs in *C. elegans*

Unlike single-gene disorders (e.g. Huntington's disease) or pathogenic diseases (e.g. Influenza), the understanding of the molecular drivers of CCDs has been a long-term puzzle in biomedical research due to the duration to develop the disease and the complexity derived from a combination of genetic, environmental, and lifestyle factors. Nevertheless, the sequencing of the human genome and the revolutionary advancement of next-generation sequencing (NGS) technologies in the past decade have transformed our approaches to studying CCDs. Advances include the discovery of early biomarkers, disease pathways, and the advancement of precision medicine based on patient genetics (Morganti et al.,

2019). Particularly, by sequencing the genome or transcriptome of healthy and diseased human populations, we can associate disease phenotypes with genetic variants (mostly SNPs) across the human genome and identify loci that may predispose or prevent CCDs complex. This approach known as genome-wide association studies (GWAS) (Frazer et al., 2009) has been widely applied and thousands of SNPs and other variants have been associated with multiple diseases. However, a major limitation of GWAS is that trait-associated SNPs may not be causative variants. There are two major barriers to define causality for GWAS hits. On one side, linking a variant to a specific gene is not trivial, as variants may influence the function of distal genes and almost 90% of single nucleotide variants (SNPs) are found in noncoding regions of the genome (Maurano et al., 2012). Further, even when clear gene candidates can be defined, the lack of an experimental system that allows testing the role of hundreds of loci *in vivo* at a reasonable pace and cost has remained the main barrier to the discovery of druggable targets potentially derived from GWAS (Korte and Farlow, 2013).

To establish the causality and to study the mechanisms of the disease-causing candidate genes, many studies utilized *in vitro* human disease models (Torrance et al., 2001). Indeed, most studies would test candidate disease genes in cultured cells, which tend to be transformed cells with altered metabolism. To better approximate the role of the gene *in vivo*, other studies would use primary cells in culture from healthy individuals; however, this *in vitro* setup assumes that the gene would act similarly *in vitro* and the natural *in vivo* context (Hudu et al., 2016).

However, it is clear that whole organisms have a broader plasticity tool set than individual cultured cells; hence, many “disease” gene targets identified *in vitro* have not translated *in vivo*. Finally, when *in vivo* studies of the candidate gene are carried out, they focus on the function of a gene in a single tissue or organ despite the body of knowledge demonstrating that a given gene can have distinct or even opposite effects on the same phenotype depending on the cell type, tissue or organ where it acts, and on other critical factors including, but not limited to, diet and microbiota tend to be overlooked.

To better understand the pathogenesis of CCDs at a cellular and molecular level, animal models are widely applied. Due to the close homology between mammalian genomes, most studies on human disease consider the mammalian models, such as the rodents, as the preeminent models to study different aspects of a disease. However, slow development, low reproductive rate, and costly maintenance make unfeasible the use of *in vivo* mammalian models to test hundreds of CCD gene candidates. Therefore, to take full advantage of the power of GWAS, it is critical to develop genetically tractable models of the disease of interest. The ideal model will have fast development, a short life span, a high reproductive rate, a conserved genome when compared to humans, and easy genetic tools. Based on these criteria, *Caenorhabditis elegans* is an ideal model organism to study the molecular bases of CCDs. *C. elegans* develop from egg to gravid adult in 3 days, live less than 30 days, produce 300-500 embryos per adult in 5 days, is fully transparent and its fully annotated genome is >65% conserved when compared to humans.

(Muschiol et al., 2009) *C. elegans* is also the only model system enabling *in vivo* whole-body or tissue-specific whole-genome RNA interference just by feeding double-stranded RNAs (dsRNAs). RNAi is delivered by simply feeding worms with *Escherichia coli* bacteria (normal lab diet for *C. elegans*) that produces dsRNA against a specific worm gene upon induction with isopropyl β -D-1-thiogalactopyranoside (IPTG) induction (Tabara et al., 1998). Whole-genome RNAi in *C. elegans* thus only requires a library of ~20,000 *E. coli* strains. Our current RNAi feeding libraries cover close to 87% of the worm genome (Kamath et al., 2003). Moreover, many cellular processes and their effectors are highly conserved from *C. elegans* to humans, which makes research in *C. elegans* translatable. Although there are important differences in terms of physiology and tissue functions, and some key mammalian genes related to many CCDs are missing in nematodes (e.g. leptin for obesity), most of the core lipid, sugar, and protein metabolism pathways and cellular signaling pathways are highly conserved between worms and mammals. For example, adipose triglyceride lipase, hormone-sensitive lipase, and lysosomal lipases play essential roles in fat breakdown and mobilization in both *C. elegans* and mammals (Wang et al., 2008). Regulators such as TOR kinase, AMPK, sterol response element binding protein (SREBP), and many other transcription factors similarly control metabolic genes and cellular responses to nutrients in *C. elegans* and mammals. Loss of function of such regulators causes similar metabolic defects such as obesity in worms and mice (Long et al., 2002; McKay et al., 2003; Sze et al., 2000).

C. elegans has been extensively used to model human CCDs, particularly, in studying Age-Related Diseases. Take neurodegenerative diseases as an example, many *C. elegans* models have been established, including Alzheimer's disease (Link, 1995), Parkinson's disease (Kuwahara et al., 2006; Lakso et al., 2003; Ved et al., 2005), Huntington's disease (Faber et al., 2002), and Amyotrophic Lateral Sclerosis (Oeda et al., 2001), and many disease mechanisms were discovered using these models. For example, it was discovered in *C. elegans* that loss of the *age-1* (phosphatidylinositol 3-OH kinase) in the insulin-like signaling pathway, results in delayed polyQ aggregation and cytotoxicity, and loss of *age-1* increases life span and healthspan by upregulating chaperone capacity (Morley et al., 2002; Parker et al., 2005). Moreover, *C. elegans* is also a preeminent model system in the study of complex diseases, such as cancer. Although all the somatic cells in the adult *C. elegans* are post-mitotic, many cancer cellular mechanisms were illustrated in *C. elegans* research in the first place. For example, programmed cell death was firstly described in *C. elegans* (Hengartner and Horvitz, 1994) and has become one of the productive fields in cancer research. One group of the most characterized oncogenic gene, Ras (*let-60* in *C. elegans*), was also first identified and characterized in the *C. elegans* multi-vulva cancer model (Ferguson and Horvitz, 1985; Horvitz and Sulston, 1980; Seydoux et al., 1993). Therefore, *C. elegans* is a great model system to study CCDs and to help expand our knowledge of the disease mechanisms.

1.2 Studying therapeutics for CCDs in *C. elegans*

C. elegans has been used to elucidate evolutionary conserved biological pathways related to human diseases for decades. On the other hand, *C. elegans* has also become a popular model to study disease treatment and for drug discovery due to the development of feasible high throughput drug and chemogenomic screens. With the transparent body, *C. elegans* is compatible with image-based drug screens using reporter strains. *C. elegans* also has advantages of fast reproductive rate and relatively small body size, and this is compatible with high throughput and high content screens (O'Reilly et al., 2014; O'Rourke et al., 2009a). The first large-scale drug screen was reported in 2006 (Kwok et al., 2006) to identify small molecules that affect the growth, survival, and locomotion. In 2010, the first automated image-based high throughput drug screen was reported to identify drugs that enhance clearance of misfolded protein using GFP reporter strain (Gosai et al., 2010). Further, *C. elegans* can be used to identify genes that are responsible for the different responses to drugs using RNAi screen combined with the drug treatments, known as chemogenomics (Jones et al., 2005). This enables the identification of the drug targets.

To date, numerous studies reported potential therapeutic drugs to treat CCDs in *C. elegans* disease models including cancer (Kobet et al., 2014; Wu et al., 2016; Ye et al., 2020), neurodegenerative diseases (Chen et al., 2015; Sohrabi et al., 2021; Voisine et al., 2007), obesity and metabolic diseases (Bouyanfif et al., 2019;

Zheng et al., 2010), and aging and age-associated diseases (Bazopoulou et al., 2017; Chen et al., 2015; Kim and Lee, 2019).

1.3 Introductory remarks

In this dissertation, I demonstrate the approaches to study the etiology of CCDs (focusing on obesity and metabolic diseases) in the model system *C. elegans* and utilize *C. elegans* as the model to study treatments and therapies for CCDs (focusing on chemotherapy), respectively. More specifically, I described the experimental and bioinformatics pipelines to identify fat regulators in obesity in *C. elegans* (**Chapter II**), established *C. elegans* diet-induced obesity (DIO) model to validate the human genetic variants that potentially cause or prevent against DIO (**Chapter III**), and identified fat regulators in *C. elegans* metabolism towards the goal of developing the first predictive model of the metabolism of obesity (**Chapter IV**). Finally, using *C. elegans-E. coli* host-microbiome system, I molecularly dissected the first diet-microbiome-host-drug 4-way interaction (**Chapter V**). Altogether, this dissertation emphasizes the variety of the approaches to study disease mechanisms and treatment of complex diseases using the invertebrate model system *C. elegans*.

CHAPTER II: Developing high-throughput RNAi screen to identify fat regulators in obesity

The methods presented in this chapter was published on *Methods Mol Biol.*

2018; 1787:129-146. using the title:

The ancient genetic networks of obesity: whole-animal automated screening for conserved fat regulators

PMID: [29736715](#) DOI: [10.1007/978-1-4939-7847-2_10](#)

Publication Author list: Wenfan Ke, Anna Drangowska-Way, Daniel Katz, Karsten Siller, Eyleen J. O'Rourke

Statement of contribution and acknowledgment

The methods described in this chapter were established based on two previous publications describing RNAi screen and bioinformatic tools developed by Dr. Eyleen O'Rourke and collaborators (Wählby et al., 2012, 2014). In particular, some pipelines described in this chapter (RNAi treatments, Cellprofiler pipelines and Cellprofiler Analyst pipelines) were adopted and modified from the previous methods developed by Dr. Carolina Wählby, Dr. Anne Carpenter, Dr. Jonah Larkins-For, Dr. Annie Lee-Conery and Dr. Eyleen O'Rourke. I optimized the methods described in this chapter for the purpose of high throughput RNAi screen for fat regulators with the help from Anna Way, Wei Ma, and undergraduate student Leila Rayyan, and advice from Dr. Eyleen O'Rourke. I also worked with Daniel Katz and Dr. Karsten Siller from the UVA high performance computing group to develop and test the pipelines for post imaging analysis on high performance computing clusters, including image stitching, data transfer, Cellprofiler analysis, and database management. This work would not have been possible without the generous support of the W. M. Keck Foundation.

2.1 Abstract

Caenorhabditis elegans is the first and only metazoan model that enables whole-body gene knock down by simply feeding their standard laboratory diet, E coli, carrying RNA interference (RNAi) expressing constructs. The simplicity of the RNAi treatment, small size, and fast reproduction rate of *C. elegans* allow us to perform whole-animal high-throughput genetic screens in wild type, mutant or otherwise genetically modified *C. elegans*. In addition, more than 65% of *C. elegans* genes are conserved in mammals including human. In particular, *C. elegans* metabolic pathways are highly conserved, which supports the study of complex diseases such as obesity in this genetically tractable model system. In this chapter, we present a detailed protocol for automated high-throughput whole-animal RNAi screening to identify the pathways promoting obesity in diet-induced and genetically-driven obese *C. elegans*. We describe an optimized high-content screening protocol to score fat mass and body fat distribution in whole animals at large scale. We provide optimized pipelines to automatically score phenotypes using the open source Cellprofiler platform within the context of supercomputer clusters. Further, we present a guideline to optimize information workflow from the automated microscope to a searchable database. The approaches described here enable unveiling the whole network of gene-gene and gene-environment interactions that define metabolic health or disease status in this proven model of human disease, but similar principles can be applied to other disease models.

2.2 Introduction

Caenorhabditis elegans has become a leading model organism to tackle important biomedical questions. It is a powerful system due to its short life span (less than 30 days), high reproduction rate (300-500 eggs per animal in total with peak around 150 eggs/day), fast development (90 hours from hatching egg to adult at 15°C), transparency of the organism and fully sequenced and annotated genome (Muschiol et al., 2009). Furthermore, *C. elegans* has a stereotypical distribution of cells identical from worm to worm and its neuronal connectome has been completely traced, providing great advantages for studying biological processes that rely on proper cell to cell, tissue to tissue, or whole-body communication (Sulston and Horvitz, 1977).

The most basic biological processes and their effectors (genes) are conserved from *C. elegans* to human, which makes research in *C. elegans* translatable to mammals and even humans. Although there are important differences in terms of tissue and organ function, and some key mammalian metabolic players are missing (i.e. leptin) most of the core lipid, sugar and protein metabolism pathways are highly conserved between worms and mammals. For example, adipose triglyceride lipase, hormone sensitive lipase, and lysosomal lipases play essential roles in fat storage and mobilization in *C. elegans* and mammals (Narbonne and Roy, 2009; Wang et al., 2008). TOR kinase, AMPK, sterol response element binding protein and many other transcription factors similarly control metabolism-gene regulation and cell responses to nutrients in *C. elegans* and mammals. Loss

of function of such regulators causes severe metabolic defects such as obesity in worms (Long et al., 2002; McKay et al., 2003; Sze et al., 2000). In addition, several pathways systemically regulating metabolism are also conserved. Importantly, the major components of the insulin-signaling pathway are conserved and chronically defective insulin signaling leads to symptoms associated with insulin resistance including obesity in worms (Garcia et al., 2015). These and other examples suggest that unwinding *C. elegans* metabolic players and how they are modulated by changing environmental factors, including food quantity and quality or genetic defects, would help us better understand metabolic disease in humans.

C. elegans is also the first model system enabling whole-genome systemic RNA interference *in vivo*. This capability is particularly critical to understand metabolic disease since metabolic status is the product of coordinated action of multiple cells and organ systems. In *C. elegans*, RNAi can be delivered by simply feeding worms with bacteria that overproduces double stranded RNA against a specific worm gene upon isopropylthiogalactoside (IPTG) induction (Tabara et al., 1998). RNAi libraries developed by Julie Ahringer's group cover close to 87% of the worm genome and these feeding constructs are readily available from Source BioScience (Kamath et al., 2003).

The fast development and reproduction rate imply that *C. elegans* can be used as an *in vivo* model to perform high-throughput (HT) screening. Automated and quantitative high-throughput screening methods have been developed and

improved throughout the past years, and these HT assays allow us to identify lead compounds in *in vivo* HT chemical screens and genes in RNAi-based screens(O'Rourke et al., 2009a).

Previously we described an improved oil red O staining technique to provide an image-based quantitative measurement of fat mass that correlated to biochemically measured triglyceride mass (O'Rourke et al., 2009b). This method uses isopropanol to preserve worm-tissue structure, which is otherwise fragile (i.e. by paraformaldehyde-based fixation). This method can be used as a powerful quantitative technique to identify genes that alter body fat mass in *C. elegans* (O'Rourke et al., 2009b). Here we present several advances to the processing and imaging of the worm populations, and we delineate considerations and solutions to the handling of the massive amount of data generated by image-based HT screening of *C. elegans*.

Comparing to our previous method, we optimized conditions in preparation, RNAi treatment and data analysis. In this chapter, we describe detailed step by step procedures with improvement on reducing non-RNAi variants such as position of the wells, growth conditions, precipitation of ORO dyes, and moreover, we incorporate the data processing power from supercomputer to enable analyses of high-resolution composite images from high-content screening experiments.

2.3 Materials

2.3.1 Bacteria and worm strains

1. RNAi Library from Ahringer laboratory can be acquired from Source BioScience.

<http://www.sourcebioscience.com/products/life-science-research/clones/rnai-resources/c-elegans-rnai-collection-ahringier/> (see Note 1)

Note 1: Two major sets of RNAi feeding libraries are currently available, the initial Ahringer library and the supplementary library. The initial Ahringer library covers 72% of the worm genome, and the supplementary library covers another 15% of all genes, so the combination of both library covers 87% of the worm genome. All the feeding library sets are delivered as glycerol stocks and should be store in -80°C freezer

2. *C. elegans* strains NL2099 (*rrf-3(pk1426)*II (see Note 2), GMW004 (*rrf-3(pk1426)* II; *daf-2(e1368)* III) can be acquired from Caenorhabditis Genetics Center (CGC)(Simmer et al., 2002). <https://cbs.umn.edu/cgc/home> (see Note 3)

*Note 2: NL2099 strain carries a 3015 base pair deletion between exon 4 to 11 of *rrf-3* gene, and this allele(pk1426) can be detected by PCR using an internal forward primer: AATTGGAAGAATGAGTCACG, an external forward primer: AAATCATACGTCATCGATGC and an external reverse primer: GCCACGAAATACCATTGCC. Amplification of genomic preps from wild type N2 strain with Internal forward primer and external reverse primer result in a 0.7kb*

band, while amplification of genomic prep from NL2099 result in a 0.85kb band. In addition, no product can be amplified on N2 strain with external forward primer and external reverse primer due to the size limiting condition of this PCR. No product can be amplified on NL2099 strain using internal forward primer and external reverse primer because the internal forward primer sits in the deleted sequence. We use NL2099 strain for screen because rrf-3 is an RNA-dependent RNA polymerase and the rrf-3(pk1426) allele makes this strain hypersensitive to RNAi. Also, worms with this allele become sterile at 25°C, which allow us to image and quantitate fat in adult worms without the interfering signal of the progeny.

Note 3: GMW004 is a double rrf-3(pk1426);daf-2 (e1368) mutant. DAF-2 is the worm insulin receptor and the e1368 allele of daf-2 is a hypomorphic thermosensitive mutation that leads to an obesity phenotype at 25°C. daf-2(e1368) is a single nucleotide substitution from G to A, causing a change of protein sequence from S573 to L573. This allele can be detected by PCR amplification of genomic DNA using forward primer CTCACCATTTGTCCCTTC and reverse primer CAATCGTCACCGTTTATCTC, followed by incubation with restriction enzyme TSP45I, which only cut wild type daf-2 allele on the mutation site.

3. L4440 empty vector transformed bacteria can be obtained from Addgene.
<https://www.addgene.org/1654/> (see Note 4)

Note 4: L4440 is the 2790bp empty plasmidic vector of the RNAi constructs. It is shipped from Addgene as transformed bacteria and generally used as negative control for C. elegans RNAi screens.

4. *daf-16* RNAi bacteria, can be found in Ahringer RNAi library, number 1717, plate 18, well H1. (see Note 5)

Note 5: DAF-16 is the C. elegans homolog of human FOXO, which is a transcription factor inhibited by insulin signaling. Reduced insulin signaling causes activation of DAF-16. Loss of DAF-16 is sufficient to rescue the obesity phenotype of daf-2 mutant worms. Hence, daf-16 RNAi can be used as a positive control in a daf-2 fat suppressor screen.

2.3.2 Reagents

1. Potassium phosphate buffer is made of 108.3g KH_2PO_4 , 35.6g K_2HPO_4 and water to 1L, pH 6.0. Sterilize by autoclaving.
2. NGM RNAi agar is made of 3g NaCl, 2.5g peptone, 17g agar and water to 1L. Sterilize by autoclave and cool to 55°C. After cooling to 55°C add in the following order: 1 mL of 5mg/mL cholesterol dissolved in ethanol, 1 mL of 1 M CaCl_2 , 1 mL of 1M MgSO_4 , and 25 mL of 1M potassium phosphate, pH 6.0, 1mM final concentration of IPTG and 1mL of 50mg/mL carbenicillin.
3. LB broth is made of 10g Bacto-tryptone, 5g yeast extract, 10g NaCl and water to 1 L, pH to 7.5 with NaOH, and sterilize by autoclaving. Before use, add 1mL of 50mg/mL carbenicillin/1L.
4. LB agar is made of 10g Bacto-tryptone, 5g yeast extract, 10g NaCl, 17g agar and water to 1 L, pH to 7.5 with NaOH, and sterilize by autoclaving. Cool down to around 55°C and add 1mL of 50mg/mL carbenicillin/1L.
5. S-basal without cholesterol buffer (S-buffer) is made of 5.85g NaCl, 1g K_2HPO_4 , 6g KH_2PO_4 , water to 1L. Sterilize by autoclaving.
6. Lysis buffer is made of 195 μL 10N NaOH, 600 μL sodium hypochlorite (Aldrich; St. Louis, MO) or commercially available bleach brands, and water to 3 mL.
7. S-buffer with 0.01% Triton-X is made by adding 100 μL of Triton-X 100% to 1L of S-buffer (resuspend with stirring bar for $\geq 1\text{h}$).
8. 60% isopropanol is made by mixing 30 mL of 100% isopropanol with 20 mL of water in a 50mL conical tube.

9. Oil red O stock solution (0.5%) is made by resuspending 0.25g of oil red O (MP, Cat. No. 155984) in 50 mL of 100% isopropanol by overnight shaking at room temperature. Prepare at least 2 days before use, and can be stored for ≥ 4 weeks at room temperature.

10. Diluted S-buffer (20%) is made of 20mL S-buffer and 80mL of distilled water.

2.3.3 Supplies and equipment

1. Omnitray single-well square plates can be obtained from Nunc Nalgene International.
2. 96-pin replicator can be obtained from V&P scientific.
3. 96-well Clear V-Bottom 2mL Polypropylene Deep Well Plate can be obtained from Corning Costar.
4. 96-well cell culture plates can be obtained from Corning Costar.
5. Breathe-Easy sealing membrane can be obtained from Sigma-Aldrich.
6. HT115 *E.coli* strain can be obtained from CGC.
7. AlumaSeal 96TM Sealing Film can be obtained from Genesee Scientific.
8. Sealing Mats for 96-well PCR Plates can be obtained from BioRad.
9. 96-well channel vacuum manifold can be obtained from V&P Scientific (product number VP 177AD).
10. 96-well PCR plates can be obtained from VWR (catalog #82006-636).
11. Petri dish (100mm X 15mm) can be obtained from VWR.
12. Sterile reservoir can be purchased from Fisher scientific.
13. 37°C shaking incubator with holders for 96-well plates can be obtained from Fisher Scientific.
14. Benchtop centrifuge with 96-well plate adaptors (Beckman Coulter Allegra X-15R with Beckman Coulter SX4750 adaptors) can be obtained from Beckman.
15. Vertical flow biological hood.
16. Comet assay 96-well slides can be obtained from Trevigen.

17. Upright or inverted microscope with an automated stage capable of doing high throughput tile capture and stitching of images of 96-well slides. (see Note 6)

Note 6: The Nikon Eclipse Ti microscope with 10X 0.45NA objective and DsRi2 camera is suitable for this purpose.

18. Digital Triple Heat Block can be obtained from VWR.

19. Multichannel pipettes and regular pipettes

2.4 Methods

2.4.1 Reagents preparation

2.4.1.1 Preparing agar plates (1 week before experiment)

1. Make and autoclave 1L LB agar as described in Materials section.
2. Place LB agar in 60°C water bath for 5-10min to cool down.
3. Add 1mL of 50mg/mL carbenicillin.
4. Pour LB agar to plates in the hood. 20ml of LB agar can be poured to 100mm Petri dish or omnitray single-well square plates.
5. Place the plates in hood for 30min to solidify.
6. Store the plates in a sealed box in 4°C. LB Agar plates can be stored in 4°C up to 1 month. (see Note 7)

Note 7: These LB carbenicillin agar square plates need to be prepared well ahead or thoroughly dried in the hood. Otherwise, moist would cross contaminate stamped RNAi clones.

2.4.1.2 Preparing NGM RNAi plates. (1 week before experiment)

1. Make and autoclave 1L NGM agar as described in material section.
2. Place NGM agar in 60°C water bath for 5-10min to cool down.
3. In a biological hood, add in the following order and thoroughly mixing after each ingredient: cholesterol, CaCl₂, MgSO₄, potassium phosphate, IPTG and

carbenicillin (volumes and stock concentrations listed in materials). Keep molten media in water bath up to right before pouring plates in the hood.

4. For 100mm petri dish, pour 20ml of NGM agar in the hood and go to step 9. For pouring 96-well cell culture plates, go to step 5.

5. Right after step 3, take a heat block pre-warmed to 70°C into the hood.

6. Bed clean aluminum foil in the heat block, place a sterile reservoir and a 96-well cell culture plate on top of the foil.

7. Pour NGM agar into the sterile reservoir.

8. Use multichannel pipettes to transfer 150µL NGM agar to every well of the 96-well plate. (see Note 8)

Note 8: Pipette tips need to be prewarmed by pipetting up and down molten NGM RNAi agar several times before transferring. While aspirating to the 96-well plates, stick the tips to the side and the bottom of the well, and aspirate slowly to prevent bubbles. It is very important to avoid bubbles in the wells because worms will crawl into the agar through bubbles, leading to irregular feeding, and making it difficult to harvest worms for further processing.

9. Place the plates in hood for 30min to solidify.

10. Store the plates in a sealed box in 4°C. NGM RNAi agar plates can be stored in 4°C up to 1 month.

2.4.1.3 Preparing Oil Red O working solution (first day of experiment)

1. Prepare 0.5% oil red O stock solution several days before as described in materials.
2. Filter the oil red O stock solution with a 0.45 μ m pore size filter.
3. Prepare a 60% working solution with filtered sterile water and shake for ≥ 2 h at room temperature.
4. Filter the solution with 0.45 μ m filter and shake for another 2 days at room temperature prior to usage.

2.4.2 Bacteria RNAi strains preparation

2.4.2.1 Growing bacteria colonies on square LB agar plate (3 days before experiment)

1. Clean the bench area with Cavicide™ and turn on the gas and fire on the bench (this step can also be performed in hood)
2. Prepare sterilized water, 95% ethanol, and 10% bleach in 3 separate containers (empty 200µl pipette boxes can be used as containers) next to the fire.
3. Briefly dip the 96-pin replicator into 10% bleach, rinse thoroughly with water and wet in 95% ethanol. Flame every side of the replicator to make sure it is sterile
4. Place the replicator back into 95% ethanol
5. Transport RNAi library to the bench with dry ice from -80°C
6. Remove the seal of the RNAi library plates next to the flame
7. Flame the replicator on flame quickly to evaporate the excess ethanol and wait for 5-15s for it to cool down. (see Note 9)

Note 9: It is important to make sure the replicator is not too hot or it would kill the bacteria. There are two extra tips on the replicator that allow the user to get a sense of the pins temperature, simply touch the two extra tips with your hand while making sure not to touch any other tip of the replicator.

8. Dip the tips of the replicator into the library plate and make sure they touch the bacteria in every single well

9. Quickly transfer and stamp the tips of replicator on the LB square plate, make smooth rounded movements to increase bacterial growth area without overlapping RNAi clones. (see Note 10)

Note 10: While stamping the replicator, it is important to be gentle and not poking into the agar. Also, every tip of the replicator has to touch the LB agar to secure the successful transferring of all RNAi clones.

10. Briefly dip the replicator into 10% bleach and repeat step 3 and 4 for each successive plate.

11. Re-seal the library plates with AlumaSeal 96™ Sealing Film and store back at -80°C (Do not ever let the library thaw!)

12. Incubate the RNAi clones seeded in the LB square plate at 37°C overnight.

13. For control RNAi clones, use sterile toothpicks or wire loop to streak bacteria on the 10cm LB agar carbenicillin 50µg/mL plates from the glycerol stock and incubate at 37°C overnight.

14. After incubation, record the RNAi clones that have no colonies.

15. The LB agar plates can be parafilm and stored at 4°C for up to 2 weeks.

2.4.2.2 Growing bacteria in 96 well deep well plate. (2 days before experiment)

1. In the biological hood, fill the 96-deep well plate with 1200µL/well of LB broth 50µg/mL carbenicillin using multichannel pipette.

2. Sterilize the bench with Cavicide™ and turn on the gas and fire on the bench.
(This step can also be performed in hood)
3. Prepare sterilized water, 95% ethanol, and 10% bleach in 3 separate containers (empty 200µl pipette boxes can be used as containers) next to the fire.
4. Dip the 96-pin replicator into 10% bleach, thoroughly rinse with water, then briefly dip in 95% ethanol and flame every side of the replicator to make sure it is sterile
5. Dip back replicator in 95% ethanol, and quickly flame again to evaporate excess ethanol. Wait for 5-15s for replicator to cool down.
6. Touch with the replicator pins the mini RNAi bacterial lawns
7. Dip the tips of the replicator into the 1.2mL LB broth Carbenicillin of two 96-deep well plates. (see Note 11)

Note 11: One 96-deep well plate worth of bacterial culture would be insufficient food to sustain the growth of ~50 worms into gravid adulthood. Two or three 96-deep well plates are preferred per RNAi library plate. In our experimental set up, 2 strains of worms (GMW004 and NL2099) are tested, so 4-6 96-deep well plates are prepared for each RNAi library plate.

8. Re-sterilize replicator by briefly dipping it into 10% bleach and repeat step 4 and 5 sequentially for the next plates.

9. Use sterile toothpicks or wire loop to pick and transfer colonies from positive and negative control 10cm LB agar carbenicillin 50µg/mL plates to all empty wells of 96 deep well plate and record these wells. (see Note 12)

Note 12: There are some RNAi clones that would not grow on the LB agar omnitray (not represented in the original library or experimental error). Take advantage of these empty wells and seed positive and negative control RNAi clones in these wells.

10. Seal the 96 deep well plates with Breathe-Easy sealing membrane and shake at 1000rpm at 37°C overnight.

2.4.2.3 Seeding RNAi bacteria in 96-well NGM RNAi plates (1 day before experiment)

1. Take out 96-deep well plates from the shaker and centrifuge for 10min at 4500rpm
2. Thoroughly clean with Cavicide™ the sink area. Next to the sink, remove the seal, and discard the supernatant into a bucket containing bleach by quick inversion of the plate. Place plates upside down on a stack of clean paper towels and move to the hood.
3. Using a 12-channel pipette, add 100µL of diluted S-buffer (20%) to each well of just one of the plates with RNAi bacterial pellets, and resuspend the bacterial pellets by vigorously pipetting.

4. Transfer bacterial suspension from plate replicate 1 to plate replicate 2 (we had grown two 96-deep well plates of culture for each RNAi clone set). Use the transferred suspension to resuspend pellets of replicate plate 2. Do not add S buffer to the second plate. (see Note 13)

Note 13: As referred in Note 11, two or three 96 deep well plates of samples are grown for each RNAi library plate to be tested. These replicates need to be combined to support the growth of ~ 50 worms into gravid adulthood. If there are two deep well plates per original plate, add 100 μ L of diluted S-buffer (20%) to the first deep well plate and resuspend the bacteria by pipetting. Then transfer the sample to the second plate and resuspend the bacteria of the second plate.

5. Add 20 μ L of distilled water to the wells located in the four edges of the plate. Then, transfer 100 μ L of the bacterial suspension into the wells of the 96-well NGM RNAi agar plate using multichannel pipette and (see Note 14)

Note 14: While transferring bacteria to the 96-well NGM RNAi agar plate, it is important to be careful not poke into the agar media. After carefully transferring 100 μ L of bacteria, it is necessary to add 20 μ L extra of water to the edge wells because these wells dry much faster than the wells at the center of the plate. If these wells become too dry, the agar may crack, worms will crawl into the cracks, and that well will not be scorable.

6. Dry the bacterial suspensions in the hood for around 5 hours, until no liquid remains (Do not over dry the plates, cover faster drying wells with breath-easy if necessary).
7. Place the lids on the NGM plates and incubate the plates overnight in 20°C incubator for induction of expression of double stranded RNAs.

2.4.3 Worm preparation

2.4.3.1 Egg preparation and synchronization (1 day before experiment)

1. Sterilize the bench with Cavicide™ and carry out the next steps next to flame.
2. Add 10-15mL of S-buffer to a worm plate with $\geq 2,000$ gravid adult worms.
3. Using S-buffer transfer worm/egg suspension to a 15mL conical tube.
4. Centrifuge at $\leq 2000g$ 30s.
5. Discard the supernatant above 3mL using sterilized glass Pasteur pipettes connected to the vacuum line.
6. Add 3mL Lysis buffer.
7. Shake vigorously for 1min and then add 9mL of S-buffer.
8. Centrifuge at 2000g for 30s.
9. Discard the supernatant above 3mL using sterilized glass Pasteur pipettes connected to the vacuum line.
10. Add 3mL Lysis buffer.
11. Shake vigorously for 1min and add 9mL S-buffer.
12. Centrifuge at 2000g for 30s.
13. Using sterilized glass Pasteur pipettes connected to the vacuum line, discard as much supernatant as you feel comfortable with, without disturbing the pellet. The volume remaining should be $\leq 500\mu\text{l}$, otherwise add 2 additional washing steps are necessary.
14. Add 14mL S-buffer.
15. Centrifuge at 2000g for 30s.

16. Wash by repeating steps 13 to 15 three times.
17. Discard as much supernatant as you feel comfortable with, without disturbing the pellet using sterilized glass Pasteur pipettes connected to the vacuum line, and fill up to the 10mL mark with S-buffer.
18. Rotate embryos in 20°C incubator for ≥ 16 hours.
19. The next day, estimate worm density as described in Note 15
20. Dilute with S-buffer or concentrate by centrifugation the worm suspension to bring the density to 10 worms/ μ L

2.4.3.2 Seeding worms (first day of experiment)

1. Take out the NGM plates with RNAi bacteria from 20°C incubator and move them to the hood.
2. In the hood, pour the worm suspension onto 50mL sterile reservoir.
3. Use a multichannel pipette to seed 5 μ L of worms from the reservoir to each well (constantly move the reservoir to maintain the worms resuspended).
4. Dry the plates in the hood for around 15min.

2.4.4 RNAi incubation (first day of experiment)

1. Move the plates to 15°C incubator and incubate for 60 hours. (see Note 16)

Note 16: The 15°C incubation can take longer or shorter than 60 hours. The development of worms needs to be checked every 2 hours starting from 50 hours till 70 hours to ensure the worms at the late L3 or early L4 stage for transferring to 25°C incubator. It is critical to not transfer daf-2 mutant worms earlier than L3 because they will enter the dauer program and arrest, and no later than L4 stage to observe full penetrance of the rrf-3 sterility phenotype.

2. Transfer the plates to 25°C incubator for 24 hours.
3. Double check the worms growing in the wells to make sure they are at gravid stage.

2.4.5 ORO staining

1. Filter the Oil Red O working solution with a 0.45 μ m filter.
2. Pour S-buffer in a reservoir. (See Note 17)

Note 17: 0.01% of Triton in the S-buffer helps prevent the worms from sticking onto the pipette tips, and reduce worm loss.

3. Using 12-channel pipette, add 100 μ L S-buffer into each well.
4. Using 12-channel pipette, transfer the whole worm suspension to a 96-well PCR plate.
5. Connect the 96-channel vacuum manifold to the vacuum pipe and calibrate the height for aspiration using a mock PCR plate with water. Calibrate to leave ~25 μ L of water behind (See Note 18)

Note 18: The amount of liquid remaining in the 96-well PCR plates is determined by the height of the 96-channel manifold. This can be adjusted and calibrated by filling water in a 96 well PCR plates and test the water level after aspiration. It is important to keep around 25 μ L of solution to minimize the chances of accidental loss of worms by aspiration.

6. Once aspirator is calibrated, aspirate the S-buffer from the 96-well PCR plates containing worms using the 96-channel vacuum manifold. (Keep around 25 μ L of S-buffer with worms)
7. Wash twice by adding and aspirating 100 μ L of S-buffer using multichannel pipettes and 96-channel vacuum manifold.
8. Using 12-channel pipette, add 60% isopropanol to each well (intentionally disrupt the worm pellet while adding the isopropanol).
9. Let worms sink for around 2min.
10. Aspirate the 60% isopropanol using 96-channel vacuum manifold.
11. Using 12-channel pipette, add 100 μ L of Oil Red O (ORO) working solution to each well. Intentionally disrupt the worm pellet while adding the ORO solution or resuspend by pipetting but do not vortex, invert, or flick the plates. Avoid ORO bulk volume or drops reaching the walls of the tubes to prevent precipitation of the dye mark.
12. Seal the 96-well PCR plates using sealing mats, and put these staining plates into a sealed box with wet paper towel. (See note 19)

Note 19: Keeping the plate completely sealed and incubating in a humid box is necessary because the ORO solution is a saturated solution, and loss of water would cause precipitation of black crystals and that prevent quantification of ORO levels.

13. Incubate the box at 25°C for 12-16 hours. (See note 20)

Note 20: It is important to restrict ORO staining to ≤ 16 hours at 25°C because longer incubation may change the tone of the ORO staining and affect the quality of the images.

14. Remove the seal and aspirate the ORO working solution using 96-channel vacuum manifold.

15. Wash the wells with 100 μ L of S-buffer twice.

16. Add 100 μ L of S-buffer 0.01% Triton.

17. Use 12-channel pipette to mount 8 μ L of worms on the Comet assay 96 well slides and carefully place the coverslips for imaging. (see Note 21)

Note 21: It requires some practice to be able to pipette up most of worms in such a small amount of liquid. To achieve this, it is important to place the tip to the very bottom of the well and aspirate as fast as possible (use “bad” pipetting procedure). Check the slide and make sure you have worms in every well. If the worms in some wells are not transferred, use a single channel pipettes to transfer again.

2.4.6 Image acquisition and data storage

To capture images from the 96-well slide, we recommend using an automated microscope or high-content screening platform. In our case, we use a Nikon Eclipse Ti microscope with an automated stage. The optics include a 10X 0.45NA objective and a DsRi2 camera. Initial storage into local SSD drives ($\geq 10\text{Tb}$) render fastest capturing rates.

2.4.7 High-Content Screening (HCS) Image Processing considerations

When performing a high-throughput image-based genetic screening, capturing, storing, and processing approximately thirty 25MB images per channel per well becomes a bottleneck due to the limited storage and processing power of regular lab computers or even workstations. For example, for the screening setup described here, each stitched RGB image of a whole well is 9001X8928 pixels, with each whole-well tiff image sized at around 250MB, and one 96-well plate representing approximately 25GB of data. Analyzing these data is an even bigger challenge than storage. Our single-worm identification algorithms, although highly accurate, are computationally demanding. Therefore, it can take from a day to a week to run a 0.25-1Tb dataset on a conventional desktop. A previous paper from our lab used compressed images to achieve analysis (5Mb *.bmp file / well). However, this is not suboptimal due to the reduction in image resolution and consequent loss of information (Wählby et al., 2014). Here we introduce the reader and potential screener to some critical aspects to be considered when embarking in a large-scale HCS.

Note 22: The images are most likely to be stored on the local computer connected to microscope. To analyze them on HPC cluster you will need to transfer them to a fast-transfer storage unit locally, remotely, or in the cloud. Your local administrator should advise you on the best available option.

2.4.7.1 Data acquisition (local versus remote)

As introduced in section 2.4.6, data acquisition begins with automated imaging of the experimental plates. These data will be written directly to a mounted PC, often the one used to set up and begin microscopic data collection. A few considerations help ensure fast data collection and transfer, including local writing space, naming conventions, and an automated transfer framework. For local storage, it is recommended to have at least 10Tb of Solid State Drive (SSD). SSD is much faster than its alternative, Hard Drive Disk (HDD), and should be used to prevent a bottleneck. Data acquisition is also the optimal step to enforce naming conventions. Since there are no built-in frameworks for naming, it is up to the screening lab to provide and enforce easy to read naming conventions that will ensure smooth data processing (see Note 23). Finally, to prevent any impedence to data collection, it is recommended to have a second mounted PC that can separately upload data to the desired server. This allows for a slower upload speed, which is often unavoidable, while still maintaining scope operation. A detailed list of our setup and examples of file naming can be found at: <http://orourkeyleenlab.wix.com/obesity-aging-lab/outreach>.

Note 23: When naming folders and images avoid whitespace. This will be useful when using a command line. If you are unable to change the names to avoid white spaces, you will need to use quotation marks at the beginning and at the end of the path to the file while using the command line.

2.4.7.2 Data processing

It is recommended that all data processing is completed on a high-processing computer (HPC) cluster. In the HPC context, image processing and analysis can be done in parallel. While some of the processing steps can be executed on a personal computer, utilization of an HPC cluster will dramatically increase computational speeds and allow for use of full resolution raw screening images. Interactive processing steps (i.e. refining worms identification) will require extra considerations, and a rudimentary knowledge of command line may be necessary to operate some of the programs described herein within the context of an HPC cluster.

First, several systems and software tools must be installed, created, or optimized. These include Cellprofiler (CP), Cellprofiler Analyst (CPA), a MySQL database (or an alternative, but CP/CPA compatible, database of your choice), and appropriate Cellprofiler pipelines. It is important to confer with a local information technologist to ensure proper installation and setup of these programs and communication with HPC cluster.

The setup and optimization of Cellprofiler pipelines for new screens may be done outside of the HPC cluster environment, which facilitates the use of CP interactive optimization tools, as long as special attention is paid to any and all naming and PATH conventions required for CP and CPA to generate and retrieve data. Cellprofiler's export and import tools work within a HPC cluster environment as

long as the final modifications to the pipeline – including image folder location and PATH names – are correctly assigned in the HPC environment. At this stage pay special attention to the MySQL database used to ensure that files are sent to the correct locations. Depending on the preferred CP analysis output, CSV data sheets can be generated instead of databases with Cellprofiler, which can then be used to manually analyze data. This approach is less robust and may result in errors due to Cellprofiler Analyst's particular file location requirements.

A comprehensive analysis of the images is possible after the initial steps are completed, and can be easily completed using the scripts provided at: <http://orourkeeyleenlab.wix.com/obesity-aging-lab/outreach>.

This process will require work on the HPC cluster through programs such as FastX or similar. FastX provides a Graphical User Interface (GUI) enabled program for HPC cluster operation, and is an easy solution for users unfamiliar with Linux or remote systems. If your institution does not have access to this program, or prefers a different one, alternatives should work just as well. Note that most alternatives may require basic command line knowledge.

2.4.7.3 Post-processing

After initial data have been collected, post-processing can be done. This may include image review, and further image analysis if necessary. It is recommended the user conducts analysis within the HPC cluster to ensure all image data can be

retrieved without permission issues. Due to the pre-established database, it should be easy to locate and retrieve any files for further use. Another consideration is kinds of storage. In particular, the differences between private user storage and shared storage. It is recommended that both be set up in all cases, the shared storage for the organization and maintenance of all raw image data sets (terabytes of information), and the private user storage for processing images, outputting data, and linking of relevant experimental metadata or information for databases. In this way private data folders would optimize for processing, and commonly used and large image files are not copied to all users, but instead located in a central location. Nevertheless, conventions of file, subfolders and folders naming should be established and strictly followed.

For users that want to compile an easy-to-use image viewer, programs such as Omero exist. Omero is an open-source program that allows for broad image organization and utilization. It may be possible to set the HPC cluster to send data outputs directly to Omero. Alternatively, integration of the MySQL database into Omero may provide the most success. These types of programs are not strictly necessary for post-processing, but may allow for additional organization and integration of screen results with data banks (i.e. wormbase, ensemble, etc). Optimal data processing and organization solutions would vary with type and scale of the screens, as well as with lab resources.

Figure 2. 1

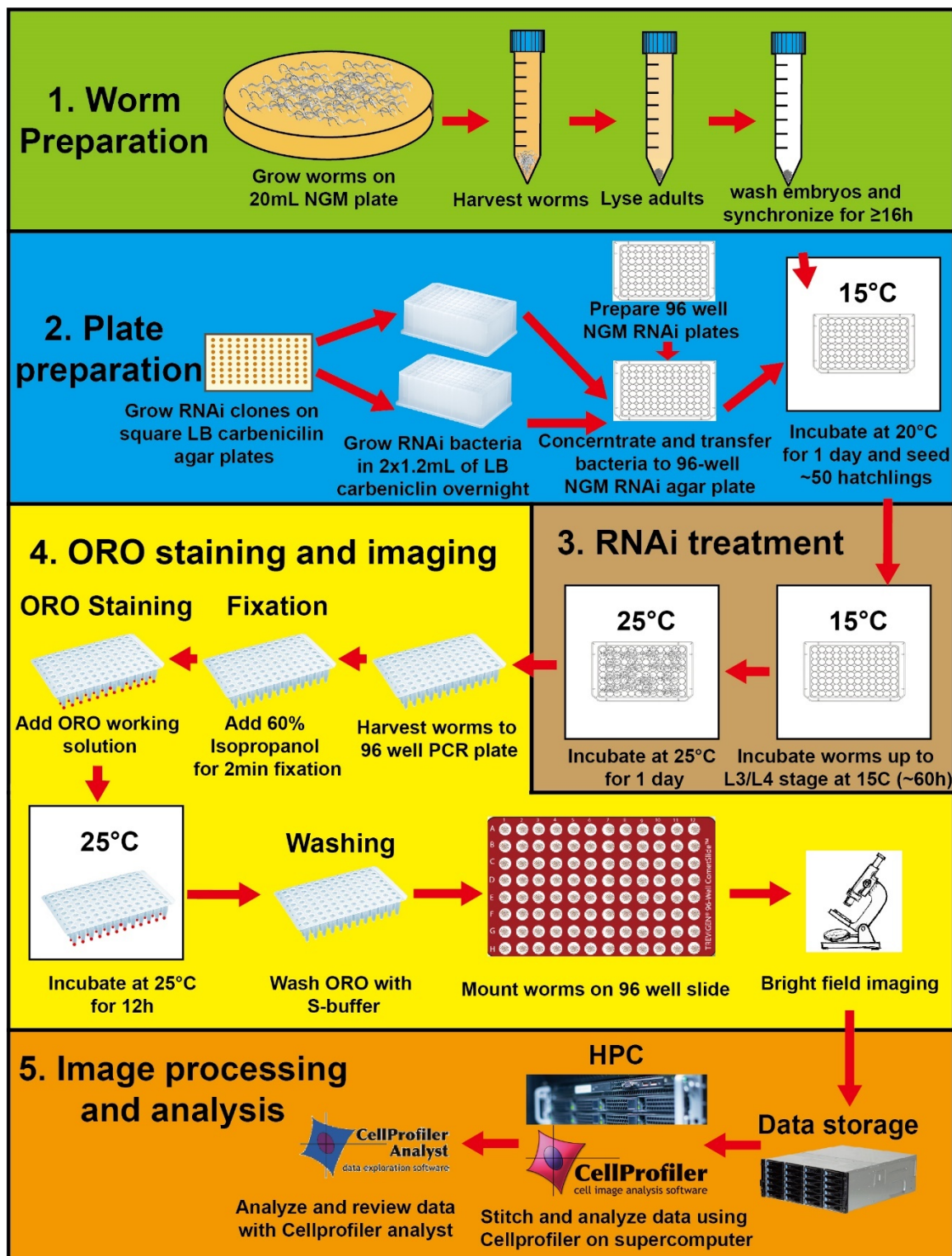


Fig. 2.1 RNAi screening workflow.

Worm preparation is shown in green (section 2.4.3); Bacterial RNAi preparation is shown in blue (section 2.4.2); Worm RNAi treatment is shown in brown (section 2.4.4); ORO staining and imaging procedures are shown in yellow (section 2.4.5 and 2.4.6), and image analysis and data transfer and processing are shown in orange (section 2.4.7).

Fig. 2.2 Post-HCS image processing workflow. Imaging data may be saved in a shared storage positioned between local computers and a local or cloud based HPC cluster. Both, home-made encoded image stitching (available at <http://orourkeyleenlab.wix.com/obesity-aging-lab/outreach>) and CellProfiler data analysis can be run on an HPC cluster. In this diagram, black arrows indicate saving and loading data to and from shared storage; green arrows indicate data processing steps within a local computer; brown arrows indicate control of programs on the HPC cluster; blue arrows indicate automated (and often parallelized) programs running in the HPC cluster; purple arrows indicate direct communication from the HPC cluster to a local computer in the pipeline 2 and 3 to optimize worm models manually; and the red arrow indicates that the output of Cellprofiler will input into Cellprofiler Analyst on the local computer for final data analysis and hit detection.

**CHAPTER III: Modeling diet-induced obesity and validating
GWAS obesity candidate genes in *C. elegans***

This work was submitted to *Genome Medicine* in 2021 using the title:

Human obesity loci established as causal obesity genes in *C. elegans*

Manuscript Author list: Wenfan Ke, Jordan Nicole Reed, Chenyu Yang, Noel Higgason, Leila Rayyan, Mete Civelek, and Eyleen Jorgelina O'Rourke

Statement of contribution and acknowledgment

The study presented in this chapter was initiated through a collaboration with Dr. Mete Civelek at UVA BME department when the Civelek group published an eQTL analysis of adipocyte to identify genes associated with cardio-metabolic traits (Civelek et al., 2017). Under the guidance of Dr. Eyleen O'Rourke and Dr. Mete Civelek, I worked with Jordan Reed (Civelek lab graduate student) to identify genes associated with human obesity and to test whether their *C. elegans* orthologs caused or prevented obesity. At the same time, I worked with undergraduate students Chenyu Yang, Noel Higgason and Leila Rayyan to establish the first *C. elegans* fructose induced obesity model and using this model to validate the function of human GWAS obesity candidate genes in animals fed a high fructose diet. Specifically, I worked with Leila and Noel to characterize the physiological and cellular response to a high fructose diet in the worms through healthspan assays, lifespan assays, lipid droplets characterization and transcription analyses. I also worked with Chenyu Yang on RNAi screening and the follow-up analysis to validate causality and characterize the candidate GWAS obesity genes.

In addition, I would like to thank Dr. Monica Driscoll and Dr. Xun Huang for generously sharing the lipid droplets reporter strains. I also specially thank Nella Solodukhina for helping manage the lab, prepare reagents and conduct some of the experiments. I also want to acknowledge the class 2020 of BIOL4005 for their help cross-validating automated scoring. I am grateful to the Keck Center for

Cellular Imaging (PI: AP; NIH-RR025616). I also want to acknowledge the *C. elegans* strains provided by the CGC, which is funded by NIH Office of Research Infrastructure Programs (P40 OD010440). Further, I would like to acknowledge UVA DoubleHoo for supporting me and the undergraduate student Leila Rayyan, and the Cardiovascular Training Grant T32HL007284 for support of Jordan Reed. This work would not have been possible without the support from NIH-DK118287 to MC, and from PEW Biomedical Scholars Award and NIH-DK087928 to Dr. Eyleen O'Rourke.

3.1 Abstract

Obesity and its comorbidities are debilitating or life-threatening for patients, and a major burden for the health system. To uncover pharmacological targets to prevent or treat obesity, several human genome-wide association studies (GWAS) have been completed, and each has identified dozens of genetic variants associated with obesity. The next challenge has remained to experimentally test which of these numerous variants are causally linked to obesity. Here we present and exploit a *C. elegans* model of diet-induced obesity (DIO) and high-throughput *in vivo* RNAi screening to test for causality 293 worm orthologs of obesity-candidate loci reported in human GWAS. We identified 14 genes that prevent obesity and 3 genes that promote DIO when silenced in *C. elegans*. We show that knock-down of the obesogenic genes not only reduces fat accumulation in primary and ectopic fat depots, but also improves the health and extends the lifespan of *C. elegans* with DIO. Further, the direction of the association between some of the human variants and obesity matches the phenotypic outcome of the loss-of-function of the *C. elegans* ortholog genes, supporting the notion that some of these genes are causally linked to obesity across phylogeny. This study not only presents novel fat regulators, it also serves as a proof of principle of the value of model systems compatible with *in vivo* high-throughput genetic screening to causally link GWAS gene candidates to human diseases that can be modeled in these systems.

3.2 Introduction

Obesity is a major risk factor for serious comorbidities including cardiovascular disease (CVD), type 2 diabetes, hypertension, stroke, neurodegenerative disease, certain cancers, and sleep apnea/sleep-disordered breathing (Ndumele et al., 2016; Poirier et al., 2006). In the past decade, obesity-derived comorbidities caused more than 4 million deaths per year and cost an average of 4 years of life lost worldwide (Flegal et al., 2016; Ng et al., 2014; Ogden et al., 2016). The increased prevalence of obesity and extreme obesity could lead to a global average reduction in life expectancy in the next decade (Lim et al., 2012; Olshansky et al., 2005). Therefore, developing effective interventions to reduce the health and economic burden of obesity is critical. Lifestyle changes including diet and exercise are the preferred strategies to reduce weight. However, several factors make the pharmacological intervention more realistic, and in some critical cases the only treatment option (Melnikova and Wages, 2006). Current pharmacological intervention is limited to a handful of weight-reducing drugs, most of which are associated with severe side effects (Kang and Park, 2012). Thus, more effective drugs with lesser side effects are urgently needed (Field et al., 2009; Rodgers et al., 2012). An important step towards developing better anti-obesity drugs is to identify druggable targets (genes). Genome-wide association studies (GWAS) are one of the most successful approaches for identifying these gene targets because they search for genetic variants associated with obesity in human populations living in their daily environments (as opposed to animal models reared in controlled environments). The genetic variants identified through GWAS can

then be mapped to genes that increase or decrease the likelihood of obesity occurrence (Hindorff et al., 2009). Currently, there are over 90 GWAS associations with obesity, metabolically healthy obesity, body mass index (BMI), waist to hip ratio (WHR), WHR adjusted for BMI, body fat distribution, and body fat percentage, with 2,537 SNPs associated with these traits (Buniello et al., 2019). Almost 90% of these variants are found in non-coding regions of the genome (Maurano et al., 2012); hence, very few variants have been mapped to effector transcripts, and only a handful have been causally linked to the disease (Gesta et al., 2011; Hainer et al., 2020; Lee et al., 2013; Loh et al., 2015, 2020; Ollmann et al., 1997; Ramos-Molina et al., 2016; Small et al., 2018; Spanswick et al., 1997; Tartaglia et al., 1995; Wang et al., 2020). A major barrier is the lack of experimental systems that enable this testing *in vivo* and at a reasonable throughput and cost (Korte and Farlow, 2013).

Genetic screening in *Caenorhabditis elegans* has proven effective at identifying drug targets for human diseases ranging from depression (e.g. Prozac) (Choy and Thomas, 1999) to metabolic disease (e.g. metformin) (Wu et al., 2016). As the first and only model organism enabling whole-genome systemic RNA interference (RNAi) *in vivo* through feeding, *C. elegans* is an ideal *in vivo* system for high throughput identification of gene function (Ke et al., 2018; O'Rourke et al., 2009a). Although *C. elegans* is evolutionarily distant from humans, core lipid, sugar, and protein metabolism pathways are highly conserved between the two species (Wang et al., 2008). Regulators such as TOR kinase and AMPK, and transcription

factors such as sterol response element binding protein (SREBP) and TFEB, similarly control metabolic genes and cellular responses to nutrients in both organisms. Loss of function of such regulators causes similar metabolic defects (e.g. obesity), in worms and mammalian systems (Long et al., 2002; McKay et al., 2003; Sze et al., 2000). Moreover, an obesity candidate gene identified in human GWAS whose ortholog is demonstrated to contribute to obesity in *C. elegans* is more likely to be a robust anti-obesity target across human populations.

In this study, we present a *C. elegans* model of diet-induced obesity (DIO), and exploit a high-throughput *in vivo* obesity screen system to test for causality genes significantly associated with obesity in human GWAS. First, we identified 340 candidate genes from published GWAS (Akiyama et al., 2017; Chu et al., 2017; Civelek et al., 2017) and built a *C. elegans* RNAi library containing 293 worm orthologs of the human-obesity candidate genes. We used our previously developed screening pipeline (Ke et al., 2018; Wählby et al., 2014) to perform an RNAi screen for genes whose inactivation alters the fat content of *C. elegans* fed a regular diet (RD). In this screen we found 14 obesity genes (inactivation leads to obesity) and 2 lean genes (inactivation leads to leanness). We also established a *C. elegans* DIO model by feeding worms a high-fructose diet (HFrD). We show that worms fed a HFrD not only have higher fat content and body size, but also exhibit shortened lifespan, locomotion defects, and impaired proteostasis. Using this DIO model, we identified 3 human-obesity candidate loci whose *C. elegans* orthologs promote HFrD-induced obesity. Furthermore, we show that inactivation of the

genes contributing to obesity also ameliorates the detrimental effects of a HFrD on *C. elegans* lifespan and healthspan. Altogether, this study provides a path to validate human GWAS obesity candidates *in vivo* in a high throughput manner for future development of pharmacological interventions to reduce the burden of obesity.

3.3 Materials and Methods

C. elegans strains

C. elegans strains N2 (Bristol, UK), NL2099 (*rrf-3(pk1426)II*), GRU101 (*gnals1 [myo-2p::yfp]*) and GRU102 (*gnals2 [myo-2p::YFP+unc-119p::Abeta1-42]*) were obtained from the Caenorhabditis Genetics Center (CGC). The tissue-specific lipid droplet reporter strains XD3971 (*xdIs143[P_{daf-22} PLIN1::GFP rol-6(su1006)]*), XD2458 (*xdIs56[P_{Y37A1B.5} PLIN1::GFP rol-6(su1006)]*), and XD1875 (*xdIs26[P_{unc-54} PLIN1::GFP rol-6(su1006)]*) were kindly gifts from Dr. Monica Driscoll and Dr. Xun Huang. Unless otherwise noted, experiments were initiated with synchronized L1 larvae obtained by egg bleaching and overnight synchronization in S-buffer.

C. elegans mediums and plates preparation

NGM (nematode growth medium) agar plates were prepared by combining 3g NaCl, 2.5g peptone, 17g agar, and water to 1L. The mixture was sterilized by autoclave and cooled to 55°C. After cooling the following reagents were added in order: 1mL of 1M CaCl₂, 1mL of 1M MgSO₄, 25mL of 1M potassium phosphate (pH=6.0). 20mL and 10mL of the mixture was added to each of the 10cm and 6cm plates. The plates were allowed to dry overnight at room temperature and stored at 4°C. RNAi NGM plates were prepared according to the same protocol, except that 3mL of IPTG (1 mM final concentration), and 1mL of 50mg/mL carbenicillin were added to the mixture directly following the addition of potassium phosphate. For 96 well RNAi plates, 200µL of the RNAi NGM was added to each well. For

HFrD plates, 10X (100mg/mL) fructose solution was supplemented to the plates to make 10mg/mL as the final concentration.

E. coli culturing

For every biological replicate fresh *E. coli* streaks or library stamps on LB-carbenicillin 50µg/mL (RNAi clones) were used. Bacterial cultures were started from single colonies or using a sterilized inoculating hedgehog, and grown overnight for 14-16h. RNAi clones were grown overnight in LB carbenicillin 50µg/mL in the absence of IPTG (or any other additives). For aeration, flasks were shaken at 250 rpm, and 1.2mL deep 96-well plates at 1,000 rpm. For targeted experiments, bacteria were harvested by centrifugation at room temperature and resuspended to OD_{600nm} = 20 in S-buffer (~20X concentrated). For screening, 1.2mL bacterial cultures were resuspended with 20µl of S-buffer. Concentrated *E. coli* were seeded onto NGM or NGM-RNAi plates immediately and never exposed to the cold.

RNAi screen

The RNAi screen for fat regulators was modified from the methods in the previous publication (Ke et al., 2018). RNAi clones from sub-libraries were transferred onto LB agar plate (Nunc Nalgene International) and grown overnight. The colonies were then inoculated into deep 96-well plates containing 1.2mL of TB Carbenicillin per well, and grown at 37°C and 1,000 rpm overnight. Cultures were pelletized, supernatants discarded and pellets resuspended in 50µl of S-buffer. 45µl of

bacterial suspension were seeded into wells containing 200 μ L of RNAi NGM plus or minus 10mg/mL fructose in 96 well plates. Once bacteria dried, 75 synchronized NL2099 hatchlings were seeded to each well and incubated at 15°C for 60h, followed by 24h incubation at 25°C. Worms were then harvested using S-buffer into 96 well PCR plates and fixed by 60% isopropanol for 10min. 200 μ L Fresh-made Oil Red O (ORO) working solution (60% ORO stock solution) from ORO stock solution (0.5% ORO in 100% isopropanol) was added after fixation and incubated at 25°C for 12h. After washing off ORO using S-buffer, worms were mounted to Comet assay 96-well slides (Trevigen) and imaged using Nikon Eclipse Ti automatic screening microscope, with 10X objectives(Plan Apo, 10X/0.45). The tile images were then stitched using the UVA high-performance computing clusters RIVANNA and deposited to the UVA Research Value Storage. The parameters of the images were measured by Cellprofiler pipelines modified from the methods in previous publications (Wählby et al., 2012, 2014) (cellprofiler.org/wormtoolbox), and the fat phenotypes were sorted by Cellprofiler Analyst, using machine learning based on principle component analysis as previously described (Wählby et al., 2014). For each image from the RD screen, if more than 50% of the worms are more obese than EV controls under RNAi treatment, we characterize the corresponding gene as obese gene; and if more than 50% of the worms are leaner than EV controls under the RNAi treatment, we characterize the corresponding gene as the lean gene. For each image from the HFrD screen, if more than 50% of the worms are leaner than EV controls under the RNAi treatment, we characterize the corresponding gene as DIO lean gene. The screen was repeated

3 times and the RNAi treatments that consistently show the same fat phenotype were characterized as high confident hits (HC). The HC obese genes, HC lean genes and HC DIO lean genes were designated for the follow-up validation on 6cm plates. For the validation, RNAi colonies were inoculated into 500mL LB at 37°C and 200 rpm overnight. Bacteria were then harvested by centrifugation at room temperature and resuspended to OD600nm = 20 in S-buffer (~20X concentrated) and seeded to the 6cm RNAi plates with or without fructose. Once bacteria dried, 300 synchronized NL2099 hatchlings were seeded to the plates and incubated at 15°C for 60h, followed by 24h incubation at 25°C. Worms were then harvested using S-buffer into 1.5mL tubes and fixed by 60% isopropanol for 10min. 1mL Fresh made Oil Red O (ORO) working solution (60% ORO stock solution) from ORO stock solution (0.5% ORO in 100% isopropanol) was added after fixation and incubated at 25°C for 12h and followed by the same imaging and processing methods as the screen. The validation experiments were also repeated 3 times and the ORO intensity was measured by ImageJ.

Aging assay

Clean and well-fed gravid adults were lysed and the progenies were synchronized in S-buffer for 20h. L1 larvae were seeded onto 6-centimeter RNAi NGM plates with 200 mL of 20X L4440 E. coli lawn, and incubate at 15°C for 60h to allow worms to develop to L3-stage. At L3-stage, 30 worms of each strain were transferred using a platinum wire to one regular diet NGM RNAi plate and one high-fructose diet NGM RNAi plate, with the target RNAi E. coli lawns seeded. The

plates were incubated at 25°C for the rest of the experiment. Immediately after incubation at 25°C after 24h (when worms reach adulthood), worms were scored daily. The number of dead and “censored” worms were recorded, and dead worms were removed from the plate by suction. Worms were determined dead if they did not respond to gentle touch by a sterilized platinum wire. Alternatively, to avoid unnecessary mechanical stress on the worms, live status was determined by placing a hot platinum wire near the head and observing avoidance. Worms were designated as “censored” if they were missing, had climbed off the NGM RNAi plate medium, had burrowed, or displayed vulval rupture or internal hatching. In accordance with the Kaplan-Meier estimate, “censored” worms were included in subsequent statistical analysis and were assumed to have the same survival probabilities as the worms that were followed for the duration of the experiment. Plates were scored until no live worms remained. The data were analyzed by GraphPad Prism, using the Mantel-Haenszel method to calculate hazard ratio and 95% CI, and the Gehan-Breslow-Wilcoxon method to calculate the p-value. The experiments were repeated 3 times for each treatment tested.

Healthspan assays

Healthspan assays were modified from the methods in previous publications (Hahm et al., 2015; Nussbaum-Krammer et al., 2015). Day3 adults were harvested from plates into 1.5mL tubes and washed 2X with S-buffer. For body bending assay, ~30 3d old worms were added to one well of a 12 wells plate (CytoOne) with 2mL of S-buffer. The plates were kept at RT for 5min before imaging. A time-

lapse (20s, with 0.05s interval) movie was taken using Zeiss Axio Zoom.v16 dissecting microscope, PlanNeoFluar Z 2.3X/0.57 FWD objective, zoom 7X. The movie was analyzed to count body bends using the ImageJ plug-in wrMTrck(www.phage.dk/plugins/wrmtrck.html). For velocity measurements, ~20 3d old worms were added to a 6cm NGM plate without E. coli lawn, and kept at RT for 5min before imaging. A time-lapse movie (2min, with 0.2s interval) was also taken using Zeiss Axio Zoom.v16 dissecting microscope, PlanNeoFluar Z 2.3X/0.57 FWD objective, zoom 7X. The movie was analyzed to measure the worm moving velocity by the ImageJ Manual Tracking plugin. For the racing assay, 50 3d old worms were transferred to a NGM plate with 50 μ L 20X lawn seeded at the opposite side of the plate. After 1h, the images of the lawn were taken by Zeiss Axio Zoom.v16 dissecting microscope, PlanNeoFluar Z 2.3X/0.57 FWD objective, zoom 7X and the number of the worms on the lawn were counted.

LD live Imaging and analysis

D1 adult LD reporter strain worms were harvested from plates and washed 2X using S-buffer. Worms were then paralyzed by 46mg/mL levamisole solution and mounted onto an agar pad as previously described (Podbilewicz and Gruenbaum, 2006). Once mounted, the images of the worms were captured by Nikon Eclipse Ti spinning disc confocal microscope, 60X/0.85NA objective, 500ms exposure time and 80% laser intensity. The images were then analyzed by ImageJ to measure the intensity and the size of the LDs.

Statistics

All statistical analyses were performed in Graphpad Prism. Outliers were detected and removed from analyses using the ROUT method. For absolute intensity measurements, LD diameter, body size, velocity, unpaired nonparametric t-test was used to make single comparisons between a specific treatment and the mock control. Ratio t-test was used to compare all ratios. The statistics of aging assay is as described in the aging assay section. Unless otherwise stated, significance was represented as follows: * $p \leq 0.05$, ** $p \leq 0.01$, *** $p \leq 0.001$ and **** $p \leq 0.0001$. Unless otherwise stated, data in this study are presented as mean values \pm SEM. All experiments were performed and quantitated at least 3 independent times.

Bioinformatics

Human gene expression data, clinical trait data, and SNP association data were previously collected and published by the Metabolic Syndrome in Men (METSIM) cohort (Civelek et al., 2017). This cohort has 770 healthy male subjects with mean BMI = 26.59 ± 3.47 . Gene expression from subcutaneous adipose tissue was measured using Affymetrix U219 microarrays, and extensive clinical phenotyping was performed, including anthropometric traits, insulin sensitivity metrics and blood metabolite levels. BMI and WHR were both reported. Correlations between gene expression and clinical traits were calculated using the biweight midcorrelation, and only significant associations are shown. Associations between SNPs and gene expression were calculated using a linear mixed model as described in Civelek et al (Civelek et al., 2017). The SNP with the most significant

gene expression within 500 kb of the transcriptional start site was designated as the eSNP. We obtained the associations between BMI and WHR from Pulit et al (Pulit et al., 2019). Human orthologs were queried for associations with human phenotypes and diseases in the GWAS catalog (Buniello et al., 2019). LocusZoom plots were generated using the BMI and WHR summary statistics from Pulit et al (Pulit et al., 2019) and genotype and gene expression data from the METSIM cohort (Civelek et al., 2017).

3.4 Results

3.4.1 *Meta-analysis of human obesity GWAS variants identifies 386 C. elegans orthologs*

To identify genes that potentially contribute to human obesity, we exploited 3 published meta-analyses of human GWAS of obesity traits (Pulit et al., 2019; Yengo et al., 2018). Together, the 3 studies report over 1,200 loci associated with an increased body-mass index (BMI) or waist/hip ratio; however, as is standard for these kinds of studies (Cheng et al., 2018; Smemo et al., 2014; Voisin et al., 2015), the majority of the variants were not linked to genes. Therefore, previous work by our group, used eQTL analysis of 770 subcutaneous adipose samples from the Metabolic Syndrome in Men (METSIM) study (Civelek et al., 2017) to link about 680 of these loci to 209 genes (Table 3.1). Additionally, a study that searched for variants associated with high BMI in a Japanese cohort of 173,430 samples, annotated 120 high-BMI gene candidates (Akiyama et al., 2017). Finally, Chu *et al.* (Chu et al., 2017) analyzed 2.6 million SNPs in up to 9,594 women and 8,738 men of European, African, Hispanic, and Asian ancestry, and based on the genomic location they predicted 11 genes as associated with ectopic fat accumulation in the cohort (Chu et al., 2017). Together, the studies predicted 340 genes associated with obesity traits in humans. Using the comparative genomic analysis tool Ortholist2 (Kim et al., 2018), we identified *C. elegans* orthologs for 67% (207 out of 340) of the human obesity candidate genes (Fig. 3.1 A; Table 3.1). However, in some cases, more than one *C. elegans* orthologs were corresponded to a human gene. Therefore, the number of *C. elegans* orthologs associated with

obesity traits in humans totaled 386. We then set up to use *in vivo* functional genomics screening to test whether these human-obesity candidate genes have correlative or causal relationships with altered fat metabolism.

Figure 3. 1

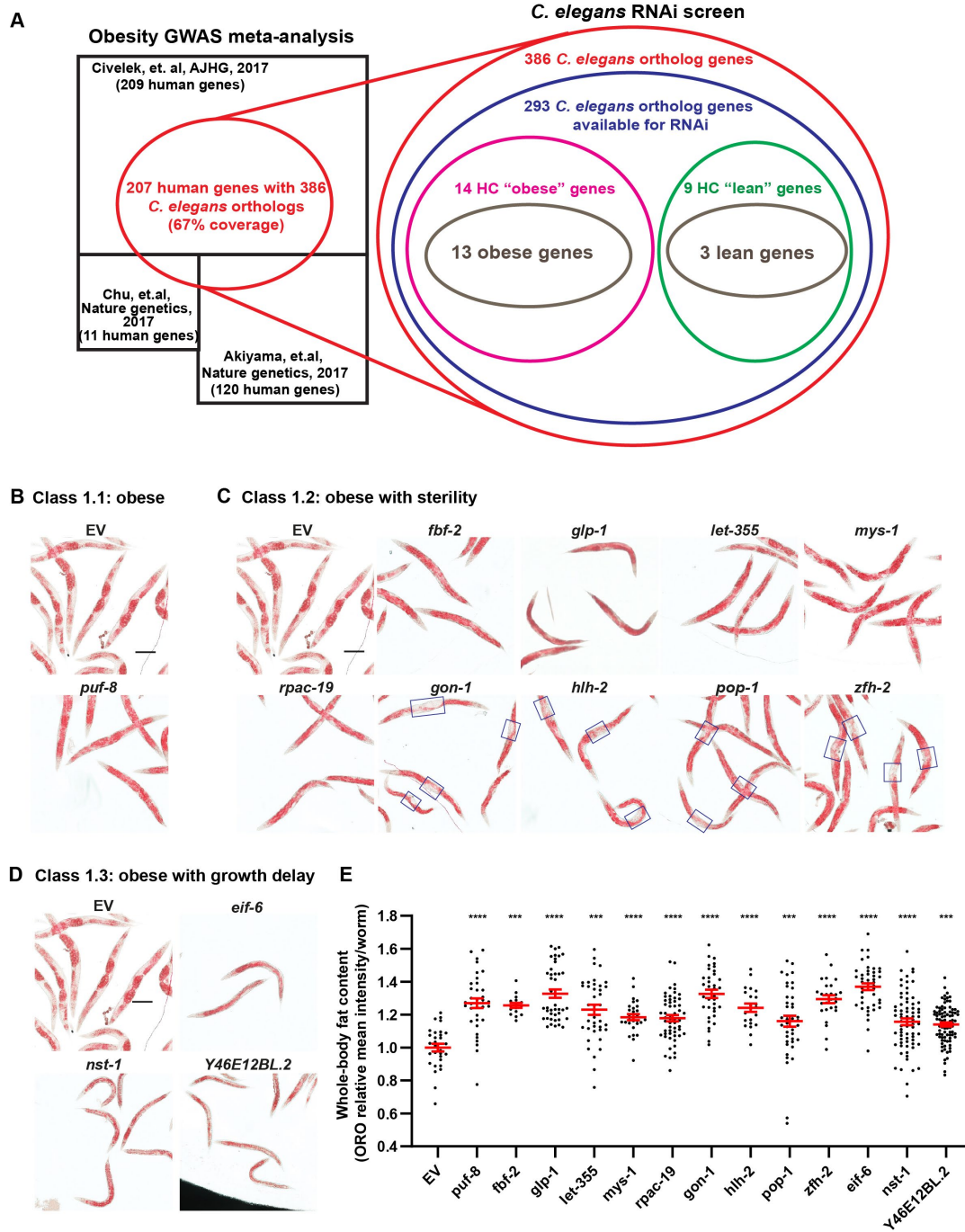


Figure 3.1. GWAS obese genes were validated through *C. elegans* RNAi screen

Throughout this figure, Error bars=S.E.M. N=numbers of independent biological replicates. * $p \leq 0.05$, ** $p \leq 0.01$, *** $p \leq 0.001$ and **** $p \leq 0.0001$.

(A) Summary of the meta-analysis and *C. elegans* RNAi screen. **(B-D)** Brightfield images of worms stained with ORO, representing body fat distribution in the worms treated with lean genes RNAi from the screen. All images are in the same magnification, scale bar=200 μ m. Obese genes were categorized into 3 groups: **(B)** obese with no secondary phenotype, **(C)** Obese with sterility, the extended fat depletion around the vulva in blue boxes, **(D)** obese with growth delay **(E)** Quantification on the relative intensity of ORO in worms as represented in **B-D**. N=3. Each data point represents the measurement of a worm. Absolute values of the intensity were normalized to the mean value of the empty vector control. Ratio t-test was used to make comparisons between empty vector control and the treatments.

3.4.2 Sixteen human-obesity gene candidates alter fat accumulation in standard-diet fed *C. elegans*

Although we identified 386 *C. elegans* orthologs of the genes associated with obesity traits in humans, only 293 of these 386 ortholog genes were available in the Ahringer (original and supplementary) (Kamath et al., 2003) or the Vidal (Rual et al., 2004) *C. elegans* genome-wide RNAi libraries (Fig. 3.1 A); therefore, we built an RNAi sub-library consisting of these 293 worm genes (Table 3.1 and workflow in Fig. 3.2 A). To increase the efficiency of the RNAi knockdown (KD) we used the RNAi-hypersensitive mutant *rrf-3(pk1426)* as the genetic background for the screen (Simmer et al., 2002). Approximately 75 *rrf-3* hatchlings were seeded in each of the RNAi and control clones of two 96-well plates (experimental replicates) and incubated at 15°C. At the L4 stage, worms were transferred to 25°C to trigger the thermosensitive RNAi-hypersensitive phenotype of *rrf-3(pk1426)*. As young adults, worms were harvested and stained with the lipid-specific dye Oil Red O (ORO) as previously described (Ke et al., 2018; Wählby et al., 2014). Body fat content was documented using high-content imaging, and the obesity phenotype was classified using Cellprofiler and Cellprofiler Analyst as we previously described (Ke et al., 2018; Wählby et al., 2014). We classified the hit genes as lean or obese based on the phenotype observed in response to RNAi treatment. Therefore, RNAi hits were classified into 3 groups: 1) obese: >50% worms in the RNAi-treated population showed higher ORO signal than empty RNAi vector control (EV), 2) wild type: fat phenotype resembling EV, and 3) lean: >50% worms in the RNAi-treated population showed lower ORO signal than EV. The

primary screen was independently repeated 3 times. The gene KDs that exhibited a consistent phenotype in all 3 repeats were classified as high-confidence (HC) genes, and selected for further validation (Fig. 3.1 A and Table 3.1 S1).

We identified 23 HC genes in the primary screen. We then retested the fat phenotype of these RNAi treatments in worms grown in standard 6 cm RNAi plates coupled to quantitation of ORO signal per worm using ImageJ. We confirmed 13 (out of 14) primary HC obese genes: *puf-8*, *fbf-2*, *glp-1*, *let-355*, *mys-1*, *rpc-19*, *gon-1*, *hlh-2*, *pop-1*, *zfh-2*, *eif-6*, *nst-1* and *Y46E12BL.2* (Fig. 3.1 B,C,D,E; Table 3.1). Of these obese genes, all but *puf-8* were sterile. Intriguingly, RNAi against *gon-1*, *hlh-2*, *pop-2* and *zfh-2* promoted a distinctive sterility phenotype, in which animals showed extended fat depletion around the vulva (Fig. 3.1 C). On the other hand, 3 obese genes – *eif-6*, *nst-1*, and *Y46E12BL.2* – additionally showed a developmental-delay phenotype (Fig. 3.1 D).

The primary screen lean hits were *rpt-5*, *hsp-4*, *let-767*, and *Y71H10B.1*. We then moved to validate these primary hits. One gene, *Y71H10B.1*, showed body fat reduction without developmental delay (Fig. 3.3 A,B). By contrast, the other three genes exhibited a severe developmental delay phenotype (Fig. 3.2 B; Table 3.1). Arrest and severe developmental delay are associated with changes in fat accumulation in *C. elegans* (Ludewig et al., 2004). Further, as previously reported (Fouad et al., 2017), we observed that body fat content increased significantly with age (Fig. 3.2 C). Therefore, we sought to test whether we could uncouple the

developmental delay from the obesity phenotype by starting the RNAi treatment at the L4 instead of the L1 stage. In animals fed RNAi from the L4 stage we found: (1) No fat phenotype for *hsp-4* (Fig. 3.2 D,E), suggesting that inactivation of this ER-stress response protein leads to the developmental delay associated with reduced fat accumulation; (2) *let-767* KD yielded adults with reduced fat content (Fig. 3.3 A,C), showing that the function of these genes in fat metabolism can be uncoupled from their role in development, and suggesting that these genes may impair development via metabolic dysfunction; and (3) surprisingly, although KD of *rpt-5* from the L1 stage impaired fat accumulation, KD of this same gene from the L4 stage caused obesity (Fig. 3.3 D,E), providing an extreme example of context-dependent gene function. Therefore, altogether, we identified 14 obese genes – *puf-8*, *eif-6*, *fbf-2*, *glp-1*, *gon-1*, *hlh-2*, *let-355*, *mys-1*, *nst-1*, *pop-1*, *rpc-19*, *rpt-5*, *Y46E12BL.2*, and *zfh-2* – and 2 lean genes – *Y71H10B.1*, *let-767*, and *mup-4* (Fig. 3.1 ; Table 3.1).

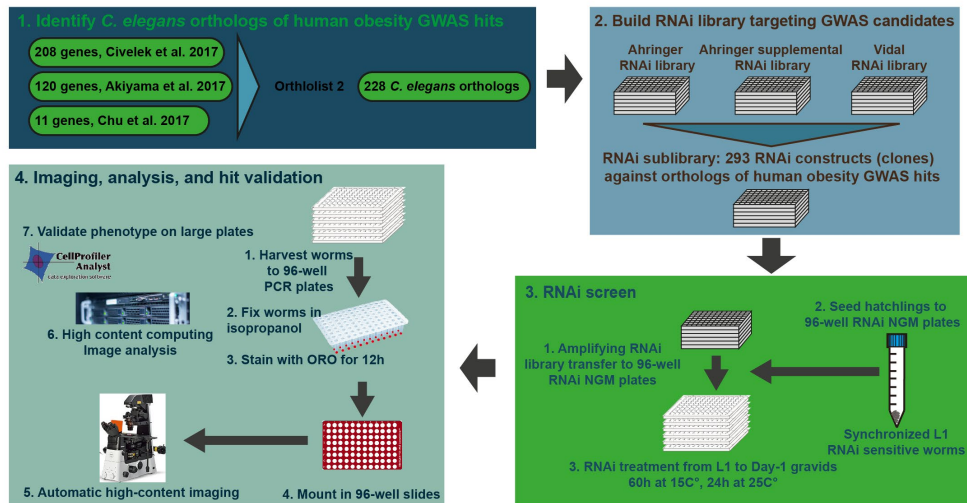
The 16 confirmed worm hits correspond to 16 human genes (Table 3.1). To identify the potentially similar contributions of the worm hits to mammalian obesity, we used three datasets: (1) Gene expression data from adipose tissue from the Hybrid Mouse Diversity Panel (Ghazalpour et al., 2012) (HMDP), a cohort of well-phenotyped male mice fed high-fat diet; (2) Subcutaneous adipose tissue gene expression data from the METSIM cohort, a cohort of thoroughly phenotyped Finnish men; and (3) the GWAS catalog (www.ebi.ac.uk/gwas/home). Using these datasets we investigated: (1) the correlations between gene expression and

anthropometric traits in mice and (2) in humans, and (3) the published associations between genetic variants and metabolic traits in GWAS studies. First, we calculated the correlation between metabolic traits and the expression of the 12 top mouse orthologs in mouse adipose tissue (Fig. 3.4 A). Most of these genes show strong correlations with obesity traits including body fat percentage, fat mass, body weight, and total mass. *Pum2*, *Polr1d*, *Notch4*, *Tcf7l2*, *Tcf12*, *Psmc3*, *Zfhx3*, and *Nt5c2* are correlated in the same direction as in *C. elegans* (*Adamts9*, *Dhx33* and *Kat8* were not measured in the mouse dataset), meaning 1) lower expression associated with increased BMI in mice and KD leading to obesity in worms or 2) lower expression associated with decreased BMI in mice and KD leading to obesity in worms. Next, we calculated the level of association between clinical traits including body mass index (BMI) and waist-to-hip ratio (WHR) with the expression of the 16 human genes in adipose tissue (Fig. 3.4 B). BMI was the most strongly associated trait, and *PUM2*, *POLR1D*, *ADAMTS9*, *NOTCH4*, *EYS*, *TCF7L2*, *KAT8* and *NT5C2* all show expression associations with BMI that go in the same direction as in *C. elegans*. Interestingly, the expression associations (Beta values) with BMI for *PUM2*, *POLR1D*, *NOTCH4*, *TCF7L2*, and *NT5C2* in humans also go in the same direction as in mice, suggesting the evolutionarily conserved functions of these genes in obesity from worms to mice and to humans. To investigate whether these genes might be implicated in obesity-derived metabolic diseases, we queried each human gene in the GWAS catalog. 15(out of 16) genes were found in loci associated with human diseases or traits (except for *DHX33*). Of these, 11 genes were associated with metabolic traits in human GWAS (Fig. 3.4 C). In total, we

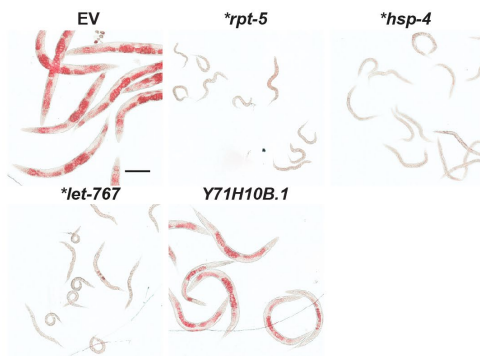
found evidence of the genes whose orthologs we showed to be causally linked to obesity in *C. elegans* could play roles in metabolic syndrome in mammalian systems.

Figure 3. 2

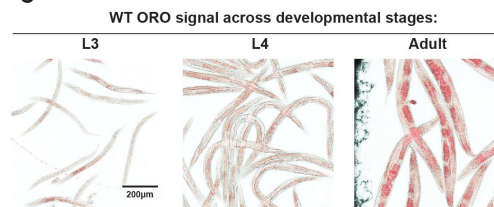
A



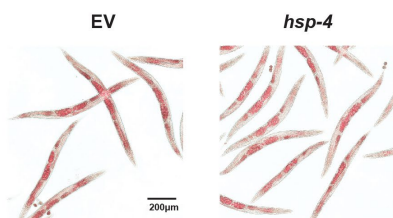
B



C



D



E

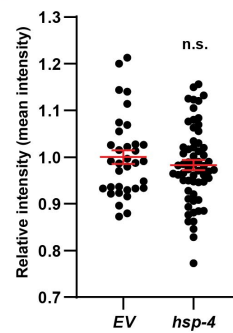


Figure 3.2

Throughout this figure, Scale bars = 200 μ m, Error bars = S.E.M. N=# independent biological replicates. Statistical significance was assessed via ratio t-test, * $p \leq 0.05$, ** $p \leq 0.01$, *** $p \leq 0.001$ and **** $p \leq 0.0001$.

(A) Overview of the strategy and pipeline of the screen. **(B)** Body fat distribution of worms treated with lean RNAi HC hits from L1 stage, stained by ORO. *Y71H10B.1* RNAi is the only lean RNAi hit without developmental delay. N=3. **(C)** body fat content of worms fed RD in different developmental stages. Left to right: L3, L4, and adult. N>5. **(D)** Validation of body fat distribution of worms treated with *hsp-4* RNAi which causes developmental delays, treated from L3 stage, showing no effect on body fat content. **(E)** Quantification on the relative intensity of ORO in worms for *hsp-4* RNAi as represented in **D**. Each data point represents the measurement of a worm. Absolute values of the intensity were normalized to the mean value of the empty vector control. N=3.

Figure 3. 3

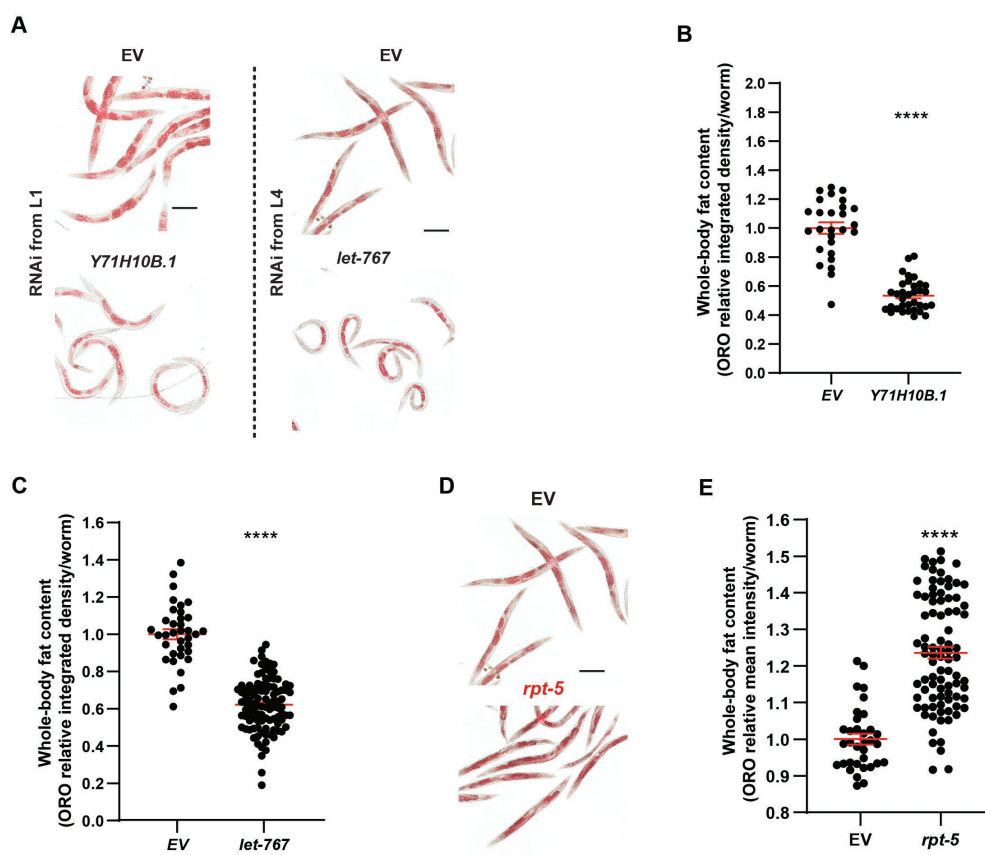


Fig. 3.3 GWAS lean genes were validated through *C. elegans* RNAi screen

Throughout this figure, Scale bars = 200 μ m, Error bars = S.E.M. N=# independent biological replicates. Statistical significance was assessed via ratio t-test, * $p \leq 0.05$, ** $p \leq 0.01$, *** $p \leq 0.001$ and **** $p \leq 0.0001$.

(A) Body fat distribution of worms treated with lean RNAi validated hits, stained by ORO. *Y71H10B.1* is the only lean gene without developmental defects. RNAi against *Y71H10B.1* started from L1 stage. *let-767* RNAi results in severe developmental arrest as described in Fig. 3.2 B, therefore, the RNAi against *let-767* started from L4 stage. **(B-C)** Quantification on the relative intensity of ORO in worms treated with **(B)** *Y71H10B.1* and **(C)** *let-767* RNAi as represented in **A**. Each data point represents the measurement of a worm. Absolute values of the intensity were normalized to the mean value of the empty vector control. N=3. **(D)** Validation of body fat distribution of worms treated with *rpt-5* RNAi that causes developmental delays, treated from L3 stage, identified as an obese gene. **(E)** Quantification on the relative intensity of ORO in worms for *rpt-5* RNAi as represented in **D**. Each data point represents the measurement of a worm. Absolute values of the intensity were normalized to the mean value of the empty vector control. N=3.

Figure 3. 4

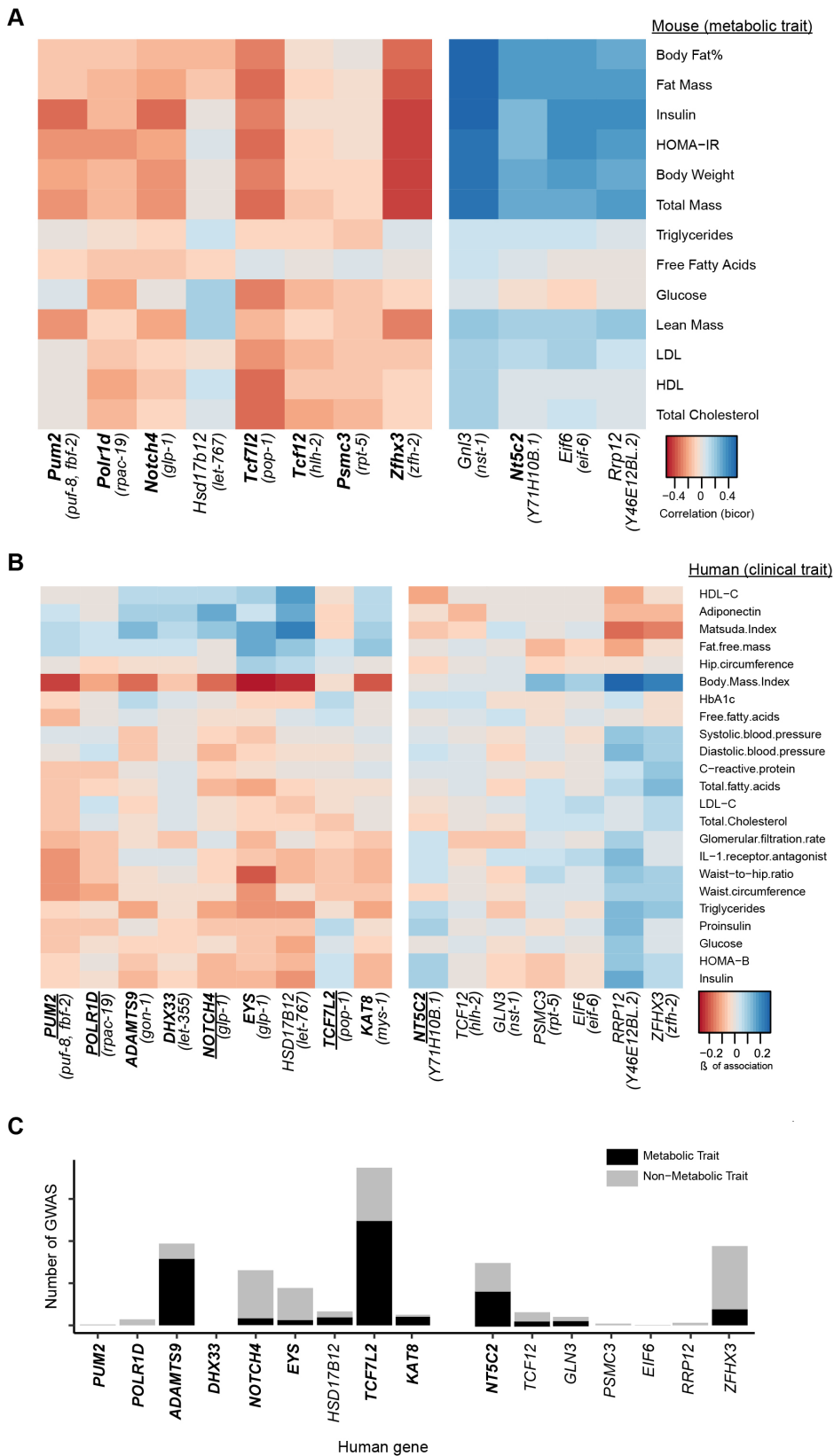


Figure 3.4 Human orthologs of *C. elegans* screen hits are implicated in human obesity

(A) Bi-weight Mid-correlations (median based correlation metric) of mouse gene expression and metabolic traits in adipose tissue of the HMDP cohort. Genes negatively associated with fat mass are shown on the left, positive association on the right. Bolded mouse ortholog names indicate that both the expression mouse ortholog and the worm gene are associated with fat storage (fat mass in mice) in the same direction. (B) Associations (Beta of association) between human gene expression and selected clinical traits in the subcutaneous adipose tissue of the METSIM cohort. Genes negatively associated with BMI are shown on the left, positive association on the right. Bolded human ortholog names indicate that both the expression human ortholog and the worm gene are associated with fat storage (BMI in humans) in the same direction. Underlined human ortholog names indicate the same effects on fat storage in both humans and mice. (C) Number of published GWAS in the GWAS catalog for each human ortholog. Color indicates association with metabolic or non-metabolic traits.

3.4.3 High-fructose diet leads to Diet-induced obesity in *C. elegans*

Excessive dietary intake of fructose has been suggested to be a major driver of the obesity epidemic (Hannou et al., 2018; Tappy and Lê, 2010), as fructose is the most common additive in industrialized foods (Hanover and White, 1993). To test the potential contribution of the human GWAS obesity candidates in the development of DIO we established a fructose-driven *C. elegans* model of DIO. We named the High-fructose diet (HFrD) the dietary regimen in which worms are grown from the L1 stage in plates of nematode growth media (NGM) supplemented with 10mg/mL of fructose. We observed that, at the adult stage, worms fed a HFrD show a significant increase in body fat content compared to those fed a regular diet (RD) (Fig. 3.5 A,B). Further, worms fed the HFrD are also larger than worms fed RD (Fig. 3.5 C), similar to the previous report showing increased body size in worms fed excessive glucose (Alcántar-Fernández et al., 2018).

Adipose is the main fat storage tissue in humans, and adipocytes with increased lipid droplet (LD) number and size are cellular hallmarks of obesity (Daemen et al., 2018). In *C. elegans*, there are no specialized adipose cells. The primary triglyceride depots are found in the worm's intestinal cells and are contained in LDs sized between 0.5–1.5 μm (Shi et al., 2013; Vrablik et al., 2015). To define whether *C. elegans* fed a HFrD would show changes in the abundance and/or size of the LDs, we used a LD reporter consisting of *Drosophila* PLIN1::GFP driven by the intestine-specific *daf-22* promoter (Laranjeiro et al., 2017; Liu et al., 2014b). In agreement with the mammalian subcellular hallmarks of obesity, we observed both,

an increase in the overall intensity (Fig. 3.5 D,E) and also in the size (Fig. 3.5 F) of the LDs in the intestine of HFrD-fed worms. Another common feature of human obesity is the increase in ectopic fat stores (fat outside the primary fat storage tissues) (van Hees et al., 2010), and excessive ectopic fat is associated with worse health outcomes (Britton and Fox, 2011) . Although *C. elegans* do not have a dedicated adipose tissue, ectopic fat is observed in mutants with metabolic dysregulation such as the insulin receptor mutant *daf-2* , in which fat is additionally observed in muscle and hypodermis (O'Rourke et al., 2009b). To further characterize the distribution of the fat stores in the HFrD worms, we used the same *Drosophila* PLIN1::GFP construct but now driven by the *unc-54* promoter to express it in the muscle, or driven by the *Y37A1B.5* promoter to express it in the hypodermis (Laranjeiro et al., 2017; Liu et al., 2014b). Again, we observed a significant increase in the LDs intensity (Fig. 3.5 D,G,H) but in this case, no change in LD size (Fig. 3.6 A,B) in neither muscle nor hypodermis of worms fed HFrD. These observations suggest excessive fat is stored in primary and ectopic tissues in *C. elegans*, subcellularly comparable to what is observed in visceral and ectopic fat depots in humans with obesity.

Obesity is defined by the World Health Organization as abnormal or excessive fat accumulation that presents a higher risk of debilitating co-morbidities and death (Ahima, 2009; Salvestrini et al., 2019; Tam et al., 2020). Therefore, we sought to test whether the increase in fat levels observed in HFrD-fed worms would meet this definition. Firstly, we evaluated the effect of HFrD on overall survival by

comparing the lifespan of HFrD-fed worms to the lifespan of the RD-fed worms. HFrD reduced the median lifespan of *C. elegans* by 69% (Gehan-Breslow-Wilcoxon test), with a 31.49 average Hazard Ratio (Mantel-Haenszel test) (Fig. 3.5 I; Table 3.2). Next, we conducted healthspan assays as described previously (Hahm et al., 2015). In the case of locomotory capacity, we found a significant reduction in body bending rate and average velocity in 3-day old worms fed HFrD when compared to worms of the same age fed RD (Fig. 3.5 J,K). In *C. elegans*, locomotion defects including impaired body bending and reduced velocity can be caused by reduced proteostasis (Fong et al., 2016), and in humans, obesity is strongly associated with neurodegenerative diseases characterized by uncurbed protein aggregation (Chatterjee et al., 2016; Cherbuin et al., 2015; Yaffe et al., 2012). Therefore, we hypothesized that high fructose levels in the *C. elegans* diet may reduce proteostasis, which would lead to an earlier onset of locomotion defects. Worms constitutively expressing a toxic form of the human A β amyloid (strain GRU102) show an earlier onset of locomotory impairment than worms expressing a non-toxic form of the human A β amyloid (strain GRU101), and this reduced locomotory capacity is due to reduced proteostasis in the neuro-locomotory system (Fong et al., 2016; Teo et al., 2019). To test the hypothesis that reduced proteostasis would contribute to the reduced locomotory capacity observed in worms fed HFrD, we fed RD or HFrD to the GRU101 and GRU102 worms. Briefly, the assay was set up by placing fifty 3-day adult worms from each condition (GRU102 \pm fructose and GRU101 \pm fructose) at one end of a 10cm NGM plate. To start the assay, 20 μ l of *E. coli* suspension (OD=20) were placed on the

plates on the opposite side of the worms. After 1h, the number of the worms fully or partially within the borders of the mini bacterial lawn was counted. We consistently found fewer worms expressing toxic A β than worms expressing the non-toxic A β in the lawns (Fig. 3.5 L), confirming the expected detrimental effect of increased protein aggregation on *C. elegans* locomotion. We also observed HFrD to be sufficient to impair *C. elegans* locomotion (Fig. 3.5 L), and, tellingly, the HFrD-derived impairment was not additive to the expression of toxic A β (Fig. 3.5 L), suggesting that HFrD and A β overexpression would have a common mechanism of toxicity, which is likely to be reduced proteostasis. Altogether, we found that overconsumption of fructose in *C. elegans* evokes several of the hallmarks of human obesity including elevated body fat content in primary and ectopic fat storage tissue subcellularly characterized by increases in the number and size of the LD, in conjunction with reduced health and lifespan.

Figure 3. 5

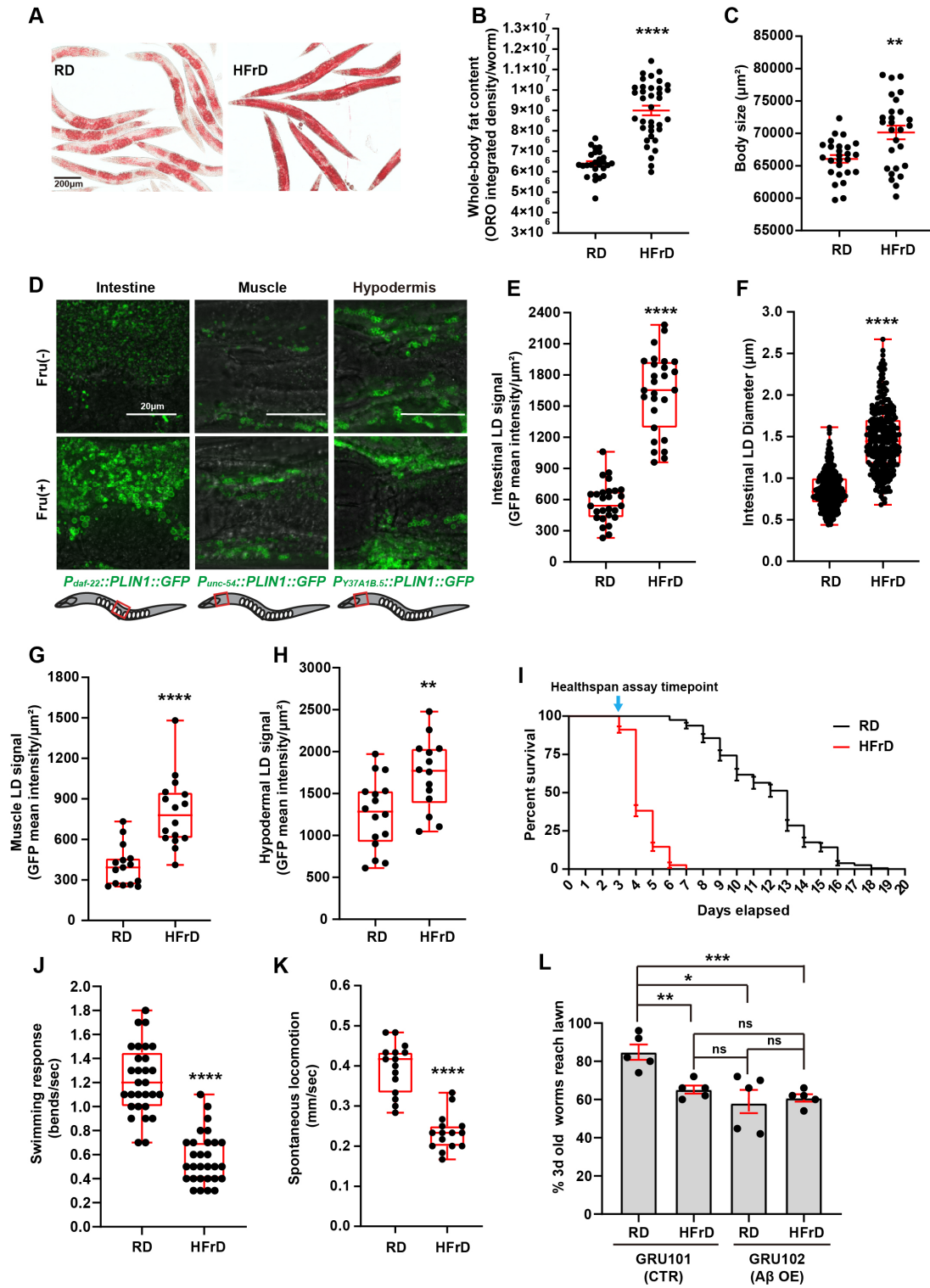


Figure 3.5 Overconsumption of fructose leads to DIO in *C. elegans*

Throughout this figure, Error bars=S.E.M. N=numbers of independent biological replicates. Unless specified, unpaired nonparametric t-tests were used to assess the significance. * $p \leq 0.05$, ** $p \leq 0.01$, *** $p \leq 0.001$ and **** $p \leq 0.0001$.

(A) Body fat distribution of worms fed RD or HFrD from L1 stage, stained by ORO. Scale bar=200 μm . **(B)** Quantification of intensity (integrated density) of ORO staining in worms for fed RD or HFrD as represented in **A**. Each data point represents the measurement of a worm. N=3. **(C)** Quantification of body size of worms fed RD or HFrD. Each data point represents the measurement of an object(worm). N=3. **(D)** Tissue-specific LD phenotype in worms fed RD (top) or HFrD (bottom), using tissue-specific LD reporter strains expressing PLIN1::GFP. Scale bar=20 μm . **(E)** Quantification of mean intensity of intestinal LDs in worms fed RD or HFrD, as represented in **D**. Each data point represents the measurement of a 0.004 mm^2 intestinal square area of a worm. N=3. **(F)** Quantification of intestinal LD size in worms fed RD or HFrD. Each data point represents the measurement of a random LD in the images. 10 worms were measured in each independent biological replicate. N=3. **(G)** Quantification of mean intensity of muscle LDs in worms fed RD or HFrD, as represented in **D**. Each data point represents the measurement of a 0.003 mm^2 muscle square area behind the pharynx of a worm. N=3. **(H)** Quantification of mean intensity of hypodermis LDs in worms fed RD or HFrD, as represented in **D**. Each data point represents the measurement of a 0.003 mm^2 hypodermis square area behind the pharynx of a worm. N=3. **(I)** Lifespan assay on worms fed RD or HFrD. N=1 is shown in this

panel, N=3 is summarized in Table 3.2 **(J)** Quantification of body bends per second of worms fed RD or HFrD in S-buffer. N=3. **(K)** Measurements of the moving velocity of worms fed RD or HFrD on bacteria-free NGM surface. N=3. **(L)** quantification of behavior assay on *C. elegans* neuron degeneration models. GRU101: worms with a pan-neuron expression of non-toxic human A β , GRU102: worms with a pan-neuron expression of toxic human A β . N=3

Figure 3. 6

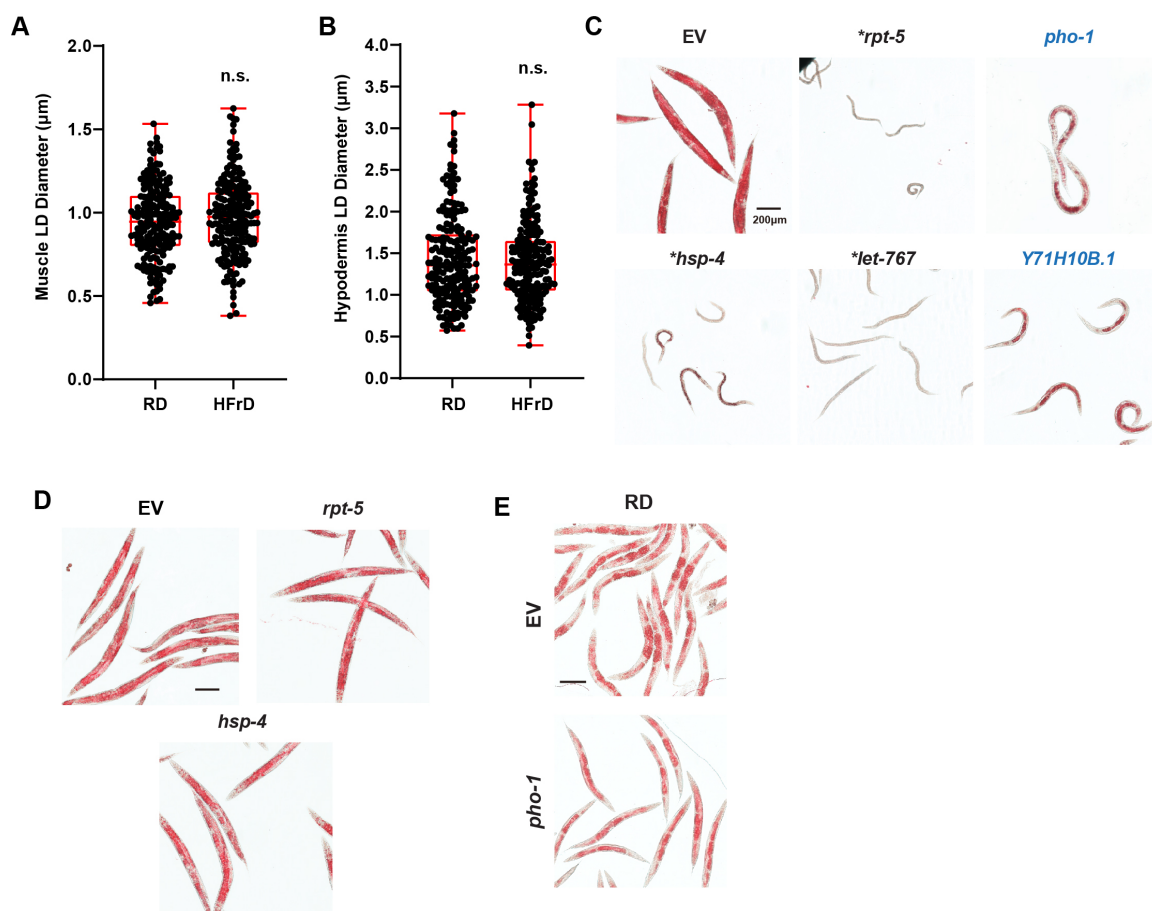


Figure 3.6

Throughout this figure, Error bars=S.E.M. N=numbers of independent biological replicates. Unless specified, unpaired nonparametric t-tests were used to assess the significance. * $p \leq 0.05$, ** $p \leq 0.01$, *** $p \leq 0.001$ and **** $p \leq 0.0001$.

(A) Quantification of muscle LD size in worms fed RD or HFrD. Each data point represents the measurement of a random LD in the images. 10 worms were measured in each independent biological replicate. N=3. **(B)** Quantification of hypodermis LD size in worms fed RD or HFrD. Each data point represents the measurement of a random LD in the images. 10 worms were measured in each independent biological replicate. N=3. **(C)** Body fat content of worms treated with HC RNAi hits from DIO screen under HFrD, worms were treated with RNAi from L1 stage and stained with ORO. *pho-1* and *Y71H10B.1* are the 2 DIO suppressors that lead to lean phenotype without developmental delay, labeled in blue. **(D)** Body fat content of worms treated with RNAi against *rpt-5* and *hsp-4* under HFrD from L4 stage and stained with ORO. No change of fat content was observed. N=3. **(E)** Body fat content of worms treated with RNAi against *pho-1* under RD from L4 stage, and stained with ORO. No change of fat content was observed. N=3.

3.4.4 Three human-obesity gene candidates cause DIO in *C. elegans*

To test the potential role of the human-obesity GWAS candidate genes in the development or the prevention of DIO, we screened the 293 human candidate genes in *C. elegans* fed 10mg/mL fructose (screen workflow similar to the RD screen described in Fig. 3.1 A but with dietary fructose supplementation to the Nematode growth media). As a result, we identified two phenotypic classes: (1) DIO: after RNAi treatment worms in these populations had phenotypes similar to the EV controls; and 2) suppressors of DIO: $\geq 50\%$ of worms in an RNAi treatment showed reduced fat content when compared to EV controls, suggesting that the gene contributes to HFrD-driven DIO in WT *C. elegans*. The RNAi treatments that showed a DIO-suppressor phenotype consistently in 3 or more independent biological replicates were considered high-confidence (HC) and selected for further study.

From the primary DIO screen, we identified 8 HC DIO-suppressor genes. Using the same rationale and approach described above (Fig. 3.2 A), we retested the 8 genes in 6cm NGM plates. We confirmed the DIO-suppressor phenotype for 5 out of the 8 HC genes. Yet, three of the retested DIO suppressors –*rpt-5*, *hsp-4*, *let-767*– led to severe developmental delay (Fig. 3.6 C; Table 3.1), while only 2 DIO suppressors – *pho-1* and *Y71H10B.1* – reduced body fat content and body size of worms fed HFrD without detrimental effect on development (Fig. 3.7 A,B,C). To further evaluate the fat phenotype of the developmentally delayed hits, we started the RNAi treatments at the L4 stage. We first found that *rpt-5* and *hsp-4* RNAi did

not alter the body fat content of worms fed HFrD (Fig. 3.6 D). We also found that L4-KD of *let-767* reduced the body fat content and the body size of worms fed HFrD (Fig. 3.7 A,D,E), suggesting that *let-767* could independently modulate fat metabolism and development. Importantly, *let-767* and *Y71H10B.1* were also lean hits in the RD screen described above (Fig. 3.2), suggesting a generic function for these genes in promoting fat accumulation. On the other hand, *rpt-5* was an obese hit in the RD screen (Fig. 3.2), in line with the observation that *rpt-5* RNAi did not reduce body fat content in worms. By contrast, *pho-1* KD only prevented obesity in worms fed HFrD, suggesting a specific function in DIO. Together, We identified and confirmed 3 genes (RNAi) –*pho-1*, *let-767* and *Y71H10B.1*– exhibiting DIO-suppressor phenotype from this HFrD screen, of which 2 genes –*let-767* and *Y71H10B.1*– were generic lean genes.

Figure 3. 7

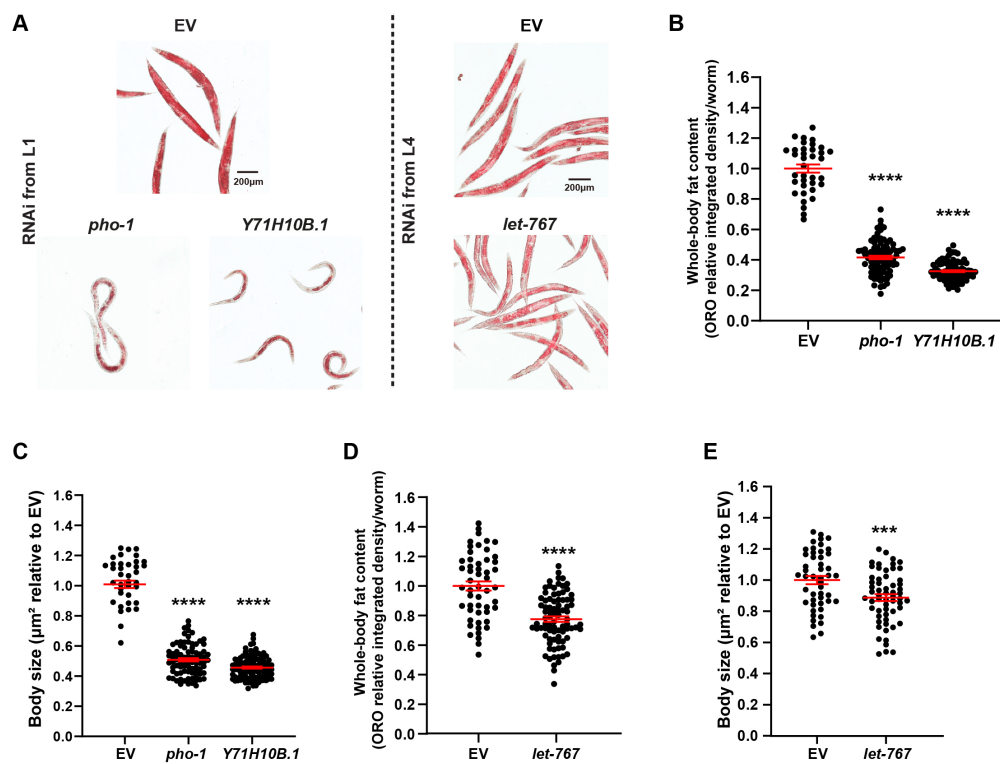


Figure 3.7 *C. elegans* DIO suppressors were identified through RNAi screen

Throughout this figure, Scale bars = 200 μ m, Error bars = S.E.M. N=# independent biological replicates. Statistical significance was assessed via ratio t-test, * $p \leq 0.05$, ** $p \leq 0.01$, *** $p \leq 0.001$ and **** $p \leq 0.0001$

(A) Body fat content of worms treated with HC RNAi hits from DIO screen under HFrD. Left: worms were treated with *pho-1* and *Y71H10B.1* RNAi from L1 stage and stained with ORO. Right: worms were treated with *let-767* RNAi from L4 stage and stained with ORO. **(B)** Quantification on the relative intensity of ORO in worms treated with *pho-1* and *Y71H10B.1* RNAi as represented in **A**. Each data point represents the measurement of a worm. Absolute values of the intensity were normalized to the mean value of the empty vector control. N=3. **(C)** Quantification of body size of worms treated with *pho-1* and *Y71H10B.1* RNAi as represented in **A**. Each data point represents the measurement of a worm. Absolute values of the body size were normalized to the mean value of the empty vector control. N=3. **(D)** Quantification on the relative intensity of ORO in worms treated with *let-767* RNAi as represented in **A**. Each data point represents the measurement of a worm. Absolute values of the intensity were normalized to the mean value of the empty vector control. N=3. **(E)** Quantification on body size of worms treated with *let-767* RNAi as represented in **A**. Each data point represents the measurement of a worm. Absolute values of the body size were normalized to the mean value of the empty vector control. N=3.

3.4.5 DIO suppressors restore *C. elegans* LD physiology in a tissue-specific manner

As described above, HFrD promotes increased accumulation of larger LDs in both primary and ectopic fat depots (Fig. 3.5 D). Using the PLIN1::GFP LD-reporter strains, we assessed whether KD of the generic lean genes *let-767*, *Y71H10B.1*, and the DIO-suppressor gene *pho-1* would suppress the LD number, size, or both phenotypes, in primary, ectopic, or both types of tissues.

C. elegans treated with RNAi against *Y71H10B.1* showed smaller LDs in the intestine (Fig. 3.8 A,B), and less overall LDs signal in the intestine, muscle, and hypodermis when animals are fed RD (Fig. 3.8 A,B,C,D) . Similarly, RNAi against *Y71H10B.1* of HfrD fed worms reduced LDs size in the intestine (Fig. 3.8 A,B), and overall LD signal in the intestine, muscle, and hypodermis (Fig. 3.8 A,B,C,D); results that are in line with the diet-independent lean phenotype of *Y71H10B.1*. On the other hand, although showing reduced LD size, RNAi treatment against *let-767*, did not significantly change LD intensity in intestine or muscle when *C. elegans* were fed RD (Fig. 3.8 A,B,C). By contrast, RNAi against *let-767* appreciably decreased the intensity of LDs signal in the hypodermis of animals fed RD, suggesting that most of the overall loss of fat observed in *let-767* RNAi-treated animals fed RD is due to loss of hypodermal fat (Fig. 3.8 A,B,C) . Distinctively, and showing the complexity of the fat-storage response to diet, *let-767* RNAi-treated worms fed HFrD showed reduced LD size and overall LD signal in the intestine, as well as decreased overall LD signal in the hypodermis (Fig. 3.8 A,B,C). Further,

LD signal did not increase in the muscle when compared to WT worms fed HFrD (Fig. 3.8 A,B,D). Therefore, *let-767* contributes to fat accumulation in the hypodermis independent of the diet and in the intestine only in HFrD, whereas they do not contribute to fat accumulation in the muscle of *C. elegans*.

Screening and validation showed that *pho-1* contributes to DIO but not basal fat accumulation in *C. elegans* (Fig. 3.7 A; Fig. 3.6 C,D; Table 3.1). Therefore, it was initially surprising to find out that RD-fed animals treated with RNAi against *pho-1* showed smaller LDs in the intestine (Fig. 3.8 A,B) and reduced overall LD signal in the hypodermis (Fig. 3.8 A,C). However, simultaneously, *pho-1*-treated worms showed a subtle increase in overall LD signal in the intestine and muscle (Fig. 3.8 A,C). Hence, we hypothesize that smaller LDs in the intestine and overall less LD content in the hypodermis, in conjunction with increased overall LD signal in intestine and muscle, may lead to a net fat signal in *pho-1* knock-down animals that is indistinguishable from WT when scoring whole-body ORO. Similarly surprising, although *pho-1* RNAi suppressed DIO, it increased LD overall signal in the intestine of worms fed HFrD (Fig. 3.8 A,D). However, *pho-1* RNAi simultaneously decreased LD overall signal in the hypodermis in animals fed HFrD (Fig. 3.8 A,B,D). The data then suggest that *pho-1* contributes to DIO mainly through enlargement of LDs in the intestine and increasing the abundance of LDs in the hypodermis, but not through changes in muscle LDs. From a different perspective, the observation that knock-down of all 3 lean genes caused a significant reduction in LD signal in the hypodermis of worms fed HFrD (Fig. 3.8

A,D) suggests that changes in hypodermal lipid content substantially contribute to DIO. Further, the only major fat-storage tissue where all lean genes reduced fat storage was the hypodermis. Also intriguing, all lean genes suppressed the enlarged body size of worms fed HFrD (Fig. 3.7 C,E); therefore, it is reasonable to hypothesize that changes in hypodermal fat stores sizably contribute to obesity and the enlarged body size observed in obese *C. elegans*.

Figure 3. 8

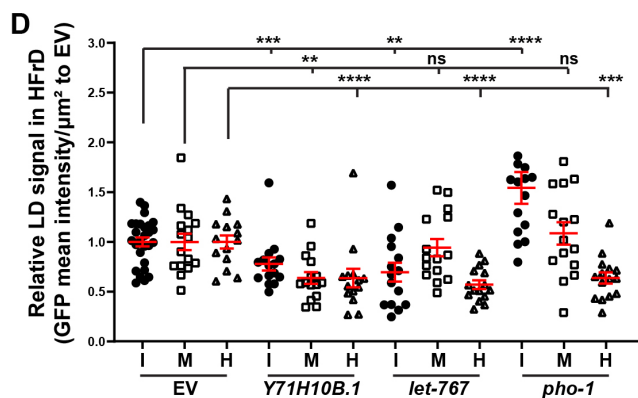
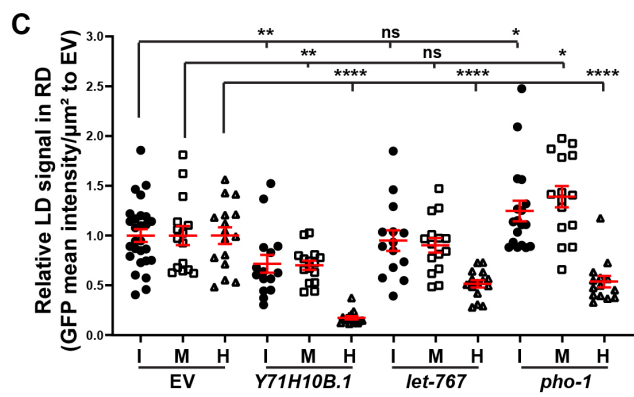
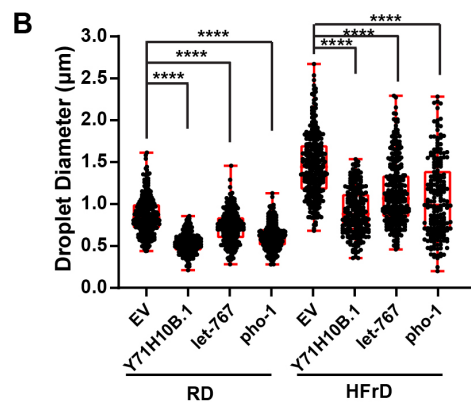
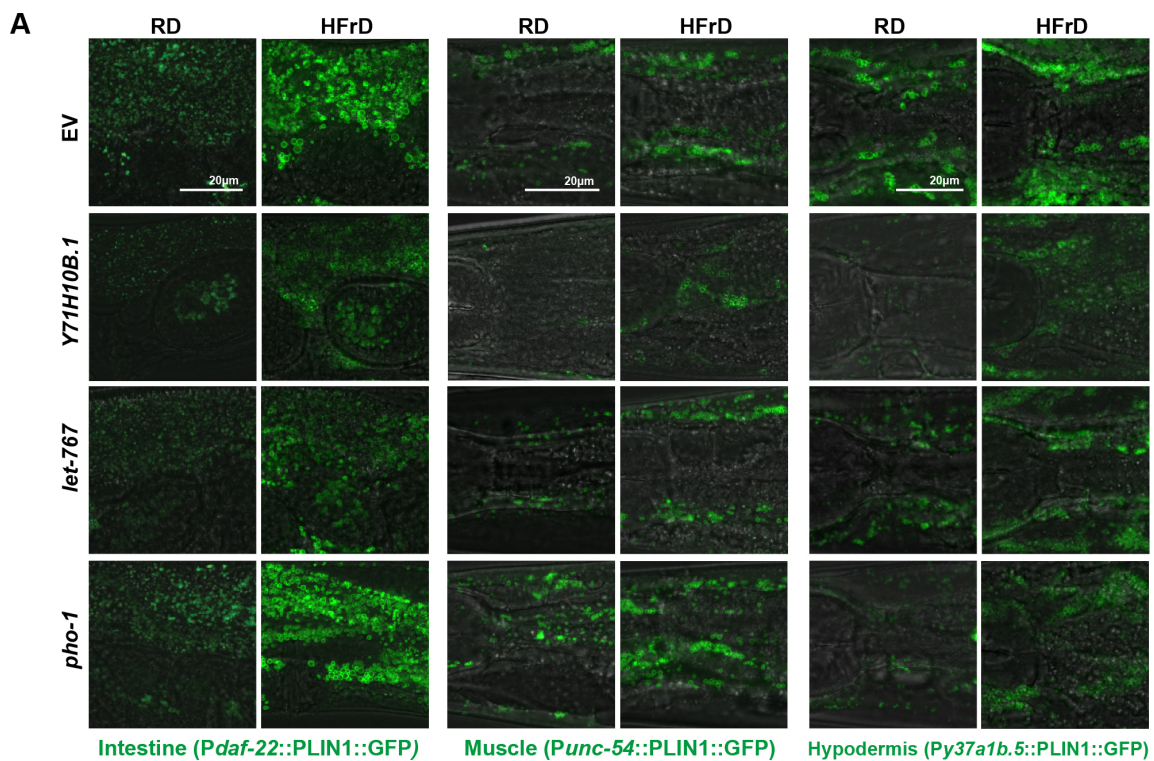


Figure 3.8 KD of DIO suppressors leads to LD phenotypes in worms fed RD and HFrD

Throughout this figure, Scale bars=20 μ m, Error bars=S.E.M. N=numbers of independent biological replicates. Unless specified, ratio t-tests were used to assess the significance. * $p \leq 0.05$, ** $p \leq 0.01$, *** $p \leq 0.001$ and **** $p \leq 0.0001$.

(A) Intestine, muscle and hypodermis LD phenotype in worms fed RD or HFrD and treated with DIO suppressors RNAi, using tissue-specific LD reporters strains XD3971, XD1875 and XD2458 respectively, expressing *Drosophila PLIN1::GFP*.

(B) Quantification of intestinal LD size in worms fed RD or HFrD and treated with DIO suppressors RNAi. Each data point represents the measurement of a random LD in the images. 10 worms were measured in each independent biological replicate. N=3. unpaired nonparametric t-tests were used to assess the significance. **(C)** Quantification of relative LDs signals in worms fed RD and treated with DIO suppressors RNAi, as represented in **A**. Each data point represents the measurement of a 0.003mm² square area of the tissue. I: intestine, M: muscle, H: hypodermis. N=3.

(D) Quantification of relative LDs signals in worms fed HFrD and treated with DIO suppressors RNAi, as represented in **A**. Each data point represents the measurement of a 0.003mm² square area of the tissue. I: intestine, M: muscle, H: hypodermis. N=3.

3.4.6 DIO suppressors restore health biomarkers and lifespan of HFrD-fed

C. elegans

DIO reduces *C. elegans* healthspan and lifespan (Fig. 3.5 I,J,K,L). Therefore, we next assessed whether the suppressors of DIO would also suppress the shortening of lifespan caused by a HFrD. For the DIO genes that do not cause a developmental delay (*pho-1* and *Y71H10B.1*), the RNAi treatment was started on synchronized hatchlings. For the genes causing developmental delay (*let-767*), RNAi was started at the L4 stage. Survival over time was assessed in ≥ 3 independent biological replicates (summarized in Table 3.3). Only lifespan reduction or extension with $p < 0.05$ (Gehan-Breslow-Wilcoxon test) in all 3 replicates was considered significant. We found that RNAi against *pho-1*, *let-767*, and *Y71H10B.1* partially suppressed the short lifespan associated with DIO (Fig. 3.9 A,B,C; Table 3.3). On the other hand, when fed RD, KD of the same genes did not alter *C. elegans* lifespan significantly (Table 3.3). To examine if KD of the genes that reduce body fat also restores *C. elegans* health, we evaluated the behavioral response to flooding (swimming response) and spontaneous locomotion of animals with KDs of the 2 generic lean genes (*let-767* and *Y71H10B.1*) and the DIO suppressor (*pho-1*). We found *Y71H10B.1* ameliorated the swimming response (Fig. 3.9 D) and that all these genes ameliorated spontaneous locomotion (Fig. 3.9 E). These findings support the notion that reducing body fat content can reduce the health and lifespan burdens associated with obesity in *C. elegans*.

Figure 3. 9

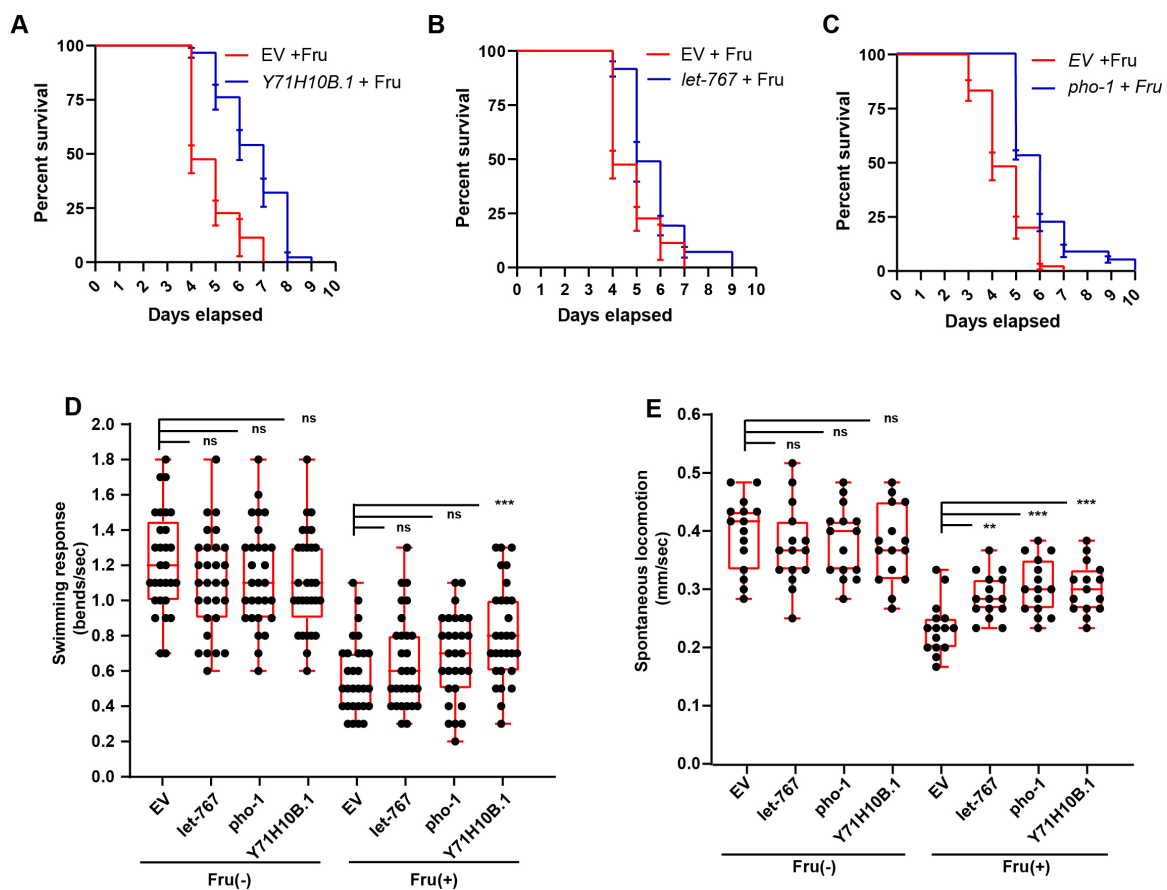


Figure 3.9 KD of DIO suppressors improves *C. elegans* healthspan and lifespan

Throughout this figure, Error bars=S.E.M. N=numbers of independent biological replicates. Unless specified, unpaired nonparametric t-tests were used to assess the significance. * $p \leq 0.05$, ** $p \leq 0.01$, *** $p \leq 0.001$ and **** $p \leq 0.0001$.

(A-D) Lifespan assay on worms fed HFrD, and treated with DIO suppressors RNAi comparing to EV. *Y71H10B.1* RNAi in **A**, *let-767* RNAi in **B**, *pho-1* RNAi in **C**. N=1 is shown in this figure, N=3 is summarized in Table 3.3 **(D)** Quantification of body bends per second of worms fed RD or HFrD and treated with DIO suppressors RNAi. N=3. **(E)** Measurements of the moving velocity on bacteria-free NGM surface of worms fed RD or HFrD and treated with DIO suppressors RNAi. N=3.

3.5 Discussion

Obesity is a complex disease influenced by various interacting factors including socioeconomic status, physical activity, eating habits, microbiota, and multiple genes acting in multiple tissues (Yang et al., 2007). This complex etiology causes challenges in understanding the molecular mechanisms of obesity and developing effective treatments. Studies aimed to elucidate the role of carbohydrates in obesity suggested that high-sugar diets could be the main factor behind the alarming increase in the incidence of obesity and metabolic syndromes. More specifically, increased fructose intake from high-fructose corn syrup (HFCS) was found to be highly correlated with the epidemic of obesity in the past 40 years. (Gross et al., 2004; Johnson et al., 2007; Marriott et al., 2010) The consumption of HFrD also has been directly linked to obesity and obesity-related metabolic syndromes in both humans and other mammalian models. (Dhingra et al., 2007; Lustig, 2010; Nakagawa et al., 2005; Toop and Gentili, 2016) Compared to glucose, fructose consumption is more detrimental in the development of obesity regarding visceral fat accumulation (Stanhope et al., 2009). Further, a recent clinical study has shown that dietary fructose restriction reduces body fat content and improves insulin kinetics in children with obesity (Schwarz et al., 2017). Previously a high glucose diet-induced obesity *C. elegans* model has been described (Lee et al., 2009; Schlotterer et al., 2009), however, a model that illustrates the consequence of overconsumption of fructose has never been introduced. In this study, for the first time, we established a simple *C. elegans* model for testing fructose overconsumption DIO. We showed that overconsumption of fructose increases the

LDs in the primary fat storage intestinal cells and the ectopic fat in muscle and hypodermis. Interestingly, the LD morphology in the fat storage tissues is also different between worms fed RD and HFrD, indicating physiological differences of the LD. Further physiological and biochemical characterization of the LDs in the worms fed HFrD compared to LD would reveal the cellular mechanisms in the development of obesity. Similar to mammalian models, we also found a lifespan and healthspan reduction of the worms fed HFrD in *C. elegans*, suggesting detrimental effects on the overconsumption of dietary fructose. More interestingly, we found that HFrD feeding disrupts the *C. elegans* behavior to seek food, suggesting impaired locomotion and cognitive capacity. We also found that such disrupted behavior is not additive with the A β overexpression, implying a role of neuron degeneration disorders in the lifespan and healthspan reduction by HFrD. It has been well documented that obesity and the related condition Type II Diabetes (T2D) are associated with increased risk of developing neurodegenerative diseases, impaired cognitive function, and reduced white matter area (Chatterjee et al., 2016; Cherbuin et al., 2015; Yaffe et al., 2012). Such association could also be validated in this *C. elegans* DIO model. Together, this *C. elegans* DIO model induced by fructose would allow us to identify novel fat regulators specifically for fructose-induced obesity and to extend our understanding of fructose metabolism in obesity.

GWAS is a powerful approach to identify loci associated with obesity because large cohorts will sample across the arc of socioeconomic statuses, physical

activity, eating habits, microbiota composition, and genetic diversity. However, connecting the resulting loci to the specific genes that promote or prevent obesity remains challenging. Obstacles include the large candidate-locus lists, defining the specific gene/s influenced by the genetic variants, and the time-consuming nature of molecular, cellular, and physiological studies (Gallagher and Chen-Plotkin, 2018). For instance, where (e.g. tissue) or when (e.g. developmental stage) should the potential effect of inactivating or hyperactivating a candidate gene be tested. As a result, comparatively few GWAS loci have been causally linked to the disease of interest. In the case of obesity, there are ~950 loci associated with BMI (Yengo et al., 2018) and ~350 loci associated with waist-hip ratio adjusted BMI (Pulit et al., 2019), yet very few genes have been validated and fewer druggable targets exist. Therefore, methods that can test the causality of GWAS loci quickly and effectively are needed. In this study, we introduced two such methods to validate potential obesity GWAS genes in a high throughput manner: bioinformatic analyses of publicly available datasets and high throughput *in vivo* RNAi screening in the model organism *C. elegans*. Using this strategy, we identified 11 novel obese genes (*fbf-2*, *gon-1*, *hlh-2*, *let-355*, *mys-1*, *nst-1*, *pop-1*, *puf-8*, *rpac-19*, *rpt-5* and *Y46E12BL.2*) and 2 novel lean/DIO suppressor genes (*let-767*, and *pho-1*). On the other hand, 3 obese genes (*eif-6*, *glp-1* and *zfh-2*) and 2 lean/DIO suppressor gene (*Y71H10B.1* and *pho-1*) were previously linked to fat metabolism and obesity.

Among the previously characterized genes, the *C. elegans* Notch, *glp-1*, has already been shown as an obese gene in *worms* in previous studies (O'Rourke et

al., 2009b; Wang et al., 2008), although its mammalian ortholog *NOTCH4* and *EYS* has not been causally linked to obesity (Both were associated with obesity in GWAS (Akiyama et al., 2017; Civelek et al., 2017)). The mammalian ortholog of *C. elegans Y71H10B.1*, named *Nt5c2*, encodes for a purine nucleotidase. *Nt5c2* KO mice gain less weight when fed a high-fat diet (Johanns et al., 2019). Therefore, the fat phenotype of the *Nt5c2* KO mice is in line with the DIO suppressor phenotype observed in *C. elegans* treated with RNAi against *Y71H10B.1*. Furthermore, using adipose tissue gene expression from the METSIM cohort, we defined that the expression of the human ortholog, *NT5C2*, positively correlates with waist-to-hip ratio and circulating triglycerides (Fig. 3.4 A). Similarly, the murine ortholog of the *C. elegans* DIO suppressor gene *pho-1*, named *Acp2*, has been characterized in one study. Comparably to the phenotypes observed in *C. elegans* treated with RNAi against *pho-1*, mice carrying a mutation in *Acp2* that impairs ACP2 acid phosphatase activity are smaller and gain less weight than the wild-type controls (Mannan et al., 2004). Further, using once again the METSIM cohort, we define that the expression of the human ortholog, *ACP2*, positively correlates with body weight and total triglycerides (Fig. 3.10). Interestingly, the function of *pho-1*-like genes in fat metabolism may be conserved even across kingdoms, as reduction of *ACP4* –the predominant ortholog of *pho-1* in Arabidopsis – leads to a decrease in total leaf lipids (Branen et al., 2003). The congruency of phenotypic effects between inactivation of *Y71H10B.1* and *pho-1* in *C. elegans* and their orthologs in mammals supports the notion that reduced function of these genes would be causally linked to obesity across animals. Further, the similarities

strengthen our confidence in the value of our nematode screening approach to defining which GWAS loci are causally linked to metabolic diseases including obesity.

However, the tight phenotypic correlation does not include all hits from our screen. Seemingly contradicting the obesity phenotype observed upon whole-body knock down of *eif-6* in *C. elegans* fed RD, *Eif6* heterozygous mice had reduced body weight gain compared to their wild-type littermates (Brina et al., 2015). Similarly, knock down of *zfh-2* in *C. elegans* leads to obesity in animals fed RD whereas heterozygous mutation of the mouse ortholog, *Zfhx3/Atbf1*, leads to reduced body weight gain (Sun et al., 2012). Nevertheless, it is difficult to evaluate the body weight phenotypes of *Eif6* and *Zfhx3* heterozygous mutant mice because these mutations lead to pleiotropic effects including perinatal mortality, growth retardation, and severe behavioral deficits (Brina et al., 2015; Sun et al., 2012), and neither body fat mass or even circulating triglycerides were reported in the single *in vivo* mouse mutant studies available to date. Furthermore, although not the case for *Eif6*, our analysis of the correlation between gene expression and metabolic traits in mice shows that reduced expression of *Zfhx3* is strongly associated with increased body fat, fat mass, and markers of metabolic syndrome including insulin sensitivity and high cholesterol (Fig. 3B). Therefore, the apparent contradictory effects of inactivating *eif-6* and *zfh-2* in *C. elegans* and their murine orthologs need further investigation.

In addition to the 3 previously characterized genes, we identified 14 *C. elegans* genes not yet causally linked to obesity. Further, the biological functions of most of these genes and their mammalian orthologs have not been fully elucidated. Nonetheless, some have been characterized to a level that enables us to propose hypotheses about their roles in fat storage. For instance, *KAT8* –the human ortholog of *C. elegans mys-1*– promotes acetylation of fatty acid synthase (FASN), which leads to reduced FASN activity (Lin et al., 2016). FASN is the terminal enzyme in *de novo* lipogenesis; therefore, it is reasonable to hypothesize that reduced *KAT8* activity might increase lipogenesis and hence promote obesity, a phenotype that would be in line with the obesity phenotype we describe here for KD of the *C. elegans* ortholog *mys-1*. Another example, *TCF7L2* –the human ortholog of *C. elegans pop-1*– has been shown as a key regulator in glucose homeostasis. It has been reported that overexpression of a nuclear isoform of *Tcf7l2* (mice ortholog) in high-fat diet-fed mice ameliorates hyperglycemia with improved glucose tolerance, while depletion of *Tcf7l2* in mice displays higher glucose levels and impairs glucose tolerance (Ip et al., 2015; Oh et al., 2012). Although the mechanism is not fully elucidated, impaired glucose homeostasis has been strongly associated with obesity in numerous studies (Abranches et al., 2015). The protective role of *Tcf7l2* in glucose homeostasis would imply a protective role in obesity, in line with our observation that knockdown of *pop-1* promotes obesity in *C. elegans*. Future studies on the role of *pop-1* in glucose homeostasis in *C. elegans* would demonstrate the function of *pop-1* and establish a causal link between obesity and glucose homeostasis.

In this study, we also characterized that knockdown of the 3 lean/DIO suppressor genes (*pho-1*, *let-767*, *Y71H10B.1*) improves the *C. elegans* healthspan and lifespan. One variant (rs75393320-C) that mapped to the human ortholog of *pho-1*, *ACP2*, has also been associated with changing HDL-C (Klarin et al., 2018). HDL-C has been suggested to have a protective role in the healthspan, especially in cardiovascular health (Brewer, 2004), suggesting a potential function of *ACP2* in cardiovascular health in mammals. With respect to *let-767*, its mammalian ortholog *HSD17B12* is a member of the hydroxysteroid dehydrogenase superfamily and is involved in the synthesis of arachidonic acid in lipid metabolism (Lima et al., 2013). As described in Fig. 3.4, *HSD17B12* is positively associated with LDL-C, and negatively associated with HDL-C, indicating a detrimental effect of *HSD17B12* in healthspan, in line with our observation that depletion of *let-767* improves the healthspan. Beside obesity and metabolic traits, 18 variants mapped to *HSD17B12* are associated with diseases-related traits (e.g. type 2 diabetes, cardiovascular disease, coronary artery diseases etc.) (www.ebi.ac.uk/gwas/). Interestingly, one variant (rs4755737) is associated with promoting longevity (Wright et al., 2019), suggesting the functions of *HSD17B12* in lifespan. A previous *in vitro* study showed that *HSD17B12* is a target of the miRNA MiR-152, which regulates cell proliferation, apoptosis and triglyceride levels in the mammary epithelial cells. In mice, *Hsd17b12* KO (Gt(A030E06)Wrst) mice do not survive beyond E8.5 stage, in line with the *C. elegans* developmental delay phenotype we observed, suggesting a conserved essential function in development (Rantakari et

al., 2010). Regarding the human ortholog of *Y71H10B.1 - NT5C2* - there are 77 variants mapped to *NT5C2* associated with a variety of the disease-related traits (beside obesity traits), including hypertension, abnormal blood pressure, coronary artery disease, and cardiovascular diseases (www.ebi.ac.uk/gwas/). Moreover, KO of *Nt5c2* (in mice) not only protects against high-fat diet induced weight gain and adiposity, but also improves insulin sensitivity and reduces hyperglycemia in mice (Johanns et al., 2019), in line with our observation on improving healthspan and lifespan in *C. elegans*.

C. elegans has been used as a simple animal model for uncovering and characterizing cellular and molecular functions of genes related to complex human diseases such as obesity. Despite significant differences with mammals including lack of specialized adipose tissue for fat storage (Srinivasan, 2015) and absence of key mammalian fat regulators such as leptin (Srinivasan et al., 2008), core metabolic pathways (e.g. Beta-oxidation) and signals regulating fat build-up and mobilization, fasting, healthspan and lifespan (e.g. insulin) are present in both *C. elegans* and mammalian (Uno and Nishida, 2016), and in some cases were first discovered in *C. elegans* and then supported by mammalian studies (e.g. DAF-16/FOXO, (Kenyon, 2011)). Clearly, there are caveats associated with using RNAi in a nematode model system to test human obesity variants. The caveats range from false negatives due to the distinct biology and anatomy of *C. elegans* and mammals –as described above– to the fact that some human variants would be gains of function whereas RNAi only enables loss of function. Nevertheless, as

demonstrated in this study, combining gene candidate generation from human GWAS with testing causality via *in vivo* RNAi in *C. elegans* can aid in identifying genes contributing to complex human diseases such as obesity.

Figure 3. 10

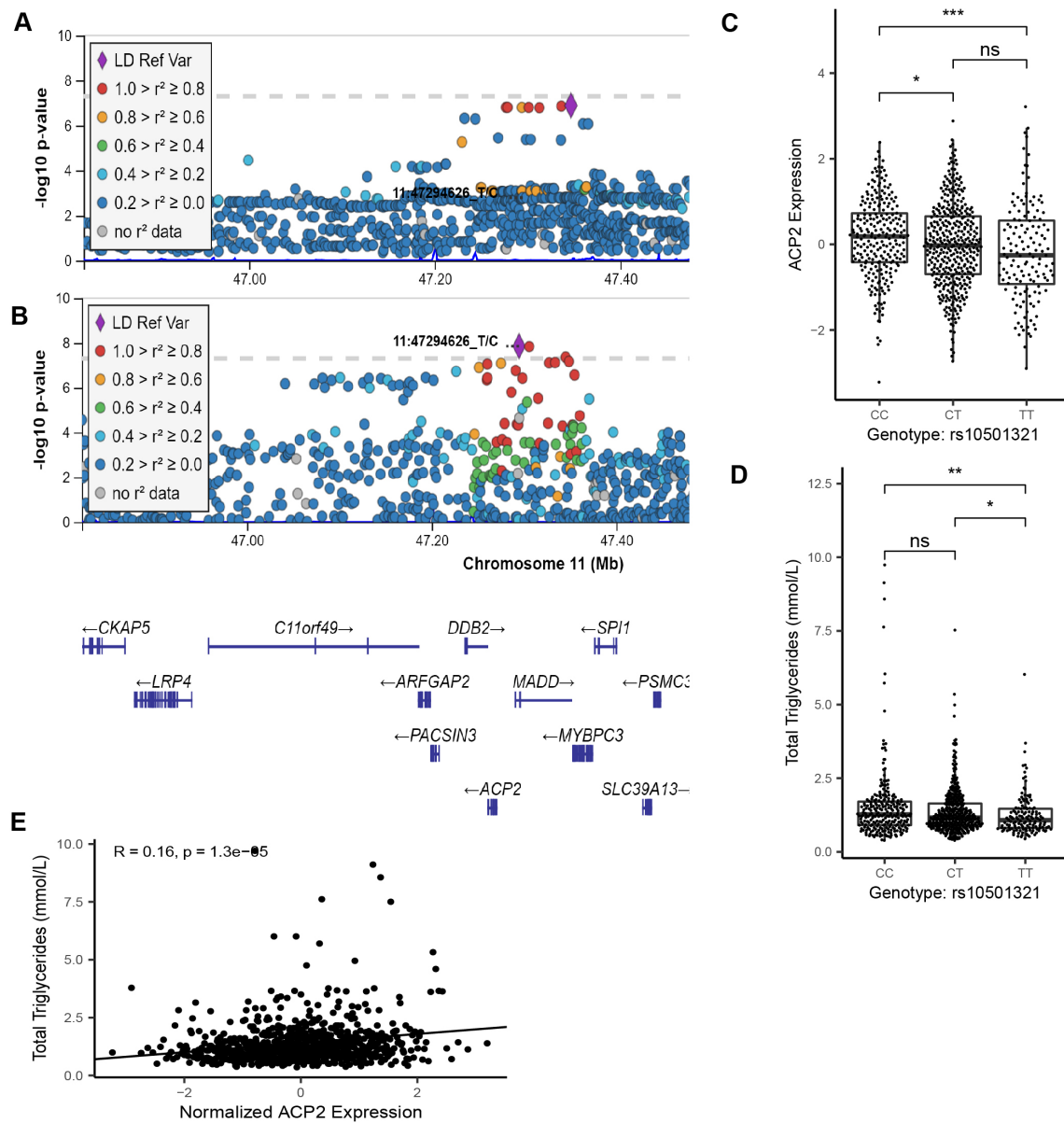


Figure 3.10

LocusZoom plots of the associations of the SNPs near *ACP2* with **(A)** BMI and **(B)** *ACP2* gene expression in subcutaneous adipose tissue in the METSIM cohort. The effect of the alleles of rs10501321 on **(C)** *ACP2* expression and **(D)** total triglycerides. **(E)** Correlation between BMI and *ACP2* (human *pho-1* ortholog) expression in the METSIM cohort.

3.6 Tables

Table 3. 1

Human GWAS obesity genes and *C. elegans* orthologs from meta-analysis

GWAS loci	Unique Human Loci ID number *	<i>C. elegans</i> gene name	<i>C. elegans</i> locus ID	<i>C. elegans</i> Unique Gene ID Number *
Validated Hits				
ACP2	2	<i>pho-1</i>	EGAP2.3	84
HSD17B12	143	<i>let-767</i>	C56G2.6	76
NT5C2	212	None	Y71H10B.1	360
ADAMTS9	3	<i>gon-1</i>	F25H8.3	132
DHX33	63	<i>let-355</i>	T05E8.3	277
EIF6	73	<i>eif-6</i>	C47B2.5	71
KAT8	154	<i>mys-1</i>	VC5.4	309
GNL3	105	<i>nst-1</i>	K01C8.9	216
POLR1D	233	<i>rpac-19</i>	F58A4.9	199
PSMC3	241	<i>rpt-5</i>	F56H1.4	193
PUM2	245	<i>puf-8</i>	C30G12.7	54
PUM2	245	<i>fbf-2</i>	F21H12.5	123
RRP12	259	None	Y46E12BL.2	333
EYS	80	<i>glp-1</i>	K07D8.1	231
NOTCH4	209	<i>glp-1</i>	K07D8.1	231
TCF12	294	<i>hlh-2</i>	M05B5.5	251
TCF7L2	295	<i>pop-1</i>	W10C8.2	319
ZFHX3	332	<i>zfh-2</i>	ZC123.3	369
Primary Hits				
MTCH2	195	<i>mtch-1</i>	F43E2.7	164
FMO1	92	None	C46H11.2	70
EYS	80	<i>mup-4</i>	K07D8.1	231
NOTCH4	209	<i>mup-4</i>	K07D8.1	231
HSPA1B	144	<i>hsp-4</i>	F43E2.8	165
PCK1	221	<i>pck-2</i>	R11A5.4	267
TAP2	291	<i>haf-8</i>	Y57G11C.1	352
TMEM245	305	None	M01F1.4	247
ZNF142	334	<i>hbl-1</i>	F13D11.2	106
Non-hits				

GWAS loci	Unique Human Loci ID number *	<i>C. elegans</i> gene name	<i>C. elegans</i> locus ID	<i>C. elegans</i> Unique Gene ID Number *
ABHD16A	1	<i>None</i>	<i>F37A4.1</i>	150
ACP2	2	<i>pho-5</i>	<i>B0361.7</i>	8
ACP2	2	<i>pho-10</i>	<i>C05C10.1</i>	24
ACP2	2	<i>pho-11</i>	<i>C05C10.4</i>	25
ACP2	2	<i>None</i>	<i>C27A2.12</i>	47
ACP2	2	<i>pho-12</i>	<i>C27A2.4</i>	48
ACP2	2	<i>pho-13</i>	<i>F07H5.9</i>	90
ACP2	2	<i>acp-5</i>	<i>F13D11.1</i>	105
ACP2	2	<i>acp-3</i>	<i>F14E5.3</i>	111
ACP2	2	<i>acp-2</i>	<i>F14E5.4</i>	112
ACP2	2	<i>acp-4</i>	<i>F14E5.6</i>	113
ACP2	2	<i>None</i>	<i>F26C11.1</i>	133
ACP2	2	<i>pho-14</i>	<i>T13B5.3</i>	285
ACP2	2	<i>pho-4</i>	<i>T16D1.2</i>	288
ACP2	2	<i>acp-1</i>	<i>ZK563.6</i>	382
ADCY3	4	<i>acy-2</i>	<i>C10F3.3</i>	37
ADCY3	4	<i>acy-3</i>	<i>C44F1.5</i>	66
ADCY3	4	<i>acy-4</i>	<i>T01C2.1</i>	272
ADCY9	5	<i>acy-1</i>	<i>F17C8.1</i>	118
AIF1	6	<i>None</i>	<i>None</i>	N/A
AK5	7	<i>None</i>	<i>C29F7.3</i>	52
AK5	7	<i>None</i>	<i>F13E6.2</i>	108
AK5	7	<i>None</i>	<i>F38B2.4</i>	155
AK5	7	<i>None</i>	<i>F40F8.1</i>	157
ALAS1	8	<i>None</i>	<i>T25B9.1</i>	299
ALDH2	9	<i>alh-1</i>	<i>F54D8.3</i>	187
ALDH2	9	<i>alh-2</i>	<i>K04F1.15</i>	222
ALKBH1	10	<i>None</i>	<i>Y51H7C.5</i>	340
AMIGO1	11	<i>None</i>	<i>None</i>	N/A
ARL3	12	<i>arl-3</i>	<i>F19H8.3</i>	121
ASCC2	13	<i>None</i>	<i>None</i>	N/A
ATF6B	14	<i>atf-6</i>	<i>F45E6.2</i>	170
ATRAID	15	<i>None</i>	<i>None</i>	N/A
ATXN1	16	<i>None</i>	<i>K04F10.1</i>	223
ATXN2L	17	<i>atx-2</i>	<i>D2045.1</i>	81
AUTS2	18	<i>None</i>	<i>None</i>	N/A

GWAS loci	Unique Human Loci ID number *	<i>C. elegans</i> gene name	<i>C. elegans</i> locus ID	<i>C. elegans</i> Unique Gene ID Number *
BAG6	19	None	None	N/A
BBS4	20	<i>bbs-4</i>	F58A4.14	198
BDNF	21	None	None	N/A
BORCS7	22	None	None	N/A
BPTF	23	<i>nurf-1</i>	F26H11.2	136
BRINP3	24	None	None	N/A
BRMS1	25	None	None	N/A
BUB3	26	<i>bub-3</i>	Y54G9A.6	347
C10orf32-ASMT	27	None	None	N/A
C1QTNF4	28	None	None	N/A
C6orf48	29	None	None	N/A
CACNB2	30	<i>ccb-1</i>	T28F2.5	306
CACNB2	30	<i>ccb-2</i>	W10C8.1	318
CADM2	31	<i>rig-5</i>	C36F7.4	59
CALCRL	32	<i>pdfr-1</i>	C13B9.4	39
CALCRL	32	ZK643.3	ZK643.3	384
CAMK1D	33	<i>cmk-1</i>	K07A9.2	230
CASD1	34	None	None	N/A
CAST	35	None	None	N/A
CBLN4	36	None	None	N/A
CBX3	37	<i>hpl-2</i>	K01G5.2	217
CBX3	37	<i>hpl-1</i>	K08H2.6	237
CCDC92	38	None	K01A2.10	214
CCK	39	None	None	N/A
CDC123	40	None	None	N/A
CDK2AP1	41	None	Y43F4B.10	330
CDKAL1	42	None	F25B5.5	128
CDKAL1	42	None	Y92H12BL.1	367
CDKN2B-AS1	43	None	None	N/A
CEP120	44	None	None	N/A
CEP70	45	None	None	N/A
CETP	46	None	None	N/A
CLIC1	47	<i>exl-1</i>	F26H11.5	137
CLIC1	47	<i>exc-4</i>	Y105E8A.22	320
CLIP1	48	<i>clip-1</i>	M01A8.2	246
CLSTN2	49	<i>casy-1</i>	B0034.3	2

GWAS loci	Unique Human Loci ID number *	<i>C. elegans</i> gene name	<i>C. elegans</i> locus ID	<i>C. elegans</i> Unique Gene ID Number *
CLUAP1	50	<i>dyf-3</i>	<i>C04C3.5</i>	18
CMPK1	51	None	<i>C29F7.3</i>	52
CMPK1	51	None	<i>F38B2.4</i>	155
CMPK1	51	None	<i>F40F8.1</i>	157
COBLL1	52	None	None	N/A
COPZ2	53	<i>copz-1</i>	<i>F59E10.3</i>	205
CPEB4	54	<i>cpb-2</i>	<i>C30B5.3</i>	53
CPEB4	54	<i>cpb-1</i>	<i>C40H1.1</i>	61
CPEB4	54	<i>fog-1</i>	<i>Y54E10A.4</i>	343
CPNE1	55	<i>cpna-2</i>	<i>B0228.4</i>	5
CPNE1	55	<i>gem-4</i>	<i>T12A7.1</i>	284
CPNE1	55	<i>nra-1</i>	<i>T28F3.1</i>	307
CRLS1	56	<i>crls-1</i>	<i>F23H11.9</i>	125
CSNK2B	57	<i>kin-10</i>	<i>T01G9.6</i>	273
CTDSP1	58	<i>scpl-1</i>	<i>B0379.4</i>	9
CWC22	59	<i>let-858</i>	<i>F33A8.1</i>	146
CYB561D1	60	None	None	N/A
CYP19A1	61	None	None	N/A
CYP27A1	62	None	<i>ZK177.4</i>	375
CYP27A1	62	<i>cyp-44A1</i>	<i>ZK177.5</i>	376
DMD	64	<i>dys-1</i>	<i>F15D3.1</i>	114
DMRTA1	65	<i>dmd-5</i>	<i>F10C1.5</i>	96
DNAJB4	66	<i>dnj-13</i>	<i>F54D5.8</i>	186
DNAJC27	67	None	None	N/A
DUSP9	68	<i>lip-1</i>	<i>C05B10.1</i>	22
DUSP9	68	<i>F13D11.3</i>	<i>F13D11.3</i>	107
EBF1	69	<i>unc-3</i>	<i>Y16B4A.1</i>	322
ECHDC1	70	None	<i>C32E8.9</i>	55
EDEM2	71	None	<i>C47E12.3</i>	72
EDEM2	71	None	<i>F10C2.5</i>	97
EHBP1	72	<i>ehbp-1</i>	<i>F25B3.1</i>	127
ENSA	74	<i>ensa-1</i>	<i>K10C3.2</i>	239
EPB41L1	75	<i>frm-1</i>	<i>ZK270.2</i>	378
ERAP1	76	None	<i>F49B2.6</i>	180
ERAP1	76	None	<i>T07F10.1</i>	279
EXOC6	77	<i>sec-15</i>	<i>C28G1.3</i>	49

GWAS loci	Unique Human Loci ID number *	<i>C. elegans</i> gene name	<i>C. elegans</i> locus ID	<i>C. elegans</i> Unique Gene ID Number *
EYA1	78	<i>eya-1</i>	C49A1.4	73
EYA2	79	<i>eya-1</i>	C49A1.4	73
EYS	80	<i>glp-1</i>	F02A9.6	87
EYS	80	<i>crb-1</i>	F11C7.4	102
EYS	80	<i>agr-1</i>	F41G3.12	161
EYS	80	<i>mua-3</i>	K08E5.3	236
EYS	80	<i>lin-12</i>	R107.8	262
EYS	80	None	T19D12.6	291
EYS	80	<i>fbn-1</i>	ZK783.1	385
FAIM2	81	<i>xbx-6</i>	F40F9.1	158
FAIM2	81	<i>tag-120</i>	F40F9.2	159
FAIM2	81	None	Y42H9AR.2	329
FAM101B	82	None	None	N/A
FAM150B	83	None	None	N/A
FAM159B	84	None	None	N/A
FAM47E	85	None	None	N/A
FAM58A	86	<i>ccnk-1</i>	F43D2.1	162
FAM60A	87	None	None	N/A
FCER1A	88	None	None	N/A
FGFR2	89	<i>egl-15</i>	F58A3.2	197
FGR	90	<i>src-2</i>	F49B2.5	179
FGR	90	<i>src-1</i>	Y92H12A.1	366
FGR,IFI6	91	None	None	N/A
FMO1	92	None	C01H6.4	14
FMO1	92	<i>fmo-4</i>	F53F4.5	184
FMO1	92	<i>fmo-5</i>	H24K24.5	209
FMO1	92	<i>fmo-1</i>	K08C7.2	232
FMO1	92	<i>fmo-2</i>	K08C7.5	233
FMO1	92	<i>fmo-3</i>	Y39A1A.19	326
FNBP4	93	None	None	N/A
FOXO3	94	<i>daf-16</i>	R13H8.1	270
FRAT2	95	None	None	N/A
FTO	96	None	None	N/A
FTO	96	None	None	N/A
FYCO1	97	<i>rabn-5</i>	F01F1.4	85
FYCO1	97	<i>eea-1</i>	T10G3.5	281

GWAS loci	Unique Human Loci ID number *	<i>C. elegans</i> gene name	<i>C. elegans</i> locus ID	<i>C. elegans</i> Unique Gene ID Number *
<i>GABRG1</i>	98	<i>ggr-1</i>	<i>C09G5.1</i>	35
<i>GABRG1</i>	98	<i>lgc-41</i>	<i>C39B10.2</i>	60
<i>GABRG1</i>	98	<i>lgc-43</i>	<i>C43F9.9</i>	64
<i>GABRG1</i>	98	<i>ggr-2</i>	<i>C45B2.4</i>	68
<i>GABRG1</i>	98	<i>lgc-48</i>	<i>C50B6.11</i>	74
<i>GABRG1</i>	98	<i>acc-2</i>	<i>C53D6.3</i>	75
<i>GABRG1</i>	98	<i>lgc-36</i>	<i>F07B10.5</i>	89
<i>GABRG1</i>	98	<i>ggr-3</i>	<i>F09C12.1</i>	94
<i>GABRG1</i>	98	<i>lgc-39</i>	<i>F09G2.5</i>	95
<i>GABRG1</i>	98	<i>lgc-51</i>	<i>F12B6.3</i>	103
<i>GABRG1</i>	98	<i>lgc-44</i>	<i>F46F3.2</i>	173
<i>GABRG1</i>	98	<i>lgc-47</i>	<i>F47A4.1</i>	174
<i>GABRG1</i>	98	<i>acc-3</i>	<i>F55D10.5</i>	189
<i>GABRG1</i>	98	<i>acc-1</i>	<i>F58G6.4</i>	202
<i>GABRG1</i>	98	<i>exp-1</i>	<i>H35N03.1</i>	211
<i>GABRG1</i>	98	<i>mod-1</i>	<i>K06C4.6</i>	229
<i>GABRG1</i>	98	<i>lgc-49</i>	<i>K10D6.1</i>	241
<i>GABRG1</i>	98	<i>lgc-54</i>	<i>T15B7.16</i>	287
<i>GABRG1</i>	98	<i>lgc-50</i>	<i>T20B12.9</i>	292
<i>GABRG1</i>	98	<i>lgc-53</i>	<i>T21F2.1</i>	294
<i>GABRG1</i>	98	<i>lgc-40</i>	<i>T24D8.1</i>	298
<i>GABRG1</i>	98	<i>acc-4</i>	<i>T27E9.9</i>	302
<i>GABRG1</i>	98	<i>lgc-55</i>	<i>Y113G7A.5</i>	321
<i>GABRG1</i>	98	<i>lgc-42</i>	<i>Y39A3B.2</i>	327
<i>GABRG1</i>	98	<i>lgc-35</i>	<i>Y46G5A.26</i>	334
<i>GABRG1</i>	98	<i>lgc-46</i>	<i>Y71D11A.5</i>	359
<i>GABRG1</i>	98	<i>lgc-52</i>	<i>Y73F8A.2</i>	363
<i>GABRG1</i>	98	<i>lgc-37</i>	<i>ZC482.5</i>	371
<i>GALNT10</i>	99	<i>gly-10</i>	<i>Y45F10D.3</i>	332
<i>GAPVD1</i>	100	<i>rme-6</i>	<i>F49E7.1</i>	182
<i>GCLC</i>	101	<i>gcs-1</i>	<i>F37B12.2</i>	153
<i>GIPC2</i>	102	<i>gipc-1</i>	<i>C35D10.2</i>	58
<i>GIPC2</i>	102	<i>gipc-2</i>	<i>F44D12.4</i>	167
<i>GIPR</i>	103	<i>pdfr-1</i>	<i>C13B9.4</i>	39
<i>GLIPR2</i>	104	None	<i>C07A4.2</i>	30
<i>GLIPR2</i>	104	None	<i>C07A4.3</i>	31

GWAS loci	Unique Human Loci ID number *	<i>C. elegans</i> gene name	<i>C. elegans</i> locus ID	<i>C. elegans</i> Unique Gene ID Number *
GLIPR2	104	<i>None</i>	<i>D2062.1</i>	82
GLIPR2	104	<i>None</i>	<i>F09B9.5</i>	93
GLIPR2	104	<i>None</i>	<i>F57B7.2</i>	194
GNPDA2	106	<i>None</i>	<i>T03F6.3</i>	276
GON4L	107	<i>gon-4</i>	<i>K04D7.5</i>	221
GP2	108	<i>None</i>	<i>None</i>	N/A
GPANK1	109	<i>None</i>	<i>ZK1320.7</i>	374
GPC6	110	<i>None</i>	<i>C03H12.1</i>	17
GPC6	110	<i>gpn-1</i>	<i>F59D12.4</i>	204
GPR101	111	<i>npr-8</i>	<i>C56G3.1</i>	77
GPR101	111	<i>None</i>	<i>F59D12.1</i>	203
GPR139	112	<i>None</i>	<i>B0334.6</i>	7
GPR26	113	<i>None</i>	<i>None</i>	N/A
GPRC5B	114	<i>None</i>	<i>None</i>	N/A
GRAMD3	115	<i>None</i>	<i>ZC328.3</i>	370
GRB14	116	<i>mig-10</i>	<i>F10E9.6</i>	98
GRM4	117	<i>mgl-2</i>	<i>F45H11.4</i>	171
GRM4	117	<i>mgl-3</i>	<i>Y4C6A.2</i>	338
GRM4	117	<i>mgl-1</i>	<i>ZC506.4</i>	372
GSDMB	118	<i>None</i>	<i>None</i>	N/A
GSTM3	119	<i>gst-16</i>	<i>F37B1.5</i>	152
GSTM3	119	<i>gst-25</i>	<i>F37F2.3</i>	154
GSTM3	119	<i>gst-1</i>	<i>R107.7</i>	261
GSTM3	119	<i>gst-41</i>	<i>R13D7.7</i>	269
GSTM3	119	<i>gst-23</i>	<i>T28A11.11</i>	303
HERC4	120	<i>herc-1</i>	<i>Y48G8AL.1</i>	336
HERPUD1	121	<i>tag-353</i>	<i>F25D7.2</i>	129
HHEX	122	<i>pha-2</i>	<i>M6.3</i>	254
HHEX	122	<i>ceh-45</i>	<i>ZK993.1</i>	386
HIF1AN	123	<i>jmid-5</i>	<i>C06H2.3</i>	28
HIRIP3	124	<i>None</i>	<i>None</i>	N/A
HLA-B	125	<i>None</i>	<i>None</i>	N/A
HLA-DMA	126	<i>None</i>	<i>None</i>	N/A
HLA-DOB	127	<i>None</i>	<i>None</i>	N/A
HLA-DRA	128	<i>None</i>	<i>None</i>	N/A
HLA-DRB5	129	<i>None</i>	<i>None</i>	N/A

GWAS loci	Unique Human Loci ID number *	<i>C. elegans</i> gene name	<i>C. elegans</i> locus ID	<i>C. elegans</i> Unique Gene ID Number *
<i>HMGA1</i>	130	<i>None</i>	<i>None</i>	N/A
<i>HMGCR</i>	131	<i>hmgr-1</i>	<i>F08F8.2</i>	91
<i>HNF4G</i>	132	<i>nhr-35</i>	<i>C07A12.3</i>	29
<i>HNF4G</i>	132	<i>nhr-64</i>	<i>C45E1.1</i>	69
<i>HNF4G</i>	132	<i>nhr-49</i>	<i>K10C3.6</i>	240
<i>HNF4G</i>	132	<i>nhr-14</i>	<i>T01B10.4</i>	271
<i>HNF4G</i>	132	<i>nhr-69</i>	<i>T23H4.2</i>	297
<i>HNRNPLL</i>	133	<i>None</i>	<i>C44B7.2</i>	65
<i>HOXA5</i>	134	<i>lin-39</i>	<i>C07H6.7</i>	32
<i>HOXA5</i>	134	<i>mab-5</i>	<i>C08C3.3</i>	33
<i>HOXA6</i>	135	<i>lin-39</i>	<i>C07H6.7</i>	32
<i>HOXA6</i>	135	<i>mab-5</i>	<i>C08C3.3</i>	33
<i>HOXA6</i>	135	<i>ceh-16</i>	<i>C13G5.1</i>	40
<i>HOXB2</i>	136	<i>vab-7</i>	<i>M142.4</i>	252
<i>HOXB2</i>	136	<i>ceh-13</i>	<i>R13A5.5</i>	268
<i>HOXB3</i>	137	<i>mab-5</i>	<i>C08C3.3</i>	33
<i>HOXB3</i>	137	<i>vab-7</i>	<i>M142.4</i>	252
<i>HOXB3</i>	137	<i>ceh-13</i>	<i>R13A5.5</i>	268
<i>HOXB4</i>	138	<i>lin-39</i>	<i>C07H6.7</i>	32
<i>HOXB4</i>	138	<i>mab-5</i>	<i>C08C3.3</i>	33
<i>HOXB4</i>	138	<i>ceh-16</i>	<i>C13G5.1</i>	40
<i>HOXB4</i>	138	<i>vab-15</i>	<i>R07B1.1</i>	258
<i>HOXB5</i>	139	<i>lin-39</i>	<i>C07H6.7</i>	32
<i>HOXB5</i>	139	<i>mab-5</i>	<i>C08C3.3</i>	33
<i>HOXC4</i>	140	<i>lin-39</i>	<i>C07H6.7</i>	32
<i>HOXC4</i>	140	<i>mab-5</i>	<i>C08C3.3</i>	33
<i>HOXC4</i>	140	<i>ceh-16</i>	<i>C13G5.1</i>	40
<i>HOXC8</i>	141	<i>mab-5</i>	<i>C08C3.3</i>	33
<i>HSD17B10</i>	142	<i>ard-1</i>	<i>F01G4.2</i>	86
<i>HSD17B12</i>	143	<i>dhs-27</i>	<i>C04F6.5</i>	19
<i>HSD17B12</i>	143	<i>stdh-1</i>	<i>C06B3.4</i>	26
<i>HSD17B12</i>	143	<i>stdh-3</i>	<i>C06B3.5</i>	27
<i>HSD17B12</i>	143	<i>stdh-2</i>	<i>F11A5.12</i>	99
<i>HSD17B12</i>	143	<i>stdh-4</i>	<i>F25G6.5</i>	130
<i>HSD17B12</i>	143	<i>dhs-5</i>	<i>F56D1.5</i>	191
<i>HSPA1B</i>	144	<i>hsp-70</i>	<i>C12C8.1</i>	38

GWAS loci	Unique Human Loci ID number *	<i>C. elegans</i> gene name	<i>C. elegans</i> locus ID	<i>C. elegans</i> Unique Gene ID Number *
<i>HSPA1B</i>	144	<i>hsp-3</i>	<i>C15H9.6</i>	44
<i>HSPA1B</i>	144	<i>hsp-1</i>	<i>F26D10.3</i>	134
<i>HSPA1B</i>	144	<i>None</i>	<i>F44E5.4</i>	168
<i>HSPA1B</i>	144	<i>None</i>	<i>F44E5.5</i>	169
<i>HUWE1</i>	145	<i>eel-1</i>	<i>Y67D8C.5</i>	356
<i>IGF2BP2</i>	146	<i>zbp-1</i>	<i>M88.5</i>	255
<i>IL13RA1</i>	147	<i>None</i>	<i>None</i>	N/A
<i>IL27</i>	148	<i>None</i>	<i>None</i>	N/A
<i>INO80E</i>	149	<i>None</i>	<i>None</i>	N/A
<i>ITGAM</i>	150	<i>None</i>	<i>None</i>	N/A
<i>ITIH4</i>	151	<i>None</i>	<i>None</i>	N/A
<i>JADE2</i>	152	<i>phf-15</i>	<i>Y53G8AR.2</i>	342
<i>JUND</i>	153	<i>None</i>	<i>None</i>	N/A
<i>KAT8</i>	154	<i>mys-2</i>	<i>K03D10.3</i>	220
<i>KCNQ1</i>	155	<i>kqt-3</i>	<i>Y54G9A.3</i>	346
<i>KIAA1429</i>	156	<i>None</i>	<i>None</i>	N/A
<i>KIAA1683</i>	157	<i>None</i>	<i>None</i>	N/A
<i>KLHL31</i>	158	<i>None</i>	<i>None</i>	N/A
<i>KNOP1</i>	159	<i>None</i>	<i>None</i>	N/A
<i>LILRB5</i>	160	<i>None</i>	<i>None</i>	N/A
<i>LIN7C</i>	161	<i>lin-7</i>	<i>Y54G11A.10</i>	345
<i>LINC00461</i>	162	<i>None</i>	<i>None</i>	N/A
<i>LINC00558</i>	163	<i>None</i>	<i>None</i>	N/A
<i>LINC01065</i>	164	<i>None</i>	<i>None</i>	N/A
<i>LINC01111</i>	165	<i>None</i>	<i>None</i>	N/A
<i>LINC01122</i>	166	<i>None</i>	<i>None</i>	N/A
<i>LINC01289</i>	167	<i>None</i>	<i>None</i>	N/A
<i>LINC01392</i>	168	<i>None</i>	<i>None</i>	N/A
<i>LINC01441</i>	169	<i>None</i>	<i>None</i>	N/A
<i>LLGL1</i>	170	<i>lgl-1</i>	<i>F56F10.4</i>	192
<i>LMO1</i>	171	<i>None</i>	<i>C26C6.6</i>	46
<i>LMO1</i>	171	<i>ttx-3</i>	<i>C40H5.5</i>	62
<i>LMO1</i>	171	<i>None</i>	<i>Y65B4A.7</i>	355
<i>LOC101927421</i>	172	<i>None</i>	<i>None</i>	N/A
<i>LOC101928435</i>	173	<i>None</i>	<i>None</i>	N/A
<i>LOC101928778</i>	174	<i>None</i>	<i>None</i>	N/A

GWAS loci	Unique Human Loci ID number *	<i>C. elegans</i> gene name	<i>C. elegans</i> locus ID	<i>C. elegans</i> Unique Gene ID Number *
LOC101929596	175	None	None	N/A
LOC102724612	176	None	None	N/A
LOC400867	177	None	None	N/A
LRP1B	178	None	F14B4.1	110
LRP1B	178	<i>lrp-1</i>	F29D11.1	142
LRP1B	178	<i>lrp-2</i>	T21E3.3	293
LSM14A	179	<i>car-1</i>	Y18D10A.17	323
LY75	180	<i>clec-51</i>	B0218.6	3
LY75	180	<i>clec-52</i>	B0218.8	4
LY75	180	<i>clec-48</i>	C14A6.1	41
LY75	180	<i>clec-148</i>	F40G9.10	160
LY75	180	<i>clec-53</i>	T03F1.10	275
LY75	180	<i>clec-49</i>	W04E12.6	313
LY75	180	<i>clec-50</i>	W04E12.8	314
LY86	181	None	None	N/A
LYPLAL1	182	<i>ath-1</i>	K04G2.5	226
MAP2K5	183	None	None	N/A
MAP3K12	184	<i>dlk-1</i>	F33E2.2	147
MAPKAP1	185	<i>sinh-1</i>	Y57A10A.20	351
MAPKAPK5-AS1	186	None	None	N/A
MC4R	187	None	None	N/A
MDH1	188	<i>mdh-1</i>	F46E10.10	172
MEGF9	189	None	VC5.2	308
METTL18	190	None	K01A11.2	213
MIR5694	191	None	None	N/A
MLL5	192	None	None	N/A
MRGPRF	193	None	None	N/A
MRPL54	194	<i>mrpl-54</i>	F25H5.6	131
MTIF3	196	None	None	N/A
MXD3	197	<i>mdl-1</i>	R03E9.1	256
MYO9A	198	<i>hum-7</i>	F56A6.2	190
NAAA	199	<i>asah-1</i>	K11D2.2	242
NAAA	199	None	Y55D5A.3	348
NCOA1	200	None	None	N/A
NEK4	201	None	None	N/A

GWAS loci	Unique Human Loci ID number *	<i>C. elegans</i> gene name	<i>C. elegans</i> locus ID	<i>C. elegans</i> Unique Gene ID Number *
NEO1	202	<i>unc-40</i>	T19B4.7	290
NFATC2IP	203	None	None	N/A
NID2	204	<i>nid-1</i>	F54F3.1	188
NIPSNAP1	205	None	K02D10.1	218
NISCH	206	None	F13E9.1	109
NLRC3	207	None	None	N/A
NLRP1	208	None	None	N/A
NOTCH4	209	<i>glp-1</i>	F02A9.6	87
NOTCH4	209	<i>crb-1</i>	F11C7.4	102
NOTCH4	209	<i>clec-78</i>	F47C12.2	175
NOTCH4	209	<i>mua-3</i>	K08E5.3	236
NOTCH4	209	<i>lin-12</i>	R107.8	262
NOTCH4	209	<i>fbn-1</i>	ZK783.1	385
NRBP1	210	<i>hpo-11</i>	H37N21.1	212
NRXN1	211	<i>nrx-1</i>	C29A12.4	51
NRXN1	211	<i>itx-1</i>	W03D8.6	311
NT5DC2	213	None	None	N/A
NTRK2	214	<i>cam-1</i>	C01G6.8	13
NTRK2	214	<i>ddr-1</i>	C25F6.4	45
NTRK2	214	<i>trk-1</i>	D1073.1	80
NUP88	215	None	None	N/A
NUPR1	216	None	None	N/A
NUTM2F	217	None	None	N/A
PACS1	218	<i>tag-232</i>	T18H9.7	289
PAX2	219	<i>egl-38</i>	C04G2.7	20
PAX2	219	<i>npax-2</i>	F48B9.5	177
PAX2	219	<i>pax-2</i>	K06B9.5	228
PBX2	220	<i>ceh-40</i>	F17A2.5	117
PBX2	220	<i>ceh-60</i>	F22A3.5	124
PBX2	220	<i>ceh-20</i>	F31E3.1	143
PCK1	221	<i>pck-3</i>	H04M03.1	206
PCK1	221	<i>pck-1</i>	W05G11.6	315
PCSK1	222	<i>kpc-1</i>	F11A6.1	100
PCSK1	222	<i>bli-4</i>	K04F10.4	224
PDZK1IP1	223	None	None	N/A
PEMT	224	None	None	N/A

GWAS loci	Unique Human Loci ID number *	<i>C. elegans</i> gene name	<i>C. elegans</i> locus ID	<i>C. elegans</i> Unique Gene ID Number *
<i>PEPD</i>	225	None	<i>K12C11.1</i>	245
<i>PEPD</i>	225	None	<i>R119.2</i>	264
<i>PEPD</i>	225	<i>pqn-59</i>	<i>R119.4</i>	265
<i>PEX6</i>	226	<i>prx-6</i>	<i>F39G3.7</i>	156
<i>PGPEP1</i>	227	None	<i>F16H6.7</i>	115
<i>PGPEP1</i>	227	None	<i>F35F10.6</i>	148
<i>PGPEP1</i>	227	None	<i>M04C9.1</i>	248
<i>PGPEP1</i>	227	None	<i>M04C9.2</i>	249
<i>PGPEP1</i>	227	None	<i>M04C9.3</i>	250
<i>PLA2R1</i>	228	<i>clec-51</i>	<i>B0218.6</i>	3
<i>PLA2R1</i>	228	<i>clec-52</i>	<i>B0218.8</i>	4
<i>PLA2R1</i>	228	<i>clec-48</i>	<i>C14A6.1</i>	41
<i>PLA2R1</i>	228	<i>clec-148</i>	<i>F40G9.10</i>	160
<i>PLA2R1</i>	228	<i>clec-53</i>	<i>T03F1.10</i>	275
<i>PLA2R1</i>	228	<i>clec-49</i>	<i>W04E12.6</i>	313
<i>PLA2R1</i>	228	<i>clec-50</i>	<i>W04E12.8</i>	314
<i>PLCD4</i>	229	<i>plc-4</i>	<i>R05G6.8</i>	257
<i>PMAIP1</i>	230	None	None	N/A
<i>PNPO</i>	231	None	<i>F57B9.1</i>	195
<i>POC5</i>	232	None	None	N/A
<i>PPM1M</i>	234	None	<i>C42C1.2</i>	63
<i>PRDM6</i>	235	None	<i>F47E1.3</i>	176
<i>PRKD3</i>	236	<i>dkf-2</i>	<i>T25E12.4</i>	300
<i>PRKD3</i>	236	<i>dkf-1</i>	<i>W09C5.5</i>	317
<i>PROCR</i>	237	None	None	N/A
<i>PRRC2A</i>	238	None	<i>F52G3.1</i>	183
<i>PRRX1</i>	239	<i>ceh-17</i>	<i>D1007.1</i>	78
<i>PRRX1</i>	239	<i>unc-42</i>	<i>F58E6.10</i>	200
<i>PRRX1</i>	239	<i>alr-1</i>	<i>R08B4.2</i>	260
<i>PSMB9</i>	240	<i>pbs-1</i>	<i>K08D12.1</i>	235
<i>PSMD5</i>	242	None	<i>F35G12.12</i>	149
<i>PSME4</i>	243	None	<i>C14C10.5</i>	42
<i>PSME4</i>	243	None	<i>T28B8.3</i>	304
<i>PSME4</i>	243	None	<i>T28B8.4</i>	305
<i>PSORS1C1</i>	244	None	None	N/A
<i>PUM2</i>	245	<i>puf-7</i>	<i>B0273.2</i>	6

GWAS loci	Unique Human Loci ID number *	<i>C. elegans</i> gene name	<i>C. elegans</i> locus ID	<i>C. elegans</i> Unique Gene ID Number *
<i>PUM2</i>	245	<i>puf-6</i>	<i>F18A11.1</i>	120
<i>PUM2</i>	245	<i>puf-5</i>	<i>F54C9.8</i>	185
<i>PUM2</i>	245	<i>fbf-1</i>	<i>H12I13.4</i>	207
<i>PUM2</i>	245	<i>puf-4</i>	<i>M4.2</i>	253
<i>PUM2</i>	245	<i>puf-9</i>	<i>W06B11.2</i>	316
<i>PUM2</i>	245	<i>puf-3</i>	<i>Y45F10A.2</i>	331
<i>PUM2</i>	245	<i>puf-11</i>	<i>Y73B6BL.38</i>	362
<i>QPCT</i>	246	None	<i>H27A22.1</i>	210
<i>RABEP1</i>	247	<i>rabn-5</i>	<i>F01F1.4</i>	85
<i>RASL11A</i>	248	None	None	N/A
<i>RBMS1</i>	249	<i>F32B4.4</i>	<i>F32B4.4</i>	144
<i>RBMS1</i>	249	None	None	N/A
<i>RBMS1</i>	249	<i>sup-26</i>	<i>R10E4.2</i>	263
<i>RFT1</i>	250	None	<i>ZK180.3</i>	377
<i>RFX7</i>	251	None	None	N/A
<i>RGS17</i>	252	<i>rgs-1</i>	<i>C05B5.7</i>	23
<i>RGS17</i>	252	<i>rgs-2</i>	<i>F16H9.1</i>	116
<i>RGS7BP</i>	253	None	None	N/A
<i>RIT2,SYT4</i>	254	None	None	N/A
<i>RPAIN</i>	255	None	None	N/A
<i>RPL27A</i>	256	None	<i>Y37E3.8</i>	324
<i>RQCD1</i>	257	None	None	N/A
<i>RREB1</i>	258	None	None	N/A
<i>RSPO3</i>	260	None	None	N/A
<i>SCARB2</i>	261	<i>scav-1</i>	<i>C03F11.3</i>	16
<i>SCARB2</i>	261	<i>scav-6</i>	<i>F07A5.3</i>	88
<i>SCARB2</i>	261	<i>scav-4</i>	<i>F11C1.3</i>	101
<i>SCARB2</i>	261	<i>scav-5</i>	<i>R07B1.3</i>	259
<i>SCARB2</i>	261	<i>scav-3</i>	<i>Y49E10.20</i>	337
<i>SCARB2</i>	261	<i>scav-2</i>	<i>Y76A2B.6</i>	364
<i>SCHLAP1</i>	262	None	None	N/A
<i>SCN2A</i>	263	None	None	N/A
<i>SCRN2</i>	264	None	None	N/A
<i>SCUBE2</i>	265	None	<i>F58E6.13</i>	201
<i>SDAD1</i>	266	<i>pro-3</i>	<i>Y39B6A.14</i>	328
<i>SDC1</i>	267	<i>sdn-1</i>	<i>F57C7.3</i>	196

GWAS loci	Unique Human Loci ID number *	<i>C. elegans</i> gene name	<i>C. elegans</i> locus ID	<i>C. elegans</i> Unique Gene ID Number *
SEC16B	268	None	F13B9.1	104
SEC16B	268	sec-16	ZK512.5	381
SH2B1	269	None	None	N/A
SLC11A1	270	smf-2	K11G12.3	243
SLC11A1	270	smf-1	K11G12.4	244
SLC11A1	270	smf-3	Y69A2AR.4	357
SLC28A3	271	slc-28.1	F27E11.1	139
SLC28A3	271	slc-28.2	F27E11.2	140
SLC38A11	272	None	None	N/A
SLC39A13	273	None	C14H10.1	43
SLC39A8	274	tag-140	T11F9.2	283
SLC39A8	274	None	Y55F3BL.2	350
SMIM4	275	None	None	N/A
SNX10	276	None	None	N/A
SNX17	277	snx-17	F17H10.3	119
SOGA3	278	tag-241	C34E11.3	57
SPATA5	279	cdc-48.3	K04G2.3	225
SRD5A3	280	None	B0024.13	1
SRR	281	None	K01C8.1	215
SRR	281	None	T01H8.2	274
SRR	281	None	Y51H7C.9	341
SSPN	282	None	None	N/A
SSR3	283	trap-3	Y38F2AR.2	325
STC1	284	None	None	N/A
STK33	285	None	F32D8.1	145
STK33	285	zyg-8	Y79H2A.11	365
STK33	285	None	ZK593.9	383
STK39	286	gck-3	Y59A8B.23	353
SUZ12P1	287	None	None	N/A
SYT4	288	snt-4	T23H2.2	296
TAF4	289	taf-4	R119.6	266
TAGLN	290	cpn-2	D1069.2	79
TAGLN	290	cpn-3	F28H1.2	141
TAGLN	290	cpn-1	F43G9.9	166
TAGLN	290	cpn-4	F49D11.8	181
TAP2	291	haf-2	F43E2.4	163

GWAS loci	Unique Human Loci ID number *	<i>C. elegans</i> gene name	<i>C. elegans</i> locus ID	<i>C. elegans</i> Unique Gene ID Number *
TAP2	291	<i>haf-4</i>	<i>W04C9.1</i>	312
TAP2	291	<i>haf-7</i>	<i>Y50E8A.16</i>	339
TAP2	291	<i>haf-9</i>	<i>ZK484.2</i>	380
TBX15	292	<i>mab-9</i>	<i>T27A1.6</i>	301
TBX15	292	<i>tbx-7</i>	<i>ZK328.8</i>	379
TBX6	293	<i>tbx-2</i>	<i>F21H11.3</i>	122
TBX6	293	<i>mls-1</i>	<i>H14A12.4</i>	208
TBX6	293	<i>tbx-7</i>	<i>ZK328.8</i>	379
TCF7L2	295	<i>egl-13</i>	<i>T22B7.1</i>	295
TFAP2B	296	<i>aptf-1</i>	<i>K06A1.1</i>	227
TFAP2B	296	<i>aptf-2</i>	<i>Y62E10A.17</i>	354
TFEC	297	<i>hlh-30</i>	<i>W02C12.3</i>	310
TIPARP	298	None	None	N/A
TMC4	299	<i>tmc-2</i>	<i>B0416.1</i>	10
TMC4	299	<i>tmc-1</i>	<i>T13G4.3</i>	286
TMC5	300	<i>tmc-2</i>	<i>B0416.1</i>	10
TMC5	300	<i>tmc-1</i>	<i>T13G4.3</i>	286
TMEM110	301	None	None	N/A
TMEM165	302	None	<i>Y54F10AL.1</i>	344
TMEM18	303	None	None	N/A
TMEM219	304	None	None	N/A
TNFAIP8	306	None	None	N/A
TNRC6B	307	None	None	N/A
TRIB2	308	<i>nipi-3</i>	<i>K09A9.1</i>	238
TRIM66	309	<i>nhl-2</i>	<i>F26F4.7</i>	135
TRIM66	309	<i>ncl-1</i>	<i>ZK112.2</i>	373
TRIM8	310	None	None	N/A
TRMO	311	None	None	N/A
TRMT112	312	None	<i>C04H5.1</i>	21
TSEN34	313	<i>tsen-34</i>	<i>K08D10.12</i>	234
TUFM	314	<i>tufm-1</i>	<i>Y71H2AM.23</i>	361
UBE2E2	315	None	None	N/A
UGGT2	316	<i>uggt-2</i>	<i>F26H9.8</i>	138
UGGT2	316	<i>uggt-1</i>	<i>F48E3.3</i>	178
UHRF1BP1	317	None	<i>C44H4.4</i>	67
UNC79	318	<i>unc-79</i>	<i>E03A3.6</i>	83

GWAS loci	Unique Human Loci ID number *	<i>C. elegans</i> gene name	<i>C. elegans</i> locus ID	<i>C. elegans</i> Unique Gene ID Number *
UQCC	319	None	None	N/A
USMG5	320	None	None	N/A
USP37	321	None	None	N/A
VAMP4	322	<i>vamp-8</i>	B0513.9	11
VAMP4	322	<i>snb-2</i>	F23H12.1	126
VAMP4	322	<i>snb-1</i>	T10H9.4	282
VAMP4	322	Y69A2AR.6	Y69A2AR.6	358
VEGFA	323	None	None	N/A
VEGFB	324	None	None	N/A
VGLL4	325	None	None	N/A
VPS13C	326	None	T08G11.1	280
VPS53	327	<i>vps-53</i>	T05G5.8	278
WARS2	328	<i>prx-10</i>	C34E10.4	56
WDPCP	329	None	None	N/A
YPEL3	330	None	B0546.4	12
YPEL3	330	None	F37A8.5	151
ZDHHC24	331	<i>dhhc-1</i>	F09B12.2	92
ZDHHC24	331	<i>dhhc-10</i>	K02G10.1	219
ZNF133	333	None	Y55F3AM.14	349
ZNF142	334	<i>spr-4</i>	C09H6.1	36
ZNF142	334	None	C28G1.4	50
ZNF169	335	None	Y55F3AM.14	349
ZNF423	336	<i>lin-13</i>	C03B8.4	15
ZNF423	336	None	C09F5.3	34
ZNF608	337	None	None	N/A
ZNF664	338	<i>egrh-3</i>	Y94H6A.11	368
ZNRF3	339	<i>plr-1</i>	Y47D3B.11	335
ZP3	340	None	None	N/A

Table 3.1 Human GWAS obesity genes and *C. elegans* orthologs from meta-analysis

340 Genes associated with obesity traits from 3 previous publications: GWAS source 1) Mete Civelek, et. al, AJHG, 2017; 2) Masato Akiyama, et.al, Nature Genetics, 2017; 3) Audrey Chu, et.al, Nature Genetics, 2017.

Table 3. 2

RD vs HFrD	Tests with equal weight for all time points		
	Log-rank	Log-rank	Log-rank
	p value	Hazard Ratio	95% CI
Rep.1	<0.0001	2.917	1.816 to 4.684
Rep.2	<0.0001	3.968	2.472 to 6.370
Rep.3	<0.0001	4.373	2.716 to 7.040
Average	N/A	3.753	N/A

RD vs HFrD	Tests with extra weight for early time points		
	Gehan-Breslow-Wilcoxon	Mantel-Haenszel	Mantel-Haenszel
	p value	Hazard Ratio	95% CI
Rep.1	<0.0001	15.6	7.488 to 32.52
Rep.2	<0.0001	47.31	24.22 to 92.44
Rep.3	<0.0001	31.56	17.30 to 57.56
Average	N/A	31.49	N/A

Table 3.2 Lifespan analysis of worms fed HFrD versus RD

Summary of 3 repeats of the lifespan analysis of worms fed HFrD versus RD.

Hazard ratios were calculated using Log-rank and Mantel-Haenszel methods.

Table 3. 3

	Rep1	Tests with equal weight for all time points			Tests with extra weight for early time points		
		Log-rank	Log-rank	Log-rank	Gehan-Breslow-Wilcoxon	Mantel-Haenszel	Mantel-Haenszel
		p value	Hazard Ratio	95% CI	p value	Hazard Ratio	95% CI
	EV HFrD vs RD	<0.0001	2.917	1.816 to 4.684	<0.0001	15.6	7.488 to 32.52
RNAi vs EV	<i>pho-1</i> RD	0.0219	0.6562	0.4013 to 1.073	0.0096	0.4871	0.2632 to 0.9012
	<i>let-767</i> RD	0.4485	0.8689	0.5438 to 1.388	0.2589	0.7954	0.4401 to 1.438
	<i>mup-4</i> RD	0.0119	1.637	0.9630 to 2.782	0.0325	2.469	1.221 to 4.992
	<i>Y71H10B.1</i> RD	0.1282	0.7631	0.4761 to 1.223	0.0307	0.6249	0.3410 to 1.145
	<i>pho-1</i> HFrD	<0.0001	0.5213	0.3409 to 0.7971	<0.0001	0.2531	0.1405 to 0.4559
	<i>let-767</i> HFrD	0.0013	0.6421	0.4257 to 0.9684	<0.0001	0.3769	0.2078 to 0.6836
	<i>mup-4</i> HFrD	0.0057	0.6924	0.4604 to 1.041	<0.0001	0.4183	0.2256 to 0.7759
	<i>Y71H10B.1</i> HFrD	<0.0001	0.385	0.2442 to 0.6071	<0.0001	0.1318	0.07146 to 0.2431

	Rep2	Tests with equal weight for all time points			Tests with extra weight for early time points		
		Log-rank	Log-rank	Log-rank	Gehan-Breslow-Wilcoxon	Mantel-Haenszel	Mantel-Haenszel
		p value	Hazard Ratio	95% CI	p value	Hazard Ratio	95% CI
	EV HFrD vs RD	<0.0001	3.968	2.472 to 6.370	<0.0001	47.31	24.22 to 92.44
RNAi vs EV	<i>pho-1</i> RD	0.8766	0.9808	0.6971 to 1.380	0.3028	0.9631	0.5990 to 1.549
	<i>let-767</i> RD	0.4266	0.9058	0.6453 to 1.272	0.101	0.827	0.5177 to 1.321
	<i>mup-4</i> RD	0.0387	1.311	0.9352 to 1.837	0.1715	1.599	1.025 to 2.494
	<i>Y71H10B.1</i> RD	0.451	0.9093	0.6473 to 1.278	0.1705	0.8363	0.5255 to 1.331
	<i>pho-1</i> HFrD	<0.0001	0.5418	0.3660 to 0.8021	<0.0001	0.1701	0.08940 to 0.3236
	<i>let-767</i> HFrD	<0.0001	0.485	0.3254 to 0.7229	<0.0001	0.1201	0.06281 to 0.2298
	<i>mup-4</i> HFrD	<0.0001	0.4166	0.2752 to 0.6306	<0.0001	0.1113	0.05989 to 0.2067
	<i>Y71H10B.1</i> HFrD	<0.0001	0.5227	0.3525 to 0.7753	<0.0001	0.142	0.07370 to 0.2736

	Rep3	Tests with equal weight for all time points			Tests with extra weight for early time points		
		Log-rank	Log-rank	Log-rank	Gehan-Breslow-Wilcoxon	Mantel-Haenszel	Mantel-Haenszel
		p value	Hazard Ratio	95% CI	p value	Hazard Ratio	95% CI
	EV HFrD vs RD	<0.0001	4.373	2.716 to 7.040	<0.0001	31.56	17.30 to 57.56
RNAi vs EV	<i>pho-1</i> RD	0.7983	1.03	0.7235 to 1.466	0.7346	1.075	0.6192 to 1.865
	<i>let-767</i> RD	0.0344	0.7866	0.5483 to 1.128	0.0057	0.5299	0.2942 to 0.9544
	<i>mup-4</i> RD	0.1991	0.8593	0.6025 to 1.225	0.0843	0.6996	0.4055 to 1.207
	<i>Y71H10B.1</i> RD	0.0057	0.7324	0.5149 to 1.042	0.0005	0.4546	0.2600 to 0.7947
	<i>pho-1</i> HFrD	<0.0001	0.5882	0.4019 to 0.8610	<0.0001	0.2862	0.1615 to 0.5072
	<i>let-767</i> HFrD	0.0029	0.6919	0.4736 to 1.011	0.0002	0.4109	0.2289 to 0.7375
	<i>mup-4</i> HFrD	0.0039	0.6622	0.4463 to 0.9825	0.0014	0.4407	0.2525 to 0.7693
	<i>Y71H10B.1</i> HFrD	<0.0001	0.5382	0.3652 to 0.7932	<0.0001	0.2516	0.1432 to 0.4422

Table 3.3 Lifespan analysis of worms treated with RNAi constructs versus EV in RD and HFrD conditions

Summary of 3 repeats of the lifespan analysis of worms treated with RNAi constructs versus EV in RD and HFrD conditions. Hazard ratios were calculated using Log-rank and Mantel-Haenszel methods.

CHAPTER IV: Metabolic profiling and modeling obesity in *C.**elegans*

Statement of contribution and acknowledgment

The modeling and the initial bioinformatic work to identify the 1535 metabolic genes in *C. elegans* was conducted by Chintan Joshi under guidance of Dr. Eyleen O'Rourke (UVA) and Dr. Nathan E. Lewis lab (UCSD). To identify the fat regulators among these metabolic genes, I performed an RNAi screen through the 1535 genes to identify those genes whose inactivation promoted or prevented obesity in 3 different conditions: 1) regular diet, 2) high-fructose diet (which leads to diet-induced obesity or DIO), and 3) in the insulin-resistant obesity *C. elegans* model, the mutant *daf-2*. I performed three biological replicates with the help from two undergraduate students, Leila Rayyan and Chenyu Yang. Leila contributed significantly especially to the development of screen pipelines (also mentioned in Chapter II) when we were troubleshooting and optimizing the conditions for the screen and the imaging systems. Chenyu Yang also contributed significantly to conduct the screen, and he also helped in preparing reagents (worms, growth plates, etc.). I developed the post-screen image processing and analysis tools and pipeline with the help of UVA HPC groups (especially Dr. Karsten Siller, also mentioned in Chapter II) to characterize the obesity phenotype as described in this chapter.

The data I collected from the image-based RNAi screen formed the foundation of this chapter. One additional phenotype we were interested in (beyond the obesity phenotype described in this chapter) is the developmental delay/arrest phenotype. This phenotype implicate that the target gene is essential for development and

growth of *C. elegans*, one of the properties of “housekeeping genes”. Taking these data from my screen, Chintan J. Joshi, Anna Way, and Dr. Eyleen O’Rourke conducted bioinformatics analysis and submitted a manuscript to *eLife* (in which I am the 2nd author), and currently available on *bioRxiv* (Joshi et al., 2021). Because the contents of this manuscript do not align with my focus of the dissertation, I omit the contents of this manuscript from this chapter.

4.1 Introduction

In the past two decades, the field of molecular biology has been shifted greatly from the studying the function genes one at a time to investigating all genes as dynamic networks underlying complexly determined phenotypes (Thompson, 1976). The desire for understanding the interaction network underlying different biological processes then emerges as a new field, termed systems biology. Technological and computational advancements have facilitated the studies of cells as a system. Since the landmark publication of the first human genome in 2001 (Lander et al., 2001), genomes from hundreds of organisms have been sequenced. The resulting data enabled genome-wide studies aimed to understand the functional interactions between genes and pathways. A variety of omics approaches such as genomics, transcriptomics, metabolomics, and proteomics are currently being used to understand network level interactions. In general, to study a biological system as a whole, four elements are needed: quantitative data, reconstruction of the network, algorithms to model intranetwork interactions in basal and perturbed conditions, and the development of theories that will explain and can predict untested changes in the network due to yet to be tested perturbations or in yet to be tested organisms (Kirschner, 2005).

To date, two models of the core metabolic reactions predicted from its genome have been generated for *C. elegans* (Gebauer et al., 2016; Watson et al., 2014). A metabolite-centered model was generated by feeding *C. elegans* with mutant libraries of *Escherichia coli* and *Comamonas aquatica* and identifying mutant

bacterial isolates that impair *C. elegans* development (Gebauer et al., 2016). This model successfully predicted the essentiality of methionine/SAM cycle and propionyl-CoA breakdown pathways on *C. elegans* development. The initial metabolic reconstruction was generated using data from several databases, and included 218 reactions from Pathologic, 263 homologous reactions from YeastCyc and EcoCyc, and comprehensive manual curation with importing homologous reactions from human metabolic reconstruction Recon 2 that have functional evidence in Wormbase or KEGG database. 1,914 reactions, 1,640 metabolites, and 979 metabolic genes in total were used to develop reconstruction of *C. elegans* metabolic reactions (Watson et al., 2014). This reconstruction was used to predict the function of some unknown genes that are required for survival, development, or aging in *C. elegans*. In collaboration with Dr. Nathan Lewis we generated a refined and predictive model of *C. elegans* metabolism by curating the published models (Gebauer et al., 2016; Yilmaz and Walhout, 2016), and testing its predictive power using experimental data. The current model contains 1535 genes, 3225 reactions, and 2328 metabolites.

Taking advantage of this metabolic model and the genetic tractability of *C. elegans*, I worked towards developing a whole-body, single-cell resolution, predictive model of obesity. Towards this goal, I developed the following: 1) a model of Diet-induced Obesity (DIO model) by feeding worms a High Fructose Diet (HFrd); 2) an insulin insensitivity obesity model by using a worm strain carrying a hypomorph mutation in the worm insulin receptor gene ortholog *daf-2*.

Increased sugar intake was found to be highly correlated with the epidemic of obesity (Gross et al., 2004; Marriott et al., 2010). The increased consumption of sugar has been largely driven by increased consumption of high-fructose sweeteners in soft drinks, breakfast cereals, baked goods, snacks, and desserts. Further, studies show that fructose, but not glucose, increases appetite and food intake. It has been shown that blood fructose induces a reduction of hypothalamic malonyl-CoA levels, whereas glucose increases hypothalamic malonyl-CoA to activate the appetite-agonist and suppress food intake (Miller et al., 2002). Moreover, fructose increases phosphorylation and activation of hypothalamic AMP kinase via promoting phosphorylation/inactivation of acetyl-CoA carboxylase with a concomitant depletion of hypothalamic ATP level; AMPK promotes fasting responses including foraging behavior. By contrast, glucose causes inhibition of AMPK (Rizkalla, 2010). Other studies showed that the expression levels of the genes encoding enzymes involved in hepatic lipogenesis, such as hepatic sterol regulatory element-binding protein (SREBP-1), fatty acid synthase (FAS), and acetyl Co-A carboxylase (ACC), is increased in mice injected with fructose (Matsuzaka et al., 2004; Mayes, 1993; Miyazaki et al., 2004). It has also been shown that although both dietary fructose and glucose induce lipogenesis, fructose causes long-term increasing expression of lipogenic enzymes, whereas glucose stimulates an insulin-dependent short-term peak induction of lipogenesis (Matsuzaka et al., 2004). Together, these studies support a model in which dietary fructose promotes obesogenic molecular and physiological changes. Together

with the epidemiological studies, the data suggest that dietary fructose would be a major driver in the epidemic of obesity acting through intricately multiorgan molecular changes that differ from those of other dietary carbohydrates. Using *C. elegans* as the model system, I developed the first worm model of fructose-induced obesity as described in **Chapter III**.

Type 2 diabetes and insulin resistance have also been associated with obesity for decades, and it has been shown that enlarged adipose tissue causes systemic insulin resistance (Reaven, 1995). However, the cellular and molecular mechanisms linking insulin resistance and obesity remain to be elucidated. The major fat depots in mammalian systems, adipocytes, have been shown to regulate systemic glucose homeostasis (Kahn and Flier, 2000; Weyer et al., 1998). Adipocytes are also well known for their function as endocrine cells. Leptin, for example, is one of the most studied adipocyte-derived hormones, and it has been shown that leptin regulates satiety, energy expenditure, and neuroendocrine function in mammalian systems (Friedman, 2000) and the deficiency of leptin or its receptor leads to obesity with severe insulin resistance. Many other studies also suggested that inflammation caused by obesity in adipose tissues is associated or functionally linked to insulin resistance and diabetes (Wu and Ballantyne, 2020). Controversially, an increasing number of recent studies suggest that insulin resistance and hyperinsulinemia could be the cause of obesity instead of the consequences of obesity (Astley et al., 2018; Czech, 2017; Nakagawa et al., 2005). Interestingly, in *C. elegans*, there is no specialized fat storage tissue such as the

white adipose tissue of mammals, and the intestine is the primary organ for lipid uptake, synthesis, storage, and mobilization (Srinivasan, 2015). *C. elegans* also lack many critical mammalian fat endocrine systems. One particular example is leptin, the central signal pathway from the adipose cell in the regulation of fat metabolism in mammals, which cannot be found in *C. elegans* (Srinivasan et al., 2008). However, despite these differences, we still observe a direct functional link between insulin resistance and obesity. It has been previously characterized that the hypomorph mutation in the worm insulin receptor ortholog *daf-2* leads to a dramatic increase of body fat content in *C. elegans* (O'Rourke et al., 2009b).

Being obesity a complex metabolic disease, we need systematic approaches to elucidate its molecular underpinnings. Thus, we aimed to obtain the quantitative tissue-level transcriptional profile of all metabolic genes in the two obesity models described above through single-cell RNAseq (scRNAseq) (The scRNAseq project is currently led by another graduate student Abbas Ghaddar) and to construct mathematical and computational *C. elegans* obesity models based on these quantitative measurements. On the other hand, in this Chapter, I obtained measurements of body fat content in the worms through ORO staining and utilized the RNAi screen methods described in **Chapter II** to identify metabolic genes that alter the body fat content in the two obesity models.

4.2 Results and discussion

To identify fat regulators for obesity in *C. elegans* using RNAi, we constructed an RNAi sub-library from the existing genome-wide RNAi libraries (Poulin et al., 2004; Rual et al., 2004). The new sublibrary targets 1372 (out of 1535) *C. elegans* predicted metabolic genes. Using this sublibrary, firstly, I screened the fat content of the wild-type worms (RNAi sensitive strain NL2099) fed the regular diet (RD). Using the screen and analysis pipeline described in Chapter II, I classified the phenotypes into three groups: normal fat (N, phenotype resemble empty vector controls), obese (O, more body fat content than empty vector controls), and lean (L, less body fat content than empty vector controls). The screen was performed in three independent biological replicates, and the RNAi constructs that lead to O or L phenotypes in all three replicates were considered as high confident (HC) hits. The constructs that result in O or L phenotypes in 2 out of the 3 replicates were considered as low confident hits, and 1 more replicate was conducted specifically on all the LC hits to further confirm the phenotypes. The confirmed LC hits were moved into the HC hits group. All HC hits were then sequence verified. Together, we identified 46 RNAi constructs that lead to the O phenotype (obesity enhancer) and 46 constructs that lead to the L phenotype (obesity suppressor). The target genes of these hits were annotated as genes that protect against obesity and the genes that promote obesity, respectively.

To identify genes that promote DIO (fructose-induced) and insulin resistance obesity, 2 independent screens were conducted using the same RNAi sublibrary.

For the DIO screen, I used the DIO model that is characterized in Chapter III, and for the insulin resistance obesity screen, I utilized the previously characterized insulin resistance obesity *C. elegans* model (*daf-2* mutant) (O'Rourke et al., 2009b). The phenotype of the worms in these screens was classified into two classes: similar (S) and less obese (LO) comparing to the obese empty vector controls. Similar to the RD screen, these screens were performed in 3 independent biological replicates and the RNAi treatments that led to LO phenotype in all 3 replicates were considered as HC hits, while the treatments that caused LO phenotype in 2 out of 3 replicates were considered as LC hits. All the LC hits were validated in one more biological replicate to identify the true hits and the true hits were moved into the HC hits group. All HC hits were then sequence verified. Together, I identified 32 HC hits (DIO suppressor) in the DIO screen and 33 genes (insulin resistance obesity suppressor) in the insulin resistance obesity screen. The target genes of these RNAi treatments were annotated as genes that promote DIO and genes that promote insulin resistance obesity, respectively.

In the outcome of the 3 screens described above, 22 out of the 46 obesity suppressors overlap with DIO suppressors, 20 of which overlap with insulin resistance obesity suppressors. 7 DIO suppressors are not overlapped with either obesity suppressors or insulin resistance obesity suppressors, whereas 3 DIO suppressors are not obesity suppressors but overlap with insulin resistance obesity suppressors. 10 insulin resistance obesity suppressors are not classified as either obesity suppressors or DIO suppressors. Taken together, we identified 66 genes

that promote obesity, of which 7 are DIO unique genes and 10 are insulin resistance obesity unique genes (Fig. 4.1, Table 4.1).

Figure 4. 1

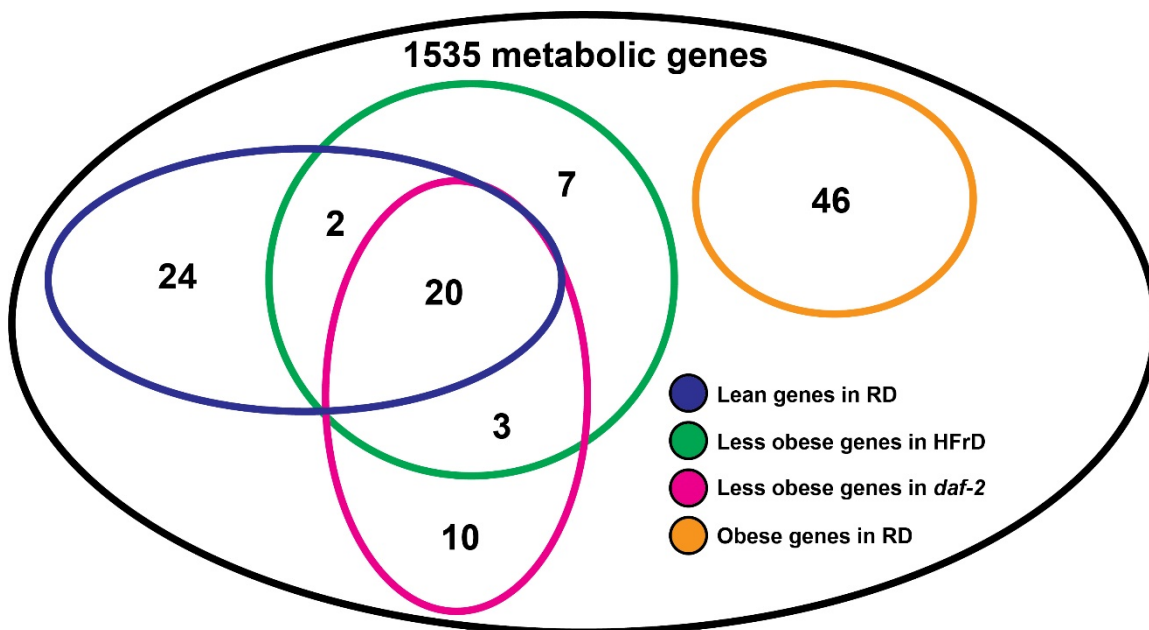


Fig. 4.1 Summary of worm model screens

3 RNAi screens were conducted targeting 1372 genes. The obesity suppressors are presented in the blue circle, the DIO suppressors are presented in the green circle, the insulin resistance obesity suppressors are presented in the pink circle, and the obesity enhancers are presented in the orange circle.

Currently, there is no computational model of obesity or a comprehensive study of the metabolic genes and pathways that contribute to obesity for any multicellular organism. To fulfill this gap, my study described the first comprehensive analysis on *C. elegans* predicted metabolic genes that contribute to obesity, using two obesity models.

Given the intricate nature of metabolic pathways, and the lack of integrated data sets or integrative tools for the analysis of metabolic pathways in multicellular organisms, traditional pathway analysis tools may miss functional patterns contained in our hit dataset. To overcome this limitation, the hits from this study will be used as a benchmark for the refinement of integrated *in silico* model of *C. elegans* metabolism.

Unlike a single cellular organism such as *E. coli* and yeast, a multicellular organism such as *C. elegans* has a much more complicated metabolic network as we need to consider cell-cell, tissue-tissue, and organ-organ interactions to gain an integrated view of metabolism in health and disease status. To better reconcile the future obesity models, we need to understand the tissue level contributions of different metabolism pathways, especially those that are causally linked to obesity in the three screens described in this chapter.

To define the tissue/s of action of the obesity genes, the next step is to use tissue-specific RNAi-mediated inactivation of the hits. Previous studies demonstrated that

C. elegans sid-1 encodes for a dsRNA channel protein that is essential for dsRNA uptake. Hence, loss of *sid-1* as in *C. elegans* strain NL3321 (*sid-1(pk3321) V*) leads to insensitivity to feeding RNAi. On the other hand, overexpression of *sid-1* (via strong tissue-specific promoters) enhances RNAi sensitivity in the target tissue (Calixto et al., 2010). The combination of a background that is insensitive to RNAi with the overexpression of a rescue/overexpression construct in specific tissues allows us to generate *C. elegans* strains that are sensitive to RNAi in single tissues or even cell types if the cell or tissue-specific promoters have been described. Multiple single-tissue *sid-1* expression strains are currently available in our lab (e.g. TU3311: neuronal overexpression, SPC272: muscle RNAi, and MGH171: intestinal RNAi). The RNAi treatment and data analysis follow the same procedures described in **Chapter II** except that the *C. elegans* strain used for the screen varies as we change the target tissue. This will allow us to generate a functional atlas of all genes contributing to obesity in a tissue-level resolution.

4.4 Tables

Table 4. 1

Fat regulators in *C. elegans* obesity models

<i>C. elegans</i> gene	Phenotype category	Sublibrary location	Human orthologs
<i>afmd-1</i>	DIO supressor	15-D03	AFMID
<i>dpm-1</i>	DIO supressor	15-C08	DPM1
<i>glct-5</i>	DIO supressor	2-F02	B3GAT1 B3GAT2 B3GAT3
<i>gpx-1</i>	DIO supressor	2-D04	GPX4 GPX7 GPX8
<i>gspd-1</i>	DIO supressor	9-D02	G6PD
<i>H23N18.4</i>	DIO supressor	10-E05	UGT3A1 UGT3A2
<i>icmt-1</i>	DIO supressor	1-C10	ICMT
<i>ipp-5</i>	DIO supressor	13-C07	INPP5A
<i>pnc-1</i>	DIO supressor	15-C07	
<i>rpia-1</i>	DIO supressor	6-E10	RPIA
<i>set-15</i>	DIO supressor	8-B01	
<i>sqv-5</i>	DIO supressor	2-D06	CHSY1 CHSY3
<i>T24C4.5</i>	DIO supressor	5-F05	PRIM1
<i>tre-3</i>	DIO supressor	15-F04	TREH
<i>vha-8</i>	DIO supressor	8-C08	ATP6V1E1 ATP6V1E2
<i>Y43F4B.5</i>	DIO supressor	7-E09	PGM2L1 PGM2
<i>ZC513.5</i>	DIO supressor	15-F05	ALG12
<i>ZK795.1</i>	DIO supressor	9-F03	IPMK
<i>ZK822.5</i>	DIO supressor	9-E03	SLC5A8 SLC5A1 SLC5A4

<i>C. elegans</i> gene	Phenotype category	Sublibrary location	Human orthologs
			SLC5A5 SLC5A9 SLC5A6 SLC5A2 SLC5A12 SLC5A10 SLC5A11 SLC5A3 SLC5A8
ZK836.2	DIO supressor	11-G11	DHTKD1 OGDH OGDHL
<i>fat-6</i>	DIO supressor & obesity supressor	9-E02	SCD SCD5
R04F11.2	DIO supressor & obesity supressor	11-H01, 17- F06	ATP5ME
<i>cbl-1</i>	insulin resistance obesity supressor	2-C07	CTH
<i>hpo-8</i>	insulin resistance obesity supressor	10-H03	HACD1 HACD2
<i>hsp-6</i>	insulin resistance obesity supressor	15-E01	HSPA9
<i>pap-1</i>	insulin resistance obesity supressor	11-E03	PAPOLA PAPOLG PAPOLB
R53.4	insulin resistance obesity supressor	4-G05	ATP5J2
<i>vha-1</i>	insulin resistance obesity supressor	17-B11	ATP6V0C
<i>vha-16</i>	insulin resistance obesity supressor	16-B09	ATP6V0D2 ATP6V0D1

<i>C. elegans</i> gene	Phenotype category	Sublibrary location	Human orthologs
<i>vha-19</i>	insulin resistance obesity suppressor	17-C06	ATP6AP1
<i>vha-9</i>	insulin resistance obesity suppressor	4-G11	ATP6V1F
<i>Y37B11A.2</i>	insulin resistance obesity suppressor	15-A12	REV3L KIAA2022
<i>vha-11</i>	insulin resistance obesity suppressor & DIO suppressor	9-H08	ATP6V1C2 ATP6V1C1
<i>vha-17</i>	insulin resistance obesity suppressor & DIO suppressor	8-G02	ATP6V0E1 ATP6V0E2
<i>vha-3</i>	insulin resistance obesity suppressor & DIO suppressor	15-C03	ATP6V0C
<i>elo-3</i>	insulin resistance obesity suppressor & DIO suppressor & obesity suppressor	8-D02	ELOVL3 ELOVL6
<i>hpo-18</i>	insulin resistance obesity suppressor & DIO suppressor & obesity suppressor	17-E02,10- C12	ATP5E ATP5EP2
<i>hyl-1</i>	insulin resistance	8-F06	CERS4 CERS5

<i>C. elegans</i> gene	Phenotype category	Sublibrary location	Human orthologs
	obesity supressor & DIO supressor & obesity supressor		CERS2 CERS3 CERS6
<i>let-754</i>	insulin resistance obesity supressor & DIO supressor & obesity supressor	6-G10	AK2 AK8
<i>sptl-1</i>	insulin resistance obesity supressor & DIO supressor & obesity supressor	16-C02	SPTLC1
<i>alg-1</i>	insulin resistance obesity supressor & obesity supressor	14-B12	AGO1 AGO2 AGO3 AGO4
<i>atp-5</i>	insulin resistance obesity supressor & obesity supressor	11-F02	ATP5H
<i>cbp-1</i>	insulin resistance obesity supressor & obesity supressor	7-B12	CREBBP EP300
<i>dyn-1</i>	insulin resistance obesity supressor & obesity supressor	14-D04	DNM1L DNM2 DNM1 MX1 MX2 DNM3
<i>ears-1</i>	insulin resistance	18-A02	EPRS

<i>C. elegans</i> gene	Phenotype category	Sublibrary location	Human orthologs
	obesity supressor & obesity supressor		
<i>elo-1</i>	insulin resistance obesity supressor & obesity supressor	8-G11	ELOVL6
<i>elo-5</i>	insulin resistance obesity supressor & obesity supressor	8-B04	ELOVL3 ELOVL6
<i>gln-6</i>	insulin resistance obesity supressor & obesity supressor	8-H03	GLUL
<i>lpin-1</i>	insulin resistance obesity supressor & obesity supressor	12-B04	LPIN2 LPIN3 LPIN1
<i>pars-1</i>	insulin resistance obesity supressor & obesity supressor	6-F04	EPRS
<i>pcp-2</i>	insulin resistance obesity supressor & obesity supressor	8-G01	PRSS16
<i>tkt-1</i>	insulin resistance obesity supressor & obesity supressor	9-A08	TKTL1 TKTL2 TKT
<i>unc-32</i>	insulin resistance	16-C12	ATP6V0A1 ATP6V0A4

<i>C. elegans</i> gene	Phenotype category	Sublibrary location	Human orthologs
	obesity supressor & obesity supressor		TCIRG1 ATP6V0A2
<i>vha-2</i>	insulin resistance obesity supressor & obesity supressor	17-B08	ATP6V0C
<i>vha-5</i>	insulin resistance obesity supressor & obesity supressor	8-F01	ATP6V0A1 ATP6V0A4 TCIRG1 ATP6V0A2
<i>aars-2</i>	obesity enhancer	1-B08	AARS2 AARS
<i>aco-2</i>	obesity enhancer	6-G11	ACO1 ACO2 IREB1
<i>acs-4</i>	obesity enhancer	6-F01	ACSL1 ACSL3 ACSL4 ACSL5 ACSL6
<i>acy-4</i>	obesity enhancer	15-F06	ADCY2 ADCY7 ADCY4 ADCY1 ADCY5 ADCY8 ADCY6 ADCY3
<i>adsl-1</i>	obesity enhancer	1-H04	ADSL
<i>B0491.5</i>	obesity enhancer	5-A08	
<i>cars-1</i>	obesity enhancer	1-A12	CARS CARS CARS2
<i>ckb-3</i>	obesity enhancer	5-H04	CHKB CHKA CHKB-CPT1B
<i>cox-15</i>	obesity enhancer	5-A04	COX15
<i>dars-2</i>	obesity enhancer	15-D09	DARS2

<i>C. elegans</i> gene	Phenotype category	Sublibrary location	Human orthologs
<i>ears-2</i>	obesity enhancer	7-G12	EARS2
<i>F12F6.7</i>	obesity enhancer	9-D05	POLD2
<i>F16B4.6</i>	obesity enhancer	10-A12,17-D07	NDUFAB1
<i>fars-1</i>	obesity enhancer	1-F04	FARSA
<i>hars-1</i>	obesity enhancer	9-C02	HARS2 HARS
<i>iars-2</i>	obesity enhancer	2-D08	IARS IARS2
<i>lars-1</i>	obesity enhancer	5-G12	LARS
<i>M153.1</i>	obesity enhancer	14-A08	PYCR2 PYCR1
<i>mars-1</i>	obesity enhancer	9-D06	MARS
<i>mys-1</i>	obesity enhancer	10-H06	KAT5 KAT8 KAT7
<i>nars-2</i>	obesity enhancer	15-B06	NARS NARS2
<i>nuo-1</i>	obesity enhancer	5-A02	NDUFV1
<i>ostb-1</i>	obesity enhancer	4-A05	DDOST
<i>plc-1</i>	obesity enhancer	13-G12	PLCE1
<i>plc-3</i>	obesity enhancer	4-G10	PLCG1 PLCG2
<i>pole-1</i>	obesity enhancer	3-A03	POLE
<i>pri-1</i>	obesity enhancer	7-B09	PRIM1
<i>rnr-2</i>	obesity enhancer	5-G10	RRM2B RRM2
<i>rpb-7</i>	obesity enhancer	3-A07	POLR2G
<i>rpc-1</i>	obesity enhancer	8-D01	POLR2A POLR3A
<i>rpc-2</i>	obesity enhancer	6-B08	POLR2B POLR3B
<i>rpom-1</i>	obesity enhancer	2-H07	POLRMT
<i>sams-1</i>	obesity enhancer	14-A03	MAT1A MAT2A

<i>C. elegans</i> gene	Phenotype category	Sublibrary location	Human orthologs
<i>sams-3</i>	obesity enhancer	8-B09	MAT1A MAT2A
<i>sams-4</i>	obesity enhancer	8-B10	MAT1A MAT2A
<i>sucl-2</i>	obesity enhancer	5-F06	SUCLG1
<i>T01B11.2</i>	obesity enhancer	8-F04	ETNPPL PHYKPL
<i>T08H10.1</i>	obesity enhancer	10-D05	AKR1B1 AKR1A1 AKR1D1 AKR1E2 AKR1B10 AKR1B15
<i>tars-1</i>	obesity enhancer	5-B05	TARS TARS2 MRPL39 TARSL2
<i>tdo-2</i>	obesity enhancer	6-C07	TDO2 TDO2
<i>ucr-2.3</i>	obesity enhancer	5-F04	UQCRC2
<i>ugt-49</i>	obesity enhancer	15-G11	UGT2B4 UGT1A6 UGT2B7 UGT8 UGT2B11 UGT1A5 UGT1A9 UGT1A8 UGT1A10 UGT1A3 UGT1A7 UGT1A4 UGT2A2 UGT2A3
<i>ugt-55</i>	obesity enhancer	11-G12	
<i>vars-1</i>	obesity enhancer	11-B05	VAR2
<i>Y41D4A.6</i>	obesity enhancer	10-A01	QRSL1
<i>yars-1</i>	obesity enhancer	18-A04	YARS
<i>acs-5</i>	obesity suppressor	7-F06	ACSL1 ACSL3 ACSL4 ACSL5

<i>C. elegans</i> gene	Phenotype category	Sublibrary location	Human orthologs
			ACSL6
<i>asb-2</i>	obesity suppressor	13-A11	ATP5F1
<i>asg-2</i>	obesity suppressor	13-D08	ATP5L ATP5L2
<i>atp-2</i>	obesity suppressor	6-B04	ATP5B
<i>cgt-3</i>	obesity suppressor	3-F10	UGCG
<i>dgk-4</i>	obesity suppressor	8-F07	DGKD DGKH DGKK DGKD
<i>dld-1</i>	obesity suppressor	9-G06	DLD
<i>elo-2</i>	obesity suppressor	9-H07	ELOVL3 ELOVL6
<i>F29C4.2</i>	obesity suppressor	7-G06	
<i>F42G8.10</i>	obesity suppressor	8-E11	NDUFB11
<i>F58F12.1</i>	obesity suppressor	3-G04	ATP5D
<i>fah-1</i>	obesity suppressor	13-D02	FAH
<i>gob-1</i>	obesity suppressor	14-D01	
<i>hxx-1</i>	obesity suppressor	2-C04	GCK HKDC1 HK1 HK2 HK3
<i>nuo-5</i>	obesity suppressor	10-B11	NDUFS1 NDUFS1
<i>pdhb-1</i>	obesity suppressor	8-A02	PDHB
<i>pyk-1</i>	obesity suppressor	2-C03	PKM PKLR PKLR
<i>sod-3</i>	obesity suppressor	14-E05	SOD2
<i>spe-5</i>	obesity suppressor	1-D02	ATP6V1B1 ATP6V1B2
<i>stt-3</i>	obesity suppressor	6-C12	STT3B STT3A
<i>T05G5.5</i>	obesity suppressor	7-B10	DCAKD

<i>C. elegans</i> gene	Phenotype category	Sublibrary location	Human orthologs
<i>vha-6</i>	obesity suppressor	5-A10	ATP6V0A1 ATP6V0A4 TCIRG1 ATP6V0A2
<i>W09C5.8</i>	obesity suppressor	2-G08	COX4I2 COX4I1
<i>ZC416.6</i>	obesity suppressor	8-A04	LTA4H

Table 4.1 Fat regulators in *C. elegans* obesity models

The result of the RNAi screen on 1535 *C. elegans* metabolic genes. The phenotypes are classified into 4 classes: 1) obesity suppressor, KD suppress the fat accumulation in worms; 2) obesity enhancer, KD enhances the fat accumulation in worms; 3) DIO suppressor, KD suppress the fat accumulation in worms fed HFrD; 4) insulin resistance obesity suppressor, KD suppress the fat accumulation in the insulin resistance obesity model.

CHAPTER V: Molecular Dissection of a Chemotherapeutic-diet-host-microbiome 4-way interaction in *C. elegans*

This work was published on *Nature Communications* 2020;11(1):2587 using the title:

Dietary serine-microbiota interaction enhances chemotherapeutic toxicity without altering drug conversion.

PMID: [32444616](#) PMCID: [PMC7244588](#) DOI: [10.1038/s41467-020-16220-w](#)

Publication Author list: Wenfan Ke*, James A. Saba*, Cong-Hui Yao, Michael A. Hilzendeger, Anna Drangowska-Way, Chintan Joshi, Vinod K. Mony, Shawna B. Benjamin, Sisi Zhang, Jason Locasale, Gary J. Patti, Nathan Lewis, and Eyleen J. O'Rourke

*James A. Saba is a co-first author of this publication

Statement of contribution and acknowledgement

The work described in this chapter was initiated by James (Jake) Saba. He made an initial observation that when we use fluorodeoxyuridine (FUdR) to sterilize the worms in aging experiments, the sterility changes depend on the *E. coli* strains we fed to the worms. From there, he tested the FUdR toxicity in worms fed 4 different *E. coli* strains, sequenced the genome of these strains, and identified the key genes in different strains of the *E. coli* that are critical to the FUdR toxicity in the worms. He also worked with me and others in the lab to test *E. coli* mutants lack of the genes he identified and validated the function of those *E. coli* genes in FUdR toxicity to worms. From there, I took over this project. To start, I revised all data from our previous work that was led by Jake (with significant contributions from all other lab members in O'Rourke lab including me, Anna Way, Dr. Vinod Mony, Shawna Benjamin and Dr. Eyleen O'Rourke) : 1) The different toxicity of the FUdR treatment among *C. elegans* raised with different bacteria strains; 2) Primary *E. coli* KO screen and follow up retests to identify critical metabolic genes in *E. coli* that alter the FUdR toxicity to worms; 3) Primary screen and some follow up validation of dietary metabolites that alter FUdR toxicity to worms, including the key observations that serine, thymidine and glycine enhance FUdR toxicity; 4) Primary RNAi screen to identify of *C. elegans* genes that alter FUdR toxicity to worms. Based on these preliminary data, I designed new experiments and turned the focus of the paper from characterizing how *E. coli* genetics and metabolism modulate FUdR toxicity to worms (which has been described thoroughly by Scott et al and Garcia et al) to how dietary metabolites influence *E. coli*'s metabolism of

FUdR and how the worms respond to the different mechanisms of FUdR toxicity from *E. coli*. Specifically, my major contribution to this publication includes: 1) retested and revised the hits from all the primary screens mentioned above (the original screen and retests mostly only have 2 or less replicates); 2) retested and confirmed that dietary thymidine enhances FUdR toxicity through pyrimidine salvage pathway by genetics, and through metabolomic analysis to further describe the bioconversion of FUMP from FUdR by *E. coli* in the pyrimidine salvage pathway; 3) established the model that dietary serine enhances FUdR toxicity through altering the *E. coli* one carbon metabolism pathway that leads to the depletion of dTMP/thymidine, resulting in thymidine starvation in worms, using both genetics and metabolomics approaches; 4) characterized that FUdR toxicity to the worms is through damaging mitochondria DNA and RNA, and leads to hyperactivation of autophagy, and consequently, autophagic cell death; 5) demonstrated that thymidine starvation by dietary serine supplementation suppresses autophagy flux in the worms, opposite from the hyperactivation of autophagy by the basal FUdR toxicity, implicating a distinct mechanism of cell death by the serine enhanced toxicity in worms.

Beside Jake and myself, the undergraduate student Michael A. Hilzendeger also made a significant contribution to this chapter. He independently characterized that the growth rate of the *E. coli* mutants we used in this study is not correlated with the FUdR toxicity, and helped me characterized the mitochondria physiology (fragmentation, membrane potential, abundance etc.) under FUdR toxicity.

The primary metabolomic measurements described in this chapter are obtained through the collaboration with Dr. Gary J. Patti's lab and Dr. Jason Locasale's lab, with the help from the graduate students and post-docs: Cong-Hui Yao (Patti lab) and Sisi Zhang (Patti lab).

In addition to the authors of the published manuscripts, I would like to thank Dr. Vincent Galy for protocol to develop anti-LGG-1 antibodies, Dr. Malene Hansen for LGG-1 reporter strain, Dr. Sidney Kushner for generous help developing HB101 RNAi competent derivative, and Dr. Xiaojing Liu and Dr. Juan Liu for optimizing and running fluorometabolite LCMS analyses. I am very grateful to Dr. Filipe Cabreiro for sharing LCMS protocol, *E. coli* strains, and general advice. I would also thank Dr. Bob Nakamoto and Dr. Yelena Peskova for training and use of their French Press. I would thank Chenyu Yang, Noel Higgason, Alexandra Loperfito, Ahtesham Najeeb Chaudhry, and Meghna Shankar for help quantitating fertility images, and specially Nella Solodukhina, Leila Rayyan, and Mikayla Marraccini for help preparing reagents and conducting some of the experiments. I am grateful to the Keck Center for Cellular Imaging for the usage of the Leica SP5X microscopy system (PI: AP; NIH-RR025616). I would also want to acknowledge the *C. elegans* strains provided by the CGC, which is funded by NIH Office of Research Infrastructure Programs (P40 OD010440). Some *E. coli* strains were provided by CGSC, which is funded by NSF/Biological Infrastructure/Living Collections Program (DBI-0742708). The HSP60 and 4A1(Tubulin) antibodies were obtained

from the Developmental Studies Hybridoma Bank, created by the NICHD of the NIH and maintained at The University of Iowa, Department of Biology. I also thank Dr. Kevin Janes and Dr. Ariel Pani for revising the manuscript for publication. Moreover, I thank UVA DoubleHoo, College Council Minerva Research Grant, Ingrassia Family Research Award, and the Jefferson Foundation for supporting me in this work. This work would not have been possible without the generous support of the W. M. Keck Foundation and PEW Charitable Trust.

5.1 Abstract

Through modifying the drug, the microbiota, or the host, diet can change the response to therapeutics. However, the mechanisms of action of the diet are mostly unknown. Using a tractable in vivo system, we define how dietary thymidine and serine convert sublethal into lethal doses of the chemotherapeutic 5'-fluorodeoxyuridine (FUdR). Thymidine promotes microbe-mediated conversion of the prodrug FUdR into toxic 5-fluorouridine-5'-monophosphate (FUMP). Serine promotes microbial nucleotide imbalance. When the main microbe-mediated toxicity mechanism is FUdR-to-FUMP conversion, death in the host involves depletion of mitochondrial RNAs and DNA and lethal activation of autophagy. When the main microbe-mediated toxicity mechanism is nucleotide imbalance, death in the host does not involve mitochondrial RNA or DNA depletion, and autophagy promotes survival. Therefore, single dietary changes can alter or even reverse the microbe and the host responses to FUdR. The four-way complexity of these diet-drug-microbiota-host interactions exemplifies the challenges faced in exploiting the therapeutic potential of the microbiota.

5.2 Introduction

Classically, diet has been thought to modulate drug efficacy and toxicity through altering the physiology of the host or by directly interfering with the pharmacodynamics of the drug (Ruggiero et al., 2012; Won et al., 2012). However, emerging evidence shows that diet can also modulate drug efficacy and toxicity through modifying the composition or physiology of the microbiota, or the interaction between the microbiota and the host (Hitchings and Kelly, 2019). In this study we utilize a tractable model system to uncover and mechanistically dissect a 4-way interaction between the amino acid serine (diet), the chemotherapeutic 5'-fluorodeoxyuridine (drug), the bacterium *E. coli* (microbiota), and the roundworm *C. elegans* (host).

Fluoropyrimidines are commonly-used chemotherapeutics, especially for cancers of the GI tract (Malet-Martino and Martino, 2002). The most accepted mechanism of action of fluoropyrimidines is inhibition of thymidylate synthase (TS). TS catalyzes the methylation of 2'-deoxyuridine-5'-monophosphate (dUMP) in position 5 of the uracil ring to produce 2'-deoxythymidine-5'-monophosphate (dTMP). TS uses the 1-carbon (1C) metabolite 5,10-methylenetetrahydrofolate (5,10-mTHF) as the indispensable methyl-group donor. TS is critical for cell survival and replication since it is the sole biosynthetic source of dTMP, which is essential for DNA synthesis. When cells are treated *in vitro* with the fluoropyrimidine 5'-fluorodeoxyuridine (FUdR), they convert FUdR into 5'-fluorodeoxyuridine monophosphate (FdUMP). FdUMP is structurally similar to dUMP, except that it

has a fluorine atom in position 5 of the uracil ring. As a consequence, FdUMP forms a stable complex with 5,10-mTHF and TS, preventing the *de novo* synthesis of dTMP. 5,10-mTHF is essential for dTMP synthesis and for the FdUMP-mediated inhibition of TS (Ducker and Rabinowitz, 2017). 1C-loaded folates are not known to transfer across membranes; thus, 5,10-mTHF must be locally generated (Ducker and Rabinowitz, 2017). 5,10-mTHF can be made from the amino acids serine and glycine. Glycine can be degraded via the glycine cleavage system (GCS) to generate NH_3 , CO_2 , and a methyl group that is incorporated into 5,10-mTHF. Separately, the reaction that converts serine to glycine also donates a 1C group to THF to form 5,10-mTHF, which is then available to participate in the methyl transfer reaction that converts dUMP into dTMP. Indeed, 1C units derived from radiolabeled serine are incorporated into nucleotides (Snell et al., 1987). Importantly, the levels of 5,10-mTHF are known to limit the efficacy of fluoropyrimidines (Malet-Martino and Martino, 2002; Ullman et al., 1978).

Several 1C-metabolites are obtained directly or indirectly from the diet, and the therapeutic value of their dietary supplementation is widely exploited (Ducker and Rabinowitz, 2017). Serving as a substrate for the synthesis of 5,10-mTHF, the 1C-metabolite folinic acid is the most efficient fluoropyrimidine potentiator (Malet-Martino and Martino, 2002). As such, the combination of fluoropyrimidines with folinic acid is the standard treatment for colon cancer (Malet-Martino and Martino, 2002). A direct intake route has been delineated for several dietary 1C-metabolites including folates, and serine (Ducker and Rabinowitz, 2017). By contrast, the

potential for bacterial uptake routes for 1C-metabolites has not been given much attention despite evidence in its favor (Kok et al., 2020). Studies in mammals show bacterially-converted dietary para-aminobenzoate-glutamate – one of the two moieties composing THF – in host tissues (Asrar and O'Connor, 2005; Rong et al., 1991), *C. elegans* studies demonstrate that *E. coli* mediates the effect of dietary supplementation of folic acid on lifespan (Maynard et al., 2018), and mouse studies show that bacterially-derived serine can affect kidney function (Nakade et al., 2018). Given that dietary 1C-metabolites, such as folinic acid, are among the most effective potentiators of fluoropyrimidine action, and that the microbiota can alter dietary 1C-metabolites or produce them from dietary precursors, 4-way interactions between dietary folates or their precursors, fluoropyrimidines, microbes, and the host, could modulate fluoropyrimidine efficacy and/or toxicity *in vivo*. In the past several years, *C. elegans* has been exploited as a model system to study complex drug-microbe-host interactions. Garcia *et al.* (García-González et al., 2017) and Scott *et al.* (Scott et al., 2017) developed a 3-way drug-microbe-*C. elegans* system revealing that microbes mediate chemotherapeutic efficacy in *C. elegans*. More recently, Pryor *et al.* developed a host-microbe-drug-dietary nutrient screen to study the interaction between *C. elegans*, *E. coli*, the biguanide metformin, and dietary nutrients (Pryor et al., 2019). Here we independently developed 3 and 4-way screening strategies to identify and mechanistically dissect the 4-way interactions that modulate FUdR toxicity in *C. elegans*.

First, we investigate the mechanism of toxicity underlying the 3-way interaction between FUdR, *E. coli*, and *C. elegans*. On the microbe side, we validate that conversion of FUdR into 5-fluorouridine monophosphate (FUMP), and not dTMP depletion, contributes to toxicity in *C. elegans*. On the host side, we define that FUdR toxicity (likely via worm-derivatives of FUMP) targets mitochondrial RNAs and DNA, and that *C. elegans* die from activation of a lethal mitochondria-to-autophagy axis. Then, we investigate the 4-way interaction between dietary metabolites, FUdR, *E. coli*, and *C. elegans*. We show that dietary supplementation with thymidine or serine transforms sublethal doses of FUdR (no apparent toxicity) into lethal ones (100% embryonic lethality) through altering the metabolism of the microbe. However, the mechanisms of action of thymidine and serine are distinct. Thymidine simply enhances the mechanisms driving the 3-way interaction, while serine acts via enabling dTMP depletion in *E. coli* and consequently in the host. Most strikingly, dietary serine redefines, or even reverts, the role that host pathways have on executing FUdR toxicity, unveiling sub-phenotypic complexity in 4-way diet-drug-microbiota-host interactions.

5.3 Material and Methods

C. elegans and E.coli strains

C. elegans strains N2 (Bristol, UK), MT2547 (*ced-4* mutant n1162) and MT4770 (*ced-9* mutant n1950) were obtained from the Caenorhabditis Genetics Center (CGC). MAH215 (Chang et al., 2017) is a kindly gift from Dr. Malene Hansen. Unless otherwise noted, experiments were initiated with synchronized L1 larvae obtained by egg bleaching and overnight synchronization in S-buffer. Wild type *E. coli* strain BW25113 and Keio KO strains were obtained from the *E. coli* Genetic Stock Center. *E. coli* strain HB101 was obtained from CGC. EORB1 and EORB1 RNAi library were constructed in our lab.

E. coli culturing and compound supplementation

For every biological replicate fresh *E. coli* streaks or library stamps on LB-carbenicillin 50µg/mL (RNAi clones) or LB-kanamycin 25µg/mL (Keio KO library) were used. Bacterial cultures were started from single colonies or using a sterilized inoculating hedgehog, and grown overnight for 14-16h. Keio clones were grown overnight in LB kanamycin 15µg/mL, RNAi clones were grown overnight in LB carbenicillin 50µg/mL in the absence of IPTG (or any other additives). The parental strain BW25113 was grown on plain LB. For aeration, flasks were shaken at 250 rpm, and 1.2mL deep 96-well plates at 1,000 rpm. For targeted experiments bacteria were harvested by centrifugation at room temperature and resuspended to OD_{600nm} = 20 in S-buffer (~20X concentrated). For screening, 1.2mL bacterial

cultures were resuspended with 20 μ l of S-buffer. Concentrated *E. coli* were seeded onto NGM or NGM-RNAi plates immediately and never exposed to the cold.

For dietary supplementation, metabolites were dissolved in water (unless otherwise stated), filter sterilized, seeded on NGM or RNAi plates, and dried in biosafety hood. Concentrated bacteria were seeded as soon as metabolites dried out. FUdR was dissolved in water to 100x concentration, filter sterilized, and added directly onto bacterial lawns immediately after lawns were dried. Seeding dietary supplement, fresh bacteria, and FUdR in that order, and adding supplements and FUdR within a 2h window of seeding fresh bacteria is critical to observe the full effect of the supplements. Synchronized hatchlings were seeded the same day for all experiments except for *C. elegans* RNAi experiments (24h later to activate RNAi). When post-developmental transfer (i.e. embryogenic competence in Fig. 5.1 e) was necessary, worms were grown in the *E. coli* background in which they were later tested.

Toxicity scoring

Imaging and image analysis

Percent hatchling was measured by taking ≥ 5 images of each treatment or mock plate per biological replicate, and at least 3 independent biological replicates were carried out for all assays. Images were taken on Zeiss Axio Zoom.v16 dissecting microscope, PlanNeoFluar Z 2.3X/0.57 FWD objective, zoom 30X. Hatchlings, live and dead eggs and adults were quantitated assisted by ImageJ object counting

tool. Values in figures are presented as “% hatchling relative to mock”, meaning the number of hatchings was first normalized to total progeny (hatchlings + live embryos + dead embryos) in each treatment and then normalized to the % hatchlings in the corresponding non-FUdR (mock) treatment. This provides a quantitative measurement controlling for other variables such as the time of scoring. For Keio clones and RNAi experiments, treatments are normalized first to mock of the same Keio clone or RNAi and then to WT, which takes into account the potential effect of the Keio or RNAi clones on worm health. However, we did not observe Keio or RNAi only effects in any of the *E. coli* or worm genes inactivations reported as hits. Estimation example: if BW25113 + 1 μ g/mL FUdR = 21 hatchlings/185 progenies (hatchlings + live embryos + dead embryos), and BW25113 untreated = 197 hatchlings/201 progenies, this implies % hatchlings for BW25113 in FUdR relative to untreated is 11.58% ($11.35/98 \times 100$). Then, if *deoA* shows hatchling/progeny ratios of 168/176 in FUdR and 194/199 in control, by the same calculation *deoA* % hatchling is 97.91%; thus, if reproducible, *deoA* is a suppressor. For enhancers, lower doses of FUdR are used and the calculations take into account the effects of FUdR relative to wild type, but in this case the WT + FUdR will show subtle toxicity. As an example, if BW25113 + 0.5 μ g/mL FUdR = 80 hatchlings/152 progenies and BW25113 untreated = 198 hatchlings/200 progenies, % hatchlings for WT BW25113 in this condition is 53.16%. If *ndk* + 0.5 μ g/mL FUdR has 25 hatchlings/148 progenies and *ndk* untreated has 205 hatchlings/208 progenies, % hatchlings in worms fed *ndk* is 17.13%, so *ndk* is an enhancer because when cultured on this *E. coli* mutant

worms produce less viable progeny than when fed wild-type *E. coli*. All toxicity measurements were repeated ≥ 3 times and the mean \pm SEM are presented.

Occasionally, embryogenic competence was calculated to identify enhancers of toxicity. The calculation is inclusive of hatchlings, live eggs and dead eggs produced per worm, and is influenced by the effect of FUdR (+/- supplements) on both the rate of development and the fertility of the P₀s. Therefore, lesser embryogenic competence or P₀ developmental delay compared to wild-type or unsupplemented reveals enhancers, whereas increased embryogenic competence reveals suppressors. Specifically, 10 worms were singly transferred to test plates, and allowed to lay progeny for 24h. Next day the total number of progeny (live + dead embryos) were counted per plate. Normalization of embryogenic competence was done as described above for %hatchlings.

Dietary metabolite 4-way screen

Amino acids were freshly dissolved to 10mg/mL in water (except tyrosine: 1mg/mL), aluminum foiled, rocked for 12h at RT, and filter sterilized. Seven 1:2 serial dilutions were made. 10 μ L per dilution were seeded in quadruplicate into 96-well plates with 100 μ L NGM per well. Once dry, wells were seeded with 8 μ L of fresh 20x HB101. Once dry, 2 plates (duplicate) were seeded with 5 μ L of 250 μ g/mL FUdR (final 12.5 μ g/mL). The remaining two plates (duplicate) were left as no FUdR controls to test the potential toxicity of the amino acids. Once dry, 25 synchronized hatchlings were seeded per well and incubated at 20°C. Altogether, the following

conditions were tested: 1) Negative control: 12.5µg/mL FUdR only, which leads to 100% sterile adults but no developmental delay; 2) Positive control: 12.5µg/mL FUdR supplemented with 5mg/mL thymidine, which leads to 100% larval arrest; 3) Amino acid toxicity control: wells supplemented only with the 8 doses of amino acids (but no FUdR), to test for the potential toxicity of the amino acids; and 4) Screening wells: wells supplemented with the 8 doses of amino acids and 12.5µg/mL FUdR. After 60 and 72h, wells were scored as follows for worm developmental stages: 1 = L1/dead, 2 = L2 larvae, 3 = L3 larvae, 4 = L4 larvae, 5 = Young adults (<5 eggs in body), 6 = Gravid adults (>5 eggs in body). Only wells which showed a ≥ 1 stage delay in FUdR + amino acid compared to FUdR only, and the AA showed no toxicity on its own, were considered hits.

Supernatant and pellet test

Saturated overnight *E. coli* cultures were re-inoculated 1:50 in liquid NGM (Nematode Growth Media without agar), and grown to $OD_{600nm} \sim 1$, at which point water (mock), Lth-FUdR (50µg/mL), or subLth-FUdR (1µg/mL) \pm thymidine (5mg/mL) or serine (1.5mg/mL) were added. After 2 more hours of incubation at 37°C, bacteria were pelleted and re-suspended in ≥ 50 volumes of water 3 times to remove residual FUdR from the bacterial suspension. On the final wash, OD_{600nm} absorbance was measured and bacteria were resuspended to $OD_{600nm} = 20$, and 100µL were seeded onto NGM plates. Once lawns were dried, 100 hatchlings were seeded and incubated at 25°C. At multiple times between 60-96h plates were imaged for scoring of developmental stages and fertility. The same setup was used

for supernatant experiments, but after centrifugation the supernatants were taken on ice, filtered-sterilized through a 0.22 μ m filter, lyophilized overnight, and resuspend in water to make 1 and 5x concentrated supernatants. 100 μ l of the sterile supernatant resuspensions were seeded on top of *upp;udk;udp* triple KO *E. coli* lawns. We used 3KO lawns to avoid in-plate conversion of FUdR remaining in the supernatant. Once supernatants dried, 100 hatchlings were seeded and incubated at 25°C. At multiple times between 60-96h, plates were imaged for scoring of developmental stages and fertility.

E. coli 4-way screen

Keio screen for mediators of SE-FUdR toxicity was performed at 25°C in 8 conditions: 1) mock (water), 2) FUdR 0.25 μ g/mL, 3) serine 1.5mg/mL, and 4-8) serine 1.5mg/mL plus FUdR from 0.05 to 0.25 μ g/mL (setup depicted in Fig. 3a). Keio clones were grown overnight in 1.2mL of LB kanamycin in deep 96-well plates at 37°C and 1,000 rpm. Cultures were pelleted, supernatants discarded and pellets resuspended in 20 μ l of S-buffer. Eight microliters of bacterial suspension were seeded into wells containing 100 μ L of NGM plus or minus serine. Once bacteria dried, 5 μ L of 1, 2, 3, 4, or 5 μ g/mL FUdR were seeded onto bacteria lawns (final doses 0.05, 0.1, 0.15, 0.2, and 0.25 μ g/mL, respectively). Once dried, 50 synchronized hatchlings were seeded and incubated at 25°C. The non-FUdR controls allowed us to determine whether any given *E. coli* KO clone would adversely affect development or fertility on their own or in combination with serine only. FUdR-only wells were scored after 60-72h relative WT *E. coli* BW25113 as

follows: -2 = no hatchlings, -1 = fewer hatchlings, 0 = similar to WT control, 1 = more hatchlings than control, 2 = similar to no-FUdR control. FUdR + serine wells were scored after 60-96h for developmental delay or embryogenic competence relative to relative WT *E. coli* BW25113 control as follows: -2 = severely delayed P0, -1 = moderate delay P0/few eggs laid, 0 = similar to control (sterile adult), 1 = some hatchlings, 2 = similar to no-serine control. Only genes showing a consistent suppressor or enhancer phenotype in FUdR plus serine condition at multiple doses or in >2 screen repeats were considered hits. All Keio hits were verified by PCR and sequencing. Primary hits are presented in Table 5.2 as: blue = suppressor of toxicity; orange= enhancer of toxicity; and white= no different from WT control. Light blue or orange, represents phenotype observed in only 1 of screen 3 repeats. Hits belonging to overrepresented metabolic pathways were retested in 6cm NGM plates and quantitated for % hatchlings in sublethal FUdR (0.25µg/mL) ± serine (1.5mg/mL), and the results are presented in main figures. Primary screen hits that were not retested in 6cm plates are depicted as NRT in Table 5.2 Retested and verified hits and non-hits are marked as “√”, and retested but not validated primary hits (phenotype did not repeat) are marked as “X”.

Bacterial growth measurements

CFU

E. coli BW25113 and HB101 were cultured and seeded in NGM ± additives plates as normally done for Lth-FUdR or SE-FUdR tests. After 48h exposure to treatments, cells were exhaustively recovered from the plates, resuspended in

equal volumes, and biomass (OD_{600nm}) and viability (CFU of serial dilutions from 10⁰-10⁻⁷) were quantitated.

Growth in liquid

HB101, BW25113 and Keio hits were hedgehog seeded from frozen stocks onto LB agar omnitray plates. Next day, 100µl of liquid NGM ± subLth-FUdR ± serine were stamp-seeded in duplicate. Absorbance at 600nm was recorded longitudinally using a SpectraMax plate reader maintained at 37°C in a continuous shaking mode. Measurements were independently carried out more than three times. Growth of *E. coli* BW25113 in complete liquid NGM in the presence of 10µM, 100µM, or 1mM 5'-iodo-dUMP relative to mock was assessed as described above. No effect on growth was observed (data not shown).

Bacteria and C. elegans Metabolomics

For Lth-FUdR and dietary supplementation-related metabolomics, single colonies of *E. coli* BW25113 or HB101 were used to inoculate 500mL of LB and incubated overnight for 14h at 37°C 250 rpm. Bacteria were harvested by centrifugation, and resuspended in 25mL of S-buffer. Concentrated bacteria were seeded on nylon membranes placed on the surface of the NGM plates to avoid “contamination” of the bacteria with NGM-agar media. For this, 5mL of concentrated bacterial suspension were dried onto 90mm Nylon membranes (VWR 7402-009) by vacuum filtration in a sterile porcelain Buchner funnel. The nylon membranes loaded with bacteria were placed on the surface of 15cm NGM agar plates with or without the

respective supplementations (i.e. \pm FUdR and \pm thymidine or \pm serine). After 24h at 25°C, *E. coli* were harvested by washing the bacteria off the membrane with 50mL of cold liquid NGM. Bacteria were then washed 2 more times with 50mL of cold water. To confirm effectiveness of the treatments, 100 μ l of bacterial suspension were seeded on NGM plates without any additives, hatchlings were seeded on these lawns, and incubated for 60h at 25°C; a time at which they were scored for progeny viability. The remaining of the washed bacterial pellets were flash frozen, lyophilized, and kept at -80°C for later extraction as described below. Samples verified via parallel hatchling-viability controls were processed for LCMS analyses.

For supernatant analyses of thymidine-enhanced toxicity, single colonies of *E. coli* BW25113 were used to inoculate 20mL of LB broth and incubated overnight for 14h at 37°C 250 rpm. Next morning cultures were pelleted, washed, and resuspended in equal volume of liquid NGM. Ten milliliters of this bacterial resuspension were used to inoculate 500mL of liquid NGM supplemented with mock, or subLth-FUdR \pm thymidine (5mg/mL), and incubated for another 2h at 37°C 250 rpm. Mock and treated cultures were then harvested by centrifugation. The supernatants were filter-sterilized to remove residual bacteria. Aliquots (10mL) were spiked in with the internal standards listed below, frozen, lyophilized, and reconstituted right before LCMS in 1:1 acetonitrile: water. The bacterial pellets were washed 2 more times with 50mL of cold water, flash frozen and lyophilized, and kept at -80°C for later extraction as described below.

To generate worm metabolomics samples, 50,000 synchronized 1-day gravid adult worms were harvested, washed in a 40 μ m mesh 1X with 50mL of NGM, incubated for 5 min in clean media to allow gut clearance, and then mesh-washed again with 50mL cold liquid NGM and 1X with 50mL of cold water, and immediately frozen in liquid nitrogen and lyophilized, and kept at -80°C for later extraction as described below.

Right before resuspending the lyophilates, a master mix of internal standards was prepared by mixing the following compounds at a final concentration of 20ng/ μ L in HPLC-grade methanol: 1) 1,3-¹⁵N₂ Uracil (Cambridge Isotope lab NLM-637-PK); 2) Uridine-¹³C₉,¹⁵N₂ 5'-triphosphate (Sigma #645672); and 3) Glycine-¹³C₂, (Sigma #283827). Then, the spike-in control master mix was diluted 1/50 in 80% methanol. 20mg of lyophilized bacteria (less than 10mg was insufficient to detect nucleotides or serine) or 5mg of lyophilized worms were resuspended in 500 μ L of the diluted internal standard solution. Samples were mixed with 200 μ L of 100 μ m silica beads and disrupted 5X for 30s in a mini-beadeaterTM-8 disruptor with cooling on ice for 2min after each cycle. Extracts were cleared through 2 rounds of 15min centrifugation at 4C and 20,000g, and then lyophilized. To measure endogenous metabolites, samples were reconstituted right before LCMS in 1:1 acetonitrile: water. Samples were separated on a Luna aminopropyl column (3 μ m, 150 mm \times 1.0 mm I.D., Phenomenex) or a CORTECS T3 column (2.7 μ m, 150 mm \times 2.1 mm I.D., Waters) and analyzed using an Agilent 6530 Q-TOF, an Agilent 6540 Q-TOF, or a Thermo Scientific Q Exactive Plus. The Luna column was used in negative

mode with the following buffers and linear gradient: A = 95% water, 5% acetonitrile (ACN), 10 mM ammonium hydroxide, 10 mM ammonium acetate; B = 95% ACN, 5% water; 100% to 0% B from 0-30 min and 0% B from 30-40 min; flow rate 50 μ L/min. The T3 column was used in positive mode with the following buffer and linear gradient: A = 95% water, 5% ACN, 10 mM ammonium acetate, 0.1% formic acid; B = 95% ACN, 5% water; 0% to 100% B from 0-30 min and 100% B from 30-40 min; flow rate 200 μ L/min. The identity of each metabolite was confirmed by comparing retention times to standard compounds and tandem MS data with the METLIN metabolite database. To measure fluorometabolites, samples were reconstituted right before LCMS in 2:1:1 water:methanol:acetonitrile, and 3 μ l were further analyzed by liquid chromatography-mass spectrometry (LC-MS) as follows. Metabolite profiling was performed using Ultimate 3000 UHPLC (Dionex) coupled to Q Exactive Plus-Mass spectrometer (QE-MS, Thermo Scientific). A hydrophilic interaction chromatography method (HILIC) employing an Xbridge amide column (100 x 2.1 mm i.d., 3.5 μ m; Waters) was used for polar metabolite separation. Detailed LC method was described previously (Liu et al., 2014a), except that mobile phase A was replaced with water containing 5 mM ammonium acetate (pH 6.8). The QE-MS is equipped with a HESI probe with related parameters set as below: heater temperature, 120 $^{\circ}$ C; sheath gas, 30; auxiliary gas, 10; sweep gas, 3; spray voltage, 3.0 kV for the positive mode and 2.5 kV for the negative mode; capillary temperature, 320 $^{\circ}$ C; S-lens, 55; scan range (m/z): 70 to 900 for pos mode (1.31 to 12.5 min) and neg mode (1.31 to 6.6 min) and 100 to 1000 for neg mode (6.61 to 12.5 min); resolution: 70000; automated gain control (AGC), 3×10^6 ions.

Customized mass calibration was performed before data acquisition. LC-MS peak extraction and integration were performed using commercially available software Sieve 2.2 (Thermo Scientific). For all metabolites, peak sizes of the target metabolites (P) were normalized to the corresponding internal standard (IS) peak area (amino acids to Glycine-13C2, nucleotides to UMP-13C9,15N2, and nucleosides to Uracil-15N2). The normalized peak value from the treatments was then normalized to the mock control from the same biological replicate. Therefore, target metabolite relative abundance was estimated as follows $(P/IS)_{\text{treatment}} / (P/IS)_{\text{mock}}$ from 3-5 independent biological replicates

EORB1 strain construction

To construct the RNAi-competent EORB1 strain, *E. coli* HB101 was first transiently made *recA+*. Then *rnc14* was interrupted with mini-Tn10 transposon introduced via P1 transduction. Transduced colonies were selected in 25µg/mL tetracycline (Tet). Tet-resistant colonies were picked and re-streaked for two rounds, and then cured of the *recA* plasmid by growing in LB at 44°C. Streaking onto LB plates containing chloramphenicol (25µg/mL) and treating with UV confirmed loss of chloramphenicol resistance and the reappearance of sensitivity to UV. Loss of RNaseIII function should prevent the maturation of rRNAs. The *rnc-* phenotype was confirmed as accumulation of the 30S rRNA precursor (Fig. 5.13 a). T7 polymerase (under the control of the *LacUV5* promoter) and the transcriptional repressor *LacI* were then introduced via lysogenization (λ DE3 Lysogenization Kit; Novagen 69734). The presence of inducible T7 polymerase was confirmed by

western blot (Fig. 5.13 b). The final EORB1 strain has the genotype [HB101], *rnc-*, *lacI-lacUV5p-T7*. EORB1 was confirmed to be competent for feeding RNAi by phenotypic analysis. RNAi against the genes *daf-2*, *unc-22*, *dpy-13*, and *pos-1* displayed the expected phenotypes when delivered via feeding RNAi from EORB1 (Fig. 5.13 c-f). To construct the EORB1 library, we miniprep (QIAprep 96-plus Miniprep Kit; Qiagen 27291) the screened constructs from HT115 Ahringer RNAi library. EORB1 was made chemically competent by CaCl_2 preparation. 5 μL of the plasmid minipreps were added to 50 μL of chemically competent EORB1 heat shocked at 42°C, and grown overnight in liquid LB-carbenicillin 50 $\mu\text{g}/\text{mL}$. Transformants underwent a second and third round of selection on solid and liquid LB-carb50, after which glycerol stocks were made.

4-way *C. elegans* RNAi screen and verification

RNAi screens were performed at 25°C in 96-well plates. RNAi clones were grown in 1.2mL of LB carbenicillin for 12-16h in 96-deep-well plates at 37°C and 1000 rpm. Cultures were harvested by centrifugation. Pellets were suspended in residual LB volume, and 8 μL were seeded into wells containing 100 μL of NGM with 50 $\mu\text{g}/\text{mL}$ carbenicillin and 5mM IPTG (though 1mM IPTG is sufficient). Wells were then seeded with $\pm 2.5\mu\text{g}/\text{mL}$ FUdR, and $\pm 5\text{mg}/\text{mL}$ thymidine or $\pm 1.5\text{mg}/\text{mL}$ serine as appropriate. After drying in biosafety hood, plates were left overnight at room temperature to allow RNAi induction. The next day, 25 L1 larvae were seeded and grown for 60-72h. At this point, controls were confirmed to have 0 hatchlings and plates were scored as follows: 0 = similar to control, 1 = ~1-10

hatchlings, 2 = ~11-50 hatchlings, 3 = ~51-100 hatchlings, 4 = >100 hatchlings, and -1= developmental delay. All RNAi hits were sequence verified. Primary hits are presented in Table 5.4 as: blue = suppressor of toxicity; orange= enhancer of toxicity; and white= no different from WT control. Light blue or orange represents phenotype observed in only 1 of screen 3 repeats. Hits belonging to overrepresented pathways were retested and quantitated for % hatchlings in 6cm plates, and the results are presented in main figures. Not retested hits are depicted as NRT in Table 5.4, while retested and verified hits and non-hits are marked as “√”, and retested but not validated RNAi clones (phenotype did not repeat) are marked as “X”.

Autophagic flux

LGG1 antibody

Anti-LGG1 (Rabbit) antibodies were generated by Covalab (Villeurbanne, France) against peptides FEKRRRAEGDKIRRKY and GQLYQDHHEEDLFLY (sequence optimized and kindly shared by Vincent Galy). Serum was immunopurified and anti-LGG-1 specificity was validated in western blots using WT, *lgg-1* RNAi and *lgg-1* OE samples as controls (Fig. 5.14 b).

Western blotting

For all but cytochrome C (cytC) samples, western blotting samples were prepared from 2 plates of 2,000 worms grown at 25°C for each treatment. After 50h, 2,000 worms from one of plates were harvested and reseeded in NGM plates with the

same additives (i.e. \pm subLth-FUdR and \pm serine) plus 20mM chloroquine (CQ). After 8h of treatment, worms were harvested from both sets of plates (\pm CQ), washed 3X with S-buffer to remove residual bacteria, and immediately frozen in liquid nitrogen. Frozen worm pellets were resuspended in 2 volumes of 1x RIPA buffer (Sigma #R0278) and sonicated. Aliquots of soluble proteins were quantitated using BCA Thermo kit (Pierce 23227), and the rest mixed with 3X SDS-PAGE sample loading buffer, and incubated for 5min at 85°C. 30 μ g of protein were loaded to each lane of a 4-12% Bis-Tris gel (Fisher NP0322BOX), and ran for 55min at 200V in MES running buffer. Gels were transferred to 0.2 μ m nitrocellulose membranes in transfer buffer (Fisher NP0006) with 20% methanol at 30V for 45min. The membranes were stained with Ponceau red to evaluate the quality of the SDS-PAGE and transfer, and then blocked with Intercept[®] (PBS) Blocking Buffer (Li-Cor 927-70001) with 0.1% Tween for 4h. Membranes were exposed to primary antibodies including α -LGG1 1:250 (custom made by Covalab), anti- α -tubulin 1:10,000 (DSHB 4A1), α -HSP-60 1:1000 (DSHB HSP60), α -cytC 1:1000 (Abcam 37BA11) overnight at 4C. Membranes were washed 3X15min with PBST (0.1% tween) and incubated with secondary antibodies 1:10,000 for 1h at room temperature (IRDye[®] 800CW Goat anti-Mouse IgG Secondary Antibody, CAT#925-32210, and IRDye[®] 800CW Goat anti-Rabbit IgG Secondary Antibody, CAT#925-32211), and imaged by Li-Cor Odyssey imager. Samples for cytC western blotting were prepared and assessed as previously described (Zhou et al., 2019).

Autophagy flux in treated animals relative to mock was calculated by measuring integrated density (I) of each band and normalized as shown in Fig. 5h. Autophagy flux relative to mock was then estimated as: $\Delta\Delta\text{LGG-1} = ((\text{LGG-1}_{\text{treatment+CQ}} / \text{Tubulin}_{\text{treatment+CQ}}) / (\text{LGG-1}_{\text{treatment no CQ}} / \text{Tubulin}_{\text{treatment no CQ}})) / ((\text{LGG-1}_{\text{mock+CQ}} / \text{Tubulin}_{\text{mock+CQ}}) / (\text{LGG-1}_{\text{mock no CQ}} / \text{Tubulin}_{\text{mock no CQ}}))$.

In vivo fluorescent reporter-based measurement of autophagic flux

Two hundred 1day-adult worms (strain MAH215) from each treatment (mock, sublth-FUdR, serine, sublth-FUdR+serine, or Lth-FUdR) were harvested with S-buffer, washed 3X, and incubated 30s with egg-prep bleaching solution. Worms were then washed 3X in S-buffer, and mounted onto agar pad on glass slides (Thermo, 3011) with #1.5 coverslip (Fisher 1.5 22X22mm). Z-stacks to measure autophagic flux in embryos were captured on Nikon Eclipse Ti spinning disc confocal microscope, 40X/1.3NA objective, 500ms exposure time and 80% laser intensity. All the images from each biological replicate were identically processed using ImageJ. Firstly, maximum projections of the fluorescent and bright field channels were created in Image J. Then the embryos were cropped out for analysis. ImageJ plot profiling combined with thresholding was used to detect and quantitate LGG-1::GFP dots. Average GFP signal of >15 individuals from ≥ 4 biological replicates are depicted for each treatment. Then, $\Delta\text{LGG-1} = \text{average GFP signal in CQ(+)} / \text{average GFP signal in CQ(-)}$ is calculated for each treatment (i.e. Lth-FUdR) and control. Lastly, all repeats (n=4) of $\Delta\text{LGG-1}_{\text{treatment}}$ and $\Delta\text{LGG-1}_{\text{control}}$ are compared using ratio t-test.

qPCR analysis

One-day gravid adults were harvested, washed in a 40 μ m nylon mesh, and quickly frozen in liquid nitrogen. Samples were kept at -80°C until RNA extraction. Total RNA was isolated using TriReagent (MRC). To quantitate expression of mitochondrially encoded RNAs (no introns), DNA was removed by DNase I (Sigma AMPD1) treatment prior to retrotranscription with random hexamer primers. All qRT-PCR reactions were performed in triplicate. Median \pm SEM of *ddCt* is reported (Pfaffl, 2001). For measurement of mitochondria to nuclear DNA ratios, 100 gravid worms from mock and treatments were lysed with SWLB (single worm lysis buffer with 0.3% proteinase K) and the supernatants containing DNA were collected and used as template. iTaq Universal SYBR Green Supermix (Biorad 1725120) reactions run in BioRad CFX96 thermocycler were analyzed using *ddCt* (Pfaffl, 2001).

Statistics and data representation

All statistical analyses were performed in Graphpad Prism. Outliers were detected and removed from analyses using the ROUT method. For %hatchlings, embryonic competency, and GFP intensity quantifications, unpaired nonparametric t-test was used to make single comparisons between a specific treatment and mock control in. Ratio t-test was used to compare all ratios including qPCR fold changes, Δ LGG-1, CFU, and normalized LC-MS ratios. Unless otherwise stated, significance was represented as follows: * $p \leq 0.05$, ** $p \leq 0.01$, *** $p \leq 0.001$ and **** $p \leq 0.0001$. All error

bars throughout this study represent S.E.M. All experiments were performed and quantitated at least 3 independent times.

5.4 Results

5.4.1 FUdR toxicity in *C. elegans* is driven by FUMP synthesis and not dTMP depletion in *E. coli*

To define if and how dietary nutrients alter the toxicity of FUdR in *C. elegans*, it is required first to identify the minimum dose leading to robust toxicity (i.e. 100% embryonic lethality) for further screens on dietary enhancers and inhibitors of the toxicity. We identified 1 ± 0.25 $\mu\text{g}/\text{mL}$ FUdR as the dose causing 100% embryonic lethality when worms were cultured on *E. coli* BW25113 (parental strain of all *E. coli* mutants used in this study), and 7.5 ± 2.5 $\mu\text{g}/\text{mL}$ FUdR as the dose causing 100% embryonic lethality when worms were cultured on *E. coli* HB101 (parental strain of all *C. elegans* RNAi clones used in this study). We hereinafter refer to these doses as Lth-FUdR (for Lethal FUdR) (Fig. 5.1 a).

We then moved on to defining the mechanism of toxicity of Lth-FUdR using a 3-way FUdR-*E. coli*-*C. elegans* high-throughput screening strategy (summarized in Fig. 5.2 a). We found that KO of *E. coli deoA* suppresses Lth-FUdR toxicity in *C. elegans* (Fig. 5.2 b,c). DeoA can convert FUdR into Fluorouracil (5-FU) (Fig. 5.2 a). Scott *et al.* demonstrated that 5-FU is also a prodrug that needs to be converted to be toxic to *C. elegans* (Scott et al., 2017). Hence, *E. coli* DeoA likely carries out one of multiple steps in the conversion of FUdR into the actual toxic derivatives. A reasonable hypothesis would be that the toxic derivative that *E. coli* produces is FUMP, as this would be in line with genetic evidence presented by Garcia *et al.* (García-González et al., 2017). However, single KO of *E. coli upp*, *udp*, or *udk*

was not sufficient to suppress Lth-FUdR toxicity in our screen or follow up retesting (Fig. 5.1 b,c). As *upp* and *udk* encode for redundant enzymes capable of converting 5-FU into FUMP, we tested a double KO. Indeed, double KO of *E. coli upp* and *udk* completely suppresses Lth-FUdR toxicity in *C. elegans* (Fig. 5.2 b,c). These results suggest that *E. coli* uses the pyrimidine ribonucleotide salvage pathway (i.e. FUdR-to-FUMP conversion pathway) to convert the prodrug FUdR into a derivative toxic to *C. elegans*. Because nucleotide polyphosphates may not be efficiently taken up by the host, FUMP would be more likely than its downstream derivatives FUDP or FUTP to be the toxic derivative that *E. coli* produces and *C. elegans* takes up. To approximate an answer to this question, we supplemented the plates with UMP (the non-fluorinated analog of FUMP), or the UMP precursors uridine and uracil. We found all 3 compounds to rescue Lth-FUdR toxicity in *C. elegans*. By contrast, supplementation with UDP only minimally rescues (possible due to residual UMP) and UTP does not rescue the toxicity (Fig. 5.1 d). These results are in line with the notion that nucleotide monophosphates or their unphosphorylated precursors can cross membranes, and hence, could be taken up by the *C. elegans* host while nucleotide polyphosphates would not, and suggest that *E. coli*-generated nucleotide polyphosphates may not be significant contributors to *E. coli* mediated FUdR toxicity in *C. elegans*. In further support of this notion, chemical inhibition of Tmk (the *E. coli* enzyme that would produce FUDP) further enhances (instead of suppressing) Lth-FUdR toxicity (Fig. 5.1 e). Similarly, KO of *ndk* (the *E. coli* gene encoding the enzyme that would produce FUTP) enhances FUdR toxicity (Fig. 5.2 d,e). Together, the data argue against *E.*

coli-generated FUDP or FUTP being significant contributors to FUdR toxicity in *C. elegans*. Another *E. coli*-generated and potentially toxic derivative of FUdR is 5'-fluorouridine (FUrd). However, KO of *yjjG* (the *E. coli* gene encoding the enzyme that produce FUrd) enhances FUdR toxicity in *C. elegans* (Fig. 5.2 d,e). Furthermore, the *upp;udk* double KO (2KO) and the *upp;udk;udp* triple KO (3KO) both rescue Lth-FUdR toxicity to the same extent (Fig. 5.1 c,f). This result argues against FUrd being a significant contributor to *E. coli*-mediated FUdR toxicity, because in the 2KO, FUrd synthesis is favored due to 5-FU to FUrd conversion, while in the 3KO, such conversion is blocked (pathway scheme in Fig. 5.2 a).

Finally, a major candidate to be an *E. coli*-generated mediator of the toxicity is FdUMP. *E. coli*-generated FdUMP could act via: 1) inhibiting *C. elegans* TS post-ingestion; or 2) inhibiting *E. coli* TS and consequently reduce the availability of thymidine in the *C. elegans* diet because *E. coli* is the main source of nucleotides for *C. elegans* (Chi et al., 2016). An essential step for both mechanisms of action is that *E. coli* thymidylate kinase (Tdk) converts FUdR into FdUMP. The result of the screen and the follow up retesting showing that KO of *tdk* enhances, instead of suppressing, Lth-FUdR toxicity (Fig. 5.2 f) argues against an FdUMP-dependent mechanism of action. In the same line, thymidine supplementation enhances, instead of rescues, Lth-FUdR toxicity (Fig. 5.2 g,h), and LCMS analyses show that the levels of dTMP did not drop in *E. coli* treated with a lethal dose of FUdR (Fig. 5.2 i). Thus, the evidence argues against FdUMP directly produced by *E. coli*, or dTMP depletion in *E. coli* contributing to Lth-FUdR toxicity in *C. elegans*.

In summary, when FUMP synthesis is blocked, we observe abrogation of the toxicity, and when FUMP synthesis or accumulation is promoted, we observe enhanced toxicity. In addition, blocking FdUMP synthesis (*tdk* KO) enhances the toxicity. Therefore, our data support a model in which FUMP would be the major link between microbe and host fluoropyrimidine metabolism, and host-generated derivatives of FUMP (e.g. FUTP or FdUTP) would promote toxicity in the host.

Figure 5. 1

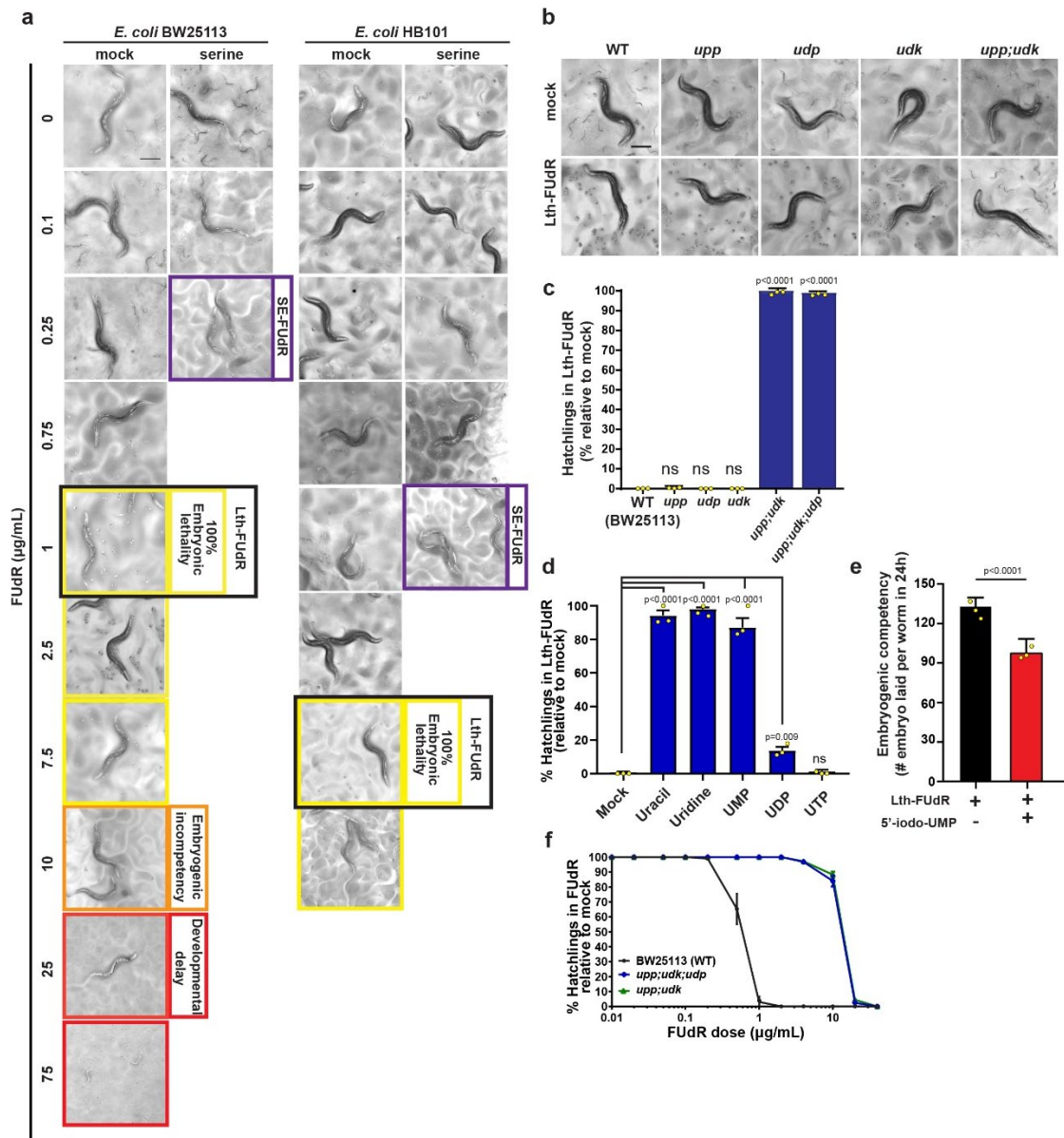


Figure 5.1 Throughout this figure % hatchlings is estimated as [(live hatchlings/(live hatchlings + live embryos + dead embryos))] in condition of interest (i.e. Lth-FUdR) relative to % hatchlings in mock of the same *E. coli* or *C. elegans* genotype; ≥ 5 images of each treatment were quantitated. Statistical significance was assessed via two-tailed unpaired nonparametric t-test for %hatchlings quantification. Scale bars = 200 μ m, error bars = S.E.M., and * $p \leq 0.05$, ** $p \leq 0.01$, *** $p \leq 0.001$, **** $p \leq 0.0001$. n= # independent biological replicates. Source data are provided as a Source Data file. Source data are provided as a Source Data file.

(a) Representative images of the toxic effect of increasing doses of FUdR in the absence or presence of 1.5mg/mL serine on *C. elegans* cultured on *E. coli* BW25113 or HB101. n>10. (b) Representative images of progeny viability of *C. elegans* exposed from L1 to mock or Lth-FUdR (1 μ g/mL) while cultured on WT *E. coli* (BW25113), or the single mutants *upp*, *udp*, and *udk*, or the double mutant *upp;udk*. (c) Quantification of percent hatchlings relative to mock of treatments represented in b plus *E. coli* triple mutant *upp;udk;udp*. n=5. (d) Quantification of % hatchlings of *C. elegans* exposed from L1 to Lth-FUdR (1 μ g/mL) in the presence of the following metabolites: Uracil 2.5mg/mL, Uridine 5mg/mL, UMP 2.5mg/mL, UDP 5mg/mL, or UTP 5mg/mL. n=3. (e) Quantification of total number of embryos (all dead) laid in 24h per worm treated with Lth-FUdR \pm the Tmk inhibitor 5'-iodo-UMP (100 μ M). n=3. (f) Quantification of % hatchlings in worms cultured on WT (BW25113), *upp;udk* double KO, or *upp;udk;udp* triple KO lawns and treated with increasing doses of FUdR (0-40 μ g/mL). FUdR dose is depicted in logarithmic scale.

Figure 5. 2

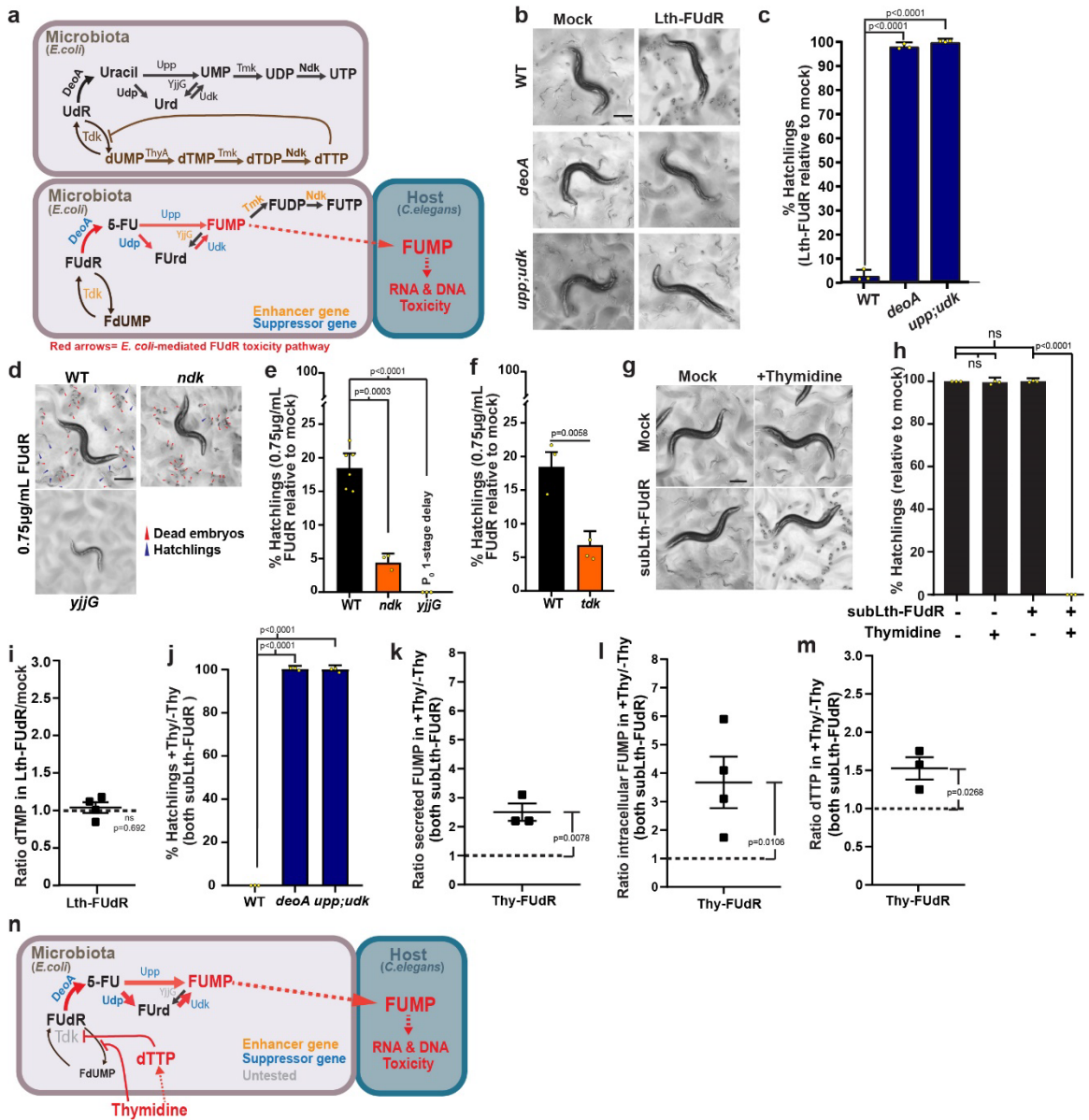


Figure 5.2 Dietary thymidine enhances FUdR-to-FUMP conversion in *E. coli*.

Throughout this figure: % hatchlings is estimated as [(live hatchlings/(live hatchlings + live embryos + dead embryos))] in the condition of interest relative to % hatchlings in mock of the same *E. coli* or *C. elegans* genotype; ≥ 5 images per treatment were quantitated; statistical significance was assessed via two-tailed unpaired nonparametric t-test. LCMS data was analyzed using one-tailed ratio t-test after ROUT outlier treatment. Data are presented as mean values \pm SEM, scale bars = 200 μ m, n= # independent biological replicates. Source data are provided as a Source Data file.

(a) Top: endogenous pyrimidine ribonucleotide salvage pathway (black font) and dTMP *de novo* synthesis pathway (brown font). Bottom: Model of *E. coli*-mediated FUdR-to-FUMP toxicity pathway. (b) Representative images of progeny viability of *C. elegans* treated with mock or Lth-FUdR while cultured on WT (BW25113), *deoA*, or *upp;udk* KO *E. coli* lawns. (c) Quantification of panel b treatments. n=3. (d) Representative images of progeny viability of *C. elegans* treated with mock or 0.75 μ g/mL FUdR (lower dose to detect enhancers) while cultured on WT (BW25113), *ndk*, or *yjjG* KO *E. coli* lawns. (e) Quantification of panel d treatments. n=3. (f) Quantification of progeny viability of *C. elegans* treated with mock or 0.75 μ g/mL FUdR while cultured on WT (BW25113) or *tdk* KO *E. coli* lawns. n=3. (g) Representative images of progeny viability of *C. elegans* treated with FUdR (0.25 μ g/mL) \pm 5mg/mL thymidine. (h) Quantification of panel g treatments. n=3. (i) LC-MS measurement of dTMP normalized to [¹³C₉,¹⁵N₂]UMP in *E. coli* treated with Lth-FUdR (5 μ g/mL) relative to mock. n=4. (j) Quantification of progeny viability of

C. elegans cultured on WT (BW25113), *upp;udk*, or *deoA* KO *E. coli* lawns treated with subLth-FUdR (0.25 μ g/mL) \pm 5mg/mL thymidine. n=3. (k) LC-MS measurement of secreted FUMP in *E. coli* supernatants normalized to [¹³C9,¹⁵N2]UMP. n=3. (l) LC-MS measurement of FUMP normalized to [¹³C9,¹⁵N2]UMP in *E. coli* pellets, n=4. (m) LC-MS measurement of dTTP normalized to [¹³C9,¹⁵N2]UMP in *E. coli* pellets, n=3. (n) Working model of *E. coli*-mediated thymidine-enhanced FUdR toxicity: 1) thymidine-derived dTTP inhibits Tdk, and 2) dietary thymidine competes with FUdR, thereby promoting FUdR-to-FUMP bioconversion.

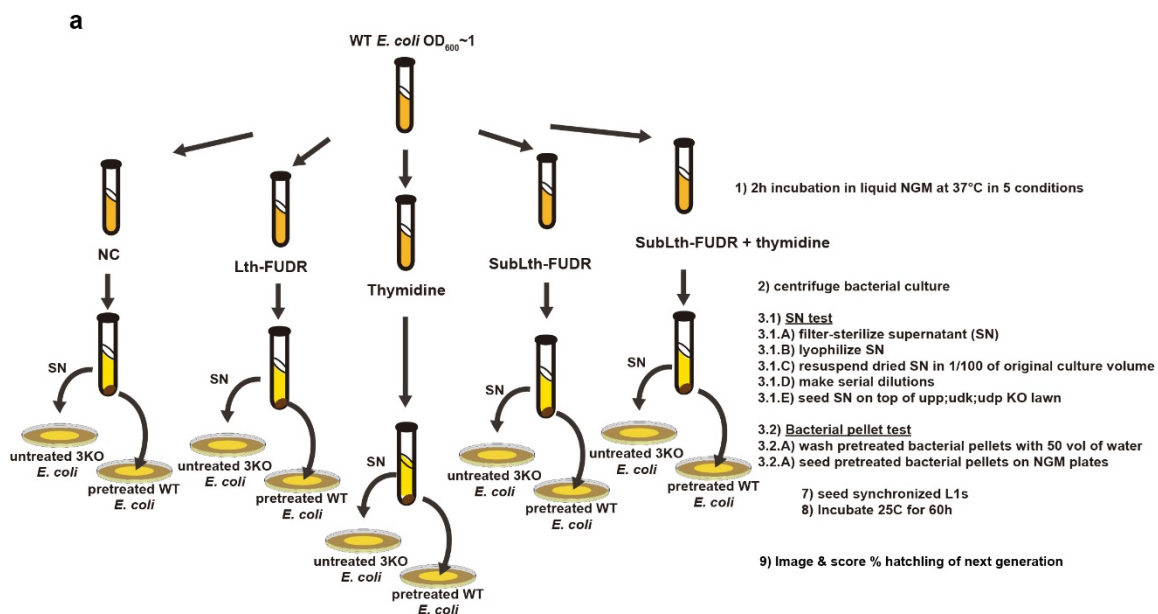
5.4.2 Dietary thymidine potentiates FUdR toxicity via promoting *E. coli* FUdR-to-FUMP conversion

The observation that in-plate supplementation with thymidine increases FUdR toxicity in *C. elegans* and that FUdR toxicity in *C. elegans* is mediated by *E. coli*, suggest that dietary thymidine, FUdR, *E. coli*, and *C. elegans* may represent an uncharacterized 4-way diet-drug-microbe-host interaction. To test the hypothesis that *E. coli* is mediating the potentiating effect of thymidine, we tested whether *E. coli* pretreated with a sublethal dose of FUdR (subLth-FUdR) plus thymidine would be more toxic to *C. elegans* than *E. coli* pretreated with subLth-FUdR alone. In this context, worms were not directly exposed to FUdR or thymidine; hence, enhanced toxicity would support the hypothesis that thymidine-enhanced FUdR toxicity is bacterially driven (Experimental setup in Fig. 5.3 a). Additionally, because the known mechanism of 5-FU toxicity is production and secretion of FUMP (Scott et al., 2017), we separated and independently tested the supernatants and pellets of *E. coli* pretreated with subLth-FUdR plus thymidine. Finally, the filter-sterilized supernatants were seeded on top of triple *upp,udp,udk* KO lawns to avoid in-plate bacterially-driven conversion of the FUdR remaining in the *E. coli* supernatants. We observed that the supernatants and the pellets of *E. coli* pretreated with Lth-FUdR and subLth-FUdR plus thymidine caused embryonic lethality, while the supernatants and pellets pretreated with subLth-FUdR or thymidine alone were not toxic to *C. elegans* (Fig. 5.3 b). Therefore, thymidine-enhanced FUdR toxicity (TE-FUdR) is bacterially driven and mediated, at least in part, by a secretable toxic compound. We first tested whether this secretable toxic compound would be the

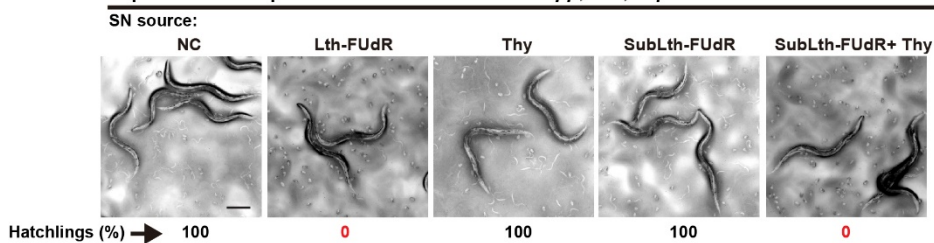
E. coli-generated FUdR-derivative FUMP. In support of this hypothesis, KO of the gene encoding the *E. coli* enzymes capable of converting FUdR into FUMP (*deoA*, or double KO of *upp* and *udk*) suppresses TE-FUdR toxicity (Fig. 5.2 j). More directly, we found a >2 fold increase in FUMP levels when we compare the supernatants and bacterial pellets of *E. coli* treated with FUdR plus thymidine relative to FUdR alone (Fig. 5.2 k,l). Therefore, dietary thymidine enhances FUdR toxicity in the *C. elegans* host through promoting FUdR-to-FUMP conversion via the pyrimidine ribonucleotide salvage pathway.

We then asked how thymidine potentiates the toxicity of FUdR. Clues came from the following: 1) KO of the gene encoding Tdk, the enzyme that can convert FUdR into FdUMP, enhances FUdR toxicity (Fig. 5.2 f). This likely occurs because by blocking the conversion of FUdR into FdUMP, we favor the conversion of FUdR into 5-FU and then FUMP (Pathway scheme in Fig. 5.2 a); 2) Tdk accepts thymidine as a substrate (ecocyc.org). Hence, thymidine can compete with FUdR and reduce the Tdk-mediated conversion of FUdR into FdUMP; and 3) Tdk is subject to end-product inhibition by dTTP (ecocyc.org). Since thymidine can serve as a substrate for the synthesis of dTTP, then dietary thymidine could promote end-product inhibition of Tdk. In support of the latter mechanism (but without ruling out the former), we observed increased levels of dTTP in TE-FUdR *E. coli* (Fig. 5.2 m). Together, the data are consistent with dietary thymidine increasing the toxicity of FUdR via indirectly promoting the conversion of FUdR into FUMP (Working model in Fig. 5.2 n).

Figure 5. 3



b Supernatant from pretreated bacteria seeded on *upp, udk, udp* lawn



Pellet of pretreated bacteria constitutes the lawn

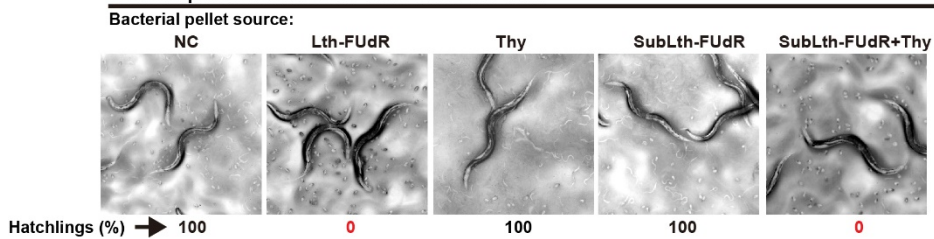


Figure 5.3

(a) Workflow of “in tube” pretreatment of *E. coli* with mock, Lth-FUdR, or subLth-FUdR \pm 5mg/mL thymidine and the follow up secreted versus intracellular (pellet) toxicity test. (b) Representative images of effect of pretreated supernatants and bacterial pellets on *C. elegans* progeny viability. n=3.

5.4.3 Dietary serine potentiates FUdR toxicity without increasing FUMP levels

After establishing that 4-way diet-drug-*E. coli*-*C. elegans* interactions such as the thymidine-FUdR-*E. coli*-*C. elegans* interaction can be detected and mechanistically dissected in our system, we sought to identify common dietary nutrients that may affect FUdR toxicity. We focused on amino acids (AA) for four reasons: 1) AA derivatives are precursors for the synthesis of nucleotides and cofactors needed to synthesize nucleotides (Locasale, 2013); 2) AAs alter chemotherapeutic efficacy in cells *in vitro* (Panosyan et al., 2014); 3) AAs are among the most highly consumed nutrients by cancer cells (Tsun and Possemato, 2015); and 4) AA-depleted diets are currently being tested to improve cancer treatment (Lukey et al., 2017). We tested 19 L-amino acids and glycine for their capacity to promote developmental delay of *C. elegans* treated with a dose of FUdR that on its own does not affect development. The conditions of the 4-way compound screen are depicted in Fig. 5.4 a and are described in the Methods section. Of the 20 AA, we found that high doses of tryptophan were toxic on their own whereas glycine and serine increased toxicity in a FUdR-specific manner (Fig. 5.4 b). Serine was a stronger toxicity potentiator than glycine, so we focused on characterizing serine-enhanced FUdR toxicity. First, we retested the capacity of serine to potentiate the toxicity of an already lethal dose of FUdR. Hatchlings seeded on *E. coli* HB101 lawns supplemented with 1.5mg/mL serine alone became fertile adults after 60h of incubation at 20° C, while hatchlings parallelly growing on 12.5µg/mL FUdR were sterile adults. However, when we combined serine and

FUdR we observed larval arrest that persisted indefinitely (Fig. 5.4 c), demonstrating that dietary supplementation of serine can potentiate the toxicity of FUdR. Furthermore, hatchlings seeded on *E. coli* HB101 lawns supplemented with 1.5mg/mL serine or a sublethal dose of FUdR (1 μ g/mL FUdR for HB101) yielded 100% fertile adult *C. elegans*; however, worms were 100% sterile when serine and FUdR were combined (Fig. 5.4 d,e). Together, the results show that dietary supplementation of serine can potentiate the toxicity of FUdR across a wide range of doses and toxicity outcomes. Hereafter, we use the term SE-FUdR toxicity to refer to the enhancement of toxicity achieved by combining a sub-lethal dose of FUdR ($\leq 0.25\mu\text{g/mL}$ for BW25113 or $\leq 1\mu\text{g/mL}$ for HB101) with dietary serine (Fig. 5.5 a).

How does dietary serine enhance FUdR toxicity in *C. elegans*? A formal possibility is that combining FUdR with serine impairs *E. coli* growth, thus leading to food scarcity in the worm. However, for all non-screening experiments presented in this study, bacteria were cultured overnight in LB in the absence of additives, and then washed and concentrated in S-buffer to $\text{OD}_{600\text{nm}} = 20$ before being seeded on nematode growth media (NGM) plates. Furthermore CFU counting of bacteria harvested from standard NGM or NGM supplemented with serine, subLth-FUdR, or subLth-FUdR plus serine shows similar bacterial viability in all conditions (Fig. 5.5 b,c). Therefore, *E. coli* lawn density and growth rates do not appear to explain SE-FUdR toxicity in our experimental setup.

We then tested whether SE-FUdR toxicity, like thymidine, was bacterially driven. As with thymidine, we pretreated liquid cultures of *E. coli* with mock, Lth-FUdR, serine, subLth-FUdR, or subLth-FUdR plus serine, and separated and tested *E. coli* supernatants and pellets independently (Experimental setup in Fig. 5.6 a). We observed toxicity in worms cultured on *E. coli* pellets pretreated with SE-FUdR (Fig. 5.4 f and Fig. 5.6 b). However, we observed no toxicity in worms exposed to supernatants of *E. coli* pretreated with SE-FUdR (Fig. 5.6 b), demonstrating that, unlike thymidine, SE-FUdR toxicity is not driven by secreted *E. coli* products, and justifying to not further characterize SE-FUdR *E. coli* supernatants in this study. Therefore, SE-FUdR toxicity is bacterially driven, but mainly via an intracellular mechanism. Based on this observation, we can formulate two hypotheses: 1) serine promotes FUdR-to-FUMP conversion but prevents FUMP secretion; or 2) serine promotes a mechanism of toxicity that is distinct from Lth-FUdR and TE-FUdR toxicity. To test the first hypothesis, we measured the levels of 5-FU and FUMP in the *E. coli* pellets, and found them to be the same in the subLth-FUdR and SE-FUdR conditions (Fig. 5.4 g,h), even though aliquots of the bacteria used for metabolite extraction showed the expected 0 and 100% embryonic lethality, respectively (Fig. 5.7 a). This lack of increase of FUMP levels in the SE-FUdR condition is in contrast with the elevated levels of FUMP observed in the TE-FUdR condition (Fig. 5.2 k,l), and supports the notion that thymidine and serine potentiate FUdR toxicity through distinct mechanisms.

Since the SE-FUdR mechanism of toxicity seems distinct from Lth-FUdR and TE-FUdR, we tested whether fluororibonucleotides other than FUMP, specifically fluorouridine (FUrd), FUDP, or FUTP, were contributing to SE-FUdR. These fluororibonucleotides were below the detection limit of our LCMS of bacteria or worms treated with subLth-FUdR or SE-FUdR (Fig. 5.7 b, and experimental details in Note 1). Nevertheless, KO of *yjjG* or *udp*, which would reduce FUrd synthesis (Pathway scheme in Fig. 5.2 a), does not reduce SE-FUdR toxicity (Fig. 5.7 c). Furthermore, blocking the conversion of FUMP-into-FUDP (through chemical treatment with 5'-iodo-UMP) and of FUDP-into-FUTP (through KO of *ndk*) further enhances SE-FUdR toxicity, arguing against FUDP or FUTP mediating SE-FUdR toxicity (Fig. 5.7 d and e, respectively). Remarkably, these data show that despite the fact that SE-FUdR toxicity is not driven by increased FUMP (Fig. 5.4 h), preventing the conversion of FUMP into FUDP or FUTP further enhances SE-FUdR toxicity. These results prompted us to think about how SE-FUdR toxicity and the FUdR-to-FUMP toxicity pathway interact. We hypothesized that sublethal levels of FUMP toxicity would be necessary to sensitize *C. elegans* to SE-FUdR toxicity. In support of this hypothesis, we found that the double KO *upp;udk*, and the triple KO *upp;udp;udk* suppress SE-FUdR toxicity in *C. elegans* (Fig. 5.4 i,j). Altogether, the results suggest that SE-FUdR is not mediated by increased conversion of FUdR into FUMP (biochemical evidence), or FUDP, FUTP or FUrd (genetic evidence) in *E. coli*. However, a sublethal level of FUMP toxicity appears to be required to sensitize *C. elegans* to SE-FUdR toxicity.

Note 1

Since the SE-FUdR mechanism of toxicity seems distinct from Lth-FUdR and TE-FUdR, fluororibonucleotides other than FUMP, specifically FUDP, FUTP, or fluorouridine (FUrd), could contribute to SE-FUdR toxicity. However, these fluororibonucleotides were below the detection limit of our LCMS of bacteria or worms treated with subLth-FUdR or SE-FUdR (Fig. 5.7 b).

This is not surprising, as previous studies (Scott et al., 2017) used a dose of fluoropyrimidine 50 fold higher (50 μ M) than the 0.25 μ g/mL (1 μ M) FUdR we use to study SE-FUdR toxicity.

SE-FUdR toxicity cannot be biochemically assessed at higher fluoropyrimidine doses because: 1) When using E. coli BW25113, doses of FUdR \geq 1 μ g/mL lead to 100% sterility. Hence, serine enhancement of toxicity cannot be assessed because further enhancement of sterility cannot be achieved; and

2) Although serine-enhanced toxicity can be observed at >10 μ g/mL FUdR in the form of developmental delay, it would not be informative to compare the metabolic profile of adults to young larvae.

Nevertheless, we used genetic and chemical inhibitor approaches to assess the potential contribution of other fluororibonucleotides, including FUDP, FUTP, FUrd, and FdUMP to SE-FUdR toxicity, and directly measured the levels of FUMP and 5-FU.

Figure 5. 4

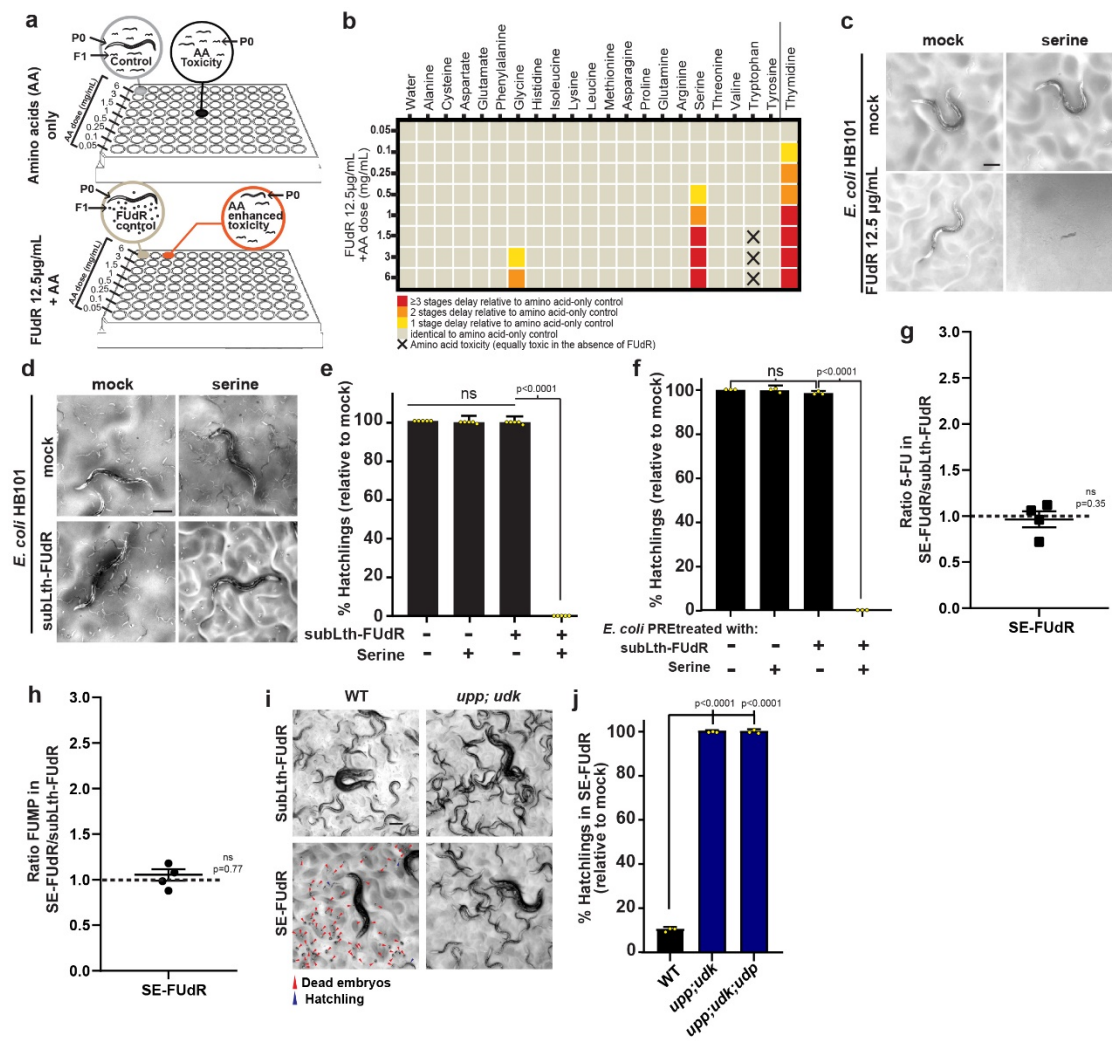


Figure 5.4 Dietary serine enhances FUdR toxicity but not FUdR-to-FUMP conversion. Throughout this figure: % hatchlings and LCMS data were analyzed as described in **Fig. 5.2**. Statistical significance was assessed via two-tailed unpaired nonparametric t-test for % hatchlings quantification. LCMS data was analyzed using one-tailed ratio t-test after ROUT outlier treatment. Data are presented as mean values +/- SEM, scale bars = 200µm, n= # independent biological replicates. Source data are provided as a Source Data file.

(a) Screen setup to search for dietary amino acids (AAs) that enhance FUdR toxicity (cause developmental delay). Worms cultured on *E. coli* HB101 were treated with 12.5 µg/mL FUdR from the L1 stage ± serial dilutions of AAs (0.05-6mg/mL). AA-only wells were included to detect AA toxicity. Wells were scored after 60h at 20°C, when FUdR-only wells show 100% embryonic lethality but no developmental delay. (b) Heat map representing degree of developmental delay caused by supplemented AAs. Color and symbol key depicted below. Thymidine is a positive control. (c) Representative images of targeted validation of developmental delay induced by co-administration of 12.5µg/mL FUdR with 1.5mg/mL of serine. Images taken after 60h of incubation at 20°C. n>3 (d) Representative images of progeny viability of *C. elegans* cultured on HB101 and treated from L1 with mock, subLth-FUdR (1µg/mL FUdR, which is sublethal because using HB101), 1.5mg/mL serine, or subLth-FUdR plus serine. n>10 (e) Quantification of % hatchlings relative to mock of treatments represented in d. n=5. (f) Quantification of % hatchlings in worms exposed to lawns of *E. coli* pretreated “in tube” with ±subLth-FUdR ±serine. In this set up worms are not directly exposed

to FUdR or serine (Fig. 5.6). n=3. **(g)** LC-MS measurement of intracellular 5-FU relative to internal standard (IS) [1,3-¹⁵N₂]Uracil in *E. coli* treated with subLth-FUdR plus serine compared to subLth-FUdR. n=4. **(h)** LC-MS measurement of intracellular FUMP relative to internal standard (IS) [¹³C₉,¹⁵N₂]UMP in *E. coli* treated with subLth-FUdR plus serine compared to subLth-FUdR. n=4. **(i)** Representative images of progeny viability of *C. elegans* cultured on WT (BW25113) or *upp;udk* KO *E. coli* lawns treated from L1 with subLth-FUdR (0.25µg/mL) ± serine. **(j)** Quantification of % hatchlings relative to mock of treatments represented in panel i and the triple *E. coli* KO *upp;udp;udk*. n=3.

Figure 5. 5

a (copy of a portion of Fig. 5.1a to avoid moving back and forth between figures)

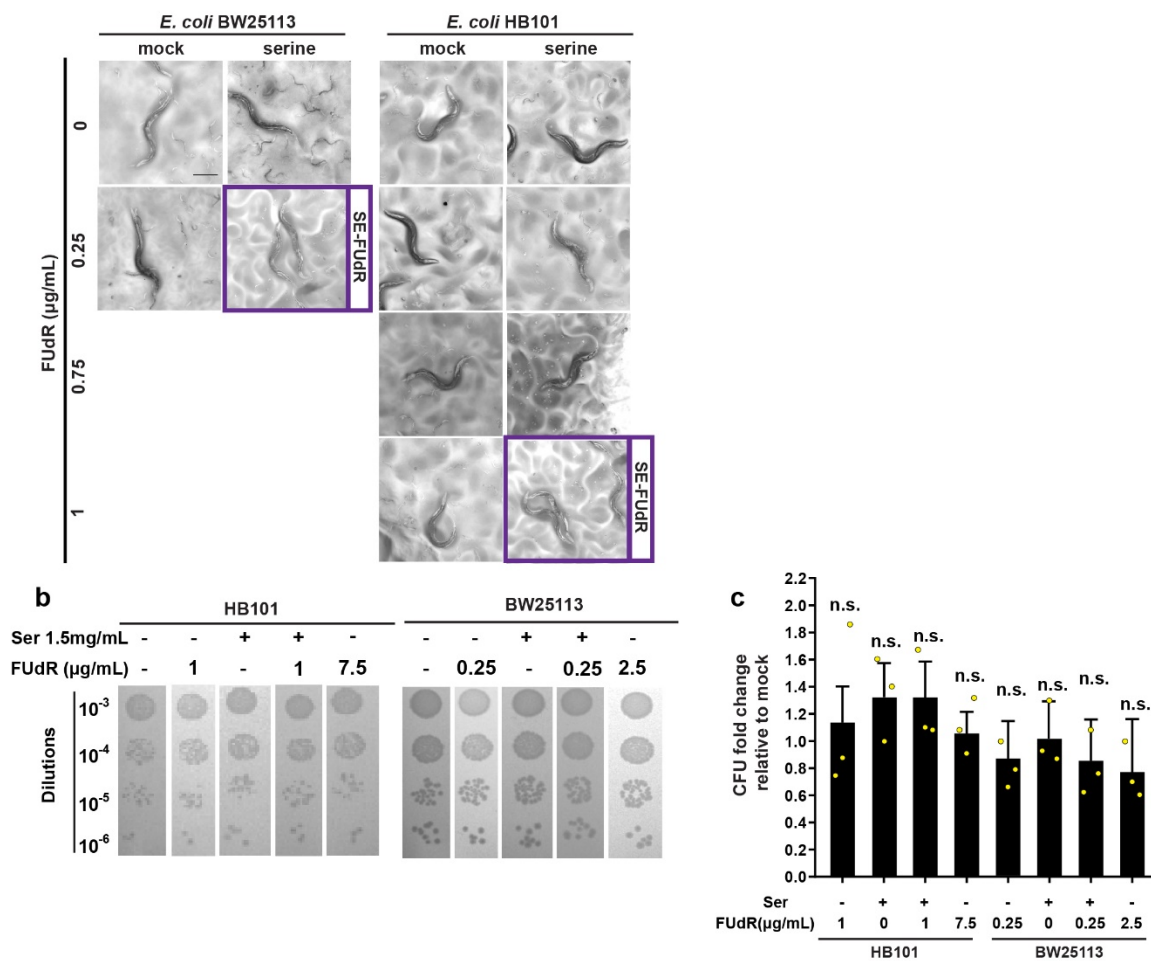
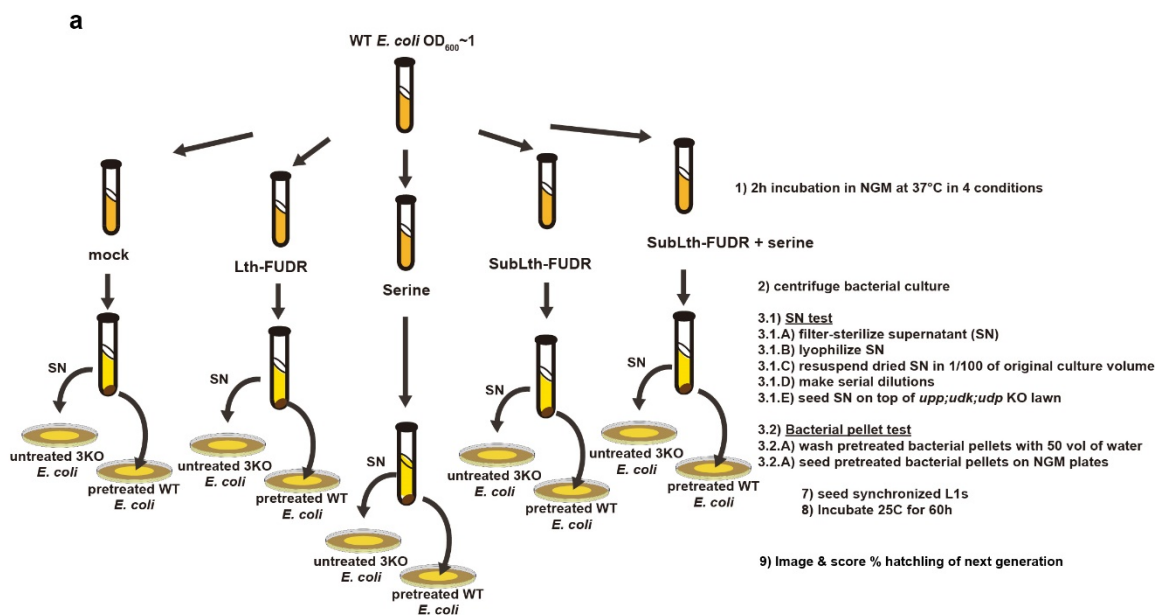


Figure 5.5 Lth-FUdR and SE-FUdR toxicity do not correlated with *E. coli* growth, viability, or bacterial virulence. Data acquisition and analysis described in Methods. Statistical significance for ratio CFU and qRT-PCR fold change was assessed using one-tail ratio t-test. Error bars represent S.E.M. * $p \leq 0.05$, ** $p \leq 0.01$, *** $p \leq 0.001$, **** $p \leq 0.0001$. n= # independent biological replicates. Source data are provided as a Source Data file.

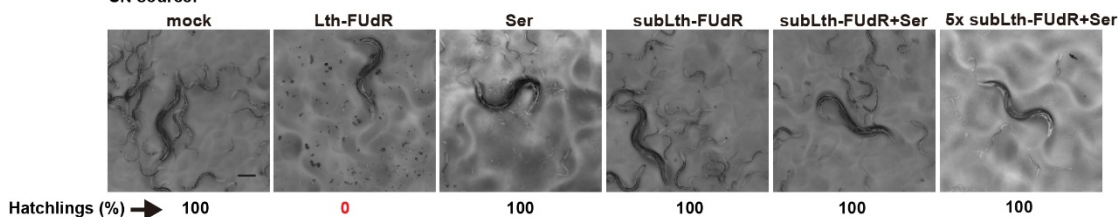
(a) Images from Fig. 5.1 a are reproduced here to avoid moving back and forth between figures. This is reproduced here to show what we define as SE-FUdR toxicity, which corresponds to $1\mu\text{g/mL}$ FUdR + 1.5mg/mL serine for worms cultured on BW25113 or its derivatives, and $7.5\mu\text{g/mL}$ FUdR + 1.5mg/mL serine for worms cultured on HB101 or its derivatives (i.e. EORB1). $n > 10$. (b) Representative images of viability of *E. coli* BW25113 and the HB101-derivative EORB1 after incubation for 48h in NGM plates supplemented with mock, subLth-FUdR, serine, subLth-FUdR plus serine, or Lth-FUdR as assessed by serial dilution for counting of colony forming units (CFU). (c) Quantification of CFU of treatments represented in panel b. Data were analyzed using ratio t-test. $n = 3$.

Figure 5. 6



b Supernatant from pretreated bacteria seeded on *upp, udk, udp* 3KO lawn

SN source:



Pellet of pretreated bacteria constitutes the lawn

Bacterial pellet source:

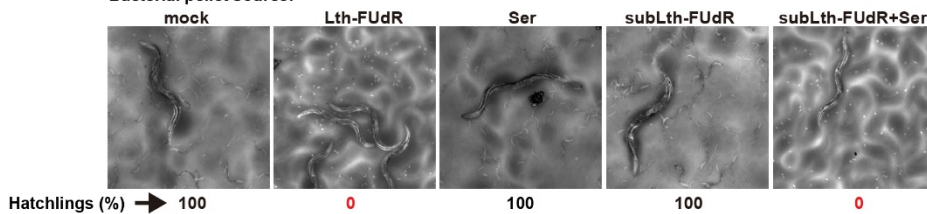


Figure 5.6

(a) Workflow of “in tube” pretreatment of *E. coli* with mock, Lth-FUdR, or subLth-FUdR ± serine and the follow up secreted versus intracellular (pellet) toxicity test.

(b) Representative images of effect of pretreated supernatants and bacterial pellets on *C. elegans* progeny viability. n=3.

Figure 5. 7

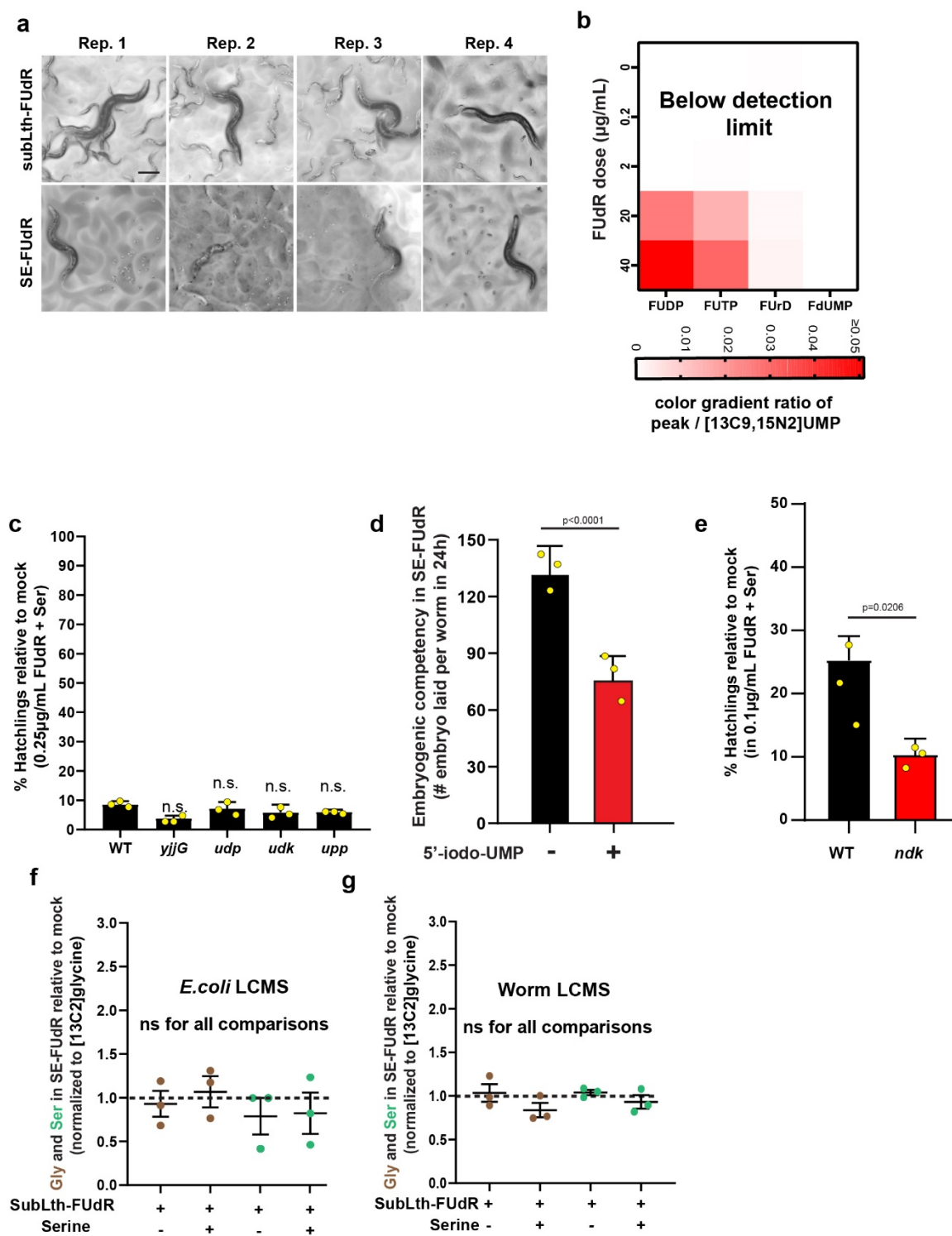


Figure 5.7 Throughout this figure % hatchlings is estimated and data analyzed as described in Fig. 5.1. Scale bars = 0.2mm, error bars represent S.E.M.. Statistical significance was assessed via two-tailed unpaired nonparametric t-test for %hatchlings quantification. LCMS data was analyzed using one-tailed ratio t-test after ROUT outlier treatment. * $p \leq 0.05$, ** $p \leq 0.01$, *** $p \leq 0.001$, **** $p \leq 0.0001$. n= # independent biological replicates. Source data are provided as a Source Data file.

(a) Representative images of progeny viability observed in worms cultured on aliquots of *E. coli* pellets used for LCMS analyses presented in Fig. 5.4 g,h, 5.11 g, and Fig. 5.7 f,g. (b) Representation of the capacity of our LCMS set up to detect FUDP, FUTP, FUdR and FdUMP in extracts *E. coli* (BW25113) treated with increasing doses of FUdR (0-40 μ g/mL). FUDP and FUTP cannot be reliably detected in samples treated with less than 20 μ g/mL FUdR. FUdR and FdUMP cannot be reliably measured even in samples treated with 40 μ g/mL FUdR (>150 fold higher than the dose we use to characterize SE-FUdR toxicity) (c) Quantification of % hatchlings relative to mock of *C. elegans* cultured on WT (BW25113), *yjjG*, *udp*, *udk*, or *upp* KO lawns treated from L1 with mock or 0.25 μ g/mL FUdR plus serine. n=3. (d) Quantification of total number of embryos (all dead) laid in 24h per worm treated with SE-FUdR \pm the Tmk inhibitor 5'-iodo-UMP (100 μ M). n=3. Data were analyzed using two-tailed unpaired nonparametric T-test. (e) Quantification of % hatchlings relative to mock of *C. elegans* cultured on WT (BW25113) or *ndk* KO lawns treated from L1 with mock or 0.1 μ g/mL FUdR plus serine (lower dose of FUdR used to enable detection of toxicity enhancer).

n=3. **(f-g)** LC-MS measurement of serine and glycine integrated peaks normalized to internal standard [13C2] glycine in **(f)** *E. coli* (WT BW25113) and **(g)** *C. elegans* cultured on WT *E. coli* BW25113, and treated with subLth-FUdR + 1.5 mg/mL serine relative to mock, n=3. Data were analyzed using ratio t-test.

5.4.4 *E. coli*'s folate-synthesis pathway is required for SE-FUdR toxicity

Having ruled out enhanced FUdR-to-FUMP conversion, we moved to uncover the main bacterially-driven mechanism of SE-FUdR toxicity. First we tested whether in-plate supplementation with serine would simply increase the levels of serine in *E. coli*, and hence, although bacterially driven, SE-FUdR would not require *E. coli*-mediated conversion of serine. Arguing against this notion, direct measurement of serine and glycine levels in *E. coli* and *C. elegans* shows no increase in the levels of these amino acids (Fig. 5.7 f,g), even when aliquots of the analyzed bacteria promote enhanced toxicity in the worm (Fig. 5.7 a). Hence, we decided to use a 4-way *E. coli* KO suppressor/enhancer screen to molecularly dissect how serine is metabolized in *E. coli* to enhance FUdR toxicity in *C. elegans*. To create our *E. coli*-KO screening library, we used *in silico* modeling based on the iJO1366 *E. coli* metabolic model to search for all *E. coli* genes within two-metabolic steps from the homologs of the mammalian fluoropyrimidine metabolic pathways (gene list in Table 5.1, and 96-well screen set up in Fig. 5.8 a). The 4-way high-throughput screen identified 29 *E. coli* genes altering SE-FUdR toxicity in *C. elegans* (Table 5.2). Genes belonging to metabolic pathways enriched among the hits were retested in 6cm NGM plates. Twelve primary hits were validated using the following criteria: 1) > or <10% hatchlings than worms seeded on WT *E. coli*; 2) p-value <0.05; and 3) growth of the *E. coli* KO clone in \pm serine \pm FUdR did not correlate with its enhancer or suppressor phenotype (Fig. 5.9). Among the SE-FUdR toxicity suppressors, *lpd* emerged as the strongest hit (Fig. 5.8 b, c). *Lpd* encodes *E. coli* lipamide dehydrogenase, which is part of three multicomponent enzymatic

complexes: pyruvate dehydrogenase, 2-oxoglutarate dehydrogenase, and the glycine cleavage complex (GCV). The GCV complex is composed of Lpd, GcvP, GcvT, and GcvH, and catalyzes the conversion of glycine into 5,10-methylene-tetrahydrofolate (5,10-mTHF). KO of *gcvP*, *gcvT*, and *gcvH*, also suppresses SE-FUdR toxicity (Fig. 5.8 c), favoring the notion that Lpd would contribute to SE-FUdR toxicity as a component of the GCV complex. However, *lpd* is a stronger suppressor than the *gcv* genes. Several distinctions exist between Lpd and the Gcv proteins. For instance, the *gcv* genes are part of a single operon transcribed by Fnr, while *lpd* is encoded as a single gene and is transcribed by Crp (ecocyc.org). In addition, Lpd is necessary for the activation of the Gcv proteins (Steiert et al., 1990). However, given the stronger suppressor phenotype of *lpd* relative to the *gcv* genes, roles for Lpd beyond the GCV complex cannot be ruled out. Nevertheless, KO of *glyA*, which encodes the enzyme that converts serine into glycine and 5,10-mTHF, also suppresses SE-FUdR toxicity (Fig. 5.8 c, and Pathway scheme in Fig. 5.8 d). Together, GlyA and the GCV complex can convert serine into 5,10-mTHF (Pathway scheme in Fig. 5.8 d); and therefore, these suppressors suggest that 5,10-mTHF may play an important role in mediating SE-FUdR toxicity. Pointing to the same direction, KO of *folP* and *folB*, suppresses SE-FUdR toxicity (Fig. 5.8 c). FolP and FolB synthesize tetrahydrofolate, which is the precursor of 5,10-mTHF (Pathway scheme in Fig. 5.8 d). Further, both the GCV complex and GlyA require the cofactor vitamin B6 (pyridoxal-5'-phosphate or PLP) to synthesize 5,10-mTHF (ecocyc.org). Hence, it is relevant that KO of the PLP-synthesis genes *pdxA*, *pdxJ*, *pdxH*, and *serC* suppress SE-FUdR toxicity (Fig. 5.8

c). Of note, the other enzymatic complexes containing Lpd, namely pyruvate dehydrogenase and 2-oxoglutarate dehydrogenase, do not use PLP as a co-factor, further favoring the notion that Lpd main contribution to SE-FUdR toxicity would be through its role as a component of the GCV complex.

Additional insight into how serine potentiates the toxicity of FUdR is garnered from the role that the serine-synthesis pathway plays in SE-FUdR toxicity. SerA, SerB, and SerC are essential for *de novo* synthesis of serine in *E. coli* (ecocyc.org). However, only KO of *serC* suppresses SE-FUdR toxicity in *C. elegans* (Fig. 5.8 c). Distinctively, SerC is involved in PLP synthesis while SerA and SerB only contribute to serine synthesis (Pathway scheme in Fig. 5.8 d). Also importantly, SerA is subject to end-product inhibition by serine. Therefore, the data suggest that serine promotes SE-FUdR toxicity via promoting the synthesis of 5,10-mTHF. Serine would promote 5,10-mTHF synthesis through at least two mechanisms (Fig. 5.8 d): 1) inhibiting its own synthesis (via SerA inhibition), thereby freeing SerC to synthesize PLP; and 2) serving as a substrate for the synthesis of 5,10-mTHF via GlyA and the GCV complex. The capacity to free SerC via end product inhibition distinguishes serine from glycine, and could underlie the observation that dietary glycine is a weaker potentiator of FUdR toxicity than serine (Fig. 5.4 b). Altogether, dietary serine promotes FUdR toxicity in *C. elegans* through a bacterially-driven mechanism that involves conversion of serine and glycine into 5,10-mTHF, and not increased bacterial conversion of FUdR-into-FUMP or accumulation of serine or glycine.

Figure 5. 8

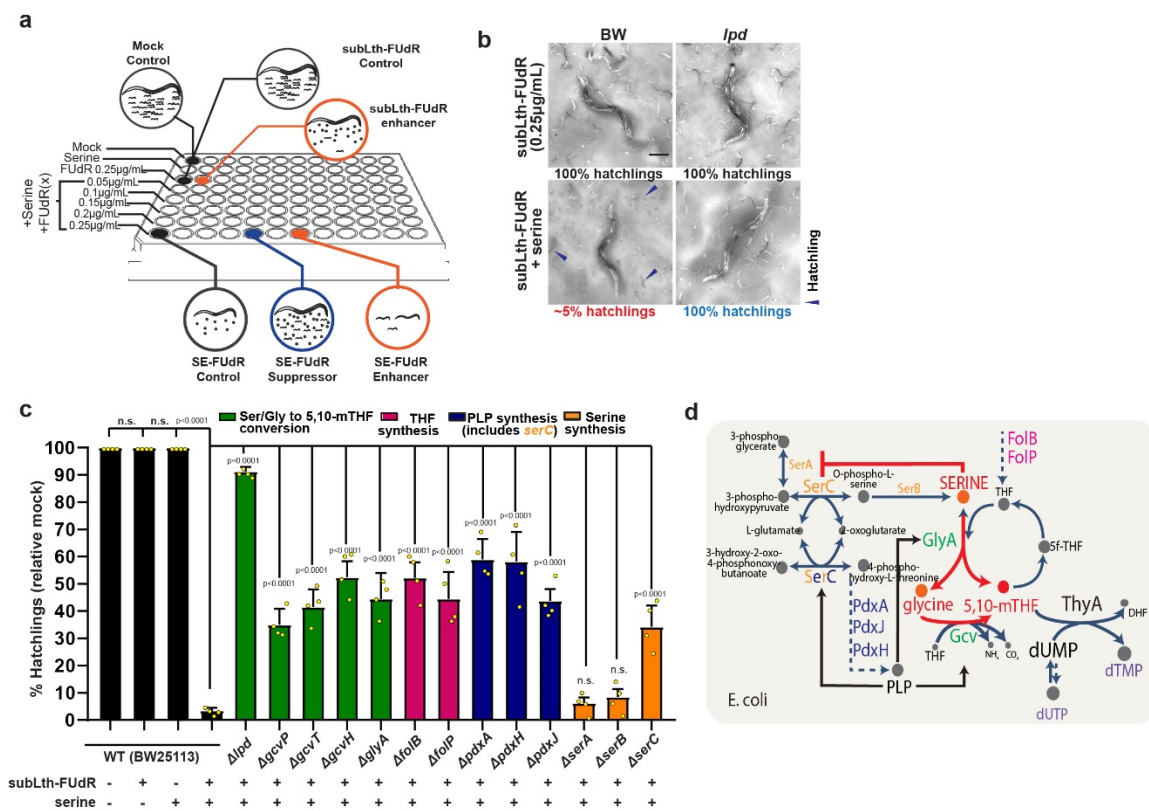


Figure 5.8 SE-FUdR toxicity requires *E. coli*'s folate and pyridoxal phosphate synthesis pathways. Throughout this figure: statistical significance was assessed via two-tailed unpaired nonparametric t-test for % hatchlings quantification. Data are presented as mean values +/- SEM, scale bars = 200µm, n= # independent biological replicates. Source data are provided as a Source Data file.

(a) Setup of 4-way *E. coli* KO screen for mediators of serine-enhanced FUdR toxicity. Screening was carried out in the BW25113 background in triplicate at 25°C in 8 conditions: 1) mock, 2) serine 1.5mg/mL, 3) subLth-FUdR 0.25µg/mL, and 4-8) serine 1.5mg/mL plus subLth-FUdR from 0.05 to 0.25µg/mL (lower doses included to detect toxicity enhancers). Each column of the 96-well plate corresponds to a different *E. coli* KO. Developmental stage and progeny viability were scored. (b) Representative images of validation of the toxicity-suppressor effect of knocking down *E. coli lpd*, making evident that SE-FUdR toxicity is bacterially driven. n=4. (c) Effect of the *E. coli* suppressors of SE-FUdR toxicity on progeny viability (% hatchlings). Images and data were analyzed as described in **Fig. 5.2**. n=4. (d) Working model of how dietary serine promotes synthesis of 5,10-mTHF in *E. coli*. Color codes of suppressor gene names are consistent with panel c. Serine relevant actions (depicted in red): 1) inhibits its own synthesis releasing *serC* to promote PLP synthesis (PLP is an essential cofactor for GlyA and the GCV complex); and 2) serves as a substrate for the synthesis of 5,10-mTHF directly via GlyA and indirectly via the GCV complex.

Figure 5. 9

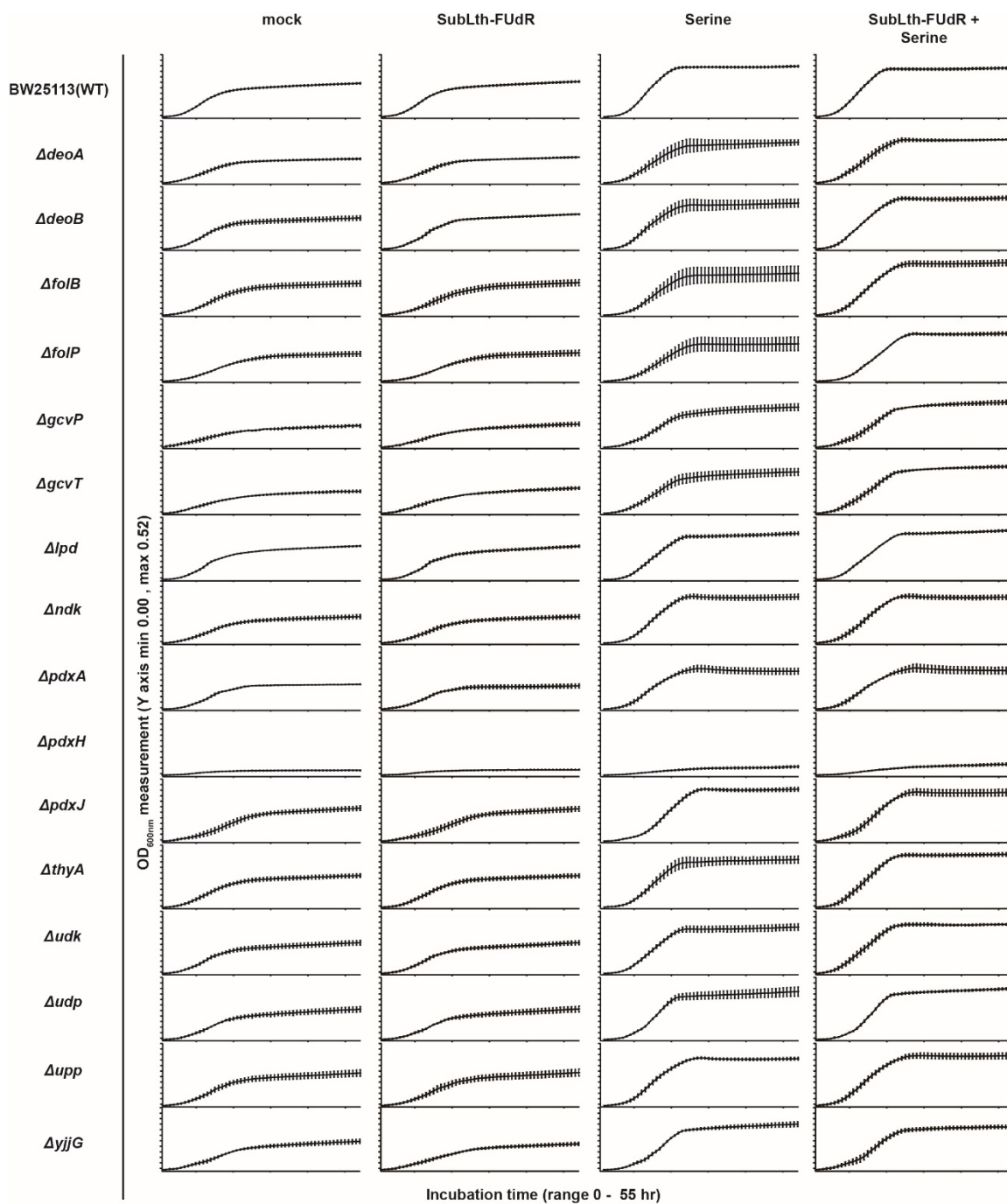


Figure 5.9 Suppression of SE-FUdR toxicity by *E. coli* KOs does not correlate with *E. coli* growth

Throughout this figure error bars represent S.E.M. Curves depict 55 h continuous biomass measurement (OD_{600nm}) of *E. coli* WT (BW25113) and KOs that alter SE-FUdR toxicity. Bacteria were cultured in complete liquid NGM containing mock, subLth-FUdR, serine, or subLth-FUdR plus serine. n=5. Source data are provided as a Source Data file.

5.4.5 Dietary serine reduces *E. coli*'s and hence *C. elegans*' dTMP pool

The observation that 5,10-mTHF synthesis in *E. coli* is essential to SE-FUdR toxicity points toward the best characterized mechanism of fluoropyrimidine toxicity: the formation of a ternary complex composed of FdUMP, 5,10-mTHF, and thymidylate synthase (TS) that inhibits TS function (Malet-Martino and Martino, 2002). Importantly, mammalian evidence suggests that 5,10-mTHF is the main limiting factor in the formation of this inhibitory complex (Malet-Martino and Martino, 2002). Hence, the next step was to define whether *E. coli*-generated 5,10-mTHF might act through inhibition of the worm TS or *E. coli* TS, or both. If worm TS is inhibited, serine would promote 5,10-mTHF synthesis in *E. coli*, elevating the levels of 5,10-mTHF in the *C. elegans* diet, and enabling the inhibition of *C. elegans*' TS (TYMS-1). Arguing against this scenario, 5,10-mTHF is known to poorly cross membranes (Ducker and Rabinowitz, 2017), and strong reduction of *C. elegans* TS expression through RNAi against *C. elegans tyms-1* (Fig. 5.10 a) does not enhance FUdR toxicity (Fig. 5.11 a). Using a similar rationale, if dietary serine enhances FUdR toxicity mainly by enabling the inhibition of *E. coli*'s TS, culturing worms on TS-deficient *E. coli* (*thyA* KO) should enhance their sensitivity to sublethal doses of FUdR. Indeed, although feeding *thyA* KO bacteria or treating with subLth-FUdR alone is not toxic to *C. elegans*, feeding *thyA* KO bacteria in the presence of sublethal levels of FUdR leads to >90% embryonic lethality in *C. elegans* (Fig. 5.11 b,c), phenocopying SE-FUdR. Furthermore, the enhanced FUdR toxicity observed in worms fed the *thyA* KO cannot be further enhanced by dietary serine (Fig. 5.11 d,e), suggesting that *thyA* KO and dietary serine enhance

FUdR toxicity through the same mechanism (see rationale of conditions for this experiment in Note 2). Another prediction of the scenario in which dietary serine enables the inhibition of *E. coli*'s TS is that SE-FUdR toxicity would depend upon *E. coli* capacity to convert FUdR into FdUMP, a reaction carried out by Tdk. In line with this prediction, we found that KO of *E. coli tdk* partially suppresses SE-FUdR toxicity (Fig. 5.11 f). The observed modest suppression is expected because KO of *tdk* would simultaneously enhance FUdR-to-FUMP bioconversion (Fig. 5.2 f and pathway scheme in Fig. 5.2 n).

The above observations are in line with a model in which dietary serine, via promoting the synthesis of 5,10-mTHF, enables the inhibition of *E. coli* ThyA, thereby reducing the levels of dTMP in the *C. elegans* diet. To test this model directly, we measured dTMP levels in *E. coli*. We found that *E. coli* treated with subLth-FUdR plus serine show reduced dTMP levels (Fig. 5.11 g). Based on the *tymS-1* versus *thyA* experiments described above (Fig. 5.11 a-e) we proposed that *C. elegans*' dTMP pool would be limited by *E. coli*'s ability to provide dTMP. Supporting this, we found that *C. elegans*' dTMP levels are reduced in the SE-FUdR condition, and that single KO of *E. coli*'s *lpd* suppresses this reduction (Fig. 5.11 g). Altogether, the data demonstrate that *E. coli*-mediated conversion of serine/glycine into 5,10-mTHF promotes a reduction of the dTMP pool in *E. coli*, and consequently in *C. elegans*.

We next reasoned that if reduced dTMP availability in the *C. elegans* diet is the main SE-FUdR toxicity mechanism, and not a mere correlation, dietary supplementation with dTMP should suppress SE-FUdR toxicity. To test this prediction, we used the complex experimental setup depicted in Fig. 5.11 h, and described in detail in Note 3. A key aspect of this experimental set up is that 5'-fluoroorotic acid (5-FO), a source of FUMP that does not need Upp/Udk-mediated conversion, is used to sensitize *C. elegans* to SE-FUdR toxicity. The first important observation we made is that serine enhances fluoropyrimidine toxicity in a *upp;udk* double KO background (Fig. 5.11 i,j). This observation is consistent with the notion that FUMP is important to sensitize to SE-FUdR toxicity but that increased flux through the pyrimidine salvage pathway is not how serine enhances toxicity (Fig. 5.4 h). Most significantly, dTMP supplementation suppresses SE-FUdR toxicity (Fig. 5.11 i,j, additional control images in Fig. 5.10 b). Therefore, the LCMS data demonstrate that dietary serine inhibits the production of dTMP in bacteria and that that in turn reduces the dTMP pool in *C. elegans*, and the dTMP-rescue data demonstrate that scarce dietary thymidine is a major contributor to death in *C. elegans*.

To go one step further and test whether precursors for the synthesis of 5,10-mTHF may limit thymidine-depletion in our experimental setup, we exposed worms to a combination of: 1) 5-FO as the source of sublethal levels of FUMP, 2) 2.5µg/mL FdUMP, and 3) *deoA E. coli* mutant as the microbe. In this condition, high levels of FdUMP can accumulate because we provide ~10 fold more FdUMP (2.5µg/mL)

than the amount of FUdR we normally use to characterize SE-FUdR (0.25µg/mL FUdR), and because the KO of *deoA* prevents the conversion of FUdR into 5-FU or FUMP. Nevertheless, despite the expected increase in FdUMP levels we see no toxicity in *C. elegans* (Fig. 5.10 c). However, supplementing these plates with as little as 150µg/mL of serine leads to >70% lethality, and from there the severity of the toxicity correlates with the amount of serine added to the system (Fig. 5.10 c).

Altogether we propose a model in which dietary serine enhances FUdR toxicity through promoting the synthesis of 5,10-mTHF, and with that the formation of the TS inhibitory complex, which results in reduced dTMP production in *E. coli* and thymidine-less death in worms (Fig. 5.11 k). Microbe-mediated thymidine starvation in *C. elegans* can be triggered genetically via KO of *E. coli thyA* or dietarily via supplementation of serine, and likely glycine, in combination with FUdR or FdUMP. Although SE-FUdR toxicity does not act through enhancing the known FUdR-to-FUMP toxicity pathway, it does require FUMP to sensitize the worm to thymidine-less death. This is in line with a previous study demonstrating that nucleotide imbalance in the microbe alone is insufficient to promote toxicity in *C. elegans* (Chi et al., 2016). Together, the data show the critical role that 4-way interactions can play in fluoropyrimidine toxicity in the host. The results also highlight the need to control animal husbandry conditions to make generalized conclusions about the role microbe and host pathways play in the response to drugs.

Note 2

A lower dose of subLth-FUdR was used in this experiment to enable detection of enhancement of toxicity when combining serine with thyA. The results also suggest that C. elegans is more dependent on E. coli's supply of dTMP than its own de novo synthesis pathway, and that inhibition of E. coli's TS is not detrimental to worms unless another concurrent insult is present (e.g. sublethal levels of FUMP toxicity).

Note 3

Set up of experiment aimed to test whether SE-FUdR toxicity can be rescued by dietary supplementation of dTMP.

This test requires a complex experimental set up because dTMP enhances FUdR-to-FUMP conversion, and hence, toxicity in C. elegans. So, if we simply add FUdR + serine + dTMP to w wild-type E. coli lawn we will see dTMP enhances, instead of rescuing the toxicity. But this would be due to confounding factors.

Hence, to test whether SE-FUdR toxicity can be rescued by dietary supplementation of dTMP we need to prevent FUdR-to-FUMP conversion. This can be easily achieved by using a upp,udk double KO or a upp,udk,udp triple KO E. coli lawn. However, this brings another challenge. That is that we need sublethal levels of FUMP toxicity for SE-FUdR toxicity to work; hence, if using E. coli lawns unable to convert FUdR into FUMP, we need an alternative source of FUMP. The simplest would be to add FUMP to the system. However, FUMP is commercially

available only as custom-made at the microgram level and it is not affordable. To overcome the need to provide FUMP in the absence of the FUdR-to-FUMP conversion pathway, we use 5'-Fluoroorotic acid (5-FO) as the source of FUMP, as E. coli converts 5-FO into FUMP in a upp;udk independent-manner (Scott et al., 2017).

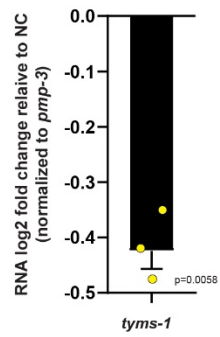
Therefore, altogether the experimental set up to test whether SE-FUdR toxicity can be rescued by dietary supplementation of dTMP includes:

- 1) upp;udk double KO lawn to avoid dTMP + FUdR promoting FUMP toxicity;*
- 2) 5-FO as the source of FUMP that is independent from Upp/Udp-Udk*
- 3) SubLth-FUdR + serine to promote SE-FUdR; and*
- 4) dTMP (1.5µg/mL) or mock to test whether dTMP supplementation rescues of SE-FUdR toxicity.*

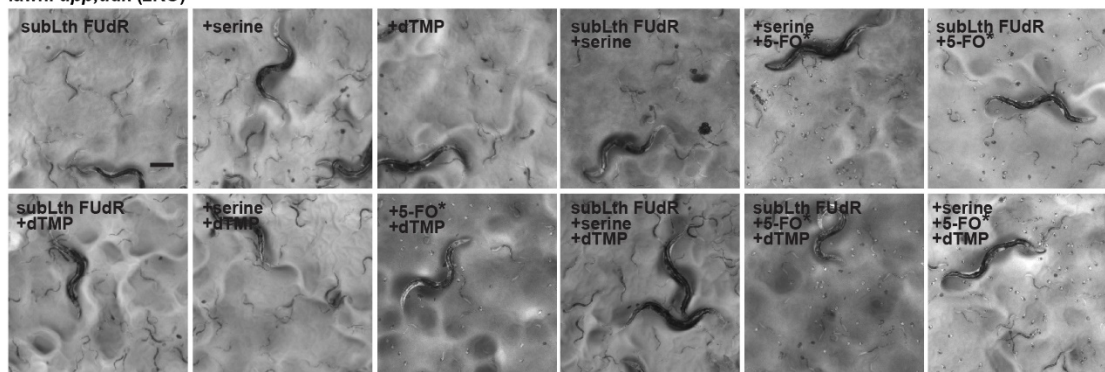
This complex experimental setup is necessary to test whether dietary thymidine rescues SE-FUdR because otherwise thymidine would simultaneously enhance Lth-FUdR toxicity (Fig. 5.2 g-n), yielding confounding results.

Figure 5. 10

a



b

lawn: *upp;udk* (2KO)

c

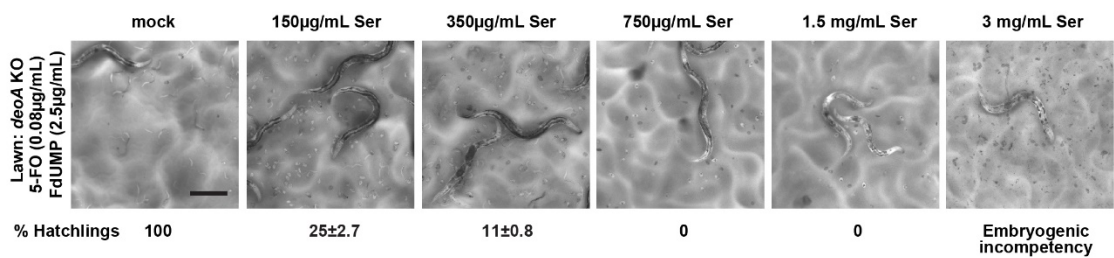


Figure 5.10 Throughout this figure, scale bars = 0.2mm, error bars represent S.E.M. * $p \leq 0.05$, ** $p \leq 0.01$, *** $p \leq 0.001$, **** $p \leq 0.0001$. n= # independent biological replicates. Source data are provided as a Source Data file.

(a). qRT-PCR analysis of aliquots of *tym-1* RNAi and EORB1 EV worms used in Fig 5.11 a. Fold change of *tym-1* expression was calculated as $\Delta\Delta CT$ as described in Methods, using *pmp-3* as reference gene. Data were analyzed using one-tailed ratio t-test, and are presented as log₂ of fold change. n=3. (b) Representative images of all control conditions in Fig. 5.11 j. n=3. (c) Representative images of effect of increasing doses of serine (0-3mg/mL) on *C. elegans* exposed to 0.08 μ g/mL 5-FO (to provide FUMP through a *upp,udk*-independent pathway) and 2.5 μ g/mL FdUMP (the main mediator of thymidine-less death) while cultured on *deoA* KO lawn (to avoid conversion of FdUMP into other fluoropyrimidines). n=3.

Figure 5. 11

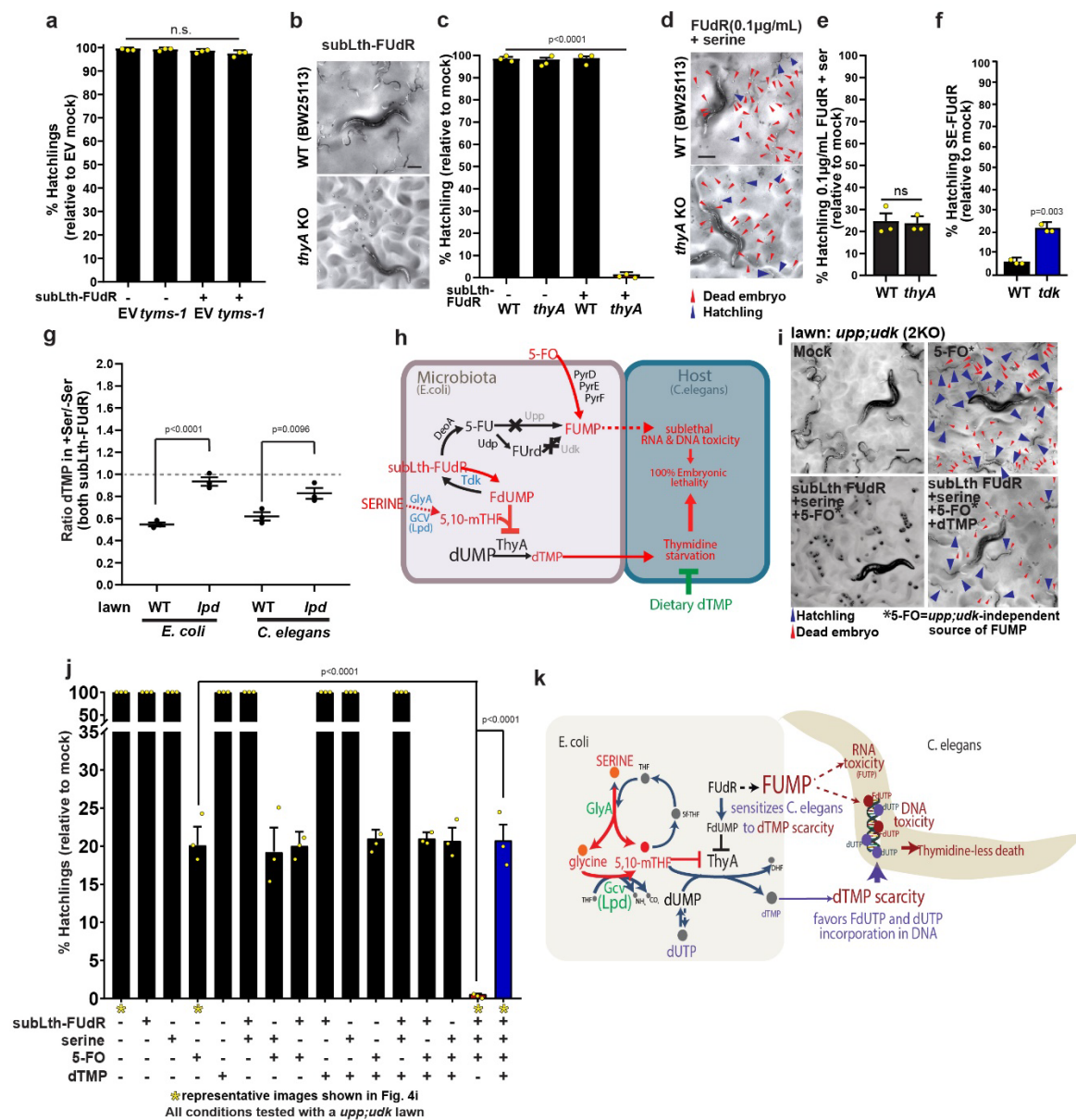


Figure 5.11 SE-FUdR promotes dTMP depletion in *E. coli* and *C. elegans*.

Throughout this figure: % hatchlings and LCMS data were analyzed as described in **Fig. 5.2** Statistical significance was assessed via two-tailed unpaired nonparametric t-test for % hatchlings quantification. LCMS data was analyzed using one-tailed ratio t-test after ROUT outlier treatment. Data are presented as mean values +/- SEM, scale bars = 200µm. n=# independent biological replicates. Source data are provided as a Source Data file.

(a) Quantification of progeny viability of *C. elegans* exposed to subLth-FUdR (1µg/mL) while cultured on EORB1 (RNAi-competent derivative of HB101) carrying empty RNAi empty vector (EV) or RNAi against *tymS-1*. n=3. See EORB1 strain development in Methods and Fig. 5.13 (b) Representative images of progeny viability of *C. elegans* exposed to subLth-FUdR (0.25µg/mL) while cultured on WT (BW25113) or *thyA* KO *E. coli* lawns. (c) Quantification of panel b treatments. n=3. (d) Representative images of progeny viability of *C. elegans* exposed to subLth-FUdR (0.1µg/mL) + serine 1.5mg/mL while cultured on WT (BW25113) or *thyA* KO *E. coli* lawns. (e) Quantification of panel d treatments. n=3. (f) Quantification of progeny viability of *C. elegans* exposed to subLth-FUdR ± serine while cultured on WT (BW25113) or *tdk* KO *E. coli* lawns. n=3. (g) LC-MS measurement of dTMP normalized to [¹³C9,¹⁵N2]UMP (Norm dTMP) in *E. coli* WT (BW25113) and *lpd* KO, and *C. elegans* cultured in these two *E. coli* strains. The ratio Norm dTMP in SE-FUdR / Norm dTMP in subLth-FUdR is depicted for each treatment. n=3. (h) Setup of dTMP-rescue experiment: 1) *upp;udk* double KO lawn avoids enhanced-FUMP toxicity otherwise driven by thymidine; 2) 5'-fluoroorotic acid (5-FO) as a source of

FUMP; 3) subLth-FUdR + serine to promote SE-FUdR; 4) \pm dTMP to test rescue of SE-FUdR toxicity. **(i)** Representative images of progeny viability of *C. elegans* cultured on *upp;udk* double KO *E. coli* lawns \pm 5-FO, \pm SE-FUdR (0.25 μ g/mL FUdR and 1.5mg/mL serine), \pm dTMP (1.5 μ g/mL) showing dTMP rescues SE-FUdR toxicity. **(j)** Quantification of treatments in panel **i** (denoted with asterisks) and other controls. n=3. **(k)** Working model of SE-FUdR toxicity. Through promoting 5,10-mTHF synthesis, dietary serine enables FdUMP-mediated inhibition of *E. coli* TS (ThyA). The consequent scarcity of dietary dTMP then exacerbates the toxic effect of sublethal FUdR, leading to DNA toxicity, and death of the worm.

5.4.6 The host distinctively responds to Lth-FUdR and SE-FUdR toxicity

Although the phenotypic outcomes of treatment with Lth-FUdR and SE-FUdR are similar, namely embryonic lethality at low doses and developmental delay at higher doses, the microbial mechanisms leading to these outcomes are distinct. Thus, we next sought to investigate whether the host response to Lth-FUdR and SE-FUdR at a sub-phenotypic level might also be distinct. We first tested whether apoptosis contributes to Lth-FUdR toxicity in *C. elegans*. We found that loss-of-function mutation of the apoptosis activator *ced-4(n1162)* and gain-of-function mutation of the apoptosis inhibitor *ced-9(n1950)* enhance toxicity (Fig. 5.12 a), arguing against apoptosis mediating Lth-FUdR toxicity in *C. elegans*.

Having used a *C. elegans* mutant approach to determine that apoptotic mechanisms do not mediate Lth-FUdR toxicity in *C. elegans*, we moved to a targeted RNAi screening approach to identify host pathways mediating Lth-FUdR and SE-FUdR toxicity. We performed 3- and 4-way *C. elegans* RNAi screens of an RNAi sublibrary composed of 361 *C. elegans* genes 2 steps away from pyrimidine, purine, and serine uptake, synthesis, metabolism, or secretion, built based on a reconciled model of *C. elegans* metabolism we are currently refining (Joshi *et al*, unpublished). We further added 26 DNA repair, autophagy, and detox pathway genes previously reported to modulate the toxicity of fluoropyrimidines or related compounds (Scott *et al.*, 2017; SenGupta *et al.*, 2013) (gene list in Table 5.3). To perform RNAi screening using the HB101 background, we developed and validated an RNAi-competent derivative of HB101 that we named EORB1 (Fig.

5.13). Using EORB1, we screened the 387-gene RNAi sublibrary in 5 conditions:

1) no additives 2) Lth-FUdR 3) serine 4) subLth-FUdR, and 5) SE-FUdR.

Figure 5. 12

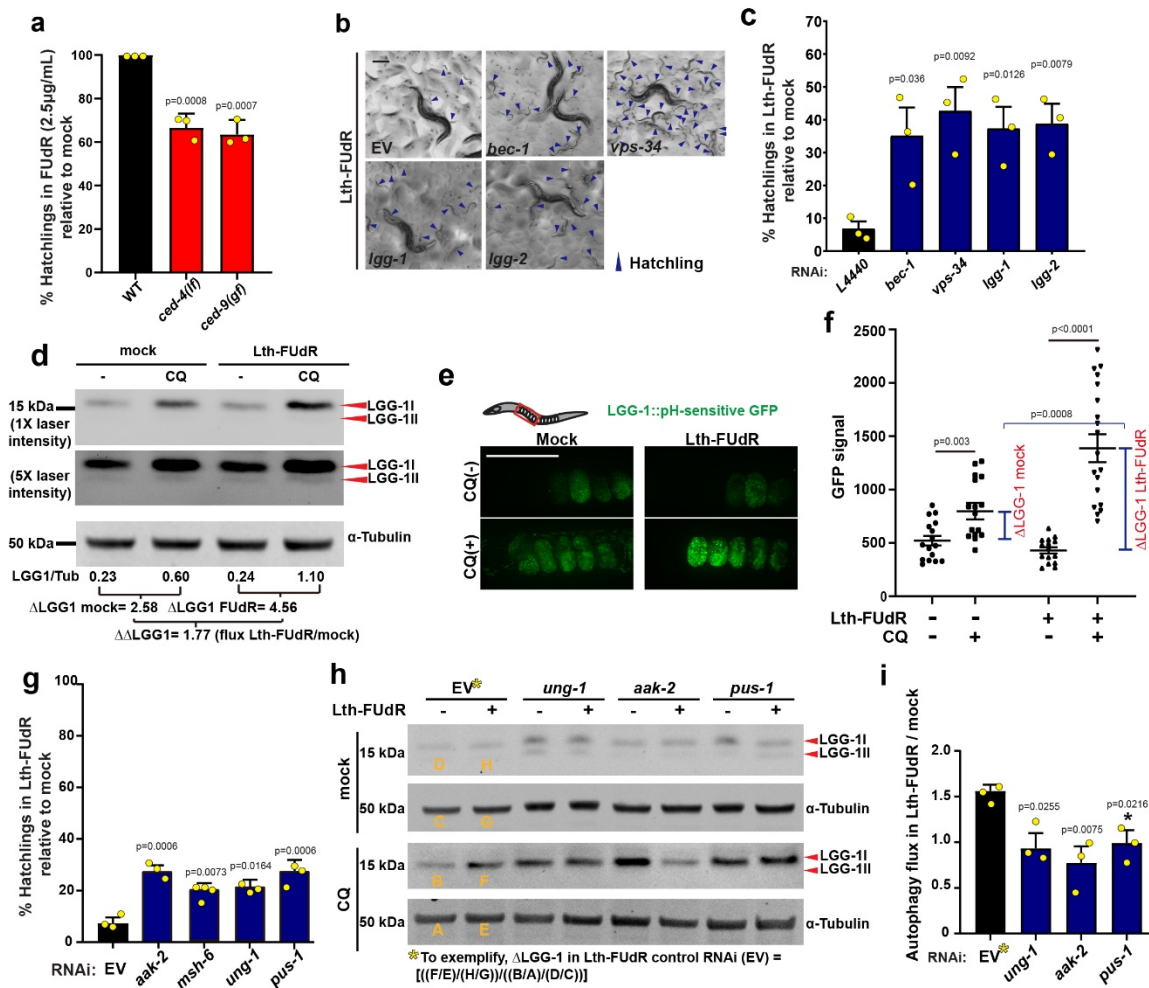


Figure 5.12 Lth-FUdR activates autophagic cell death in *C. elegans*. Throughout this figure: % hatchlings was analyzed as described in **Fig. 5.2** Statistical significance was assessed via two-tailed unpaired nonparametric t-test for % hatchlings quantification. Statistical significance for Western blotting ratio was assessed via one-tailed ratio t-test. Data are presented as mean values +/- SEM, * $p \leq 0.05$, n=# independent biological replicates. Source data are provided as a Source Data file.

(a) Quantification of progeny viability of WT, *ced-4(n1162)*, and *ced-9(n1950)* mutant *C. elegans* exposed to 2.5 μ g/mL FUdR (lower dose of FUdR used to enable detection of enhancers). n=3. (b) Representative images of progeny viability of *C. elegans* exposed to Lth-FUdR while cultured on EORB1 EV or autophagy RNAi clones. Scale bar = 200 μ m. (c) % hatchling quantification of treatments represented in panel b. n=3. (d) Representative α LGG-1 western blotting of worms cultured on EORB1 lawn \pm Lth-FUdR (7.5 μ g/mL) \pm 8h exposure to 20mM chloroquine (lysosomal inhibitor). Two different exposures of α LGG-1 blot are depicted. Autophagy flux estimation and data interpretation described in main text and Methods. n=10. (e) *In vivo* imaging of embryos expressing LGG-1::GFP(pH-sensitive) treated with \pm Lth-FUdR (7.5 μ g/mL) and \pm 8h of 20mM chloroquine. Scale bar = 100 μ m. (f) Quantification of GFP signal of treatments represented in panel e, two-tailed, unpaired, nonparametric t-test. LGG-1::GFP data acquisition, analyses, and interpretation described in main text and Methods. Unpaired nonparametric one-tailed t-test was used to singly compare average GFP signal in (+)CQ to (-)CQ (denoted with black brackets and asterisks), and

one-tailed ratio t-test was used to compare Δ LGG-1 ratios (denoted with blue brackets and asterisks). n=3. **(g)** Quantification of progeny viability of *C. elegans* exposed to Lth-FUdR (7.5 μ g/mL) while cultured on EORB1 EV or RNAi against *aak-2*, *msh-6*, *ung-1*, or *pus-1*. n=3. **(h)** Representative α LGG-1 western blotting of worms cultured on EORB1 EV or RNAi against *ung-1*, *aak-2* or *pus-1* \pm Lth-FUdR (7.5 μ g/mL) \pm 8h of 20mM chloroquine. Approach, data analyses and interpretation described in main text and Methods. **(i)** Autophagy flux quantification as depicted in panel **h**, and described in methods. n=3.

Figure 5. 13

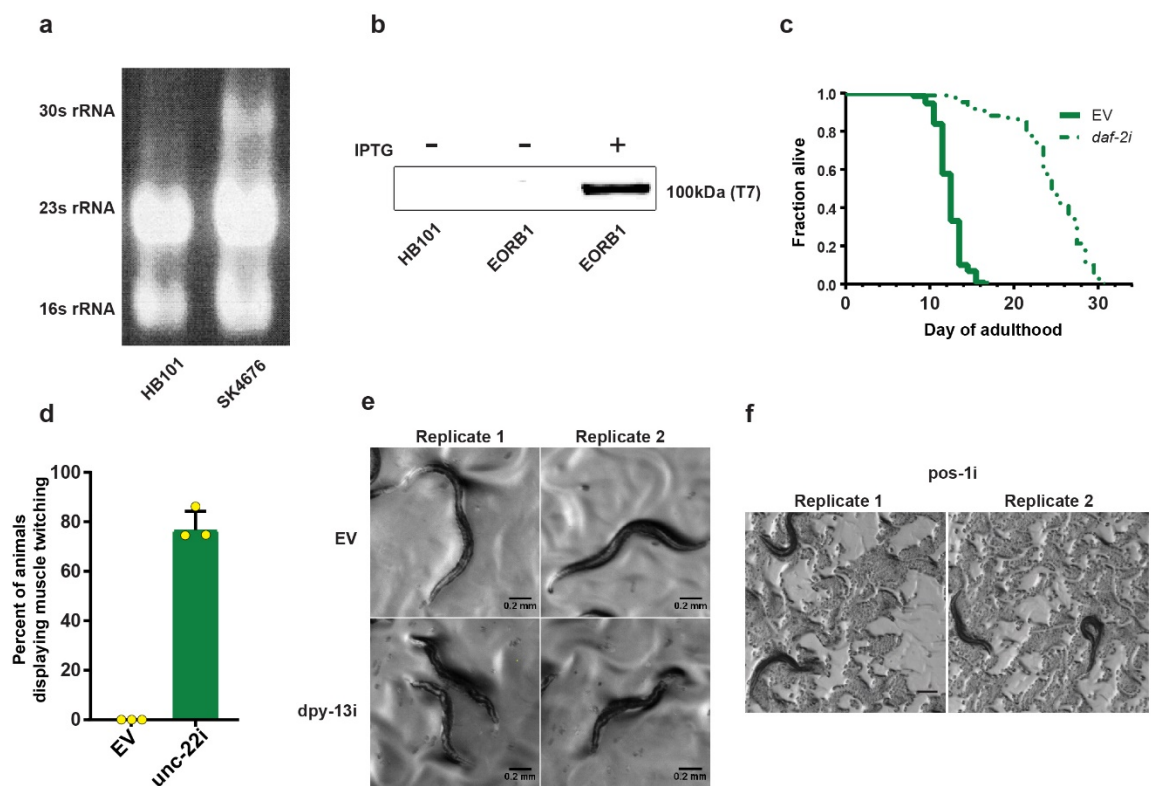


Figure 5.13 Validation of EORB1 (an RNAi-competent derivative of HB101).

Source data are provided as a Source Data file.

(a) HB101 *rnc*- derivative, but not HB101 parental, accumulates 30S rRNA precursor. (b) IPTG-inducible T7 polymerase is expressed in EORB1 but not in the HB101 parental strain. (c-f) EORB1 is competent for feeding RNAi: (c) RNAi against *daf-2* extends *C. elegans* lifespan ~2-fold, (d) *unc-22* causes muscle twitching in >75% of animals. n=3 independent biological replicates. (e) *dpy-13* causes a dumpy phenotype in 100% of animals (2 representative experiments shown for control and RNAi), and (f) *pos-1* causes 100% sterility (2 representative experiments shown for RNAi).

5.4.6.1 Host response to Lth-FUdR toxicity

SenGupta *et al.*(SenGupta *et al.*, 2013) and Scott *et al.*(Scott *et al.*, 2017) demonstrated that 5-FU activates autophagy in *C. elegans*, and that death requires the autophagy-related genes *bec-1* (*C. elegans* ortholog of BECLIN 1) and *atg-7* (E1-like enzyme involved in conjugation of the ubiquitin-like proteins LGG-1 and ATG-12 to autophagic membranes)(Scott *et al.*, 2017; SenGupta *et al.*, 2013). In accordance with these reports, our 3-way RNAi screen identified 4 autophagy genes as suppressors of Lth-FUdR toxicity in *C. elegans* (Table 5.4 and Fig. 5.12 b,c). To better define the role of autophagy, we used 3 approaches to assess the levels of autophagy in worms treated with Lth-FUdR. First, we assessed transcriptional levels of autophagy genes whose expression correlates well with levels of autophagic flux in *C. elegans*(Zhang *et al.*, 2015b), and found increased expression of *atg-16.2*, *atg-18*, and *bec-1* in worms treated with Lth-FUdR (Fig. 5.14 a). Second, we assessed autophagy at the protein level. The most cited approaches to measure autophagy in *C. elegans* are the measurement of the number of LGG-1::GFP punctae in *in vivo* imaging analyses, and using α -GFP antibodies to measure LGG-1::GFP in western blotting assays (Palmisano and Meléndez, 2016). However, in isolation, these approaches could be misleading as LGG-1 is subject to autophagic degradation and thus an increased LGG-1::GFP signal could indicate either increased autophagy initiation (increased flux) or decreased lysosomal turnover (decreased flux). Thus, to better assess autophagic flux in *C. elegans*, we developed and immunopurified antibodies against LGG-1. We validated the antibodies using *lgg-1* RNAi and LGG-1 overexpression worms

(Fig. 5.14 b). We then measured autophagic flux in worms by exposing them to the relevant treatments \pm the lysosomal inhibitor chloroquine (CQ). Because CQ blocks lysosomal turnover, the magnitude of the difference in LGG-1 signal between plus and minus CQ reflects the relative level of autophagic flux in any particular condition and can then be compared between conditions (a.k.a. $\Delta\Delta$ LGG-1; see methods for additional details on calculations). Using this metric, we observed 1.5-2 fold increases in autophagic flux in the Lth-FUdR condition (Fig. 5.12 d). Third, since our toxicity readout is embryonic lethality, we assessed autophagic flux in the embryo. For this, we used a previously reported LGG-1 transgenic line (Chang et al., 2017) in combination with CQ. In this reporter strain, LGG-1 is fused to a pH-sensitive GFP. Hence, unless lysosomal acidification is perturbed, the GFP signal corresponds to non-acidic autophagosomes (AP). By contrast, in animals treated with an agent that alkalinizes the lysosome (i.e. CQ), the GFP signal corresponds to AP + autolysosomes (AL); hence, the ratio $\text{GFP}_{\text{CQ}(+)}/\text{GFP}_{\text{CQ}(-)} = \Delta\text{LGG-1}$ for a given treatment or control. The simplest interpretations of this readout follow: 1) basal autophagic flux: whichever $\Delta\text{LGG-1}$ is observed in wild-type unperturbed animals; 2) reduced or blocked autophagic flux: $\Delta\text{LGG-1}$ is smaller (statistically significant) than $\Delta\text{LGG-1}$ in the control; and 3) increased autophagic flux: $\Delta\text{LGG-1}$ is larger (statistically significant) than $\Delta\text{LGG-1}$ in the control. Using this metric, we found a $\Delta\text{LGG-1}$ of $\sim 50\%$ in mock and $\sim 300\%$ in Lth-FUdR (Fig. 5.12 e,f), suggesting Lth-FUdR strongly increases autophagic flux. Altogether, Lth-FUdR promotes high levels of autophagy, and 4 different autophagy genes mediate death in the Lth-FUdR condition. Death not only

concurrent, but also dependent on autophagy is the definition of autophagic cell death (ACD). Hence, we propose that worms treated with lethal doses of FUdR are dying through ACD.

In line with ACD mediating Lth-FUdR toxicity in *C. elegans*, we found that RNAi against *aak-2* suppresses toxicity (Fig. 5.12 g). *aak-2* encodes for the catalytic subunit of AMP-activated protein kinase (AMPK), a central energy homeostasis kinase that promotes the activation of autophagy (Kim et al., 2011) and has been functionally linked to ACD (Ha et al., 2017). AMPK responds to several stresses including DNA damage (Zhang et al., 2015a). Among our RNAi screen hits, we found two DNA repair/damage-related enzymes, MSH-6 and UNG-1 (Fig. 5.12 g). The mismatch-repair enzyme MSH-6 has been shown to mediate 5-FU toxicity in *C. elegans* (Scott et al., 2017; SenGupta et al., 2013). By contrast, *ung-1* has not been previously shown to mediate fluoropyrimidine toxicity in *C. elegans*. UNG1 is a DNA repair enzyme that catalyzes the removal of uracil misincorporated in DNA. However, if it enters a futile lesion/repair cycle, as when an excess of FdUTP is available to be incorporated into DNA (Pettersen et al., 2011; Seiple et al., 2006), then it promotes DNA damage. Hence, we hypothesized that UNG-1 and AMPK would be part of an axis that activates lethal levels of autophagy in response to FUdR. In support of this hypothesis, we found that RNAi against *ung-1* and *aak-2* suppresses the activation of autophagy otherwise observed in animals treated with lethal doses of FUdR (Fig. 5.12 h,i). Another RNAi hit, *pus-1* (Fig. 5.12 g), provides additional insight into how Lth-FUdR toxicity would be executed in *C. elegans*.

From yeast to mammals pseudouridine synthase (PUS1) converts uridines present in several RNA classes into pseudouridines (Ansmant et al., 2000; Chen and Patton, 1999), and pseudouridylation is required for proper maturation and stability of RNAs (Spenkuch et al., 2014). However, when uracil is fluorinated PUS1 is irreversibly linked to it (Gu et al., 1999; Huang et al., 1998), reducing the pool of functional RNAs and promoting toxicity (Zhao and Yu, 2007). We then tested whether PUS-1 dysfunction would also be upstream of ACD. Indeed, we found that *pus-1* RNAi suppresses the hyperactivation of autophagy (Fig. 5.12 h,i). Altogether the data show that UNG-1, AMPK, and PUS-1 are upstream of autophagy in the pathway that promotes death in animals treated with a lethal dose of FUdR. Further, that the suppressors of embryonic lethality also suppress the increased autophagic flux, reinforces the notion that ACD executes death in the Lth-FUdR condition.

In addition to being functionally dysregulated by fluoropyrimidines, mammalian UNG1 and PUS1 share a mitochondrial subcellular localization (Bykhovskaya et al., 2004; Slupphaug et al., 1993). This was intriguing because mitochondrial lipids are emerging as key upstream players in non-apoptotic cell death (Dixon et al., 2015; Magtanong et al., 2016; Nikolettou et al., 2013), and, in this sense, the Lth-FUdR suppressor *pld-1* is particularly informative because its mammalian homolog, PLD1, produces a lipid signal that activates autophagy (Dall'Armi et al., 2010). We therefore hypothesized that lipid signals might link mitochondrial dysfunction caused by Lth-FUdR to the activation of lethal levels of autophagy. In support of this hypothesis, we found that *ipla-2*, *T28F3.5*, *C03H5.4*, *T09B9.3*, and

pld-1 not only suppress Lth-FUdR toxicity (Fig. 5.15 a,b) but they also suppress enhanced autophagy (Fig. 5.15 c,d), in line with a model in which lipid signals link mitochondrial dysfunction to ACD.

We then embarked on defining what it is that Lth-FUdR does to the mitochondria. A previous study, found that cytochrome C (cytC) abundance is a good predictor of activation of lethal autophagy downstream of loss of mitochondrial membrane integrity (Zhou et al., 2019). However, in the context of Lth-FUdR, cytC levels do not correlate with toxicity (Fig. 5.14 c). This result suggests that loss of mitochondrial membrane integrity is one of several possible insults to the mitochondria that can trigger lethal autophagy, but it is unlikely to be the one triggering it in animals treated with FUdR. In addition, mitochondrial leakage is the most established trigger of apoptosis (Wang and Youle, 2009). Hence, the cytC negative result is in line with apoptosis not being a mediator of Lth-FUdR toxicity (Fig. 5.12 a). We then searched for other insults that may promote the activation of autophagy in animals treated with FUdR. We found no changes in the mitochondrial oxidative stress response as measured by *gst-4* expression (Fig. 5.14 d), or the mtUPR response as measured by *hsp-6* mRNA (Fig. 5.14 d) and HSP-60 protein levels (Fig. 5.14 c). However, we did find reduced levels of mitochondrial DNA (Fig. 5.15 e) and mitochondrially-encoded mRNAs (Fig. 5.15 f) and rRNA (Fig. 5.15 g) in worms treated with a lethal dose of FUdR. These results align well with PUS-1 and UNG-1 mediating Lth-FUdR toxicity because in mammals futile activation of mitochondrial UNG1 and malfunction of mitochondrial

PUS1 leads to mitochondrial DNA and RNA toxicity, and mitochondrial dysfunction *in vitro* and *in vivo* (Bykhovskaya et al., 2004; Endres et al., 2004). Therefore, although future studies are warranted to fully dissect the mechanisms executing death in animals treated with lethal doses of FUdR, the data presented here fit a model in which FUdR derivatives (likely FUTP and FdUTP) would be incorporated into the host mitochondrial RNAs and DNA, impairing mitochondrial RNA maturation (via PUS-1 inhibition), and promoting mito DNA damage (via futile UNG-1 activity). In turn, AMPK and lipid signals would transduce mitochondrial damage to the cytosol to activate lethal levels of autophagy.

Figure 5. 14

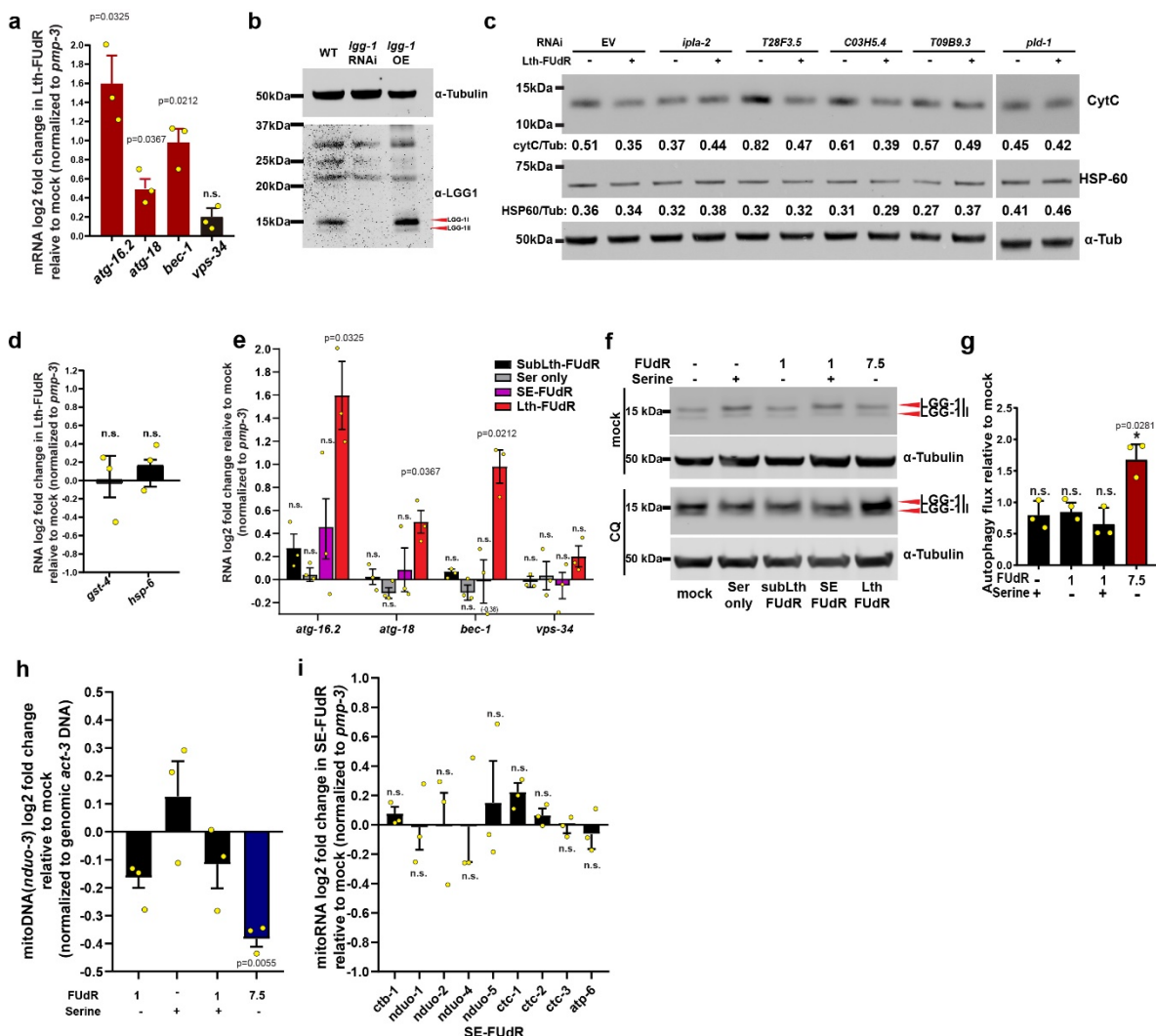


Figure 5.14 Throughout this figure, error bars represent S.E.M. Statistical significance was assessed using one-tailed ratio t-test. * $p \leq 0.05$, ** $p \leq 0.01$, *** $p \leq 0.001$, **** $p \leq 0.0001$. n= # independent biological replicates. Source data are provided as a Source Data file.

(a) qRT-PCR analysis of autophagy genes in worms cultured on EORB1 lawn and treated with Lth-FUdR. Fold change was calculated as $\Delta\Delta CT$ as described in Methods, using *pmp-3* as reference gene. Data are presented as log₂ of fold change. n=3 **(b)** The specificity of α -LGG1 antibody was validated by western blotting of whole lysates of *C. elegans* fed RNAi against *lgg-1* and of a transgenic line overexpressing *lgg-1* (MAH215). α -Tubulin (4A1) was used as loading reference. Red arrows point to LGG1I and LGG1II bands. n=1 **(c)** Representative western blotting analysis of endogenous cytochrome C (cytC) and of HSP-60 in worms treated with Lth-FUdR and fed EORB1 EV or RNAi targeting mitochondrial genes that suppress Lth-FUdR toxicity. Quantification of band intensity relative to α -Tubulin is depicted. n=3. **(d)** qRT-PCR analysis of mito oxidative stress response (*gst-4*) and mitoUPR (*hsp-6*) in worms treated with Lth-FUdR relative to mock. Analysis and quantification as described in panel **a**. n=3. **(e)** qRT-PCR analysis of autophagy genes in worms cultured on EORB1 lawn and treated with subLth-FUdR, serine, SE-FUdR, or Lth-FUdR. Analysis and quantification as described in panel **a**. n=3. **(f)** Western blotting analysis of α -LGG1 in worms cultured on EORB1 and treated with mock, serine, subLth-FUdR, SE-FUdR, and Lth-FUdR \pm 20mM Chloroquine. **(g)** Quantification of LGG-1 relative to α -Tubulin in treatments represented in panel **f**. Analysis and quantification as described in Fig. 5.12 h n=3.

Data analyzed using ratio t-test. **(h)** qPCR analysis of mitochondrial DNA content (*nduo-3*) relative to nuclear DNA (*act-3*) in subLth-FUdR, serine, SE-FUdR and Lth-FUdR relative to mock. Data presented as log₂ fold change and statistically analyzed using ratio t-test. n=3. **(i)** qRT-PCR analysis of the expression/stability of mitochondrially-encoded genes in worms treated with SE-FUdR. Quantification and analysis as described in panel **a**. n=3.

Figure 5. 15

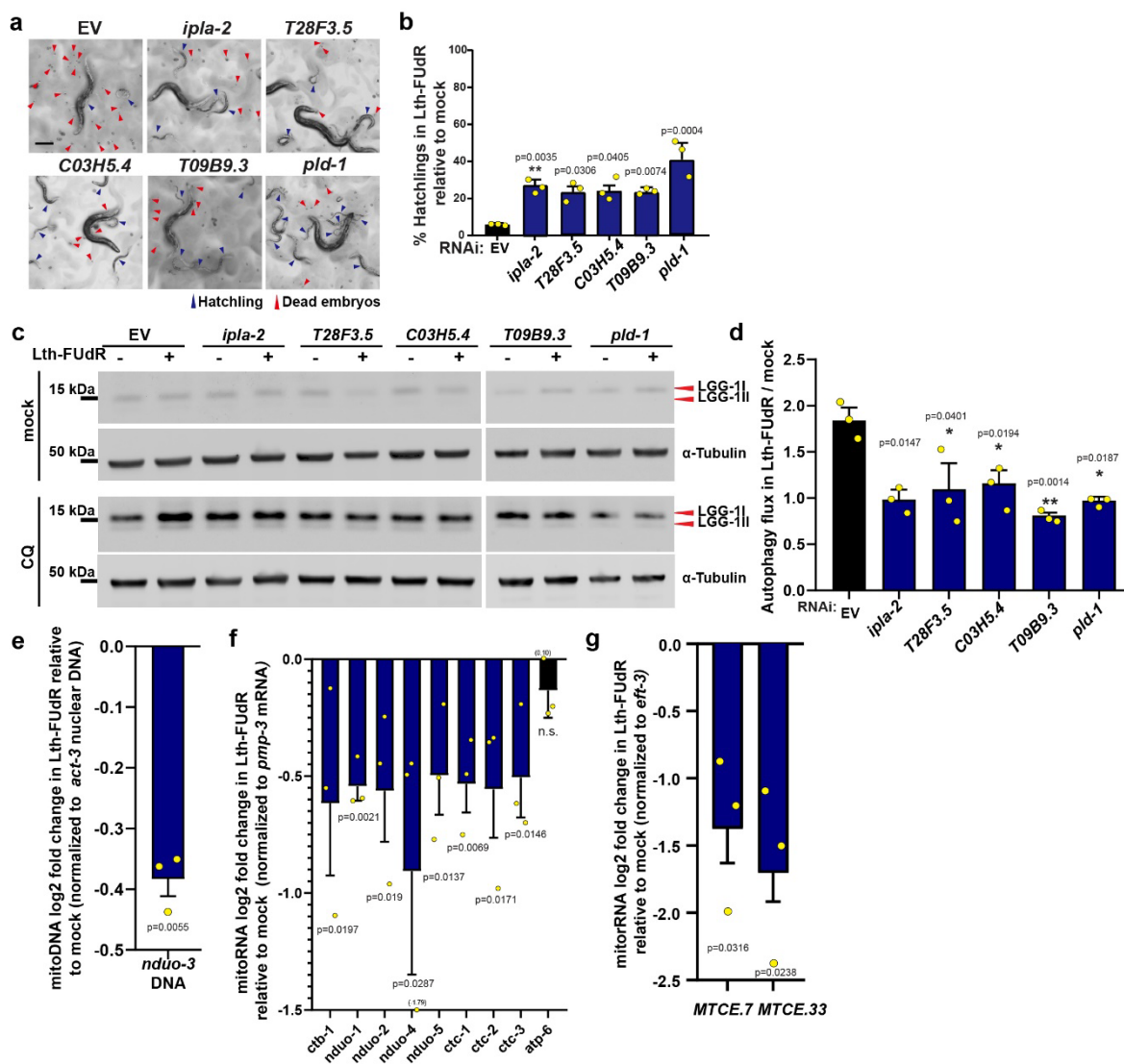


Figure 5.15 Autophagy activation in Lth-FUdR depends on mitochondrial lipid metabolism. Throughout this figure: % hatchlings was analyzed as described in

Fig. 5.2 Statistical significance for %hatchlings quantification was assessed via two-tailed unpaired nonparametric t-test. Statistical significance for Western blotting ratio and qPCR fold change was assessed via one-tailed ratio t-test. Data are presented as mean values +/- SEM, scale bars = 200µm. n= # independent biological replicates. Source data are provided as a Source Data file.

(a) Representative images of progeny viability of *C. elegans* exposed to Lth-FUdR (7.5µg/mL) while cultured on EORB1 EV or RNAi targeting mitochondrial genes. n=3. (b) Quantification of treatments represented in panel a. n=3. (c) Representative αLGG-1 western blotting analysis of worms exposed to ± Lth-FUdR (7.5µg/mL) ± 8h of 20mM chloroquine while cultured on EORB1 EV or RNAi targeting mitochondrial genes. Data acquisition as described in Methods. (d) Quantification of autophagy flux of treatments represented in panel c. Autophagy flux estimation and interpretation as described in **Fig. 5.12 h-i**, main text, and Methods. n=3. (e) qPCR analysis of mitochondrial DNA content (*nduo-3*) relative to nuclear DNA (*act-3*) in Lth-FUdR worms relative to mock. n=3. (f) qRT-PCR analysis of the expression/stability of mitochondrially-encoded mRNAs relative to the nuclearly encoded mRNA *pmp-3* in worms treated with Lth-FUdR relative to mock. n=3. (g) qRT-PCR analysis of mitochondrially encoded rRNAs normalized to *eft-3* (as previously described) in worms treated with Lth-FUdR relative to mock. n=3.

5.4.6.2 Serine-enhanced FUdR toxicity

Since the major toxicity mechanism in the SE-FUdR condition is the classic inhibition of TS, and thymidine-less death has been linked to apoptosis, we first tested whether apoptosis was contributing to SE-FUdR toxicity in *C. elegans*. However, we found the apoptosis mutants *ced-4(n1162)* and *ced-9(n1950)* to further enhance SE-FUdR toxicity (Fig. 5.16 a), arguing against apoptosis mediating toxicity in this condition. We then moved onto perform 4-way RNAi screening for *C. elegans* genes mediating SE-FUdR toxicity. The screen hits revealed that the host response to SE-FUdR is remarkably distinct from the response to Lth-FUdR. From the 9 genes that were hits in both screens, only 2 show the same phenotype in both conditions (Fig. 5.16 b and Table 5.4). One of these genes is *ung-1* which suppresses Lth-FUdR (Fig. 5.12 g) and SE-FUdR (Fig. 5.16 c) toxicity. In contrast, the other 7 genes that are hits in both screens show opposite phenotypes. *pus-1* suppresses Lth-FUdR toxicity (Fig. 5.12 g) and enhances SE-FUdR toxicity (Fig. 5.16 c), which is in line with a more prevalent role for RNA toxicity in the Lth-FUdR than in the SE-FUdR condition. Most striking, the autophagy genes, as a class, have opposite phenotypes in the two screens. While autophagy mediates Lth-FUdR toxicity, RNAi against the autophagy genes *bec-1*, *atg-7*, *lgg-1*, *lgg-2*, and *vps-34* further enhances SE-FUdR toxicity (Fig. 5.16 d,e), suggesting that autophagy promotes death downstream of fluororibonucleotide toxicity, but protects from death during thymidine starvation. One autophagy gene, *atg-7*, acts distinctively as its inactivation does not suppress Lth-FUdR toxicity but

enhances SE-FUdR toxicity. However, autophagy independent from ATG-7 (a.k.a. non-conventional autophagy) has been reported (Chang et al., 2013; Nishida et al., 2009), and ATG7 modulates the DNA damage-responsive tumor suppressor and cell-death mediator p53 (Lee et al., 2012). Therefore, the protective role of ATG-7 in SE-FUdR toxicity may occur through mechanisms distinct from autophagy. We then measured the levels of autophagy in the SE-FUdR toxicity condition. We found no changes in the levels of expression of autophagy genes (Fig. 5.14 e) or autophagic flux by western blots of gravid adults (Fig. 5.14 f,g). However, when exposed to serine, embryos show similar GFP signal in the absence and presence of CQ (Fig. 5.16 f,g), suggestive of reduced autophagic flux. Altogether, although several aspects of the death mechanisms remain to be elucidated, it is clear that Lth-FUdR and SE-FUdR are distinctively executed in the host. Further supporting this notion, we observe no changes in mitochondrial DNA (Fig. 5.14 h) or RNA content (Fig. 5.14 i) in the SE-FUdR condition, and, correspondingly, AMPK and the lipid metabolism genes that suppress Lth-FUdR toxicity do not suppress SE-FUdR toxicity (Fig. 5.16 b). Altogether, the results show that dietary serine not only changes metabolic flux in *E. coli*, and with that the level of toxicity of FUdR, but also redefines the host response to FUdR toxicity (Working model in Fig. 5.16 h).

Figure 5. 16

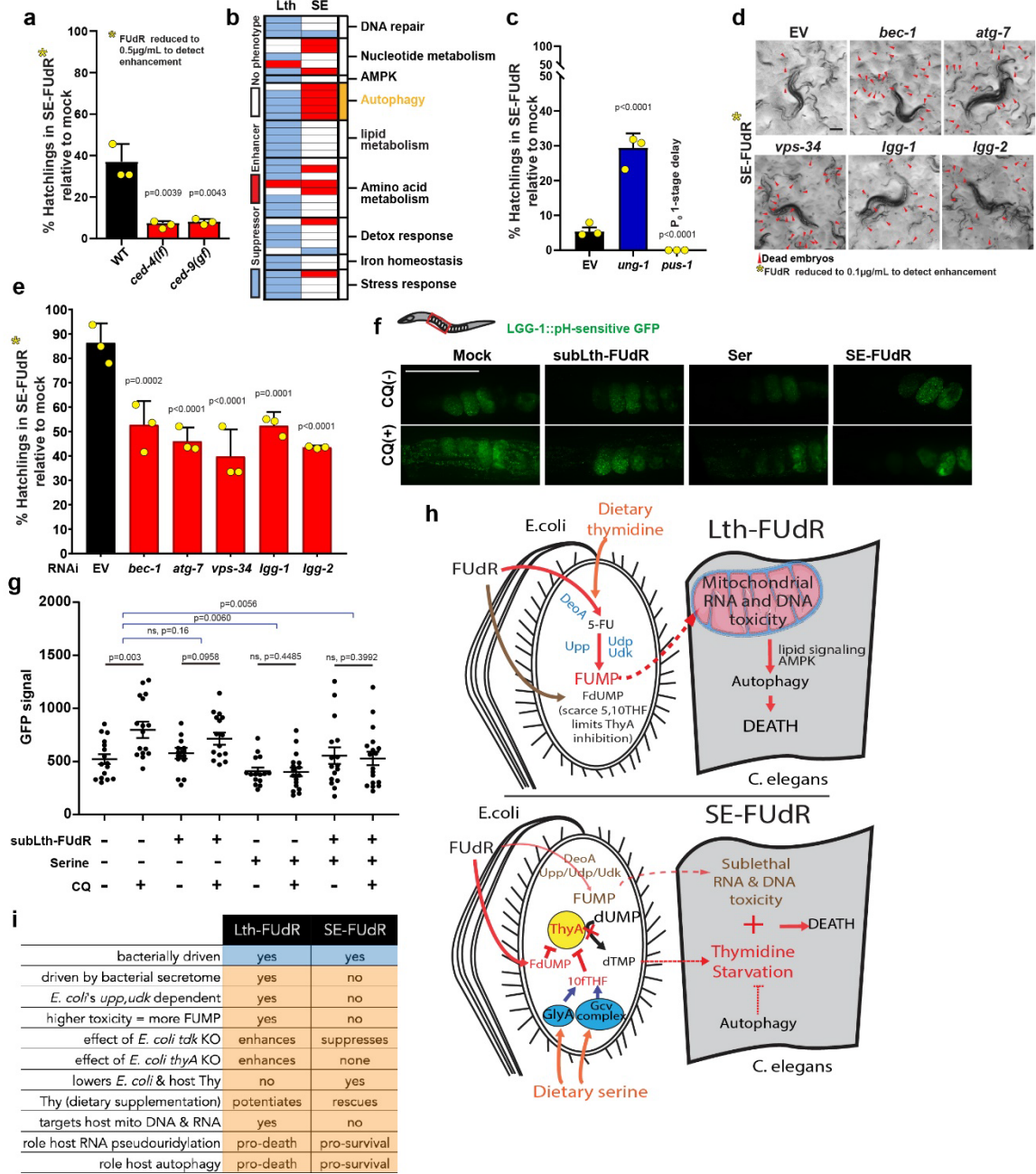


Figure 5.16 Host response to Lth-FUdR and SE-FUdR are distinct. Throughout this figure: % hatchlings was analyzed as described in **Fig. 5.2** Statistical significance was assessed via two-tailed unpaired nonparametric t-test for % hatchlings quantification. Data are presented as mean values +/- SEM. n= # independent biological replicates. Source data are provided as a Source Data file.

(a) Quantification of progeny viability of WT, *ced-4(n1162)*, and *ced-9(n1950)* mutant *C. elegans* cultured on EORB1 lawns treated with 0.5µg/mL plus 1.5mg/mL serine (lower dose of FUdR used to enable detection of SE-FUdR enhancers). n=3.

(b) GO Distribution of the 3-way (left) and 4-way (right) hits from the *C. elegans* RNAi screen for modulators of Lth-FUdR and SE-FUdR, respectively. Enriched functional class (Fisher's exact test $p < 0.005$) denoted yellow.

(c) Quantification of progeny viability of *C. elegans* exposed to SE-FUdR (1µg/mL FUdR) while cultured on EORB1 EV or RNAi against *ung-1* or *pus-1*. n=3.

(d) Representative images of progeny viability of *C. elegans* cultured on EORB1 EV or autophagy RNAi lawns treated with 0.1µg/mL plus 1.5mg/mL serine (lower dose of FUdR used to enable detection of enhancers). Scale bar= 200µm. n=3.

(e) Quantification of treatments represented in panel d. n=3.

(f) *In vivo* imaging of embryos expressing LGG-1::GFP(pH-sensitive) treated in EORB1 lawns with 1µg/mL FUdR, 1.5mg/mL serine, and FUdR plus serine, ± 6h on 20mM chloroquine. Scale bar = 100µm. n=3.

(g) Quantification of GFP signal of treatments represented in panel f. Analysis as described in **Fig. 5.12 f**. In this panel * $p = 0.052$. n=3.

(h) Working model of the host response to Lth-FUdR and SE-FUdR. In the Lth-FUdR condition, some derivatives of FUMP generated in the worm (e.g. FUTP) misincorporate into mitochondrial

RNAs preventing RNA maturation and function, while others (e.g. FdUTP) are incorporated into DNA, promoting detrimental levels of DNA repair. Then lipid signals and AMPK link the consequent mitochondrial dysfunction to the activation of autophagic cell death. In the SE-FUdR condition, mito RNAs and DNA are not major targets. Instead, *C. elegans* die of dTMP deficiency, and its consequent thymidine-less death, which autophagy can alleviate. (i) List of distinctive characteristics of Lth-FUdR and SE-FUdR.

5.5 Discussion

Diet and microbiota are attractive targets for therapeutic intervention. However, the dominance of correlative and *in vitro* studies on the effects that diet and microbiota have on the host response to drugs has limited the development of therapeutic interventions targeting diet, microbiota, or both. Here, we used a tractable system that enables molecular dissection of 4-way diet, drug, microbe, host interactions *in vivo*. With this 4-way model system, we dissected the microbe and host response to FUdR, and how they both change when serine is supplemented to the diet.

We first show that Lth-FUdR toxicity is bacterially driven. However, the amount of thymidine that *E. coli* provides to *C. elegans* does not play a role in Lth-FUdR toxicity in our experimental setup. But when serine is supplemented to the diet, this changes. Dietary serine enables the inhibition of *E. coli*'s TS, reducing the dTMP pool in *E. coli* and consequently in *C. elegans*. Together, the data presented here suggest that the precursors for the synthesis of 5,10-mTHF are limiting in our experimental setup. As a practical corollary, the fact that supplementation with a single dietary metabolite can greatly enhance the potency of *E. coli*-mediated FUdR toxicity as well as shift its mechanism of action emphasizes the need to employ standardized media conditions when studying drug mechanisms in model organisms. Indeed, in *C. elegans* research, peptone concentrations from different commercial providers are not standardized. Thus, some results garnered from *C. elegans* studies using drugs supplemented to the media may be influenced by the varied nutrient compositions of media and the consequent distinct interactions with

microbial and host metabolism. More broadly, the mechanisms of action of dietary thymidine and serine show that the microbiota can affect the efficacy or toxicity of drugs through at least two mechanisms: 1) directly, via metabolizing the drug (i.e. conversion of FUdR into FUMP; thymidine mechanism); and 2) indirectly, via converting dietary nutrients into metabolites that alter the mechanism of action of the drug (i.e. conversion of dietary serine into 5,10-mTHF enabling thymidine-less death; serine mechanism).

The significance of using simplified tractable models of microbe-host co-metabolism resides in unveiling the complexity of the molecular interactions that may affect drug treatment outcomes, and serving as guide for mechanistic studies in higher organisms. At first sight, *C. elegans* may seem too unique to inform host-microbiota interactions in higher organisms. Bacteria serve as microbiota and food source in *C. elegans* (Samuel et al., 2016). Hence, bacteria are the principal source of micro and macronutrients, and this may seem different from mammals. However, the mammalian gut microbiota plays a critical role in providing essential nutrients and in digesting the complex carbohydrates, proteins, and fats that reach the lower gastrointestinal tract in mammals (Oliphant and Allen-Vercoe, 2019). Furthermore, bacterial lysis, and the consequent release of cell content, is part of the normal mammalian gut dynamics (Derrien and van Hylckama Vlieg, 2015). The enterohepatic system permits exchange of metabolites, byproducts, and xenobiotics between the intraluminal intestine, the bloodstream, and animal tissues (Watkins and Klaassen, 2018). Indeed, microbiota-derived metabolites

including nucleosides and nucleotides can be found in blood and other mammalian-host organs (Fergus et al., 2015; Nakayama et al., 1997; Proietti et al., 2019). Furthermore, studies in mammals show bacterially-converted dietary folates, and bacterially-derived serine in host tissues (Asrar and O'Connor, 2005; Nakade et al., 2018; Rong et al., 1991). It is also notable that panels of probiotic bacteria that include *E. coli* can differentially activate chemotherapeutics *in vitro* (Lehouritis et al., 2015, 2016). Therefore, although only suggestive, the current mammalian evidence is in line with diet being capable of modulating fluoropyrimidine efficacy and toxicity through altering the metabolism of gut microbes in the clinical setting. Diet and microbes could account, at least in part, for the variability in fluoropyrimidine responsiveness that cannot be explained by the genetics of the patient or the tumor (Scartozzi et al., 2011). Most important, and exemplifying the value of simplified model systems, the notion introduced here that microbe-derived “natural” metabolites can have a significant impact on the efficacy and toxicity of drugs is relevant on its own, because even the most detailed studies to date base the screens for microbial activities modulating drug efficacy or toxicity on biochemical searches for microbe-derived drug derivatives (degradation products or modified versions of the administered drug)(Zimmermann et al., 2019). Our work reveals a limitation of these drug-derivative screens, as they would miss microbiota activities (i.e. conversion of dietary serine into 5,10-mTHF) capable of, for example, transforming a non-lethal dose of FUdR into a lethal one.

Notwithstanding, the most surprising finding from this work is that dietary serine also alters, and in cases reverses, the role that host pathways play in the response to FUdR. Examples include RNA modification (*pus-1*) and autophagy (*bec-1*, *lgg-1*, *lgg-2*, and *vps-34*) executing death in the Lth-FUdR condition and protecting from death in the SE-FUdR condition. Furthermore, even for genes playing similar roles in both conditions, the underlying mechanisms may be distinct. For instance, *ung-1* is the only gene with a suppressor phenotype in both conditions. Nevertheless, based on the mitochondrial DNA results, it is likely that UNG-1's toxic role is due to a futile cycle of removal and reincorporation of fluorouracil in the mitochondrial DNA of FUdR-treated animals. However, in the SE-FUdR condition, mitochondrial DNA is not depleted and fluororibonucleotide toxicity is not the main mechanism of *E. coli*-driven toxicity. Instead, the combination of low levels of dTTP and relative high levels of dUTP and FdUTP would favor the incorporation of fluorinated and non-fluorinated uracils in genomic DNA as previously reported (Seiple et al., 2006; Van Triest et al., 2000). Hence, it is likely that in the SE-FUdR condition, UNG-1 is toxic because it enters a futile cycle of removal and reincorporation of uracil into the genomic DNA. Altogether, even when a surface-level interpretation of the outcome (100% embryonic lethality) would lead one to believe that the same mechanisms underlie death in these two conditions - dead embryos look grossly identical, worms and bacteria are isogenic, and the drug is the same - the underlying mechanisms in the microbe and the host in the presence or absence of dietary supplementation with serine are distinct to the point that the same molecular players have opposite roles (Fig. 5.16 i). Although our

study identifies these striking sub-phenotypic distinctions, it leaves many questions unanswered. Future studies would be necessary to fully dissect the underlying death mechanisms in both the Lth-FUdR and SE-FUdR conditions. This will likely be a challenging endeavor, since the mechanisms by which cells die of thymidine-less death have remained unknown for decades (Khodursky et al., 2015; Van Triest et al., 2000). Nevertheless, the understanding that distinct mechanisms can underlie the same treatment outcomes should guide future research; in particular, it should encourage limiting the use of correlative studies for translational purposes.

Humans host more than 1,500 species in the gut, and the composition varies between and within individuals (Almeida et al., 2019). Each of these microbes can distinctly metabolize dietary components and drugs. The dietary-nutrient and drug derivatives from each microbe can be further metabolized or alter the physiology of other microbes and the host, building chains of events alternatively or simultaneously triggered by dietary, drug, microbe and host metabolites, byproducts, and signaling molecules. Hence, we can speculate that the complexity of drug-microbe-host co-metabolism *in vivo* is astronomical. Therefore, the complexity of the simplified 4-way interactions presented here highlight both the extensive need for mechanistic studies, and the challenges we face to realize the full therapeutic potential of the microbiota.

5.6 Tables

Table 5. 1

List of *E. coli* genes screened from the Keio *E. coli* knock-out library.

Gene name	B number	Gene name	B number	Gene name	B number
<i>alsA</i>	b4087	<i>mrcB</i>	b0149	<i>sdaA</i>	b1814
<i>alsB</i>	b4088	<i>mutM</i>	b3635	<i>sdaB</i>	b2797
<i>alsC</i>	b4086	<i>nadC</i>	b0109	<i>sdaC</i>	b2796
<i>aphA</i>	b4055	<i>ndk</i>	b2518	<i>serA</i>	b2913
<i>apt</i>	b0469	<i>nei</i>	b0714	<i>serB</i>	b4388
<i>cdd</i>	b2143	<i>nlpD</i>	b2742	<i>serC</i>	b0907
<i>cmk</i>	b0910	<i>nrdD</i>	b4238	<i>solA</i>	b1059
<i>codA</i>	b0337	<i>nth</i>	b1633	<i>sstT</i>	b3089
<i>codB</i>	b0336	<i>nupC</i>	b2393	<i>surE</i>	b2744
<i>cpdA</i>	b3032	<i>nupG</i>	b2964	<i>tdcC</i>	b3116
<i>cpdB</i>	b4213	<i>ompC</i>	b2215	<i>tdcG</i>	b4471
<i>crp</i>	b3357	<i>ompF</i>	b0929	<i>tdk</i>	b1238
<i>cyaA</i>	b3806	<i>ompN</i>	b1377	<i>thiD</i>	b2103
<i>cycA</i>	b4208	<i>pabA</i>	b3360	<i>thiE</i>	b3993
<i>cysE</i>	b3607	<i>pabB</i>	b1812	<i>thyA</i>	b2827
<i>damX</i>	b3388	<i>pabC</i>	b1096	<i>tnaA</i>	b3708
<i>dcd</i>	b2065	<i>pdxA</i>	b0052	<i>trpA</i>	b1260
<i>dedD</i>	b2314	<i>pdxH</i>	b1638	<i>trpB</i>	b1261
<i>deoA</i>	b4382	<i>pdxJ</i>	b2564	<i>trpD</i>	b1263
<i>deoB</i>	b4383	<i>pdxK</i>	b2418	<i>tsx</i>	b0411
<i>deoD</i>	b4384	<i>pdxY</i>	b1636	<i>udk</i>	b2066
<i>dksA</i>	b0145	<i>pepA</i>	b4260	<i>udp</i>	b3831
<i>dosP</i>	b1489	<i>pepB</i>	b2523	<i>ugpQ</i>	b3449
<i>entF</i>	b0586	<i>pepD</i>	b0237	<i>upp</i>	b2498

Gene name	B number	Gene name	B number	Gene name	B number
<i>fis</i>	b3261	<i>pepN</i>	b0932	<i>uraA</i>	b2497
<i>folB</i>	b3058	<i>phnN</i>	b4094	<i>ushA</i>	b0480
<i>folM</i>	b1606	<i>phoB</i>	b0399	<i>xapA</i>	b2407
<i>folP</i>	b3177	<i>phoE</i>	b0241	<i>xapB</i>	b2406
<i>fruR</i>	b0080	<i>pncB</i>	b0931	<i>yaaJ</i>	b0007
<i>gcvH</i>	b2904	<i>prkB</i>	b3355	<i>ybiV</i>	b0822
<i>gcvP</i>	b2903	<i>purD</i>	b4005	<i>ybjI</i>	b0844
<i>gcvT</i>	b2905	<i>purF</i>	b2312	<i>yccR</i>	b0959
<i>glpQ</i>	b2239	<i>purH</i>	b4006	<i>ycdG</i>	b1006
<i>glyA</i>	b2551	<i>purN</i>	b2500	<i>ydfG</i>	b1539
<i>glyS</i>	b3559	<i>purR</i>	b1658	<i>yeaV</i>	b1801
<i>gpt</i>	b0238	<i>purT</i>	b1849	<i>yeiA</i>	b2147
<i>gshB</i>	b2947	<i>purU</i>	b1232	<i>yeiT</i>	b2146
<i>hisG</i>	b2019	<i>pyrE</i>	b3642	<i>yfaO</i>	b2251
<i>hpt</i>	b0125	<i>pyrF</i>	b1281	<i>yfbR</i>	b2291
<i>ihfA</i>	b1712	<i>rbsA</i>	b3749	<i>ygfA</i>	b2912
<i>ihfB</i>	b0912	<i>rbsB</i>	b3751	<i>yggC</i>	b2928
<i>kbl</i>	b3617	<i>rbsC</i>	b3750	<i>ygjF</i>	b3068
<i>lpd</i>	b0116	<i>rbsD</i>	b3748	<i>yhfW</i>	b3380
<i>lpp</i>	b1677	<i>rbsK</i>	b3752	<i>yigB</i>	b3812
<i>ltaE</i>	b0870	<i>recX</i>	b2698	<i>yjfF</i>	b4231
<i>mazG</i>	b2781	<i>rfe</i>	b3784	<i>yjjG</i>	b4374
<i>metF</i>	b3941	<i>rihA</i>	b0651	<i>ytfQ</i>	b4227
<i>metH</i>	b4019	<i>rihB</i>	b2162	<i>ytfR</i>	b4485
<i>mrcA</i>	b3396	<i>rihC</i>	b0030	<i>ytfT</i>	b4230

Table 5.1 List of *E. coli* genes screened from the Keio *E. coli* knock-out library.

List is comprised of genes found by iJO1366 model to be associated 1-2 steps away from homologs of mammalian fluoropyrimidine metabolic pathways. In total 147 loss of function mutants in the background *E. coli* strain BW25113 were screened.

Table 5. 2

Hits of Keio screen for mediators of SE-FUdR toxicity

Gene	Keio	Biological process (EC)	Verified
<i>codA</i>	b0337	Deamination of cytosine to uracil (3.5.4.1)	NT
<i>crp</i>	b3357	cAMP receptor protein, regulates transcription	√
<i>cysE</i>	b3607	Serine synthesis (2.3.1.30)	NT
<i>dcd</i>	b2065	dUTP synthesis from dCTP (3.5.4.13)	NT
<i>deoA</i>	b4382	thymine/uracil synthesis from	√
<i>deoB</i>	b4383	PRPP synthesis (5.4.2.7)	NT
<i>dksA</i>	b0145	Regulates rRNA transcription	NT
<i>dosP</i>	b1489	c-di-GMP hydrolysis (3.1.4.52)	NT
<i>folB</i>	b3058	THF synthesis (4.1.2.25)	√
<i>folP</i>	b3177	THF synthesis (2.5.1.15)	√
<i>gcvP</i>	b2903	10fTHF synthesis (1.4.4.2)	√
<i>gcvT</i>	b2905	10fTHF synthesis (2.1.2.10)	√
<i>lpd</i>	b0116	10fTHF synthesis (1.8.1.4)	√
<i>metF</i>	b3941	5,10-methylene-THF metabolism (1.5.1.20)	X
<i>nlpD</i>	b2742	Divisome associated factor	NT
<i>pdxA</i>	b0052	Pyridoxal-5-phosphate synthesis	√
<i>pdxH</i>	b1638	Pyridoxal-5-phosphate synthesis and salvage	√
<i>pdxJ</i>	b2564	Pyridoxal-5-phosphate synthesis (2.6.99.2)	√
<i>pepD</i>	b0237	Muropeptide degradation (3.4.13.18)	NT
<i>phoE</i>	b0241	Outer membrane phosphate transport	NT
<i>rbsK</i>	b3752	Ribose degradation (2.7.1.15)	NT
<i>serC</i>	b0907	Serine synthesis (2.6.1.52)	√
<i>upp</i>	b2498	UMP salvage 2.4.2.9	X
<i>yjjG</i>	b4374	Pyrimidine nucleotidase (3.1.3.5)	X

Gene	Keio	Biological process (EC)	Verified
<i>ndk</i>	b2518	UTP/CTP synthesis (2.7.4.6)	√
<i>pabC</i>	b1096	PABA/tetrahydrofolate synthesis (4.1.3.38)	NT
<i>sdaB</i>	b2797	Serine degradation	NT
<i>udk</i>	b2066	UMP/CMP salvage (2.7.1.48)	X
<i>udp</i>	b3831	Uracil salvage (2.4.2.3)	X

Table 5.2 Hits of Keio screen for mediators of SE-FUdR toxicity.

Primary hits are presented as: blue = suppressor of toxicity; orange= enhancer of toxicity; and white= no different from WT control. Light blue or orange, represents phenotype observed in only 1-2 of 3 screen repeats. Hits belonging to overrepresented metabolic pathways were retested in 6cm NGM plates and quantitated for % hatchlings in sublethal FUdR (unless otherwise stated 0.25 μ g/mL) \pm serine (1.5mg/mL), and the results are presented in main figures. Primary screen hits that were not retested in 6cm plates are depicted as NRT. Retested and verified hits (colored cells) and non-hits (white cells) are marked as “√”, and retested but not validated primary hits (phenotype did not repeat) are marked as “X”.

Table 5. 3

List of *C. elegans* genes tested in the EORB1 Lth-FUdR, and SE-FUdR RNAi screens.

<i>Gene name</i>	Sequence ID	<i>Gene name</i>	Sequence ID	<i>Gene name</i>	Sequence ID
<i>B0001.4</i>	B0001.4	<i>glna-3</i>	F30F8.2	<i>acs-3</i>	T08B1.6
<i>gna-1</i>	B0024.12	<i>fasn-1</i>	F32H2.5	<i>ech-1.2</i>	T08B2.7
<i>vps-34</i>	B0025.1	<i>nhr-8</i>	F33D4.1	<i>fars-1</i>	T08B2.9
<i>B0205.6</i>	B0205.6	<i>gst-38</i>	F35E8.8	<i>T08D2.2</i>	T08D2.2
<i>let-363</i>	B0261.2	<i>mlcd-1</i>	F35G12.1	<i>acd-10</i>	T08G2.3
<i>B0272.3</i>	B0272.3	<i>alh-3</i>	F36H1.6	<i>T09B4.8</i>	T09B4.8
<i>B0272.4</i>	B0272.4	<i>F37B12.2</i>	F37B12.2	<i>T09B9.3</i>	T09B9.3
<i>rpia-1</i>	B0280.3	<i>acs-4</i>	F37C12.7	<i>gars-1</i>	T10F2.1
<i>ckb-3</i>	B0285.10	<i>gst-25</i>	F37F2.3	<i>T10F2.2</i>	T10F2.2
<i>ckb-1</i>	B0285.8	<i>pha-4</i>	F38A6.1	<i>T12B3.3</i>	T12B3.3
<i>ckb-2</i>	B0285.9	<i>F38B6.4</i>	F38B6.4	<i>agxt-1</i>	T14D7.1
<i>B0303.3</i>	B0303.3	<i>F40F8.1</i>	F40F8.1	<i>T19B4.3</i>	T19B4.3
<i>psd-1</i>	B0361.5	<i>F41E6.5</i>	F41E6.5	<i>skn-1</i>	T19E7.2
<i>acly-2</i>	B0365.1	<i>tatn-1</i>	F42D1.2	<i>bec-1</i>	T19E7.3
<i>B0395.3</i>	B0395.3	<i>moc-3</i>	F42G8.6	<i>T19H12.6</i>	T19H12.6
<i>cat-2</i>	B0432.5	<i>ech-3</i>	F43H9.1	<i>oga-1</i>	T20B5.3
<i>B0478.3</i>	B0478.3	<i>sptl-2</i>	F43H9.2	<i>cts-1</i>	T20G5.2
<i>mtrr-1</i>	C01G6.6	<i>ppt-1</i>	F44C4.5	<i>T21C9.6</i>	T21C9.6
<i>rnr-2</i>	C03C10.3	<i>exo-1</i>	F45G2.3	<i>T21D12.7</i>	T21D12.7
<i>C03H5.4</i>	C03H5.4	<i>ipla-2</i>	F47A4.5	<i>T22G5.1</i>	T22G5.1
<i>pdhb-1</i>	C04C3.3	<i>acs-16</i>	F47G6.2	<i>sptl-3</i>	T22G5.5
<i>pld-1</i>	C04G6.3	<i>F52A8.5</i>	F52A8.5	<i>alh-13</i>	T22H6.2
<i>C05C10.3</i>	C05C10.3	<i>cep-1</i>	F52B5.5	<i>gna-2</i>	T23G11.2

<i>Gene name</i>	Sequence ID	<i>Gene name</i>	Sequence ID	<i>Gene name</i>	Sequence ID
<i>mel-32</i>	C05D11.11	<i>aat-3</i>	F52H2.2	<i>rnr-1</i>	T23G5.1
<i>basl-1</i>	C05D2.3	<i>F52H2.4</i>	F52H2.4	<i>T24C12.3</i>	T24C12.3
<i>bas-1</i>	C05D2.4	<i>acaa-2</i>	F53A2.7	<i>T25B9.1</i>	T25B9.1
<i>icl-1</i>	C05E4.9	<i>F53C11.3</i>	F53C11.3	<i>acdh-7</i>	T25G12.5
<i>sucl-1</i>	C05G5.4	<i>sms-2</i>	F53H8.4	<i>jhdm-1</i>	T26A5.5
<i>mthf-1</i>	C06A8.1	<i>cbs-2</i>	F54A3.4	<i>ckc-1</i>	T27A10.3
<i>trxr-1</i>	C06G3.7	<i>F54C8.1</i>	F54C8.1	<i>T27A3.6</i>	T27A3.6
<i>folt-1</i>	C06H2.4	<i>pcs-1</i>	F54D5.1	<i>gst-23</i>	T28A11.11
<i>C07E3.9</i>	C07E3.9	<i>alh-1</i>	F54D8.3	<i>mlh-1</i>	T28A8.7
<i>glna-1</i>	C09F9.3	<i>gpx-8</i>	F55A3.5	<i>T28F3.5</i>	T28F3.5
<i>gpx-5</i>	C11E4.1	<i>F55G1.5</i>	F55G1.5	<i>mys-1</i>	VC5.4
<i>gpx-3</i>	C11E4.2	<i>alh-6</i>	F56D12.1	<i>cpt-6</i>	W01A11.5
<i>cbl-1</i>	C12C8.2	<i>cdo-1</i>	F56F10.3	<i>decr-1.2</i>	W01C9.4
<i>glt-1</i>	C12D12.2	<i>pept-3</i>	F56F4.5	<i>aars-1</i>	W02B12.6
<i>got-2.2</i>	C14F11.1	<i>elo-1</i>	F56H11.4	<i>ndx-2</i>	W02G9.1
<i>C15B12.1</i>	C15B12.1	<i>F58A6.1</i>	F58A6.1	<i>sars-2</i>	W03B1.4
<i>kynu-1</i>	C15H9.7	<i>acox-6</i>	F58F9.7	<i>W03D8.8</i>	W03D8.8
<i>cysl-1</i>	C17G1.7	<i>F59A7.7</i>	F59A7.7	<i>glt-7</i>	W03G1.1
<i>sptl-1</i>	C23H3.4	<i>cysl-4</i>	F59A7.9	<i>fat-5</i>	W06D12.3
<i>qns-1</i>	C24F3.4	<i>F59F4.1</i>	F59F4.1	<i>pus-1</i>	W06H3.2
<i>dpyd-1</i>	C25F6.3	<i>frh-1</i>	F59G1.7	<i>ctps-1</i>	W06H3.3
<i>C27A7.1</i>	C27A7.1	<i>tat-2</i>	H06H21.10	<i>ipla-3</i>	W07A8.2
<i>C27A7.3</i>	C27A7.3	<i>pms-2</i>	H12C20.2	<i>W07E11.1</i>	W07E11.1
<i>cka-1</i>	C28D4.2	<i>H14N18.4</i>	H14N18.4	<i>W07E6.3</i>	W07E6.3
<i>gln-6</i>	C28D4.3	<i>mboa-2</i>	H19N07.4	<i>lap-2</i>	W07G4.4
<i>gsto-1</i>	C29E4.7	<i>sms-1</i>	H21P03.3	<i>ace-1</i>	W09B12.1
<i>C29F7.3</i>	C29F7.3	<i>H24K24.3</i>	H24K24.3	<i>pod-2</i>	W09B6.1

<i>Gene name</i>	Sequence ID	<i>Gene name</i>	Sequence ID	<i>Gene name</i>	Sequence ID
<i>C30H6.7</i>	C30H6.7	<i>msh-2</i>	H26D21.2	<i>gln-3</i>	Y105C5B.28
<i>C31H1.5</i>	C31H1.5	<i>K01C8.1</i>	K01C8.1	<i>ech-7</i>	Y105E8A.4
<i>C31H5.6</i>	C31H5.6	<i>tdc-1</i>	K01C8.3	<i>hpvt-1</i>	Y105E8B.5
<i>lgg-1/2</i>	C32D5.9/ZK593.6	<i>bcat-1</i>	K02A4.1	<i>hpo-20</i>	Y110A2AL.12
<i>C32F10.8</i>	C32F10.8	<i>K02D7.1</i>	K02D7.1	<i>tyms-1</i>	Y110A7A.4
<i>mys-4</i>	C34B7.4	<i>ahcy-1</i>	K02F2.2	<i>Y17G7B.3</i>	Y17G7B.3
<i>acs-19</i>	C36A4.9	<i>K02F3.2</i>	K02F3.2	<i>sms-3</i>	Y22D7AL.8
<i>dhfr-1</i>	C36B1.7	<i>mys-2</i>	K03D10.3	<i>cars-1</i>	Y23H5A.7
<i>hsp-6</i>	C37H5.8	<i>gln-2</i>	K03H1.1	<i>unc-25</i>	Y37D8A.23
<i>C44B7.7</i>	C44B7.7	<i>gta-1</i>	K04D7.3	<i>prdx-6</i>	Y38C1AA.11
<i>got-2.1</i>	C44E4.3	<i>alh-2</i>	K04F1.15	<i>Y38F2AR.12</i>	Y38F2AR.12
<i>gln-1</i>	C45B2.5	<i>K05B2.4</i>	K05B2.4	<i>Y39B6A.3</i>	Y39B6A.3
<i>gsr-1</i>	C46F11.2	<i>acd-8</i>	K05F1.3	<i>Y39E4A.3</i>	Y39E4A.3
<i>acs-17</i>	C46F4.2	<i>dao-3</i>	K07E3.3	<i>thk-1</i>	Y43C5A.5
<i>C47B2.2</i>	C47B2.2	<i>K07E3.4</i>	K07E3.4	<i>Y43F4B.5</i>	Y43F4B.5
<i>tars-1</i>	C47D12.6	<i>fmo-2</i>	K08C7.5	<i>Y44A6D.5</i>	Y44A6D.5
<i>sars-1</i>	C47E12.1	<i>dnj-15</i>	K08D10.2	<i>ace-2</i>	Y44E3A.2
<i>acox-5</i>	C48B4.1	<i>gst-3</i>	K08F4.11	<i>Y45F10D.4</i>	Y45F10D.4
<i>cho-1</i>	C48D1.3	<i>gst-2</i>	K08F4.6	<i>gst-10</i>	Y45G12C.2
<i>C49F5.5</i>	C49F5.5	<i>gst-4</i>	K08F4.7	<i>msh-6</i>	Y47G6A.11
<i>cka-2</i>	C52B9.1	<i>pah-1</i>	K08F8.4	<i>Y47G6A.22</i>	Y47G6A.22
<i>C53D5.5</i>	C53D5.5	<i>uda-1</i>	K08H10.4	<i>pcaf-1</i>	Y47G6A.6
<i>atic-1</i>	C55F2.1	<i>ent-2</i>	K09A9.3	<i>men-1</i>	Y48B6A.12
<i>acly-1</i>	D1005.1	<i>K09H11.1</i>	K09H11.1	<i>ace-4</i>	Y48B6A.7
<i>acs-22</i>	D1009.1	<i>nhr-49</i>	K10C3.6	<i>ace-3</i>	Y48B6A.8
<i>gcsh-1</i>	D1025.2	<i>K10D2.7</i>	K10D2.7	<i>Y48G10A.1</i>	Y48G10A.1
<i>pyc-1</i>	D2023.2	<i>cysl-2</i>	K10H10.2	<i>cept-2</i>	Y49A3A.1

<i>Gene name</i>	Sequence ID	<i>Gene name</i>	Sequence ID	<i>Gene name</i>	Sequence ID
<i>mpst-1</i>	D2023.5	<i>sodh-1</i>	K12G11.3	<i>tat-1</i>	Y49E10.11
<i>gstk-2</i>	D2024.7	<i>sodh-2</i>	K12G11.4	<i>pstk-1</i>	Y49E10.22
<i>pyr-1</i>	D2085.1	<i>dld-1</i>	LLC1.3	Y51H7C.9	Y51H7C.j
<i>gbh-1</i>	D2089.5	<i>snf-6</i>	M01G5.5	<i>hsf-1</i>	Y53C10A.12
<i>glna-2</i>	DH11.1	<i>asns-2</i>	M02D8.4	<i>ctl-2</i>	Y54G11A.5
E01A2.1	E01A2.1	<i>dhs-28</i>	M03A8.1	<i>ctl-1</i>	Y54G11A.6
<i>maoc-1</i>	E04F6.3	<i>hat-1</i>	M03C11.4	<i>nprr-1</i>	Y54G2A.17
acd-12	E04F6.5	M05B5.4	M05B5.4	<i>ung-1</i>	Y56A3A.29
<i>ndx-6</i>	EEED8.8	<i>gbh-2</i>	M05D6.7	<i>daf-22</i>	Y57A10C.6
<i>alh-9</i>	F01F1.6	<i>gmps-1</i>	M106.4	<i>unc-51</i>	Y60A3A.1
<i>tkt-1</i>	F01G10.1	<i>gss-1</i>	M176.2	<i>algn-7</i>	Y60A3A.14
<i>ech-8</i>	F01G10.2	<i>atg-7</i>	M7.5	Y62E10A.13	Y62E10A.13
<i>ech-9</i>	F01G10.3	R02D3.1	R02D3.1	<i>acs-13</i>	Y65B4BL.5
<i>gfat-1</i>	F07A11.2	<i>metr-1</i>	R03D7.1	<i>daao-1</i>	Y69A2AR.5
F07A11.5	F07A11.5	<i>gst-5</i>	R03D7.6	<i>alh-12</i>	Y69F12A.2
<i>aat-2</i>	F07C3.7	<i>gpx-7</i>	R03G5.5	<i>fard-1</i>	Y71H10A.2
<i>acox-1</i>	F08A8.1	R05F9.6	R05F9.6	Y71H10B.1	Y71H10B.1
<i>acox-2</i>	F08A8.2	<i>plc-4</i>	R05G6.8	Y73B6BL.29	Y73B6BL.29
<i>acox-3</i>	F08A8.3	<i>gpx-2</i>	R05H10.5	<i>plc-2</i>	Y75B12B.6
<i>acox-4</i>	F08A8.4	<i>ech-4</i>	R06F6.9	<i>acs-5</i>	Y76A2B.3
<i>apy-1</i>	F08C6.6	<i>gst-36</i>	R07B1.4	Y7A9A.1	Y7A9A.1
F08F3.4	F08F3.4	<i>acs-15</i>	R07C3.4	<i>gpx-4</i>	Y94H6A.4
F09E5.3	F09E5.3	<i>mig-23</i>	R07E4.4	ZC155.4	ZC155.4
F09G2.8	F09G2.8	<i>cpt-2</i>	R07H5.2	<i>cbs-1</i>	ZC373.1
F10F2.2	F10F2.2	<i>cysl-3</i>	R08E5.2	<i>hap-1</i>	ZC395.7
<i>acs-14</i>	F11A3.1	<i>exo-3</i>	R09B3.1	<i>cha-1</i>	ZC416.8
<i>gst-8</i>	F11G11.1	<i>hacd-1</i>	R09B5.6	<i>ears-1</i>	ZC434.5

<i>Gene name</i>	Sequence ID	<i>Gene name</i>	Sequence ID	<i>Gene name</i>	Sequence ID
<i>gst-7</i>	F11G11.2	<i>acs-18</i>	R09E10.3	<i>pspy-1</i>	ZC506.3
<i>gst-6</i>	F11G11.3	<i>R102.4</i>	R102.4	<i>nit-1</i>	ZK1058.6
<i>gst-44</i>	F13A7.10	<i>gst-1</i>	R107.7	<i>cth-2</i>	ZK1127.10
<i>ldh-1</i>	F13D12.2	<i>cbp-1</i>	R10E11.1	<i>tph-1</i>	ZK1290.2
<i>alh-8</i>	F13D12.4	<i>R12C12.1</i>	R12C12.1	<i>gstk-1</i>	ZK1320.1
<i>F13H8.9</i>	F13H8.9	<i>R12E2.11</i>	R12E2.11	<i>lap-1</i>	ZK353.6
<i>F19B6.1</i>	F19B6.1	<i>daf-16</i>	R13H8.1	<i>eat-4</i>	ZK512.6
<i>F19G12.2</i>	F19G12.2	<i>R151.2</i>	R151.2	<i>ZK563.7</i>	ZK563.7
<i>F20D1.9</i>	F20D1.9	<i>mboa-6</i>	R155.1	<i>pyk-2</i>	ZK593.1
<i>gfat-2</i>	F22B3.4	<i>dtmk-1</i>	R53.2	<i>ZK643.2</i>	ZK643.2
<i>fars-3</i>	F22B5.9	<i>T01B11.2</i>	T01B11.2	<i>upp-1</i>	ZK783.2
<i>cth-1</i>	F22B8.6	<i>aak-2</i>	T01C1.8	<i>ent-1</i>	ZK809.4
<i>ckb-4</i>	F22F7.5	<i>got-1.2</i>	T01C8.5	<i>ZK822.5</i>	ZK822.5
<i>dlat-1</i>	F23B12.5	<i>T02G5.4</i>	T02G5.4	<i>hdl-1</i>	ZK829.2
<i>gcst-1</i>	F25B4.1	<i>T02G5.7</i>	T02G5.7	<i>gdh-1</i>	ZK829.4
<i>hmgs-1</i>	F25B4.6	<i>kat-1</i>	T02G5.8	<i>elpc-3</i>	ZK863.3
<i>F25B5.3</i>	F25B5.3	<i>kars-1</i>	T02G5.9	<i>nit-1</i>	ZK892.2
<i>F25B5.6</i>	F25B5.6	<i>T03D8.6</i>	T03D8.6		
<i>F25E2.3</i>	F25E2.3	<i>ppat-1</i>	T04A8.5		
<i>asns-1</i>	F25G6.6	<i>decr-1.3</i>	T05C12.3		
<i>pyk-1</i>	F25H5.3	<i>T05E7.1</i>	T05E7.1		
<i>gln-5</i>	F26D10.10	<i>ech-6</i>	T05G5.6		
<i>gpx-1</i>	F26E4.12	<i>apn-1</i>	T05H10.2		
<i>F26H9.5</i>	F26H9.5	<i>pdha-1</i>	T05H10.6		
<i>aat-1</i>	F27C8.1	<i>alh-4</i>	T05H4.13		
<i>acs-20</i>	F28D1.9	<i>atl-1</i>	T06E4.3		
<i>acs-2</i>	F28F8.2	<i>umps-1</i>	T07C4.1		

<i>Gene name</i>	Sequence ID	<i>Gene name</i>	Sequence ID	<i>Gene name</i>	Sequence ID
<i>aars-2</i>	F28H1.3	<i>T07F10.1</i>	T07F10.1		
<i>nkat-1</i>	F28H6.3	<i>alh-5</i>	T08B1.3		

Table 5.3. List of *C. elegans* genes tested in the EORB1 Lth-FUdR, and SE-FUdR RNAi screens.

387 gene knockdowns were tested in duplicate or triplicate in Lth-FUdR and SE-FUdR.

Table 5. 4

Symbol	Biological process	Lth-	SE-
<i>vector</i>			
<i>F19G12.2</i>	DNA damage response	NT	NT
<i>msh-6</i>	mismatch repair of DNA (previously shown in	√	√
<i>ung-1</i>	base-excision repair of DNA	√	√
<i>cdd-1</i>	cytidine/deoxycytidine conversion to	NT	NT
<i>cdd-2</i>	cytidine/deoxycytidine conversion to	NT	NT
<i>H24K24.3</i>	alcohol dehydrogenase providing formate for	NT	NT
<i>K02D7.1</i>	purine nucleoside phosphorylase	NT	NT
<i>pus-1</i>	Catalyzes pseudouridylation. Toxic covalent complex	√	√
<i>tym-1</i>	dTMP synthesis	X	X
<i>aak-2</i>	AMPK subunit	√	√
<i>atg-7</i>	Autophagy (previously shown in Sengupta et al.,	X	√
<i>bec-1</i>	Autophagy (previously shown in Sengupta et al.,	√	√
<i>lgg-1/2</i>	Autophagy	√	√
<i>vps-34</i>	Autophagy	√	√
<i>acly-1</i>	conversion of acetate and CoA into acetyl-CoA	X	√
<i>C30H6.7</i>	conversion of pyruvate to acetyl-CoA (lipogenesis)	X	√
<i>T28F3.5</i>	conversion of acetyl-CoA to malonyl-CoA	√	√
<i>gbh-1</i>	carnitine synthesis (lipid transport into mitochondria)	X	√
<i>ipla-2</i>	similar to phospholipase A2	√	√
<i>C03H5.4</i>	similar to phospholipase A2	√	√
<i>pld-1</i>	similar to phospholipase D1	√	√
<i>T09B9.3</i>	glycerophosphodiesterase	√	√
<i>aat-2</i>	amino acid transport	NT	NT
<i>aat-3</i>	amino acid transport	NT	NT
<i>C15B12.1</i>	lysine catabolism	NT	NT
<i>cysl-1</i>	cysteine synthesis	NT	NT

Symbol	Biological process	Lth-	SE-
<i>cysl-4</i>	cysteine synthesis	NT	NT
<i>got-2.2</i>	aspartate catabolism	NT	NT
<i>pstk-1</i>	seryl-tRNA phosphorylation	NT	NT
<i>snf-6</i>	amino acid transport	NT	NT
<i>fmo-2</i>	Detox response	NT	NT
<i>daf-16</i>	Detox transcription factor	NT	NT
<i>C49F5.5</i>	histone acetylation	NT	NT
<i>pcs-1</i>	Detox response	NT	NT
<i>skn-1</i>	Detox transcription factor	NT	NT
<i>mpst-1</i>	iron-sulfur complex formation	NT	NT
<i>Y45F10D.4</i>	iron homeostasis	NT	NT
<i>ctl-2</i>	oxidative stress response	NT	NT
<i>gst-3</i>	oxidative stress response	NT	NT
<i>gpx-8</i>	oxidative stress response	NT	NT
<i>gpx-5</i>	oxidative stress response	NT	NT

Table 5.4 *C. elegans* suppressors and enhancers of Lth-FUdR and SE-FUdR toxicity

Primary RNAi hits are presented as: blue = suppressor of toxicity; orange= enhancer of toxicity; and white= no different from WT control. Light blue or orange, represents phenotype observed in only 1-2 of 3 screen repeats. Hits belonging to overrepresented metabolic pathways were retested in 6cm NGM plates and quantitated for % hatchlings in sublethal FUdR (unless otherwise stated 1µg/mL) ± serine (1.5mg/mL), and the results are presented in main figures. Primary screen hits that were not retested in 6cm plates are depicted as NRT. Retested and

verified hits (colored cells) and non-hits (white cells) are marked as “√”, and retested but not validated primary hits (phenotype did not repeat) are marked as “X”.

CHAPTER VI: Conclusion

Summary of this dissertation

In this dissertation, I introduce the different methods and approaches to study the complex chronic disease (CCD) that has the highest incidence rate – obesity, and I describe a study on the efficacy of the treatment for one of the deadliest CCD – cancer, respectively, using *C. elegans* as the model system.

In **Chapter II**, I developed the experimental and post-experimental data analysis pipelines to perform high throughput, high content, image-based reverse genetics screen for fat regulators by taking advantage of the model system *C. elegans*, as the first and the only *in vivo* model system that enables fast and simple genome-wide RNAi screen through feeding. This method is the fundamental approach that was implemented in **Chapter II** and **Chapter IV**.

In **Chapter III**, I established and characterized the first fructose-induced obesity *C. elegans* model. I found that the worms fed high fructose diet (HFrD) not only carry the high body fat content phenotype, but exhibit many healthspan deficiencies, including reduction of lifespan, impaired locomotion, and indications of neurodegenerative diseases. Using this model, I conducted an RNAi screen on 293 *C. elegans* orthologs of human genes that were associated with obesity from three previously published datasets, and causally linked 17 genes to obesity *in vivo*. Within these 17 genes, 4 genes promote obesity and fructose-induced obesity, while 13 genes protect against obesity. Further, I found that depletion of

each of the 4 genes that promote obesity improves the *C. elegans* lifespan, suggesting the potential targets for developing intervention against obesity.

In **Chapter IV**, I described the approaches to understand the mechanism of obesity systematically. Using the single-cell RNAseq datasets from *C. elegans* fructose-induced obesity (described in Chapter III) and insulin resistance obesity model (described in a previous publication(O'Rourke et al., 2009b)), our team and our collaborators are capable of developing the first obesity metabolic computation model with tissue level resolution. To refine and reconcile this model, I conducted an RNAi screen on 1372 *C. elegans* predicted metabolic genes in both the fructose-induced obesity model and the insulin resistance obesity model. I identified 46 genes that promote obesity and 46 genes that inhibit obesity under the regular diet (RD), 32 genes that promote obesity under HFrD, and 33 genes that promote obesity under insulin resistance condition. The result of this screen is served as a great hypothesis generator to describe the metabolic pathways that contribute to the development of obesity.

In **Chapter V**, I focus on chemotherapeutic drug efficacy. Using the *C. elegans-E. coli* host-microbiome system, I described a host-microbiome-diet-drug 4-way interaction that alters the efficacy of one of the most commonly used GI cancer drug, 5'-fluorodeoxyuridine (FUdR). I characterized that dietary serine enhances FUdR efficacy through *E. coli* one-carbon metabolism and the inhibition of thymidine synthase ThyA, and ultimately leads to thymidine starvation in the host

C. elegans. In contrast, dietary thymidine enhances FUdR efficacy by promoting the bioconversion of FUdR to its active form FUMP (the basal FUdR toxicity pathway), through enhancing the *E. coli* pyrimidine salvage pathway. Most strikingly, although both dietary serine and thymidine enhance FUdR efficacy through modulating microbiome (*E. coli*)'s metabolism, the host (*C. elegans*) response to these two different types of enhancement of efficacy is opposite in mechanism. The basal FUdR toxicity pathway from *E. coli* damages the *C. elegans* mitochondria DNA and RNA, resulting in activation of mitochondria lipid signals to autophagy machinery, and hyperactivates the *C. elegans* autophagy causing autophagic cell death. While serine enhanced FUdR toxicity suppresses the *C. elegans* autophagy that protects against cell death.

Simplicity is the ultimate sophistication.

C. elegans, a 1mm long multicellular organism consist of only ~1000 cells, is one of the simplest animal model systems to study biological questions (Corsi et al., 2015). CCDs, the most deadly group of diseases that are responsible for ~80% of the death in the US in the past decade (Murphy et al., 2021), are the most complicated questions in the biomedical studies. How do we use such a simple system to tackle such complicated biomedical problems? The answer is *simple*.

The procedures to inactivate a gene expression using RNAi in *C. elegans* are the simplest comparing to other *in vivo* animal models. In mammalian systems such as mice, the *in vivo* RNAi requires the generation of transgenic lines expressing

shRNA targeting the gene of interest (Premisirut et al., 2011). Such procedures are time-consuming and are not compatible with high throughput functional genomics. In non-mammalian vertebrate systems such as zebrafish and *Xenopus*, microinjection of Morpholino phosphorodiamidate antisense oligonucleotides (MOs) are usually used to inactivate target gene expression through inhibiting transcription or splicing machinery (Bedell et al., 2011; Summerton, 1999). However, there are many caveats in the use of MOs. Firstly, the injection of MOs is usually conducted in the early embryonic stages, and such an invasive procedure could be difficult and unprecise. More importantly, MOs have been shown to have strong cytotoxicity and side effects, including boosting the target gene transcription to compensate for the inhibition of translation (Heasman et al., 2001) and activating p53 to induce unexpected cell death (Robu et al., 2007). These limitations diminish the accuracy of the MOs-based experiments in studying the functions of genes. In the invertebrate systems, *Drosophila melanogaster* is the only other animal model system that enables genome-wide RNAi screen (Mohr, 2014). However, the *in vivo* RNAi screens in drosophila use the Gal4-UAS system and require making crosses to screen the phenotype in the F1 generation. This procedure takes tremendous custody in terms of stock maintenance and flies picking. Unlike all these more complicated model systems described above, *C. elegans* RNAi machinery can be simply activated by feeding the worms with *E. coli* containing the plasmids that express target dsRNA. The inactivation of the genes can be achieved at any time point during the development in one generation. Due to the fast rate of reproduction and development, the RNAi screen in *C. elegans* is

highly compatible with high throughput, large-scale approaches, and to study all the potential genes and pathways that involve in a multigenic CCD. In the human genetics studies on CCDs, the greatest challenge is to causally validate the tremendous numbers of genetic variants that have been associated with the diseases (Cano-Gamez and Trynka, 2020). It has been reported that by 2016, there were 3835 genes associated with human diseases, mostly CCDs, but only 84 genes were causally validated (Gallagher and Chen-Plotkin, 2018). With such a small number of the genes that were causally validated, it is very difficult to draw the big picture of the disease mechanisms and to search for the best druggable target for treatments. In **Chapter III**, using the *C. elegans* model, I causally linked 17 GWAS obesity candidate genes in a screen of 293 genes. Further, in **Chapter IV**, I causally linked 112 metabolic genes to obesity in a screen of 1372 metabolic genes in *C. elegans*. Together, as a proof of principle, in the studies described in this dissertation alone, I validated the causality of 1665 genes and found 129 genes promote or inhibit obesity in *C. elegans*. Although evolutionary, *C. elegans* is distant from humans, and many genes and pathways are different from those in humans, the fundamental cellular and molecular pathways are mostly conserved. Nevertheless, additional validation of the functions of these genes in more complicated models are vital. On the other hand, if a gene has conserved functions in a disease in both *C. elegans* and Humans, this gene is likely to be involved in a critical pathway for us to understand the disease mechanisms.

The human body consists of 11 organ systems and trillions of cells. Most of the CCDs are multisystem diseases caused by deficiencies in cell-cell, tissue-tissue, organ-organ communication. In obesity, for example, human adipose tissues secrete several adipokines include leptin (Zhang et al., 1994), TNF- α (Trayhurn and Wood, 2004), IL-6 (Engström et al., 2003), and growth factors (Blüher, 2016). These signals are critical in the regulation of glucose homeostasis, angiogenesis, inflammation, blood pressure, lipid metabolism, haemostasis, and appetite (Trayhurn, 2005). Disruption of these signals leads to obesity and obesity-related metabolic syndromes. Further, the function of a gene or a pathway in different cell and organ systems may be involved in different mechanisms in CCDs, and some may have opposite roles. Taking angiotensin II receptor type I (AT1) as an example, Although the diet-induced body weight gain is attenuated in the *Agtr1* global knockout mice, studies have shown that AT1 specifically in the paraventricular nucleus of the hypothalamus has a protective role against obesity (Littlejohn and Grobe, 2015). The tissue level complexity of the disease mechanisms is one of the key challenges in studying CCDs. *C. elegans* only consist of ~1000 cells but are composed of similar basic tissues as in other animals (e.g. nerve, muscle, gut, skin, etc.). Although many key cell types in some CCDs are missing (e.g. adipocytes in obesity), and some key regulatory systems (e.g. leptin in obesity) do not exist in *C. elegans*, the basic cellular and metabolic pathways are mostly conserved, and alternative cell types are often found in *C. elegans* resemble the missing cell types in human diseases (e.g. intestinal cells as major fat depots in worms, similar to adipocytes in humans). Nevertheless, such simplicity allows us to conduct tissue-

specific analysis or single-cell analysis to understand the disease mechanisms in different tissues. In **Chapter IV**, I described generating an integrative and comprehensive metabolic atlas in *C. elegans* obesity with tissue level resolution using single-cell RNA-Seq, RNAi, and tissue-specific RNAi. Such an atlas would shed light on the underappreciated tissue-specific metabolic pathways and the interactions between cells and tissues in obesity.

C. elegans is also a rising system in the studies of the microbiome (Zhang et al., 2017). The natural microbiome of *C. elegans* is composed of thousands of Operational Taxonomic Units (OTUs), demonstrating extensive diversity (Dirksen et al., 2016; Samuel et al., 2016). However, In standard laboratory conditions, as established by Dr. Sydney Brenner in the 1970s, the single bacteria species *E. coli* is served as both the food source and microbiome of *C. elegans* for easier visualization and mating of the worms (Brenner, 1974). A few strains of *E. coli* are commonly used for different purposes, includes the wild type K12 strain (Browning et al., 2013; Depuydt et al., 2013), uracil auxotroph strain OP50 (Brenner, 1974), the K12 and B hybrid strain HB101 that forms low-viscosity lawn (Avery and Shtonda, 2003; Boyer and Roulland-Dussoix, 1969; Davis et al., 1995), and the K12-derived strain HT115 (D3) for RNAi because of the disruption of the RNase III gene in this strain(Kamath et al., 2003; Rual et al., 2004). Many tools and reagents are available for both *E. coli* and *C. elegans* to establish simple *C. elegans* – *E. coli* host-microbiome disease models. On the *C. elegans* side, many human CCD models were previously established, including neurodegenerative

disease (Kuwahara et al., 2006; Lakso et al., 2003; Ved et al., 2005), cancer (Ferguson and Horvitz, 1985; Horvitz and Sulston, 1980; Seydoux et al., 1993), and obesity (described in **Chapter II, III, and IV**). While on the *E. coli* side, the current *E. coli* Keio deletion collection containing approximately 4000 mutants covering 93% of *E. coli* genes (Baba et al., 2006), and this collection can be used to screen for any host phenotypes. For example, two previous studies (García-González et al., 2017; Scott et al., 2017) and particularly my study as described in **Chapter V** on fluoropyrimidine also used the *C. elegans* – *E. coli* system and characterized the key metabolic pathways in *E. coli* that alter the drug efficacy through screens on *E. coli* Keio library. More specifically, through diet – drug – *E. coli* – *C. elegans* 4-way analysis, we characterized the complicated interactions that change fluoropyrimidine efficacy through completely different metabolic pathways and further influence the host response to the drug. These key bacteria metabolic pathways affect fluoropyrimidine, including one-carbon metabolism and pyrimidine salvage pathways are highly conserved in prokaryotes, and are present in most human gut microbiome species (Javdan et al., 2020). Taken together, This *C. elegans* – *E. coli* simplified host-microbe system allows us to study the host-microbe interactions at the molecular level in many diseases and treatments.

To summarize, my studies demonstrate the use of the simple model system *C. elegans* to tackle complicated biological questions related to human complex chronic diseases. These studies provide cellular and molecular insights not only

for us to better understand disease mechanisms but also to develop interventions and to investigate the changes in drug efficacy under a variety of circumstances.

References

- Abranches, M.V., Oliveira, F.C.E. de, Conceição, L.L. da, and Peluzio, M. do C.G. (2015). Obesity and diabetes: the link between adipose tissue dysfunction and glucose homeostasis. *Nutr Res Rev* 28, 121–132.
- Ahima, R.S. (2009). Connecting obesity, aging and diabetes. *Nat. Med.* 15, 996–997.
- Akiyama, M., Okada, Y., Kanai, M., Takahashi, A., Momozawa, Y., Ikeda, M., Iwata, N., Ikegawa, S., Hirata, M., Matsuda, K., et al. (2017). Genome-wide association study identifies 112 new loci for body mass index in the Japanese population. *Nat. Genet.* 49, 1458–1467.
- Alcántar-Fernández, J., Navarro, R.E., Salazar-Martínez, A.M., Pérez-Andrade, M.E., and Miranda-Ríos, J. (2018). *Caenorhabditis elegans* respond to high-glucose diets through a network of stress-responsive transcription factors. *PLoS One* 13, e0199888.
- Almeida, A., Mitchell, A.L., Boland, M., Forster, S.C., Gloor, G.B., Tarkowska, A., Lawley, T.D., and Finn, R.D. (2019). A new genomic blueprint of the human gut microbiota. *Nature* 568, 499–504.
- Anderson, G., and Horvath, J. (2004). The growing burden of chronic disease in America. *Public Health Rep.* 119, 263–270.
- Ansmant, I., Massenet, S., Grosjean, H., Motorin, Y., and Branlant, C. (2000). Identification of the *Saccharomyces cerevisiae* RNA:pseudouridine synthase

- responsible for formation of psi(2819) in 21S mitochondrial ribosomal RNA. *Nucleic Acids Res.* **28**, 1941–1946.
- Asrar, F.M., and O'Connor, D.L. (2005). Bacterially synthesized folate and supplemental folic acid are absorbed across the large intestine of piglets. *J. Nutr. Biochem.* **16**, 587–593.
- Astley, C.M., Todd, J.N., Salem, R.M., Vedantam, S., Ebbeling, C.B., Huang, P.L., Ludwig, D.S., Hirschhorn, J.N., and Florez, J.C. (2018). Genetic Evidence That Carbohydrate-Stimulated Insulin Secretion Leads to Obesity. *Clin. Chem.* **64**, 192–200.
- Avery, L., and Shtonda, B.B. (2003). Food transport in the *C. elegans* pharynx. *J. Exp. Biol.* **206**, 2441–2457.
- Baba, T., Ara, T., Hasegawa, M., Takai, Y., Okumura, Y., Baba, M., Datsenko, K.A., Tomita, M., Wanner, B.L., and Mori, H. (2006). Construction of *Escherichia coli* K-12 in-frame, single-gene knockout mutants: the Keio collection. *Mol. Syst. Biol.* **2**, 2006.0008.
- Bazopoulou, D., Chaudhury, A.R., Pantazis, A., and Chronis, N. (2017). An automated compound screening for anti-aging effects on the function of *C. elegans* sensory neurons. *Sci. Rep.* **7**, 9403.
- Bedell, V.M., Westcot, S.E., and Ekker, S.C. (2011). Lessons from morpholino-based screening in zebrafish. *Brief. Funct. Genomics* **10**, 181–188.
- Blüher, M. (2016). Adipose tissue inflammation: a cause or consequence of obesity-related insulin resistance? *Clin. Sci.* **130**, 1603–1614.

- Bouyanfif, A., Jayarathne, S., Koboziev, I., and Moustaid-Moussa, N. (2019). The Nematode *Caenorhabditis elegans* as a Model Organism to Study Metabolic Effects of ω -3 Polyunsaturated Fatty Acids in Obesity. *Adv. Nutr.* *10*, 165–178.
- Boyer, H.W., and Roulland-Dussoix, D. (1969). A complementation analysis of the restriction and modification of DNA in *Escherichia coli*. *J. Mol. Biol.* *41*, 459–472.
- Branen, J.K., Shintani, D.K., and Engeseth, N.J. (2003). Expression of antisense acyl carrier protein-4 reduces lipid content in *Arabidopsis* leaf tissue. *Plant Physiol.* *132*, 748–756.
- Brenner, S. (1974). The genetics of *Caenorhabditis elegans*. *Genetics* *77*, 71–94.
- Brewer, H.B. (2004). High-density lipoproteins: a new potential therapeutic target for the prevention of cardiovascular disease. *Arterioscler. Thromb. Vasc. Biol.* *24*, 387–391.
- Brina, D., Miluzio, A., Ricciardi, S., Clarke, K., Davidsen, P.K., Viero, G., Tebaldi, T., Offenhäuser, N., Rozman, J., Rathkolb, B., et al. (2015). eIF6 coordinates insulin sensitivity and lipid metabolism by coupling translation to transcription. *Nat. Commun.* *6*, 8261.
- Britton, K.A., and Fox, C.S. (2011). Ectopic fat depots and cardiovascular disease. *Circulation* *124*, e837–41.
- Browning, D.F., Wells, T.J., França, F.L.S., Morris, F.C., Sevastyanovich, Y.R., Bryant, J.A., Johnson, M.D., Lund, P.A., Cunningham, A.F., Hobman, J.L., et

- al. (2013). Laboratory adapted *Escherichia coli* K-12 becomes a pathogen of *Caenorhabditis elegans* upon restoration of O antigen biosynthesis. *Mol. Microbiol.* 87, 939–950.
- Buniello, A., MacArthur, J.A.L., Cerezo, M., Harris, L.W., Hayhurst, J., Malangone, C., McMahon, A., Morales, J., Mountjoy, E., Sollis, E., et al. (2019). The NHGRI-EBI GWAS Catalog of published genome-wide association studies, targeted arrays and summary statistics 2019. *Nucleic Acids Res.* 47, D1005–D1012.
- Buttorff, C., Ruder, T., and Bauman, M. (2017). Multiple Chronic Conditions in the United States (RAND Corporation).
- Bykhovskaya, Y., Casas, K., Mengesha, E., Inbal, A., and Fischel-Ghodsian, N. (2004). Missense mutation in pseudouridine synthase 1 (PUS1) causes mitochondrial myopathy and sideroblastic anemia (MLASA). *Am. J. Hum. Genet.* 74, 1303–1308.
- Calixto, A., Chelur, D., Topalidou, I., Chen, X., and Chalfie, M. (2010). Enhanced neuronal RNAi in *C. elegans* using SID-1. *Nat. Methods* 7, 554–559.
- Cano-Gamez, E., and Trynka, G. (2020). From GWAS to function: using functional genomics to identify the mechanisms underlying complex diseases. *Front. Genet.* 11, 424.
- Chang, J.T., Kumsta, C., Hellman, A.B., Adams, L.M., and Hansen, M. (2017). Spatiotemporal regulation of autophagy during *Caenorhabditis elegans* aging. *eLife* 6, e18459

- Chang, T.-K., Shrivage, B.V., Hayes, S.D., Powers, C.M., Simin, R.T., Wade Harper, J., and Baehrecke, E.H. (2013). Uba1 functions in Atg7- and Atg3-independent autophagy. *Nat. Cell Biol.* *15*, 1067–1078.
- Chatterjee, S., Peters, S.A.E., Woodward, M., Mejia Arango, S., Batty, G.D., Beckett, N., Beiser, A., Borenstein, A.R., Crane, P.K., Haan, M., et al. (2016). Type 2 diabetes as a risk factor for dementia in women compared with men: A pooled analysis of 2.3 million people comprising more than 100,000 cases of dementia. *Diabetes Care* *39*, 300–307.
- Chen, J., and Patton, J.R. (1999). Cloning and characterization of a mammalian pseudouridine synthase. *RNA* *5*, 409–419.
- Chen, X., Barclay, J.W., Burgoyne, R.D., and Morgan, A. (2015). Using *C. elegans* to discover therapeutic compounds for ageing-associated neurodegenerative diseases. *Chem. Cent. J.* *9*, 65.
- Cheng, M., Mei, B., Zhou, Q., Zhang, M., Huang, H., Han, L., and Huang, Q. (2018). Computational analyses of obesity associated loci generated by genome-wide association studies. *PLoS One* *13*, e0199987.
- Cherbuin, N., Sargent-Cox, K., Fraser, M., Sachdev, P., and Anstey, K.J. (2015). Being overweight is associated with hippocampal atrophy: the PATH Through Life Study. *Int. J. Obes.* *39*, 1509–1514.
- Chi, C., Ronai, D., Than, M.T., Walker, C.J., Sewell, A.K., and Han, M. (2016). Nucleotide levels regulate germline proliferation through modulating GLP-1/Notch signaling in *C. elegans*. *Genes Dev.* *30*, 307–320.

- Choy, R.K., and Thomas, J.H. (1999). Fluoxetine-resistant mutants in *C. elegans* define a novel family of transmembrane proteins. *Mol. Cell* *4*, 143–152.
- Chu, A.Y., Deng, X., Fisher, V.A., Drong, A., Zhang, Y., Feitosa, M.F., Liu, C.-T., Weeks, O., Choh, A.C., Duan, Q., et al. (2017). Multiethnic genome-wide meta-analysis of ectopic fat depots identifies loci associated with adipocyte development and differentiation. *Nat. Genet.* *49*, 125–130.
- Civelek, M., Wu, Y., Pan, C., Raulerson, C.K., Ko, A., He, A., Tilford, C., Saleem, N.K., Stančáková, A., Scott, L.J., et al. (2017). Genetic Regulation of Adipose Gene Expression and Cardio-Metabolic Traits. *Am. J. Hum. Genet.* *100*, 428–443.
- Corsi, A.K., Wightman, B., and Chalfie, M. (2015). A Transparent Window into Biology: A Primer on *Caenorhabditis elegans*. *Genetics*, *200*, 387–407.
- Czech, M.P. (2017). Insulin action and resistance in obesity and type 2 diabetes. *Nat. Med.* *23*, 804–814.
- Daemen, S., van Polanen, N., and Hesselink, M.K.C. (2018). The effect of diet and exercise on lipid droplet dynamics in human muscle tissue. *J. Exp. Biol.* *221*.
- Dall'Armi, C., Hurtado-Lorenzo, A., Tian, H., Morel, E., Nezu, A., Chan, R.B., Yu, W.H., Robinson, K.S., Yeku, O., Small, S.A., et al. (2010). The phospholipase D1 pathway modulates macroautophagy. *Nat. Commun.* *1*, 142.
- Davis, M.W., Somerville, D., Lee, R.Y., Lockery, S., Avery, L., and Fambrough, D.M. (1995). Mutations in the *Caenorhabditis elegans* Na,K-ATPase alpha-

subunit gene, *eat-6*, disrupt excitable cell function. *J. Neurosci.* *15*, 8408–8418.

Depuydt, G., Xie, F., Petyuk, V.A., Shanmugam, N., Smolders, A., Dhondt, I., Brewer, H.M., Camp, D.G., Smith, R.D., and Braeckman, B.P. (2013). Reduced insulin/insulin-like growth factor-1 signaling and dietary restriction inhibit translation but preserve muscle mass in *Caenorhabditis elegans*. *Mol. Cell Proteomics* *12*, 3624–3639.

Derrien, M., and van Hylckama Vlieg, J.E.T. (2015). Fate, activity, and impact of ingested bacteria within the human gut microbiota. *Trends Microbiol.* *23*, 354–366.

Dhingra, R., Sullivan, L., Jacques, P.F., Wang, T.J., Fox, C.S., Meigs, J.B., D'Agostino, R.B., Gaziano, J.M., and Vasan, R.S. (2007). Soft drink consumption and risk of developing cardiometabolic risk factors and the metabolic syndrome in middle-aged adults in the community. *Circulation* *116*, 480–488.

Dirksen, P., Marsh, S.A., Braker, I., Heitland, N., Wagner, S., Nakad, R., Mader, S., Petersen, C., Kowallik, V., Rosenstiel, P., et al. (2016). The native microbiome of the nematode *Caenorhabditis elegans*: gateway to a new host-microbiome model. *BMC Biol.* *14*, 38.

Dixon, S.J., Winter, G.E., Musavi, L.S., Lee, E.D., Snijder, B., Rebsamen, M., Superti-Furga, G., and Stockwell, B.R. (2015). Human haploid cell genetics

reveals roles for lipid metabolism genes in nonapoptotic cell death. *ACS Chem. Biol.* *10*, 1604–1609.

Ducker, G.S., and Rabinowitz, J.D. (2017). One-Carbon Metabolism in Health and Disease. *Cell Metab.* *25*, 27–42.

Endres, M., Biniszkiwicz, D., Sobol, R.W., Harms, C., Ahmadi, M., Lipski, A., Katchanov, J., Mergenthaler, P., Dirnagl, U., Wilson, S.H., et al. (2004). Increased postischemic brain injury in mice deficient in uracil-DNA glycosylase. *J. Clin. Invest.* *113*, 1711–1721.

Engström, G., Hedblad, B., Stavenow, L., Lind, P., Janzon, L., and Lindgärde, F. (2003). Inflammation-sensitive plasma proteins are associated with future weight gain. *Diabetes* *52*, 2097–2101.

Faber, P.W., Voisine, C., King, D.C., Bates, E.A., and Hart, A.C. (2002). Glutamine/proline-rich PQE-1 proteins protect *Caenorhabditis elegans* neurons from huntingtin polyglutamine neurotoxicity. *Proc. Natl. Acad. Sci. USA* *99*, 17131–17136.

Fergus, C., Barnes, D., Alqasem, M.A., and Kelly, V.P. (2015). The queuine micronutrient: charting a course from microbe to man. *Nutrients* *7*, 2897–2929.

Ferguson, E.L., and Horvitz, H.R. (1985). Identification and characterization of 22 genes that affect the vulval cell lineages of the nematode *Caenorhabditis elegans*. *Genetics* *110*, 17–72.

Field, B.C.T., Chaudhri, O.B., and Bloom, S.R. (2009). Obesity treatment: novel peripheral targets. *Br. J. Clin. Pharmacol.* *68*, 830–843.

- Flegal, K.M., Kruszon-Moran, D., Carroll, M.D., Fryar, C.D., and Ogden, C.L. (2016). Trends in obesity among adults in the united states, 2005 to 2014. *JAMA* 315, 2284–2291.
- Fong, S., Teo, E., Ng, L.F., Chen, C.-B., Lakshmanan, L.N., Tsoi, S.Y., Moore, P.K., Inoue, T., Halliwell, B., and Gruber, J. (2016). Energy crisis precedes global metabolic failure in a novel *Caenorhabditis elegans* Alzheimer Disease model. *Sci. Rep.* 6, 33781.
- Fouad, A.D., Pu, S.H., Teng, S., Mark, J.R., Fu, M., Zhang, K., Huang, J., Raizen, D.M., and Fang-Yen, C. (2017). Quantitative Assessment of Fat Levels in *Caenorhabditis elegans* Using Dark Field Microscopy. *G3 (Bethesda)* 7, 1811–1818.
- Frazer, K.A., Murray, S.S., Schork, N.J., and Topol, E.J. (2009). Human genetic variation and its contribution to complex traits. *Nat. Rev. Genet.* 10, 241–251.
- Friedman, J.M. (2000). Obesity in the new millennium. *Nature* 404, 632–634.
- Gallagher, M.D., and Chen-Plotkin, A.S. (2018). The Post-GWAS Era: From Association to Function. *Am. J. Hum. Genet.* 102, 717–730.
- Garcia, A.M., Ladage, M.L., Dumesnil, D.R., Zaman, K., Shulaev, V., Azad, R.K., and Padilla, P.A. (2015). Glucose induces sensitivity to oxygen deprivation and modulates insulin/IGF-1 signaling and lipid biosynthesis in *Caenorhabditis elegans*. *Genetics* 200, 167–184.

- García-González, A.P., Ritter, A.D., Shrestha, S., Andersen, E.C., Yilmaz, L.S., and Walhout, A.J.M. (2017). Bacterial metabolism affects the *c. elegans* response to cancer chemotherapeutics. *Cell* 169, 431–441.e8.
- Gebauer, J., Gentsch, C., Mansfeld, J., Schmeißer, K., Waschina, S., Brandes, S., Klimmasch, L., Zamboni, N., Zarse, K., Schuster, S., et al. (2016). A Genome-Scale Database and Reconstruction of *Caenorhabditis elegans* Metabolism. *Cell Syst.* 2, 312–322.
- Gesta, S., Bezy, O., Mori, M.A., Macotela, Y., Lee, K.Y., and Kahn, C.R. (2011). Mesodermal developmental gene *Tbx15* impairs adipocyte differentiation and mitochondrial respiration. *Proc. Natl. Acad. Sci. USA* 108, 2771–2776.
- Ghazalpour, A., Rau, C.D., Farber, C.R., Bennett, B.J., Orozco, L.D., van Nas, A., Pan, C., Allayee, H., Beaven, S.W., Civelek, M., et al. (2012). Hybrid mouse diversity panel: a panel of inbred mouse strains suitable for analysis of complex genetic traits. *Mamm. Genome* 23, 680–692.
- Gosai, S.J., Kwak, J.H., Luke, C.J., Long, O.S., King, D.E., Kovatch, K.J., Johnston, P.A., Shun, T.Y., Lazo, J.S., Perlmutter, D.H., et al. (2010). Automated high-content live animal drug screening using *C. elegans* expressing the aggregation prone serpin $\alpha 1$ -antitrypsin Z. *PLoS One* 5, e15460.
- Gross, L.S., Li, L., Ford, E.S., and Liu, S. (2004). Increased consumption of refined carbohydrates and the epidemic of type 2 diabetes in the United States: an ecologic assessment. *Am. J. Clin. Nutr.* 79, 774–779.

- Gu, X., Liu, Y., and Santi, D.V. (1999). The mechanism of pseudouridine synthase I as deduced from its interaction with 5-fluorouracil-tRNA. *Proc. Natl. Acad. Sci. USA* *96*, 14270–14275.
- Ha, S., Jeong, S.-H., Yi, K., Chung, K.M., Hong, C.J., Kim, S.W., Kim, E.-K., and Yu, S.-W. (2017). Phosphorylation of p62 by AMP-activated protein kinase mediates autophagic cell death in adult hippocampal neural stem cells. *J. Biol. Chem.* *292*, 13795–13808.
- Hahm, J.-H., Kim, S., DiLoreto, R., Shi, C., Lee, S.-J.V., Murphy, C.T., and Nam, H.G. (2015). *C. elegans* maximum velocity correlates with healthspan and is maintained in worms with an insulin receptor mutation. *Nat. Commun.* *6*, 8919.
- Hainer, V., Aldhoon Hainerová, I., Kunešová, M., Taxová Braunerová, R., Zamrazilová, H., and Bendlová, B. (2020). Melanocortin pathways: suppressed and stimulated melanocortin-4 receptor (MC4R). *Physiol. Res.* *69*, S245–S254.
- Hannou, S.A., Haslam, D.E., McKeown, N.M., and Herman, M.A. (2018). Fructose metabolism and metabolic disease. *J. Clin. Invest.* *128*, 545–555.
- Hanover, L.M., and White, J.S. (1993). Manufacturing, composition, and applications of fructose. *Am. J. Clin. Nutr.* *58*, 724S–732S.
- Heasman, J., Wessely, O., Llangland, R., Craig, E.J., and Kessler, D.S. (2001). Vegetal localization of maternal mRNAs is disrupted by VegT depletion. *Dev. Biol.* *240*, 377–386.

- Hengartner, M.O., and Horvitz, H.R. (1994). Programmed cell death in *Caenorhabditis elegans*. *Curr. Opin. Genet. Dev.* 4, 581–586.
- Hindorff, L.A., Sethupathy, P., Junkins, H.A., Ramos, E.M., Mehta, J.P., Collins, F.S., and Manolio, T.A. (2009). Potential etiologic and functional implications of genome-wide association loci for human diseases and traits. *Proc. Natl. Acad. Sci. USA* 106, 9362–9367.
- Hitchings, R., and Kelly, L. (2019). Drug metabolism as a community effort. *Cell Metab.* 30, 235–237.
- Horvitz, H.R., and Sulston, J.E. (1980). Isolation and genetic characterization of cell-lineage mutants of the nematode *Caenorhabditis elegans*. *Genetics* 96, 435–454.
- Huang, L., Pookanjanatavip, M., Gu, X., and Santi, D.V. (1998). A conserved aspartate of tRNA pseudouridine synthase is essential for activity and a probable nucleophilic catalyst. *Biochemistry* 37, 344–351.
- Hudu, S.A., Alshrari, A.S., Syahida, A., and Sekawi, Z. (2016). Cell culture, technology: enhancing the culture of diagnosing human diseases. *J. Clin. Diagn. Res.* 10, DE01–5.
- Ip, W., Shao, W., Song, Z., Chen, Z., Wheeler, M.B., and Jin, T. (2015). Liver-specific expression of dominant-negative transcription factor 7-like 2 causes progressive impairment in glucose homeostasis. *Diabetes* 64, 1923–1932.

- Javdan, B., Lopez, J.G., Chankhamjon, P., Lee, Y.-C.J., Hull, R., Wu, Q., Wang, X., Chatterjee, S., and Donia, M.S. (2020). Personalized mapping of drug metabolism by the human gut microbiome. *Cell* *181*, 1661–1679.e22.
- Johanns, M., Kviklyte, S., Chuang, S.-J., Corbeels, K., Jacobs, R., Herinckx, G., Vertommen, D., Schakman, O., Duparc, T., Cani, P.D., et al. (2019). Genetic deletion of soluble 5'-nucleotidase II reduces body weight gain and insulin resistance induced by a high-fat diet. *Mol. Genet. Metab.* *126*, 377–387.
- Johnson, R.J., Segal, M.S., Sautin, Y., Nakagawa, T., Feig, D.I., Kang, D.-H., Gersch, M.S., Benner, S., and Sánchez-Lozada, L.G. (2007). Potential role of sugar (fructose) in the epidemic of hypertension, obesity and the metabolic syndrome, diabetes, kidney disease, and cardiovascular disease. *Am. J. Clin. Nutr.* *86*, 899–906.
- Joly, P., Touraine, C., Georget, A., Dartigues, J.-F., Commenges, D., and Jacqmin-Gadda, H. (2013). Prevalence projections of chronic diseases and impact of public health intervention. *Biometrics* *69*, 109–117.
- Jones, A.K., Buckingham, S.D., and Sattelle, D.B. (2005). Chemistry-to-gene screens in *Caenorhabditis elegans*. *Nat. Rev. Drug Discov.* *4*, 321–330.
- Joshi, C.J., Ke, W., Drangowska-Way, A., O'Rourke, E.J., and Lewis, N.E. (2021). What are housekeeping genes? *BioRxiv*.
- Kahn, B.B., and Flier, J.S. (2000). Obesity and insulin resistance. *J. Clin. Invest.* *106*, 473–481.

- Kamath, R.S., Fraser, A.G., Dong, Y., Poulin, G., Durbin, R., Gotta, M., Kanapin, A., Le Bot, N., Moreno, S., Sohrmann, M., et al. (2003). Systematic functional analysis of the *Caenorhabditis elegans* genome using RNAi. *Nature* 421, 231–237.
- Kang, J.G., and Park, C.-Y. (2012). Anti-Obesity Drugs: A Review about Their Effects and Safety. *Diabetes Metab J* 36, 13–25.
- Ke, W., Drangowska-Way, A., Katz, D., Siller, K., and O'Rourke, E.J. (2018). The Ancient Genetic Networks of Obesity: Whole-Animal Automated Screening for Conserved Fat Regulators. *Methods Mol. Biol.* 1787, 129–146.
- Kenyon, C. (2011). The first long-lived mutants: discovery of the insulin/IGF-1 pathway for ageing. *Philos. Trans. R. Soc. Lond. B, Biol. Sci.* 366, 9–16.
- Khodursky, A., Guzmán, E.C., and Hanawalt, P.C. (2015). Thymineless Death Lives On: New Insights into a Classic Phenomenon. *Annu. Rev. Microbiol.* 69, 247–263.
- Kim, E.J.E., and Lee, S.J.V. (2019). Recent progresses on anti-aging compounds and their targets in *Caenorhabditis elegans*. *Translational Medicine of Aging.* 3, 121-124.
- Kim, J., Kundu, M., Viollet, B., and Guan, K.-L. (2011). AMPK and mTOR regulate autophagy through direct phosphorylation of Ulk1. *Nat. Cell Biol.* 13, 132–141.
- Kim, W., Underwood, R.S., Greenwald, I., and Shaye, D.D. (2018). OrthoList 2: A New Comparative Genomic Analysis of Human and *Caenorhabditis elegans* Genes. *Genetics* 210, 445–461.

- Kirschner, M.W. (2005). The meaning of systems biology. *Cell* 121, 503–504.
- Klarin, D., Damrauer, S.M., Cho, K., Sun, Y.V., Teslovich, T.M., Honerlaw, J., Gagnon, D.R., DuVall, S.L., Li, J., Peloso, G.M., et al. (2018). Genetics of blood lipids among ~300,000 multi-ethnic participants of the Million Veteran Program. *Nat. Genet.* 50, 1514–1523.
- Kobet, R.A., Pan, X., Zhang, B., Pak, S.C., Asch, A.S., and Lee, M.-H. (2014). *Caenorhabditis elegans*: A Model System for Anti-Cancer Drug Discovery and Therapeutic Target Identification. *Biomol. Ther. (Seoul)* 22, 371–383.
- Kok, D.E., Steegenga, W.T., Smid, E.J., Zoetendal, E.G., Ulrich, C.M., and Kampman, E. (2020). Bacterial folate biosynthesis and colorectal cancer risk: more than just a gut feeling. *Crit. Rev. Food Sci. Nutr.* 60, 244–256.
- Korte, A., and Farlow, A. (2013). The advantages and limitations of trait analysis with GWAS: a review. *Plant Methods* 9, 29.
- Kuwahara, T., Koyama, A., Gengyo-Ando, K., Masuda, M., Kowa, H., Tsunoda, M., Mitani, S., and Iwatsubo, T. (2006). Familial Parkinson mutant alpha-synuclein causes dopamine neuron dysfunction in transgenic *Caenorhabditis elegans*. *J. Biol. Chem.* 281, 334–340.
- Kwok, T.C.Y., Ricker, N., Fraser, R., Chan, A.W., Burns, A., Stanley, E.F., McCourt, P., Cutler, S.R., and Roy, P.J. (2006). A small-molecule screen in *C. elegans* yields a new calcium channel antagonist. *Nature* 441, 91–95.
- Lakso, M., Vartiainen, S., Moilanen, A.-M., Sirviö, J., Thomas, J.H., Nass, R., Blakely, R.D., and Wong, G. (2003). Dopaminergic neuronal loss and motor

deficits in *Caenorhabditis elegans* overexpressing human alpha-synuclein. *J. Neurochem.* **86**, 165–172.

Lander, E.S., Linton, L.M., Birren, B., Nusbaum, C., Zody, M.C., Baldwin, J., Devon, K., Dewar, K., Doyle, M., FitzHugh, W., et al. (2001). Initial sequencing and analysis of the human genome. *Nature* **409**, 860–921.

Laranjeiro, R., Harinath, G., Burke, D., Braeckman, B.P., and Driscoll, M. (2017). Single swim sessions in *C. elegans* induce key features of mammalian exercise. *BMC Biol.* **15**, 30.

Lee, I.H., Kawai, Y., Fergusson, M.M., Rovira, I.I., Bishop, A.J.R., Motoyama, N., Cao, L., and Finkel, T. (2012). Atg7 modulates p53 activity to regulate cell cycle and survival during metabolic stress. *Science* **336**, 225–228.

Lee, K.Y., Yamamoto, Y., Boucher, J., Winnay, J.N., Gesta, S., Cobb, J., Blüher, M., and Kahn, C.R. (2013). Shox2 is a molecular determinant of depot-specific adipocyte function. *Proc. Natl. Acad. Sci. USA* **110**, 11409–11414.

Lee, S.-J., Murphy, C.T., and Kenyon, C. (2009). Glucose shortens the life span of *C. elegans* by downregulating DAF-16/FOXO activity and aquaporin gene expression. *Cell Metab.* **10**, 379–391.

Lehouritis, P., Cummins, J., Stanton, M., Murphy, C.T., McCarthy, F.O., Reid, G., Urbaniak, C., Byrne, W.L., and Tangney, M. (2015). Local bacteria affect the efficacy of chemotherapeutic drugs. *Sci. Rep.* **5**, 14554.

- Lehouritis, P., Stanton, M., McCarthy, F.O., Jeavons, M., and Tangney, M. (2016). Activation of multiple chemotherapeutic prodrugs by the natural enzymolome of tumour-localised probiotic bacteria. *J. Control. Release* 222, 9–17.
- Lim, S.S., Vos, T., Flaxman, A.D., Danaei, G., Shibuya, K., Adair-Rohani, H., Amann, M., Anderson, H.R., Andrews, K.G., Aryee, M., et al. (2012). A comparative risk assessment of burden of disease and injury attributable to 67 risk factors and risk factor clusters in 21 regions, 1990-2010: a systematic analysis for the Global Burden of Disease Study 2010. *Lancet* 380, 2224–2260.
- Lima, D., Machado, A., Reis-Henriques, M.A., Rocha, E., Santos, M.M., and Castro, L.F.C. (2013). Cloning and expression analysis of the 17 β hydroxysteroid dehydrogenase type 12 (HSD17B12) in the neogastropod *Nucella lapillus*. *J. Steroid Biochem. Mol. Biol.* 134, 8–14.
- Lin, H.-P., Cheng, Z.-L., He, R.-Y., Song, L., Tian, M.-X., Zhou, L.-S., Groh, B.S., Liu, W.-R., Ji, M.-B., Ding, C., et al. (2016). Destabilization of fatty acid synthase by acetylation inhibits de novo lipogenesis and tumor cell growth. *Cancer Res.* 76, 6924–6936.
- Link, C.D. (1995). Expression of human beta-amyloid peptide in transgenic *Caenorhabditis elegans*. *Proc. Natl. Acad. Sci. USA* 92, 9368–9372.
- Littlejohn, N.K., and Grobe, J.L. (2015). Opposing tissue-specific roles of angiotensin in the pathogenesis of obesity, and implications for obesity-

- related hypertension. *Am. J. Physiol. Regul. Integr. Comp. Physiol.* **309**, R1463–73.
- Liu, X., Ser, Z., and Locasale, J.W. (2014a). Development and quantitative evaluation of a high-resolution metabolomics technology. *Anal. Chem.* **86**, 2175–2184.
- Liu, Z., Li, X., Ge, Q., Ding, M., and Huang, X. (2014b). A lipid droplet-associated GFP reporter-based screen identifies new fat storage regulators in *C. elegans*. *J Genet Genomics* **41**, 305–313.
- Locasale, J.W. (2013). Serine, glycine and one-carbon units: cancer metabolism in full circle. *Nat. Rev. Cancer* **13**, 572–583.
- Loh, N.Y., Neville, M.J., Marinou, K., Hardcastle, S.A., Fielding, B.A., Duncan, E.L., McCarthy, M.I., Tobias, J.H., Gregson, C.L., Karpe, F., et al. (2015). LRP5 regulates human body fat distribution by modulating adipose progenitor biology in a dose- and depot-specific fashion. *Cell Metab.* **21**, 262–273.
- Loh, N.Y., Minchin, J.E.N., Pinnick, K.E., Verma, M., Todorčević, M., Denton, N., Moustafa, J.E.-S., Kemp, J.P., Gregson, C.L., Evans, D.M., et al. (2020). RSPO3 impacts body fat distribution and regulates adipose cell biology in vitro. *Nat. Commun.* **11**, 2797.
- Long, X., Spycher, C., Han, Z.S., Rose, A.M., Müller, F., and Avruch, J. (2002). TOR deficiency in *C. elegans* causes developmental arrest and intestinal atrophy by inhibition of mRNA translation. *Curr. Biol.* **12**, 1448–1461.

- Ludewig, A.H., Kober-Eisermann, C., Weitzel, C., Bethke, A., Neubert, K., Gerisch, B., Hutter, H., and Antebi, A. (2004). A novel nuclear receptor/coregulator complex controls *C. elegans* lipid metabolism, larval development, and aging. *Genes Dev.* *18*, 2120–2133.
- Lukey, M.J., Katt, W.P., and Cerione, R.A. (2017). Targeting amino acid metabolism for cancer therapy. *Drug Discov. Today* *22*, 796–804.
- Lustig, R.H. (2010). Fructose: metabolic, hedonic, and societal parallels with ethanol. *J. Am. Diet. Assoc.* *110*, 1307–1321.
- Magtanong, L., Ko, P.J., and Dixon, S.J. (2016). Emerging roles for lipids in non-apoptotic cell death. *Cell Death Differ.* *23*, 1099–1109.
- Malet-Martino, M., and Martino, R. (2002). Clinical studies of three oral prodrugs of 5-fluorouracil (capecitabine, UFT, S-1): a review. *Oncologist* *7*, 288–323.
- Mannan, A.U., Roussa, E., Kraus, C., Rickmann, M., Maenner, J., Nayernia, K., Krieglstein, K., Reis, A., and Engel, W. (2004). Mutation in the gene encoding lysosomal acid phosphatase (*Acp2*) causes cerebellum and skin malformation in mouse. *Neurogenetics* *5*, 229–238.
- Marriott, B.P., Olsho, L., Hadden, L., and Connor, P. (2010). Intake of added sugars and selected nutrients in the United States, National Health and Nutrition Examination Survey (NHANES) 2003-2006. *Crit. Rev. Food Sci. Nutr.* *50*, 228–258.
- Martin, A.B., Hartman, M., Lassman, D., Catlin, A., and National Health Expenditure Accounts Team (2021). National health care spending in 2019:

steady growth for the fourth consecutive year. *Health Aff. (Millwood)* 40, 14–24.

Matsuzaka, T., Shimano, H., Yahagi, N., Amemiya-Kudo, M., Okazaki, H., Tamura, Y., Iizuka, Y., Ohashi, K., Tomita, S., Sekiya, M., et al. (2004). Insulin-independent induction of sterol regulatory element-binding protein-1c expression in the livers of streptozotocin-treated mice. *Diabetes* 53, 560–569.

Maurano, M.T., Humbert, R., Rynes, E., Thurman, R.E., Haugen, E., Wang, H., Reynolds, A.P., Sandstrom, R., Qu, H., Brody, J., et al. (2012). Systematic localization of common disease-associated variation in regulatory DNA. *Science* 337, 1190–1195.

Mayes, P.A. (1993). Intermediary metabolism of fructose. *Am. J. Clin. Nutr.* 58, 754S–765S.

Maynard, C., Cummins, I., Green, J., and Weinkove, D. (2018). A bacterial route for folic acid supplementation. *BMC Biol.* 16, 67.

McKay, R.M., McKay, J.P., Avery, L., and Graff, J.M. (2003). *C elegans*: a model for exploring the genetics of fat storage. *Dev. Cell* 4, 131–142.

Melnikova, I., and Wages, D. (2006). Anti-obesity therapies. *Nat. Rev. Drug Discov.* 5, 369–370.

Miller, C.C., Martin, R.J., Whitney, M.L., and Edwards, G.L. (2002). Intracerebroventricular injection of fructose stimulates feeding in rats. *Nutr. Neurosci.* 5, 359–362.

- Miyazaki, M., Dobrzyn, A., Man, W.C., Chu, K., Sampath, H., Kim, H.-J., and Ntambi, J.M. (2004). Stearoyl-CoA desaturase 1 gene expression is necessary for fructose-mediated induction of lipogenic gene expression by sterol regulatory element-binding protein-1c-dependent and -independent mechanisms. *J. Biol. Chem.* 279, 25164–25171.
- Mohr, S.E. (2014). RNAi screening in *Drosophila* cells and in vivo. *Methods* 68, 82–88.
- Morganti, S., Tarantino, P., Ferraro, E., D'Amico, P., Viale, G., Trapani, D., Duso, B.A., and Curigliano, G. (2019). Complexity of genome sequencing and reporting: Next generation sequencing (NGS) technologies and implementation of precision medicine in real life. *Crit. Rev. Oncol. Hematol.* 133, 171–182.
- Morley, J.F., Brignull, H.R., Weyers, J.J., and Morimoto, R.I. (2002). The threshold for polyglutamine-expansion protein aggregation and cellular toxicity is dynamic and influenced by aging in *Caenorhabditis elegans*. *Proc. Natl. Acad. Sci. USA* 99, 10417–10422.
- Murphy, S.L., Xu, J., Kochanek, K.D., Arias, E., and Tejada-Vera, B. (2021). Deaths: final data for 2018. *Natl. Vital Stat. Rep.* 69, 1–83.
- Muschiol, D., Schroeder, F., and Traunspurger, W. (2009). Life cycle and population growth rate of *Caenorhabditis elegans* studied by a new method. *BMC Ecol.* 9, 14.

- Nakade, Y., Iwata, Y., Furuichi, K., Mita, M., Hamase, K., Konno, R., Miyake, T., Sakai, N., Kitajima, S., Toyama, T., et al. (2018). Gut microbiota-derived D-serine protects against acute kidney injury. *JCI Insight* 3.
- Nakagawa, T., Tuttle, K.R., Short, R.A., and Johnson, R.J. (2005). Hypothesis: fructose-induced hyperuricemia as a causal mechanism for the epidemic of the metabolic syndrome. *Nat. Clin. Pract. Nephrol.* 1, 80–86.
- Nakayama, H., Kinouchi, T., Kataoka, K., Akimoto, S., Matsuda, Y., and Ohnishi, Y. (1997). Intestinal anaerobic bacteria hydrolyse sorivudine, producing the high blood concentration of 5-(E)-(2-bromovinyl)uracil that increases the level and toxicity of 5-fluorouracil. *Pharmacogenetics* 7, 35–43.
- Narbonne, P., and Roy, R. (2009). *Caenorhabditis elegans* dauers need LKB1/AMPK to ration lipid reserves and ensure long-term survival. *Nature* 457, 210–214.
- Ndumele, C.E., Matsushita, K., Lazo, M., Bello, N., Blumenthal, R.S., Gerstenblith, G., Nambi, V., Ballantyne, C.M., Solomon, S.D., Selvin, E., et al. (2016). Obesity and subtypes of incident cardiovascular disease. *J. Am. Heart Assoc.* 5.
- Ng, M., Fleming, T., Robinson, M., Thomson, B., Graetz, N., Margono, C., Mullany, E.C., Biryukov, S., Abbafati, C., Abera, S.F., et al. (2014). Global, regional, and national prevalence of overweight and obesity in children and adults during 1980-2013: a systematic analysis for the Global Burden of Disease Study 2013. *Lancet* 384, 766–781.

- Nikoletopoulou, V., Markaki, M., Palikaras, K., and Tavernarakis, N. (2013). Crosstalk between apoptosis, necrosis and autophagy. *Biochim. Biophys. Acta* 1833, 3448–3459.
- Nishida, Y., Arakawa, S., Fujitani, K., Yamaguchi, H., Mizuta, T., Kanaseki, T., Komatsu, M., Otsu, K., Tsujimoto, Y., and Shimizu, S. (2009). Discovery of Atg5/Atg7-independent alternative macroautophagy. *Nature* 461, 654–658.
- Nussbaum-Krammer, C.I., Neto, M.F., Brielmann, R.M., Pedersen, J.S., and Morimoto, R.I. (2015). Investigating the spreading and toxicity of prion-like proteins using the metazoan model organism *C. elegans*. *J. Vis. Exp.* 52321.
- O'Reilly, L.P., Luke, C.J., Perlmutter, D.H., Silverman, G.A., and Pak, S.C. (2014). *C. elegans* in high-throughput drug discovery. *Adv. Drug Deliv. Rev.* 69-70, 247–253.
- O'Rourke, E.J., Conery, A.L., and Moy, T.I. (2009a). Whole-animal high-throughput screens: the *C. elegans* model. *Methods Mol. Biol.* 486, 57–75.
- O'Rourke, E.J., Soukas, A.A., Carr, C.E., and Ruvkun, G. (2009b). *C. elegans* major fats are stored in vesicles distinct from lysosome-related organelles. *Cell Metab.* 10, 430–435.
- Oeda, T., Shimohama, S., Kitagawa, N., Kohno, R., Imura, T., Shibasaki, H., and Ishii, N. (2001). Oxidative stress causes abnormal accumulation of familial amyotrophic lateral sclerosis-related mutant SOD1 in transgenic *Caenorhabditis elegans*. *Hum. Mol. Genet.* 10, 2013–2023.

- Ogden, C.L., Carroll, M.D., Lawman, H.G., Fryar, C.D., Kruszon-Moran, D., Kit, B.K., and Flegal, K.M. (2016). Trends in Obesity Prevalence Among Children and Adolescents in the United States, 1988-1994 Through 2013-2014. *JAMA* 315, 2292–2299.
- Oh, K.-J., Park, J., Kim, S.S., Oh, H., Choi, C.S., and Koo, S.-H. (2012). TCF7L2 modulates glucose homeostasis by regulating CREB- and FoxO1-dependent transcriptional pathway in the liver. *PLoS Genet.* 8, e1002986.
- Oliphant, K., and Allen-Vercoe, E. (2019). Macronutrient metabolism by the human gut microbiome: major fermentation by-products and their impact on host health. *Microbiome* 7, 91.
- Ollmann, M.M., Wilson, B.D., Yang, Y.K., Kerns, J.A., Chen, Y., Gantz, I., and Barsh, G.S. (1997). Antagonism of central melanocortin receptors in vitro and in vivo by agouti-related protein. *Science* 278, 135–138.
- Olshansky, S.J., Passaro, D.J., Hershov, R.C., Layden, J., Carnes, B.A., Brody, J., Hayflick, L., Butler, R.N., Allison, D.B., and Ludwig, D.S. (2005). A potential decline in life expectancy in the United States in the 21st century. *N. Engl. J. Med.* 352, 1138–1145.
- Palmisano, N.J., and Meléndez, A. (2016). Detection of Autophagy in *Caenorhabditis elegans* Using GFP::LGG-1 as an Autophagy Marker. *Cold Spring Harb. Protoc.* 2016, pdb.prot086496.
- Panosyan, E.H., Wang, Y., Xia, P., Lee, W.-N.P., Pak, Y., Laks, D.R., Lin, H.J., Moore, T.B., Cloughesy, T.F., Kornblum, H.I., et al. (2014). Asparagine

depletion potentiates the cytotoxic effect of chemotherapy against brain tumors. *Mol. Cancer Res.* 12, 694–702.

Parker, J.A., Arango, M., Abderrahmane, S., Lambert, E., Tourette, C., Catoire, H., and Néri, C. (2005). Resveratrol rescues mutant polyglutamine cytotoxicity in nematode and mammalian neurons. *Nat. Genet.* 37, 349–350.

Pettersen, H.S., Visnes, T., Vågbø, C.B., Svaasand, E.K., Doseth, B., Slupphaug, G., Kavli, B., and Krokan, H.E. (2011). UNG-initiated base excision repair is the major repair route for 5-fluorouracil in DNA, but 5-fluorouracil cytotoxicity depends mainly on RNA incorporation. *Nucleic Acids Res.* 39, 8430–8444.

Pfaffl, M.W. (2001). A new mathematical model for relative quantification in real-time RT-PCR. *Nucleic Acids Res.* 29, e45.

Podbilewicz, B., and Gruenbaum, Y. (2006). Live Imaging of *Caenorhabditis elegans*: preparation of samples. *CSH Protoc* 2006.

Poirier, P., Giles, T.D., Bray, G.A., Hong, Y., Stern, J.S., Pi-Sunyer, F.X., Eckel, R.H., American Heart Association, and Obesity Committee of the Council on Nutrition, Physical Activity, and Metabolism (2006). Obesity and cardiovascular disease: pathophysiology, evaluation, and effect of weight loss: an update of the 1997 American Heart Association Scientific Statement on Obesity and Heart Disease from the Obesity Committee of the Council on Nutrition, Physical Activity, and Metabolism. *Circulation* 113, 898–918.

- Poulin, G., Nandakumar, R., and Ahringer, J. (2004). Genome-wide RNAi screens in *Caenorhabditis elegans*: impact on cancer research. *Oncogene* 23, 8340–8345.
- Premisrirut, P.K., Dow, L.E., Kim, S.Y., Camiolo, M., Malone, C.D., Miething, C., Scuoppo, C., Zuber, J., Dickins, R.A., Kogan, S.C., et al. (2011). A rapid and scalable system for studying gene function in mice using conditional RNA interference. *Cell* 145, 145–158.
- Proietti, M., Perruzza, L., Scribano, D., Pellegrini, G., D'Antuono, R., Strati, F., Raffaelli, M., Gonzalez, S.F., Thelen, M., Hardt, W.-D., et al. (2019). ATP released by intestinal bacteria limits the generation of protective IgA against enteropathogens. *Nat. Commun.* 10, 250.
- Pryor, R., Norvaisas, P., Marinos, G., Best, L., Thingholm, L.B., Quintaneiro, L.M., De Haes, W., Esser, D., Waschina, S., Lujan, C., et al. (2019). Host-Microbe-Drug-Nutrient Screen Identifies Bacterial Effectors of Metformin Therapy. *Cell* 178, 1299–1312.e29.
- Pulit, S.L., Stoneman, C., Morris, A.P., Wood, A.R., Glastonbury, C.A., Tyrrell, J., Yengo, L., Ferreira, T., Marouli, E., Ji, Y., et al. (2019). Meta-analysis of genome-wide association studies for body fat distribution in 694 649 individuals of European ancestry. *Hum. Mol. Genet.* 28, 166–174.
- Ramos-Molina, B., Martin, M.G., and Lindberg, I. (2016). PCSK1 variants and human obesity. *Prog. Mol. Biol. Transl. Sci.* 140, 47–74.

- Rantakari, P., Lagerbohm, H., Kaimainen, M., Suomela, J.-P., Strauss, L., Sainio, K., Pakarinen, P., and Poutanen, M. (2010). Hydroxysteroid (17 β) dehydrogenase 12 is essential for mouse organogenesis and embryonic survival. *Endocrinology* *151*, 1893–1901.
- Reaven, G.M. (1995). Pathophysiology of insulin resistance in human disease. *Physiol. Rev.* *75*, 473–486.
- Rizkalla, S.W. (2010). Health implications of fructose consumption: A review of recent data. *Nutr. Metab. (Lond.)* *7*, 82.
- Robu, M.E., Larson, J.D., Nasevicius, A., Beiraghi, S., Brenner, C., Farber, S.A., and Ekker, S.C. (2007). p53 activation by knockdown technologies. *PLoS Genet.* *3*, e78.
- Rodgers, R.J., Tschöp, M.H., and Wilding, J.P.H. (2012). Anti-obesity drugs: past, present and future. *Dis. Model. Mech.* *5*, 621–626.
- Rong, N., Selhub, J., Goldin, B.R., and Rosenberg, I.H. (1991). Bacterially synthesized folate in rat large intestine is incorporated into host tissue folyl polyglutamates. *J. Nutr.* *121*, 1955–1959.
- Rual, J.-F., Ceron, J., Koreth, J., Hao, T., Nicot, A.-S., Hirozane-Kishikawa, T., Vandenhaute, J., Orkin, S.H., Hill, D.E., van den Heuvel, S., et al. (2004). Toward improving *Caenorhabditis elegans* phenome mapping with an ORFeome-based RNAi library. *Genome Res.* *14*, 2162–2168.

- Ruggiero, A., Cefalo, M.G., Coccia, P., Mastrangelo, S., Maurizi, P., and Riccardi, R. (2012). The role of diet on the clinical pharmacology of oral antineoplastic agents. *Eur. J. Clin. Pharmacol.* *68*, 115–122.
- Salvestrini, V., Sell, C., and Lorenzini, A. (2019). Obesity may accelerate the aging process. *Front. Endocrinol. (Lausanne)* *10*, 266.
- Samuel, B.S., Rowedder, H., Braendle, C., Félix, M.-A., and Ruvkun, G. (2016). *Caenorhabditis elegans* responses to bacteria from its natural habitats. *Proc. Natl. Acad. Sci. USA* *113*, E3941–9.
- Scartozzi, M., Maccaroni, E., Giampieri, R., Pistelli, M., Bittoni, A., Del Prete, M., Berardi, R., and Cascinu, S. (2011). 5-Fluorouracil pharmacogenomics: still rocking after all these years? *Pharmacogenomics* *12*, 251–265.
- Schlotterer, A., Kukudov, G., Bozorgmehr, F., Hutter, H., Du, X., Oikonomou, D., Ibrahim, Y., Pfisterer, F., Rabbani, N., Thornalley, P., et al. (2009). *C. elegans* as model for the study of high glucose-mediated life span reduction. *Diabetes* *58*, 2450–2456.
- Schwarz, J.-M., Noworolski, S.M., Erkin-Cakmak, A., Korn, N.J., Wen, M.J., Tai, V.W., Jones, G.M., Palii, S.P., Velasco-Alin, M., Pan, K., et al. (2017). Effects of dietary fructose restriction on liver fat, de novo lipogenesis, and insulin kinetics in children with obesity. *Gastroenterology* *153*, 743–752.
- Scott, T.A., Quintaneiro, L.M., Norvaisas, P., Lui, P.P., Wilson, M.P., Leung, K.-Y., Herrera-Dominguez, L., Sudiwala, S., Pessia, A., Clayton, P.T., et al. (2017).

Host-Microbe Co-metabolism Dictates Cancer Drug Efficacy in *C. elegans*.
Cell 169, 442–456.e18.

Seiple, L., Jaruga, P., Dizdaroglu, M., and Stivers, J.T. (2006). Linking uracil base excision repair and 5-fluorouracil toxicity in yeast. *Nucleic Acids Res.* 34, 140–151.

SenGupta, T., Torgersen, M.L., Kassahun, H., Vellai, T., Simonsen, A., and Nilsen, H. (2013). Base excision repair AP endonucleases and mismatch repair act together to induce checkpoint-mediated autophagy. *Nat. Commun.* 4, 2674.

Seydoux, G., Salvage, C., and Greenwald, I. (1993). Isolation and Characterization of Mutations Causing Abnormal Eversion of the Vulva in *Caenorhabditis elegans*. *Dev. Biol.* 157, 423–436.

Shi, X., Li, J., Zou, X., Greggain, J., Rødkær, S.V., Færgeman, N.J., Liang, B., and Watts, J.L. (2013). Regulation of lipid droplet size and phospholipid composition by stearoyl-CoA desaturase. *J. Lipid Res.* 54, 2504–2514.

Simmer, F., Tijsterman, M., Parrish, S., Koushika, S.P., Nonet, M.L., Fire, A., Ahringer, J., and Plasterk, R.H.A. (2002). Loss of the putative RNA-directed RNA polymerase RRF-3 makes *C. elegans* hypersensitive to RNAi. *Curr. Biol.* 12, 1317–1319.

Slupphaug, G., Markussen, F.H., Olsen, L.C., Aasland, R., Aarsaether, N., Bakke, O., Krokan, H.E., and Helland, D.E. (1993). Nuclear and mitochondrial forms of human uracil-DNA glycosylase are encoded by the same gene. *Nucleic Acids Res.* 21, 2579–2584.

- Small, K.S., Todorčević, M., Civelek, M., El-Sayed Moustafa, J.S., Wang, X., Simon, M.M., Fernandez-Tajes, J., Mahajan, A., Horikoshi, M., Hugill, A., et al. (2018). Regulatory variants at KLF14 influence type 2 diabetes risk via a female-specific effect on adipocyte size and body composition. *Nat. Genet.* *50*, 572–580.
- Smemo, S., Tena, J.J., Kim, K.-H., Gamazon, E.R., Sakabe, N.J., Gómez-Marín, C., Aneas, I., Credidio, F.L., Sobreira, D.R., Wasserman, N.F., et al. (2014). Obesity-associated variants within FTO form long-range functional connections with IRX3. *Nature* *507*, 371–375.
- Snell, K., Natsumeda, Y., and Weber, G. (1987). The modulation of serine metabolism in hepatoma 3924A during different phases of cellular proliferation in culture. *Biochem. J.* *245*, 609–612.
- Sohrabi, S., Mor, D.E., Kaletsky, R., Keyes, W., and Murphy, C.T. (2021). High-throughput behavioral screen in *C. elegans* reveals Parkinson's disease drug candidates. *Commun. Biol.* *4*, 203.
- Spanswick, D., Smith, M.A., Groppi, V.E., Logan, S.D., and Ashford, M.L. (1997). Leptin inhibits hypothalamic neurons by activation of ATP-sensitive potassium channels. *Nature* *390*, 521–525.
- Spenkuch, F., Motorin, Y., and Helm, M. (2014). Pseudouridine: still mysterious, but never a fake (uridine)! *RNA Biol.* *11*, 1540–1554.
- Srinivasan, S. (2015). Regulation of body fat in *Caenorhabditis elegans*. *Annu. Rev. Physiol.* *77*, 161–178.

- Srinivasan, S., Sadegh, L., Elle, I.C., Christensen, A.G.L., Faergeman, N.J., and Ashrafi, K. (2008). Serotonin regulates *C. elegans* fat and feeding through independent molecular mechanisms. *Cell Metab.* 7, 533–544.
- Stanhope, K.L., Schwarz, J.M., Keim, N.L., Griffen, S.C., Bremer, A.A., Graham, J.L., Hatcher, B., Cox, C.L., Dyachenko, A., Zhang, W., et al. (2009). Consuming fructose-sweetened, not glucose-sweetened, beverages increases visceral adiposity and lipids and decreases insulin sensitivity in overweight/obese humans. *J. Clin. Invest.* 119, 1322–1334.
- Steiert, P.S., Stauffer, L.T., and Stauffer, G.V. (1990). The *lpd* gene product functions as the L protein in the *Escherichia coli* glycine cleavage enzyme system. *J. Bacteriol.* 172, 6142–6144.
- Sulston, J.E., and Horvitz, H.R. (1977). Post-embryonic cell lineages of the nematode, *Caenorhabditis elegans*. *Dev. Biol.* 56, 110–156.
- Summerton, J. (1999). Morpholino antisense oligomers: the case for an RNase H-independent structural type. *Biochim. Biophys. Acta* 1489, 141–158.
- Sun, X., Fu, X., Li, J., Xing, C., Martin, D.W., Zhang, H.H., Chen, Z., and Dong, J.-T. (2012). Heterozygous deletion of *Atbf1* by the Cre-loxP system in mice causes preweaning mortality. *Genesis* 50, 819–827.
- Sze, J.Y., Victor, M., Loer, C., Shi, Y., and Ruvkun, G. (2000). Food and metabolic signalling defects in a *Caenorhabditis elegans* serotonin-synthesis mutant. *Nature* 403, 560–564.

- Tabara, H., Grishok, A., and Mello, C.C. (1998). RNAi in *C. elegans*: soaking in the genome sequence. *Science* 282, 430–431.
- Tam, B.T., Morais, J.A., and Santosa, S. (2020). Obesity and ageing: Two sides of the same coin. *Obes. Rev.* 21, e12991.
- Tappy, L., and Lê, K.-A. (2010). Metabolic effects of fructose and the worldwide increase in obesity. *Physiol. Rev.* 90, 23–46.
- Tartaglia, L.A., Dembski, M., Weng, X., Deng, N., Culpepper, J., Devos, R., Richards, G.J., Campfield, L.A., Clark, F.T., Deeds, J., et al. (1995). Identification and expression cloning of a leptin receptor, OB-R. *Cell* 83, 1263–1271.
- Teo, E., Ravi, S., Barardo, D., Kim, H.-S., Fong, S., Cazenave-Gassiot, A., Tan, T.Y., Ching, J., Kovalik, J.-P., Wenk, M.R., et al. (2019). Metabolic stress is a primary pathogenic event in transgenic *Caenorhabditis elegans* expressing pan-neuronal human amyloid beta. *eLife* 8.
- Thompson, R.H.S. (1976). Trends in biochemical sciences. *Biochem Educ* 4, 37.
- Toop, C.R., and Gentili, S. (2016). Fructose Beverage Consumption Induces a Metabolic Syndrome Phenotype in the Rat: A Systematic Review and Meta-Analysis. *Nutrients* 8.
- Torrance, C.J., Agrawal, V., Vogelstein, B., and Kinzler, K.W. (2001). Use of isogenic human cancer cells for high-throughput screening and drug discovery. *Nat. Biotechnol.* 19, 940–945.

- Trayhurn, P. (2005). Endocrine and signalling role of adipose tissue: new perspectives on fat. *Acta. Physiol. Scand.* *184*, 285–293.
- Trayhurn, P., and Wood, I.S. (2004). Adipokines: inflammation and the pleiotropic role of white adipose tissue. *Br. J. Nutr.* *92*, 347–355.
- Van Triest, B., Pinedo, H.M., Giaccone, G., and Peters, G.J. (2000). Downstream molecular determinants of response to 5-fluorouracil and antifolate thymidylate synthase inhibitors. *Ann. Oncol.* *11*, 385–391.
- Tsun, Z.-Y., and Possemato, R. (2015). Amino acid management in cancer. *Semin. Cell Dev. Biol.* *43*, 22–32.
- Ullman, B., Lee, M., Martin, D.W., and Santi, D.V. (1978). Cytotoxicity of 5-fluoro-2'-deoxyuridine: requirement for reduced folate cofactors and antagonism by methotrexate. *Proc. Natl. Acad. Sci. USA* *75*, 980–983.
- Uno, M., and Nishida, E. (2016). Lifespan-regulating genes in *C. elegans*. *NPJ Aging Mech. Dis.* *2*, 16010.
- van den Akker, M., Buntinx, F., Metsemakers, J.F., Roos, S., and Knottnerus, J.A. (1998). Multimorbidity in general practice: prevalence, incidence, and determinants of co-occurring chronic and recurrent diseases. *J. Clin. Epidemiol.* *51*, 367–375.
- van Hees, A.M.J., Saris, W.H.M., Hul, G.B., Schaper, N.C., Timmerman, B.E., Lovegrove, J.A., Roche, H.M., and Blaak, E.E. (2010). Effects of dietary fat modification on skeletal muscle fatty acid handling in the metabolic syndrome. *Int. J. Obes.* *34*, 859–870.

- Ved, R., Saha, S., Westlund, B., Perier, C., Burnam, L., Sluder, A., Hoener, M., Rodrigues, C.M.P., Alfonso, A., Steer, C., et al. (2005). Similar patterns of mitochondrial vulnerability and rescue induced by genetic modification of alpha-synuclein, parkin, and DJ-1 in *Caenorhabditis elegans*. *J. Biol. Chem.* *280*, 42655–42668.
- Voisin, S., Almén, M.S., Zheleznyakova, G.Y., Lundberg, L., Zarei, S., Castillo, S., Eriksson, F.E., Nilsson, E.K., Blüher, M., Böttcher, Y., et al. (2015). Many obesity-associated SNPs strongly associate with DNA methylation changes at proximal promoters and enhancers. *Genome Med.* *7*, 103.
- Voisine, C., Varma, H., Walker, N., Bates, E.A., Stockwell, B.R., and Hart, A.C. (2007). Identification of potential therapeutic drugs for huntington's disease using *Caenorhabditis elegans*. *PLoS One* *2*, e504.
- Vrablik, T.L., Petyuk, V.A., Larson, E.M., Smith, R.D., and Watts, J.L. (2015). Lipidomic and proteomic analysis of *Caenorhabditis elegans* lipid droplets and identification of ACS-4 as a lipid droplet-associated protein. *Biochim. Biophys. Acta* *1851*, 1337–1345.
- Wählby, C., Kametsky, L., Liu, Z.H., Riklin-Raviv, T., Conery, A.L., O'Rourke, E.J., Sokolnicki, K.L., Visvikis, O., Ljosa, V., Irazoqui, J.E., et al. (2012). An image analysis toolbox for high-throughput *C. elegans* assays. *Nat. Methods* *9*, 714–716.
- Wählby, C., Conery, A.L., Bray, M.-A., Kametsky, L., Larkins-Ford, J., Sokolnicki, K.L., Veneskey, M., Michaels, K., Carpenter, A.E., and O'Rourke, E.J. (2014).

- High- and low-throughput scoring of fat mass and body fat distribution in *C. elegans*. *Methods* 68, 492–499.
- Wang, C., and Youle, R.J. (2009). The role of mitochondria in apoptosis*. *Annu. Rev. Genet.* 43, 95–118.
- Wang, M.C., O'Rourke, E.J., and Ruvkun, G. (2008). Fat metabolism links germline stem cells and longevity in *C. elegans*. *Science* 322, 957–960.
- Wang, P., Loh, K.H., Wu, M., Morgan, D.A., Schneeberger, M., Yu, X., Chi, J., Kosse, C., Kim, D., Rahmouni, K., et al. (2020). A leptin-BDNF pathway regulating sympathetic innervation of adipose tissue. *Nature* 583, 839–844.
- Watkins, J.B., and Klaassen, C.D. (2018). Absorption, enterohepatic circulation, and fecal excretion of toxicants. In *Comprehensive Toxicology*, (Elsevier), pp. 99–112.
- Watson, E., MacNeil, L.T., Ritter, A.D., Yilmaz, L.S., Rosebrock, A.P., Caudy, A.A., and Walhout, A.J.M. (2014). Interspecies systems biology uncovers metabolites affecting *C. elegans* gene expression and life history traits. *Cell* 156, 759–770.
- Weyer, C., Tataranni, P.A., Snitker, S., Danforth, E., and Ravussin, E. (1998). Increase in insulin action and fat oxidation after treatment with CL 316,243, a highly selective beta3-adrenoceptor agonist in humans. *Diabetes* 47, 1555–1561.

- Wolff, J.L., Starfield, B., and Anderson, G. (2002). Prevalence, expenditures, and complications of multiple chronic conditions in the elderly. *Arch. Intern. Med.* 162, 2269–2276.
- Won, C.S., Oberlies, N.H., and Paine, M.F. (2012). Mechanisms underlying food-drug interactions: inhibition of intestinal metabolism and transport. *Pharmacol. Ther.* 136, 186–201.
- Wright, K.M., Rand, K.A., Kermany, A., Noto, K., Curtis, D., Garrigan, D., Slinkov, D., Dorfman, I., Granka, J.M., Byrnes, J., et al. (2019). A Prospective Analysis of Genetic Variants Associated with Human Lifespan. *G3 (Bethesda)* 9, 2863–2878.
- Wu, H., and Ballantyne, C.M. (2020). Metabolic inflammation and insulin resistance in obesity. *Circ. Res.* 126, 1549–1564.
- Wu, L., Zhou, B., Oshiro-Rapley, N., Li, M., Paulo, J.A., Webster, C.M., Mou, F., Kacergis, M.C., Talkowski, M.E., Carr, C.E., et al. (2016). An ancient, unified mechanism for metformin growth inhibition in *c. elegans* and cancer. *Cell* 167, 1705–1718.e13.
- Yaffe, K., Falvey, C., Hamilton, N., Schwartz, A.V., Simonsick, E.M., Satterfield, S., Cauley, J.A., Rosano, C., Launer, L.J., Strotmeyer, E.S., et al. (2012). Diabetes, glucose control, and 9-year cognitive decline among older adults without dementia. *Arch. Neurol.* 69, 1170–1175.
- Yang, W., Kelly, T., and He, J. (2007). Genetic epidemiology of obesity. *Epidemiol Rev* 29, 49–61.

- Ye, F.B., Hamza, A., Singh, T., Flibotte, S., and Hieter, P. (2020). A Multimodal Genotoxic Anticancer Drug Characterized by Pharmacogenetic Analysis in *Caenorhabditis elegans*. *Genetics*. 215(3), 609-621.
- Yengo, L., Sidorenko, J., Kemper, K.E., Zheng, Z., Wood, A.R., Weedon, M.N., Frayling, T.M., Hirschhorn, J., Yang, J., Visscher, P.M., et al. (2018). Meta-analysis of genome-wide association studies for height and body mass index in ~700000 individuals of European ancestry. *Hum. Mol. Genet.* 27, 3641–3649.
- Yilmaz, L.S., and Walhout, A.J.M. (2016). A *Caenorhabditis elegans* Genome-Scale Metabolic Network Model. *Cell Syst.* 2, 297–311.
- Zhang, D., Tang, B., Xie, X., Xiao, Y.-F., Yang, S.-M., and Zhang, J.-W. (2015a). The interplay between DNA repair and autophagy in cancer therapy. *Cancer Biol. Ther.* 16, 1005–1013.
- Zhang, F., Berg, M., Dierking, K., Félix, M.-A., Shapira, M., Samuel, B.S., and Schulenburg, H. (2017). *Caenorhabditis elegans* as a Model for Microbiome Research. *Front. Microbiol.* 8, 485.
- Zhang, H., Chang, J.T., Guo, B., Hansen, M., Jia, K., Kovács, A.L., Kumsta, C., Lapierre, L.R., Legouis, R., Lin, L., et al. (2015b). Guidelines for monitoring autophagy in *Caenorhabditis elegans*. *Autophagy* 11, 9–27.
- Zhang, Y., Proenca, R., Maffei, M., Barone, M., Leopold, L., and Friedman, J.M. (1994). Positional cloning of the mouse obese gene and its human homologue. *Nature* 372, 425–432.

- Zhao, X., and Yu, Y.-T. (2007). Incorporation of 5-fluorouracil into U2 snRNA blocks pseudouridylation and pre-mRNA splicing in vivo. *Nucleic Acids Res.* *35*, 550–558.
- Zheng, J., Enright, F., Keenan, M., Finley, J., Zhou, J., Ye, J., Greenway, F., Senevirathne, R.N., Gissendanner, C.R., Manaois, R., et al. (2010). Resistant starch, fermented resistant starch, and short-chain fatty acids reduce intestinal fat deposition in *Caenorhabditis elegans*. *J. Agric. Food Chem.* *58*, 4744–4748.
- Zhou, B., Kreuzer, J., Kumsta, C., Wu, L., Kamber, K.J., Cedillo, L., Zhang, Y., Li, S., Kacergis, M.C., Webster, C.M., et al. (2019). Mitochondrial permeability uncouples elevated autophagy and lifespan extension. *Cell* *177*, 299–314.e16.
- Zimmermann, M., Zimmermann-Kogadeeva, M., Wegmann, R., and Goodman, A.L. (2019). Mapping human microbiome drug metabolism by gut bacteria and their genes. *Nature* *570*, 462–467.